EARTH RESOURCES SHUTTLE IMAGING RADAR

Earth Resources Shuttle Imaging Radar

Contract NAS-9-14273

October 1975

RADAR AVIONICS DIVISION
AEROSPACE GROUPS
Hughes Aircraft Company • Culver City, California

PAGE MISSING FROM AVAILABLE VERSION

CONTENTS

CONTENTS (Continued)

1.0 INTRODUCTION

This is a report on a preliminary design of a Synthetic Array Radar (SAR) intended for experimental use with the Space Shuttle program that will be operated during the 1980's. The radar is called Earth Resources Shuttle Imaging Radar (ERSIR). Its primary purpose is to determine the usefulness of SAR in monitoring and managing earth resources. This report describes the design developed for the ERSIR, discusses tradeoffs made during its evolution, and indicates design questions that are still to be resolved.

ERSIR consists of a flight sensor for collecting the raw radar data and a ground sensor used both for reducing these radar data to images and for extracting earth resources information from the data. The flight sensor consists of two high powered coherent, pulse radars, one that operates at L and the other at X-band. Both are dual polarized. The transmitted power at L-band is 200 watts and at X-band it is 500 watts. In order to incorporate maximum simplicity into the flight sensor, the receiver output signal is converted to digital form and then recorded with various ancillary signals after a few data operations directed at maximizing the efficiency of recording. Data on the tape can be either transmitted via a digital data link to a ground terminal, or the tape can be delivered to the ground station after the shuttle lands. In either event a data tape is the source of input to the ground system, where the data are first processed to form calibrated images on both data tape and film. Extraction of earth resource data from the tape data is facilitated by a wide variety of operations available to the experimenter for analyzing the radar images.

OBJECTIVES AND COMPROMISES

During the evolution of this design, much attention was given to the needs of the experimenters who will use it. Counsel was sought from those knowledgeable in geology and agriculture as well as from those knowledgeable in the application of radar to these fields. Also advantage was taken of the Microwave Sensing Survey reported in JPL's Shuttle Imaging Radar Study.* All helped in determining frequencies, polarizations, resolution and calibration goals. By the time Hughes entered the ERSIR program, goals for swath width and vertical look angles (angle between radar beam and line-of-sight) had already been established. Very little outside information was available on the amount of diversity needed, i.e., how many independent samples of the power of each resolution cell are needed. The question was resolved mainly on the basis of Hughes own studies of diversity; similarly questions on image quality requirements were resolved primarily on the basis of Hughes own experience.

Aside from these inherent characteristics of the radar data to be collected, user needs related to the processing of this data must be considered in the design. Certain of the processing requirements are obvious, such as the need to record image output on data tape and the need to process the data in reasonably short times. Other requirements are not so obvious. These fall mainly into the category of processing flexibility including such considerations as the kinds of operations that experimenters would like to perform on the data.

The overall approach to the ERSIR design was to come as close as technical risk and cost would allow in satisfying what were seen as the totality of experimenter needs. Where knowledge of user needs was uncertain, as for image processing, requirements that appeared most reasonable were suggested.

As this design developed, attention was given to the demands placed on the Shuttle and its payload of experiments. The principal direct effects of ERSIR on the Shuttle are those which relate to payload weight, prime power loading, vehicle drag, and expenditure of reaction control fuel.

---

*Shuttle Imaging Radar Study, System Definition Report, J.G. Mehlis and E.A. Cohen, Aug. 5, 1974, Jet Propulsion Laboratory, Pasadena, CA.

The relationship between weight and prime power is inverse. The trade-off was resolved by minimizing SAR prime power while considering other constraints; this forced the total SAR weight up to 1094 kg. From the shuttle standpoint this appeared the most satisfactory approach.

Shuttle drag and reaction control fuel expenditure were both increased slightly in favor of simplifying the SAR space and ground units; the penalty imposed on the Shuttle system seems small. During ERSIR operation the shuttle flies sideways, in an orientation that produces maximum drag (Fig 1-1). This is in contrast to nose first orientation, in which its longitudinal axis and velocity vector are aligned, an orientation that incurs minimum drag. This slightly increases the Shuttle's hourly loss of velocity (Table 1-1), but it reduces the complexity and cost of the ERSIR antenna deployment mechanism.

Also, during ERSIR operation the Shuttle reaction control system uses the payload inertial guidance unit as a reference for attitude control, to keep the antenna pointing within about ± 0.3 degrees (2σ) of the required direction. This requires the reaction control system to expend fuel at a greater rate than otherwise, but greatly reduces the complexity of the ground system processor. Also, this assumes that the ERSIR design includes a resolution of about 25 m x 25 m. Should the resolution be significantly reduced, tight control of beam point may no longer be justified since processor simplification will have been precluded by the finer resolution itself.

TABLE 1-1. ORBITAL VELOCITY LOSS PER HOUR

Shuttle Flight Direction	Velocity Loss Per One Hour (km/sec)*
Sideways (Z-axis vertical)	2.5×10^{-4}
Nose forward (Z-axis vertical)	7.2×10^{-5}

*Reference: Space shuttle system payload accommodations, page 3-33

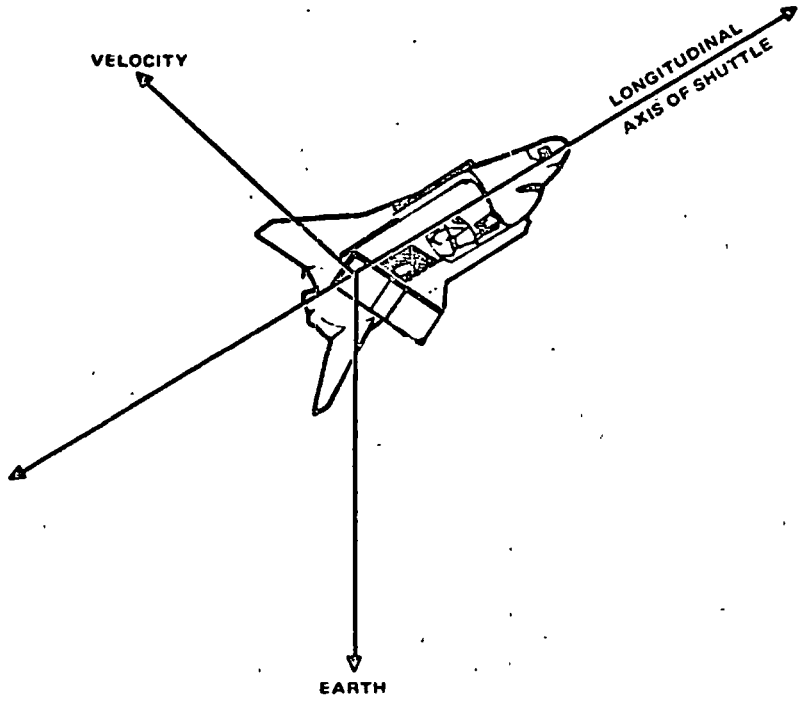

Figure 1-1. Orientation for radar survey (sideways flight).

Compatibility with other experiments was also considered in establishing the ERSIR design; the interference of ERSIR with other experimental equipment in a common Space Lab payload was to be the minimum compatible with the allowable technical risk and cost. The principal consideration here was the method of deploying the ERSIR antenna structure. This includes both the extent to which it is deployed and also its final orientation. The ERSIR baseline design calls for the minimum deployment that will allow an unobscured view of the ground from the other pallets while the shuttle is in inverted flight. If the ERSIR antenna is reduced in length to about 7.5 m, and the obscuration of another pallet were permitted, then cost and risk of antenna deployment could be reduced.

SELECTION OF FREQUENCIES

It appeared that one user would have need for frequencies extending from UHF to K_u-band; it also appeared that the inclusion of four band frequencies UHF, L, X and K_u would satisfy all user needs. Initially it was attempted to include three of these frequencies, UFH, L, and X-bands, in a single design. Because of limitations placed on the available aperture by the size of the Space Lab's pallets and the Space Lab's internal launch envelope it was necessary for the L and X-band antennas to look through the UHF antenna. The maximum aperture height available was three meters (possibly plus 10 percent), while to attain the desired swath widths and vertical look angles, the L and X-bands together used all this available aperture height. In consequence, it was necessary to overlay the UHF antenna on the combined L, X band antennas. While this was possible, the development was considered costly; moreover it involved a moderate amount of technical risk, since it required folding the combined antenna system for stowage. For this reason UHF was not included as a principal frequency; if it were to be incorporated, it would be flown separately from an X and L system.

K_u-band was included, at this time, for a different reason. To produce information significantly different from X-band it would need to be significantly higher in frequency than the X-band, which is 9.0 GHz. This means a frequency of at least 16 or 17 GHz. Fabricating the long antenna array needed for these frequencies (at least 6 m) requires special shop techniques for maintaining tolerances on flatness. Furthermore, because of the shuttle's thermal environment, maintaining this flatness requires a more difficult and higher risk design than for X-band. Another disadvantage of these higher K_u-band frequencies is that they may need greater transmitter prime power for the same signal-to-noise ratio, when mapping diffuse type scatterers, such as wheat fields, under moderately adverse propagation conditions. An example is the presence of low stratus clouds without precipitation. Increasing the ERSIR baseline X-band frequency to 16 or 17 GHz would require increasing the system prime power by roughly 4.4 kW. Therefore, early in the program, prime power, technical risk and development cost were recognized as the main reasons for not pursuing K_u-band (16 GHz).

Later in the program a point was made that L and K_u-bands would be preferable to L and X-bands for making agricultural measurements. It was noted that even 13 or 14 GHz would be preferable to 9 Hz, because backscattering of plant biomass is more sensitive to the higher frequency. Fabrication of the antenna for this frequency is about 30 percent higher in cost, but presents no significant increase in technical risk. Although the base line design of ERSIR continues to be L and X bands for reason of continuity of effort, the X-band could be changed readily to K_u-band (13 GHz).

RESOLUTION AND FREQUENCY SELECTION

The baseline resolution of 25 m x 25 m, measured in ground coordinates, strongly influences the complexity of the required ground processing. The baseline design includes ground processing that is moderately complex, primarily because of the need to do range closure compensation for L-band on the ground instead of before recording. If, however, the L-band frequency were increased from 1.04 GHz to 2 GHz, then probably range compensation could precede recording. This change would simplify the ground processor considerably and should be incorporated into the ERSIR design if possible.

A secondary ground resolution capability of 12.5 m x 12.5 m is also available with the ERSIR at this time. It is secondary because the system records full swath widths for only the 25 m x 25 m resolution, and the ground processor capacity for mass data reduction is sized to accommodate this larger resolution. A swath with width of 45 km can be recorded in the 12.5 m resolution mode. Although with the appropriate software the system can reduce the 12 m resolution data, the program will be more complex because of the increased range closure complexity; for a given terrain area the data reduction time will be roughly 16 times greater than for 25 m resolution.

CALIBRATION

For some applications, such as agricultural crop assessment, the average radar backscattering cross section (σ_o) must be measured with considerable accuracy; consequently radar calibration must provide for all

the radar parameters which effect that measurement. In this study calibration errors were categorized in terms of their long term components (highly correlated over several orbits) and short term components (highly correlated over only 10 km or 20 km). Goals that appear realistic in terms of hardware performance have been set for each. Short term and long term error goals are each 1.8 dB with a 95 percent confidence. The RMS error goal is 2.6 dB.

The appropriateness of these goals should be reviewed by user groups.

DIVERSITY (NUMBER OF LOOKS)

Position diversity is used in the ERSIR design; every resolution cell is looked at by four different synthetic array beams as the Shuttle sweeps by (see Figures 1-2 and 1-3). These four looks are nearly independent when the resolution cell contains a diffuse backscatterer such as a wheat field, or plowed ground. The imagery resulting from these four looks consists of four maps which can be averaged together, or in any way desired by the experimenter.

A logical question is: "Why not use the totality of recorded radar data to obtain a smaller azimuth resolution?" This can be done; but with a significant increase in complexity of the ground processor software. If at a later time it is decided that a finer azimuth resolution is desirable only a change in the ground processor software will be needed.

DESIGN ALTITUDE AND COVERAGE

The design altitude for ERSIR operation is 200 km, but it will perform acceptably up to 400 km. At the design altitude, a swath having a width of up to 85 km can be mapped, and this swath can be offset anywhere from 35 km to 365 km from the ground track (see Figure 1-4). The vertical look angle of the inner edge of the minimum offset swath is 10 degrees, and that of the outer edge of the maximum offset swath is 60 degrees.

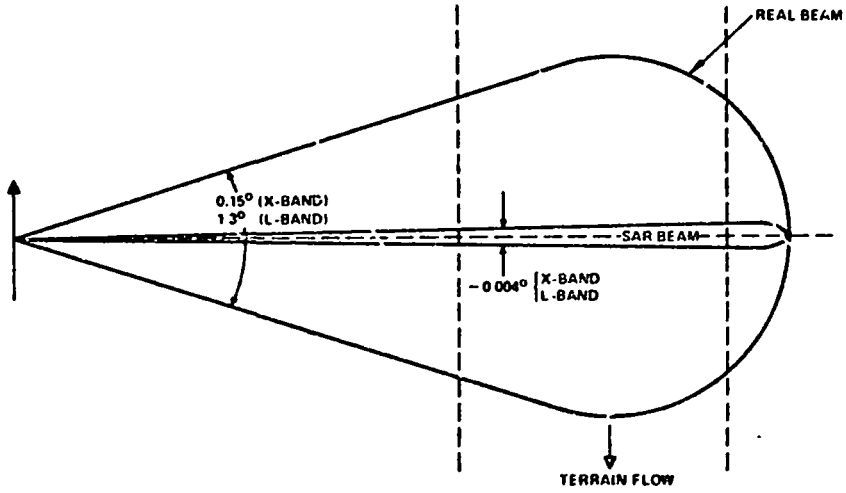

Figure 1-2. Single look synthetic array beam (25 m resolution).

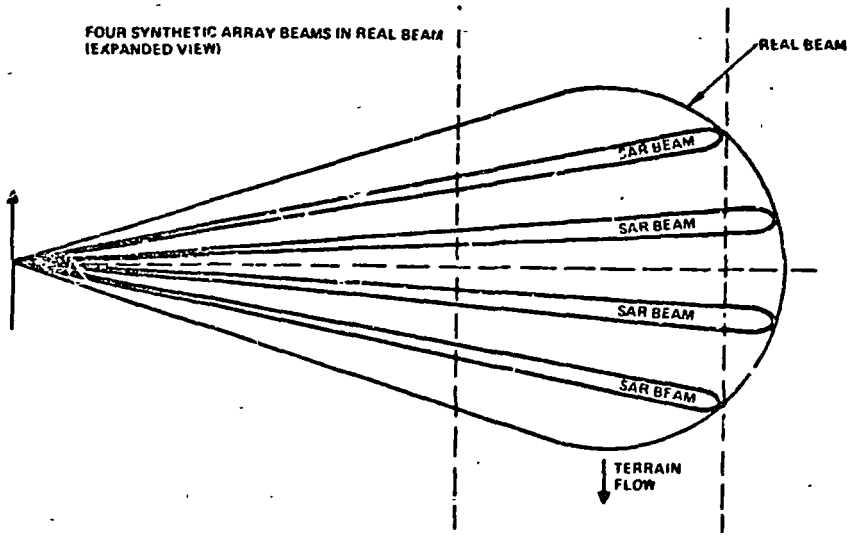

Figure 1-3. ERSIR four look imagery.

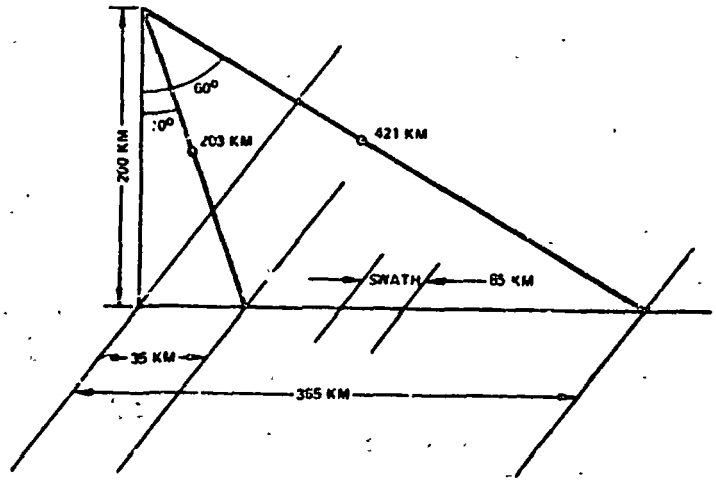

Figure 1-4. Geometry.

ERSIR SPACE AND GROUND SYSTEMS

In ERSIR the raw radar data is recorded digitally in-flight and converted into images on the ground (see Figure 1-5). Raw radar data are collected simultaneously at X-band (9.0 GHz) and L-band (1.04 GHz), and at each frequency. Vertical and horizontal polarization data are recorded separately. Either vertical or horizontal polarization can be selected for transmission at each frequency. Consequently, either an L-band combination of

$$L_{VH} \text{ and } L_{VV}, \text{ or } L_{HH} \text{ and } L_{HV}$$

plus, an X-band combination of either

$$X_{VH} \text{ and } X_{VV} \text{ or } X_{HH} \text{ and } X_{HV}$$

can be selected. After these raw radar data are converted to images by the ground processor, maps will be made for each combination. For example, if raw data were simultaneously collected for L_{VH}, L_{VV}, X_{HV}, and X_{HH} then there would be maps (images) for each. More specifically because of diversity there will be: four maps at L_{VH}, four maps at L_{VV}, four maps at X_{HV}, and four maps at X_{HH}, a total of 16 maps. Each of these maps will be the same swath.

One of the important ground system design questions that needs answering is: How precisely must the different maps be registered? That is,

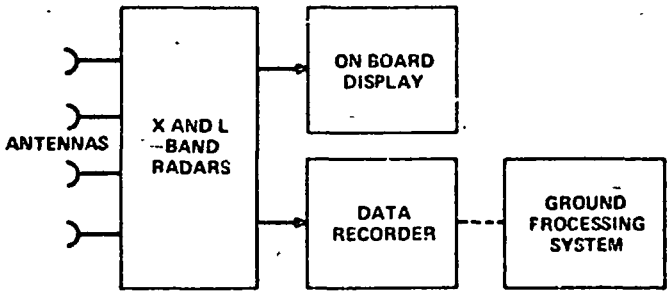

Figure 1-5. Imaging radar for the space shuttle.

how precisely must experimenters align the resolution cells of one map with those of another? Most likely, for the four diversity looks (maps) within a single frequency-polarization combination, the resolution cells should be matched (registered) so that corresponding looks at the same ground cell are identified. This is a straightforward processor operation. Further, the 8 maps of both polarizations can be registered at the same time. Registration of the L-band and X-band data is still straightforward but more complicated.

Raw radar data can be transferred from the Space Shuttle to the Ground System by either a digital communication link, or by moving the tapes to the ground site after Shuttle landing. In the ERSIR design, sufficient tape is carried for recording four hours of full radar operation. The weight cost is 176 kg (22 reels of tape). This storage capacity can be reduced to the extent that communication capacity is available. Although at full operation rate at which data enters the recorder is 260 Mbits/sec, the recorders can be slowed by a ratio of 10:1 to provide communication channel input rates as low as 26 Mbits/sec.

The Ground System forms the images, and records them on both data tape and film. It also provides a means for analyzing the data.

SUMMARY OF ERSIR PARAMETERS AND PERFORMANCE

A summary of the ERSIR baseline parameters is given in Table 1-2.

A summary of coverage and image quality is given in Table 1-3. Resolutions as fine as 6M are specified there, although, 25M is indicated as the design resolutions. The distinction between primary and secondary resolutions has been made previously. It should be added here that a 6 m x 6 m resolution is available only incidently, as the required transmitter and receiver bandwidths are needed for achieving the 12.5 m x 12.5 m resolution at the small vertical look angles (10 to 20 degrees). This, of course, means that the 6 m resolution is available for only the larger vertical look angles (30 to 60 degrees). Also, in the 6 m resolution mode swath widths are limited to 22 km by the available processor short term storage.

TABLE 1-2. BASELINE PARAMETERS

Characteristics	Radar	
	X-band	L-band
Frequency	9.0 GHz	1.04 GHz
Transmit polarizations	V or H	V or H
Receiver polarizations	V and H	V and H
PRF range, Hz	1200-1800	1200-1800
Transmitter average power out, watts	500 W	200 W
Transmitter peak power	17 kW	6.8 kW
Antenna azimuth beamwidth	0.15°	1.3°
Elevation beamwidth	6.3°, 9.4°, 18.9°	6.3°, 9.4°, 18.9°
Total antenna aperture, height x length	3M x 10.7M	
Total system weight (including 22 tapes)	1271 kg	

TABLE 1-3. COVERAGE AND IMAGE QUALITY SUMMARY FOR BASELINE

Resolution	6 m to 25 m*
Minimum signal to thermal noise (12.5 m resolution)*	8 dB
Minimum signal to total background noise*	7 dB (full swath) 8 dB (middle swath)
Look angles from vertical	10° to 60°
Range offsets	75 km to 365 km
Swath width	to 85 km
Number of looks	4 at 12.5 m and 25 m* 1 at 6 m
Dynamic range (image on data tape) $-21\ \text{dB} \leq \sigma_0 \leq -10\ \text{dB}$	50 dB

*Design resolution is 25 m

Total background noise in the "minimum signal-to-total background noise" consists of all the noise sources contributing to the noise appearing in the image. It includes these sources:

receiver thermal noise
analog-to-digital converter quantization noise
SAR filter integrated sidelobes
range pulse compression integrated sidelobes
range PRF ambiguous noise
azimuth PRF ambiguous noise
transmitter noise

For a fixed swath both the minimum signal-to-thermal noise and the minimum signal-to-total background noise appear at the swatch edges; in particular, the minimum signal-to-total background noise of 7 dB and minimum signal-to-thermal noise for 8 dB is used in defining swath width. Thus, the swath widths called out in this report have at least these characteristics throughout the swath. The "middle swath" referred to in Table 1-2 is specifically the middle-third of the swath.

2.0 FUNCTIONAL DESCRIPTION

2.1 SPACE SYSTEM FUNCTIONAL DESCRIPTION

Space Sensor Functions

The space shuttle imaging radar is the active sensor link between various areas on the earth's surface and the ground processor system. The combination of space and ground processors furnish the user community with information on earth resources experiments and surveys. The space sensor carries out the following functions:

- Illuminates selected terrain swaths
- Pre-processes the reflected energy
- Records the raw data
- Produces an on-board display of the scene

Ground processing functions are discussed in Section 2.2

The space sensor is configured for dual frequency, dual polarization, and multi-look terrain imaging. Figure 2-1 illustrates the use of a planar array antenna in space for illuminating the swath by means of multiple beams that form multi-look images. Two antennas, one at X-band and one at L-band illuminate the terrain with either vertically or horizontally polarized energy. Four antennas are used for receiving, as shown in Figure 2-2.

The space sensor pre-processes ground reflected signals in the four receiver channels and records the raw sensor data for subsequent transmittal to the ground processing system. Cross-polarized signal data (VH or HV) are recorded for each band. This supplies information on depolarizing characteristics of the terrain.

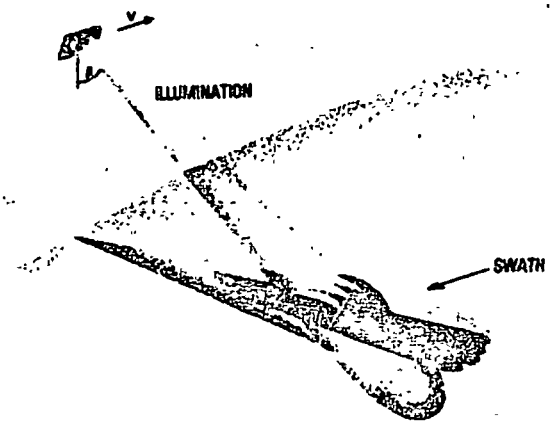

Figure 2-1. Multi-looks and signal-to-noise.

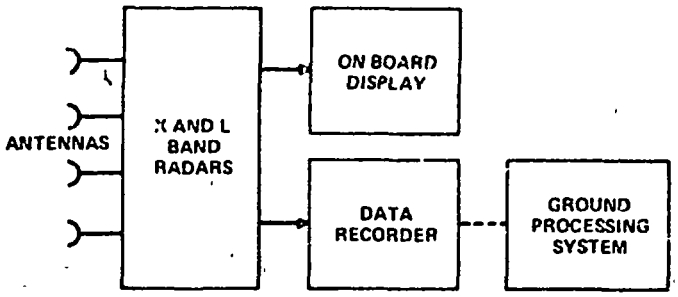

Figure 2-2. Imaging radar for the space shuttle.

An on-board display presents passing scene imagery of the selected swath for one of the four receiver channels. This optional feature makes possible one display of single channel imagery with an unfocused resolution of about 100 meters (X-band) to 200 meters (L-band). This may be compared with simultaneous four channel, 12.5 meter imagery (25 meters baseline design) processed on the ground.

The space sensor is basically a simple assembly of the two dual-polarized radars with data buffering and recording. Figure 2-3 shows the principal units of the baseline design, which includes the optional on-board

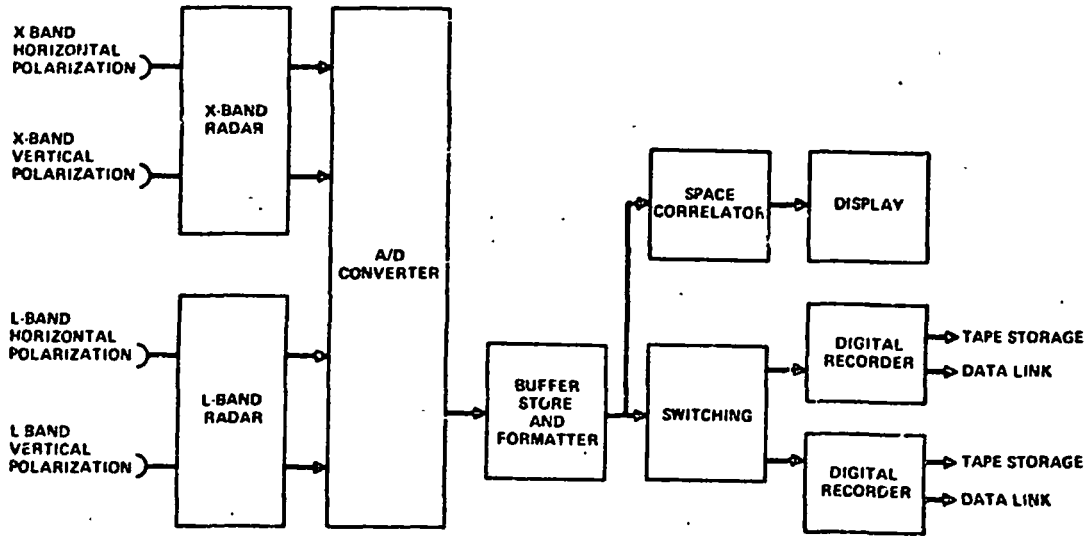

Figure 2-3. Principal units of ERSIR baseline design.

display. The two recorders may be used alternately to provide continuous data acquisition. One recorder can store data, while the other is employed for data link or both may be used simultaneously for data storage at a higher rate (260 MB's).

The space sensor functions fall into two broad categories: (1) functions which relate primarily to swath selection; and (2) functions which relate primarily to swath recording.

The Swath Selection Process

The swath selection process involves functions which determine antenna vertical position, antenna beamwidth, swath resolution and image quality. These functions are interrelated and the sensor is designed with sets of mutually consistent parameters to produce imaging of the designated swath with the designated swath resolution (25 meters, nominally), and with acceptable quality. Accordingly, the antenna is designed to permit selection of one of three available vertical beams: a broad beam for wide swath coverage (to 85 KM) near nadir, an intermediate beam (9.5 degrees) for intermediate offset ranges and a narrow beam (6 degrees) for imaging swaths at

large look angles. Geometrical and resolution characteristics involved in the selection process are illustrated in Figure 2-4.

The resolution characteristics of the selected swath are determined by the bandwidth of the transmitted waveform. For a fixed short range resolution, r_s, the resolution r_g varies across the swath. r_s is related to the transmitted waveform bandwidth by the following:

$$r_s = C/2B = 150/B \text{ meters} \tag{2-1}$$

$$r_g = r_s \csc\beta \text{ meters} \tag{2-2}$$

where

C is the velocity of light

B is the waveform bandwidth (MHz)

β is the look angle.

The block diagram in Figure 2-5 shows major SAR space functions. The prf and pulse duration of the transmitted waveform determine the average power (500 watts at X-band, 200 watts at L-band); the resolution is

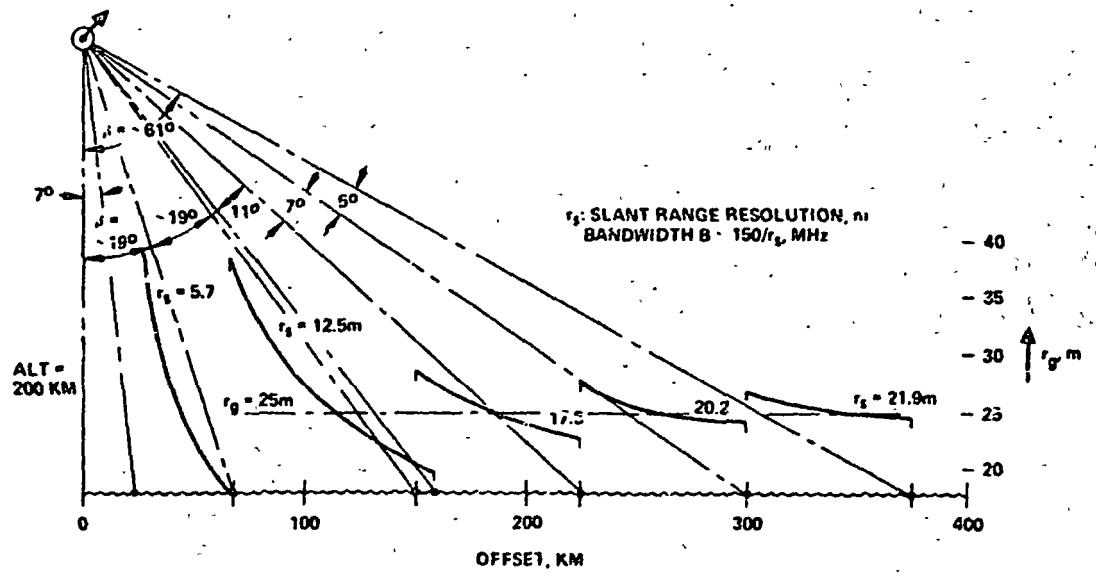

Figure 2-4. Resolutions and bandwidths vs swaths.

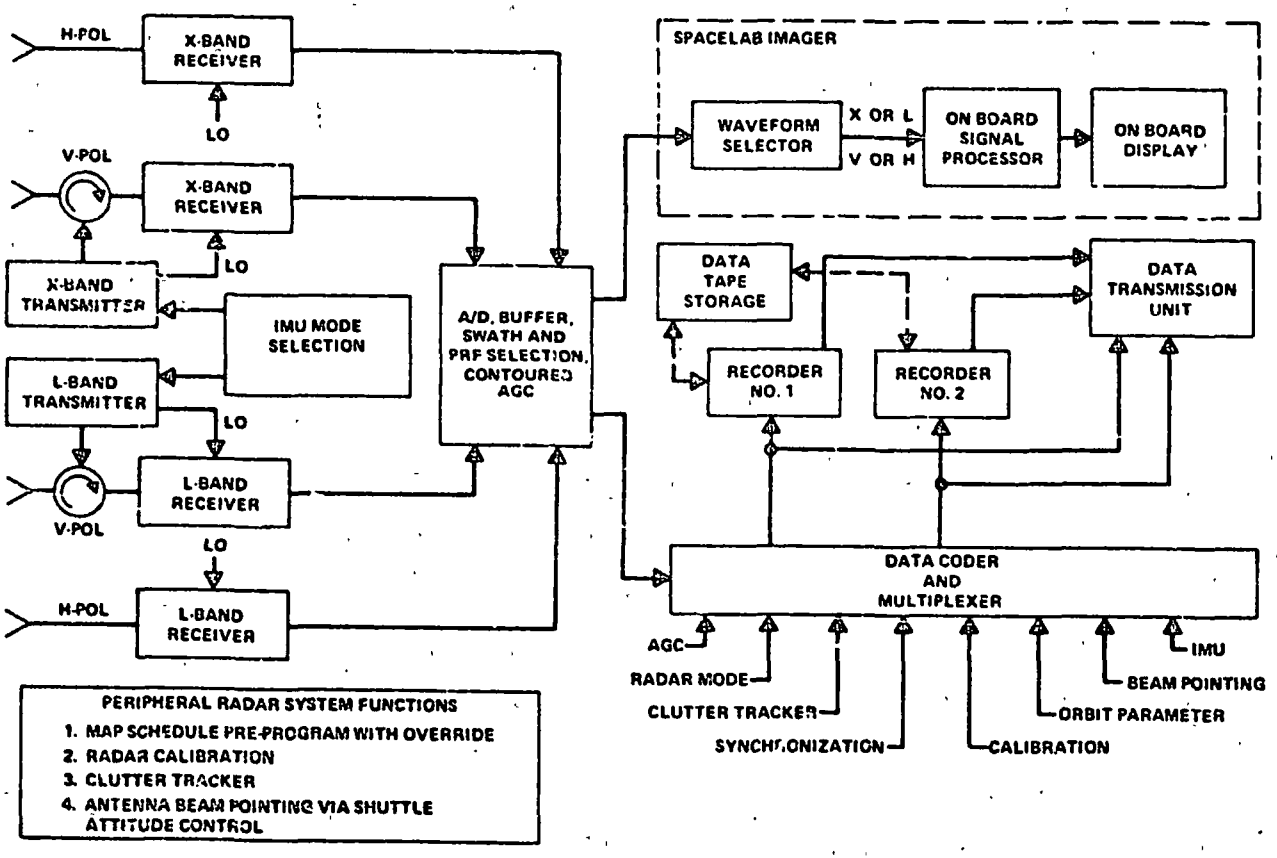

Figure 2-5. SAR space functions.

provided by the pulse compression bandwidth B in equation 2-1 above. The wavefo-m selections are based upon two image quality considerations: (1) signal-to-noise ratio (pulse duration) and (2) range and azimuth ambiguity suppression (prf and vertical beamwidth).

The receiver channel bandwidth is also a factor in the selection process. The appropriate bandwith is obtained by selecting one of seven filters before A/D conversion. The available bandwidths bracket the 6 to 27 MHz range required for 25 meters resolution at look angles varying from 15° to 60°.

The Record Process

The following list of space sensor functions relate primarily to the record process: (1) antenna beam pointing in azimuth; (2) calibration; (3) range contour AGC and A/D conversion and (4) buffering.

The A/D and buffer in Figure 2-5 link the radar signals to the data recording process. The buffer conserves bandwidth and time to make the data recording process efficient. This is possible with raw data for multi-look imagery because the time interval between successive prf intervals of data is large in comparsion to the time delay interval of the swath width:

$$T_p = \frac{C}{2\ prf} > \Delta R_s \qquad (2\text{-}3)$$

where $\Delta R_s \simeq \Delta R_g \sin\beta$; ΔR_g is swath and ΔR_s is the corresponding slant range interval, β is look angle. The buffer expands the raw data to fill the interval T_p, resulting in a stream of uniform, closely packed data for the tape recorders. The multi-look ground processing precludes presumming because the prf is not large in comparison to the SAR data bandwidth.

Range contour AGC and the A/D conversion functions contribute to the efficiency of the recording process and to dynamic range performance. With the contour AGC function, the data are recorded at 5 bits IQ yet retain a dynamic range that is equivalent to 8 bits. This is done with the help of a digital AGC technique. The range swath is divided into segments of 1 to 10 KM and for each receiver AGC is applied independently to each segment.

The resulting AGC profiles are encoded with the 5 bit (IQ) data stream. The ground processor employs an AGC inversion process to restore the equivalence of 8-bits (I,Q) dynamic range (See Section 4.2).

The space sensor provides calibration data for the ground processor to help make its operation accurate and its measurements meaningful. The data comprise critical parameters for transmitter power, receiver gain, and sensor noise level. These data are recorded and transmitted to the ground processing station with the raw radar data. Programmed calibration routines are supplied for this purpose. In addition, the calibration function includes built-in test continuous monitoring as a normal routine that maintains and up-dates transmitter power and receiver gain calibration data. Updating the receiver AGC calibration is important because receiver AGC changes during the data acquisition process to accommodate signal level changes of a general nature, such as occur when crossing seas, lakes and land-water boundaries.

The calibration facilities use replicas of the transmitter waveform both to provide parameter data used in calibration and for continuous monitoring. Data are provided on waveform as well as the mean value of receiver gain. Parameter data for estimating sensor noise are provided by special calibration routines established for that purpose (See Section 4.4).

The accuracy of azimuth beam pointing simplifies the ground processor, reducing its cost and increasing its reliability. The antenna is positioned near an optimum azimuth angle, which results in minimum range closure compensation.

The azimuth beam pointing function uses the IPS (inertial pointing subsystem) to provide a stable and accurate antenna azimuth position, which is determined by the Spacelab attitude. The result is a simplification in ground processor requirements, saving the expense of more complex ground processor equipment. The IPS Antenna beam pointing function stabilizes the antenna near an azimuth position which results in minimum range closure compensation.

With the IPS, expected accuracies are $\pm 0.3^{o}$ degree or better and this accuracy satisfies the requirements for a single range closure compensation per swath (L-band; single look at 1 GHz and four looks at 2 GHz). The

requirement for doppler compensation at X-band is also simplified. (See Section 4.4.)

2.2 GROUND SYSTEM FUNCTIONAL DESCRIPTION

The purpose of the Ground System is to provide a diversity of experimenters with the kinds of SAR data they need and also to provide a means of extracting information and developing techniques for data extraction. The data output available for off-site investigation will be of two kinds, image data tape and photographic copy. Both types of outputs will include calibration and navigational indexing. The site data extraction mode is conversational. The experimenter can command the system to carry out operations on the data that he specifies, observe within one or two minutes the resulting image or numerical results on CRT's, revise his specified operations, see the new results, and so on.

In the ground system, images are formed first by digital correlation, after which they are calibrated (Figure 2-6). Not all of the uncalibrated image data is of the same quality because it comes from different parts of the real antenna beam; therefore, the data are indexed in the calibration process according to its estimated signal-to-noise ratio. Navigational data and identifying symbols are also included. Once the calibrated and labeled data is generated, it becomes an input to the computer and display units.

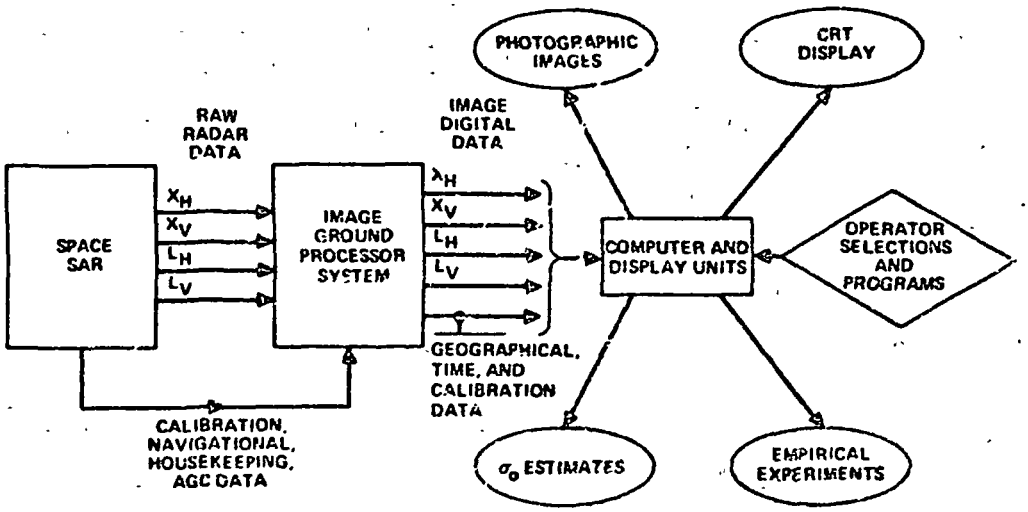

Figure 2-6. ERSIR outputs.

Whatever program has been read into the computer for the particular experiment at hand determines whether photographic images, CRT displays, or additional processing will be applied to the imaged data prior to display, or whether numerical estimates of image characteristics, such as the average backscatter coefficient, will be made.

All 16 of the images of the swath will be registered so that experimenters can form new maps by combining individual resolution cells in arbitrary ways, and in general carry out a wide range of empirical investigation (Figure 2-7). This will permit performing multi-frequency, dual-polarization experiments that can be carried out at present only with great difficulty.

Data Processor Function

The data processor, in response to its input commands, first forms the single-look calibrated image at each of the requested frequencies and polarizations, and then does the post image processing. Post image processing is controlled by the computer program read into the computer for the

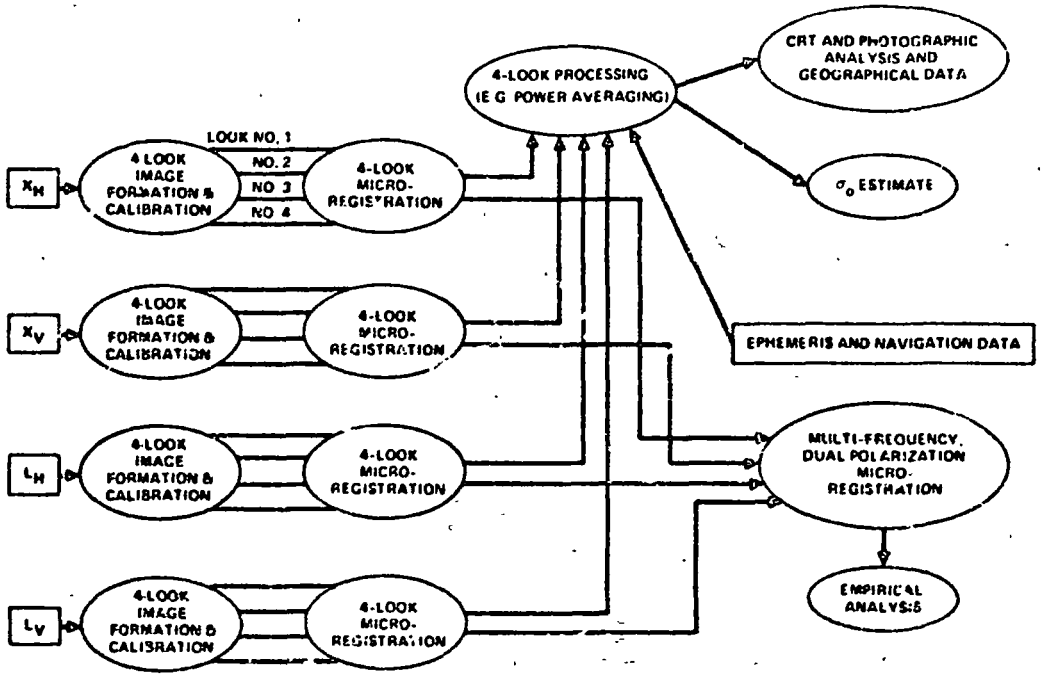

Figure 2-7. Principal functions of ground processes.

experiment at hand, and is limited principally by the amount of data available, image quality, and the precision of multiple image registration. Once the several single look images are formed, calibrated, and registered an extremely wide range of processing options is available to the experimenter. For example new images can be composed from multiple images; image enhancement can be applied to single images. Images can be subjected to spectral analysis and also to statistical analysis.

The formation of single-look calibrated images is basic to all processing done on the raw radar data. This is carried out in two steps. First, the uncalibrated image is formed, and then it is calibrated. After image formation, the several images to be used in the experiment are registered (termed micro-registrations in the illustrations).

Uncalibrated Image Formation

There are several steps required in the formation of the uncalibrated image, namely those listed below:

- AGC inversion
- SAR Beam and Real Beam Alignment
- Pulse Compression
- Correction for envelope closure
- Determine and apply focusing
- SAR filter formation (correlation)

All of the Input data required for these operations is recorded on the data tape. In addition to the raw radar data recorded various ancillary signals such as navigation and AGC Data also are included (see Figure 2-8). If shuttle ephemeris data are available, they can be used with the shuttle navigation data to improve data quality.

AGC Inversion (see Figure 2-8)

In the shuttle, to preserve the maximum dynamic range of the radar data with the minimum data rate, the raw radar data is scaled before it is recorded, in an amount determined by the AGC voltage. Before any images can be formed this scaling must be inverted. The amount of this adjustment is determined by means of the ancilliary AGC data on the data tape.

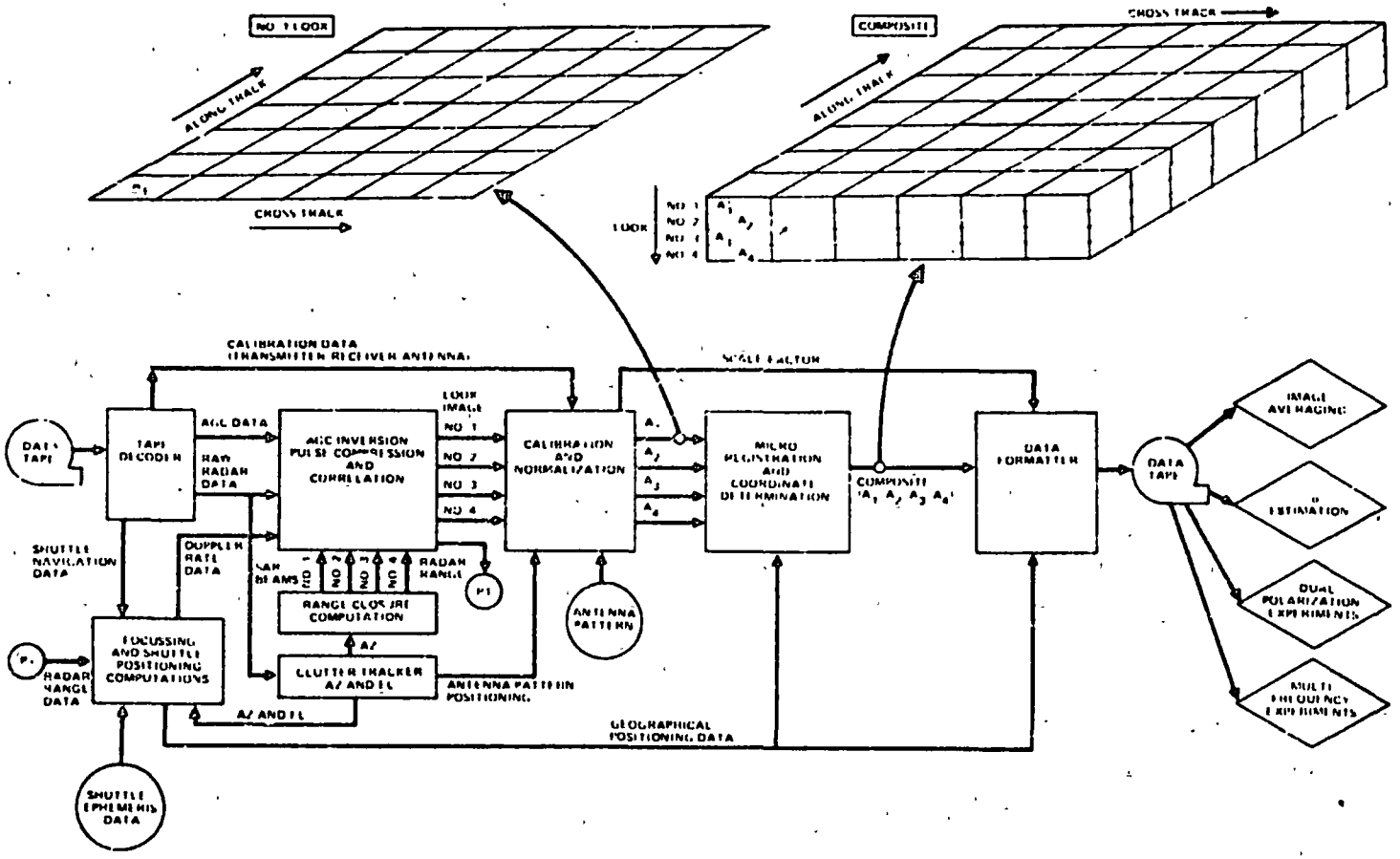

Figure 2-8. Image formation and registration (1-frequency, 1-polarization, 4 looks).

SAR Beam and Real Beam Alignment

The SAR doppler filters (SAR beam) must be centered within the real antenna beam. To do this a clutter tracker locates the doppler center of real antenna beam to within about five percent of its beamwidth. Clutter tracking is done on the uncompressed raw radar data and before range closure compensation.

Once the main beam doppler center is determined, the SAR filters are positioned symmetrically about this center. However first pulse compression, range closure compensation, and focusing must be applied to the raw radar data (Figure 2-9).

Pulse Compression and Range Closure Compensation

Linear chirp pulse compression and range closure compensation are done in the same unit, which is essentially a digital delay line pulse compressor (Figure 2-10). Range closure compensation removes the relative range motion of a ground cell during formation of each synthetic array. For

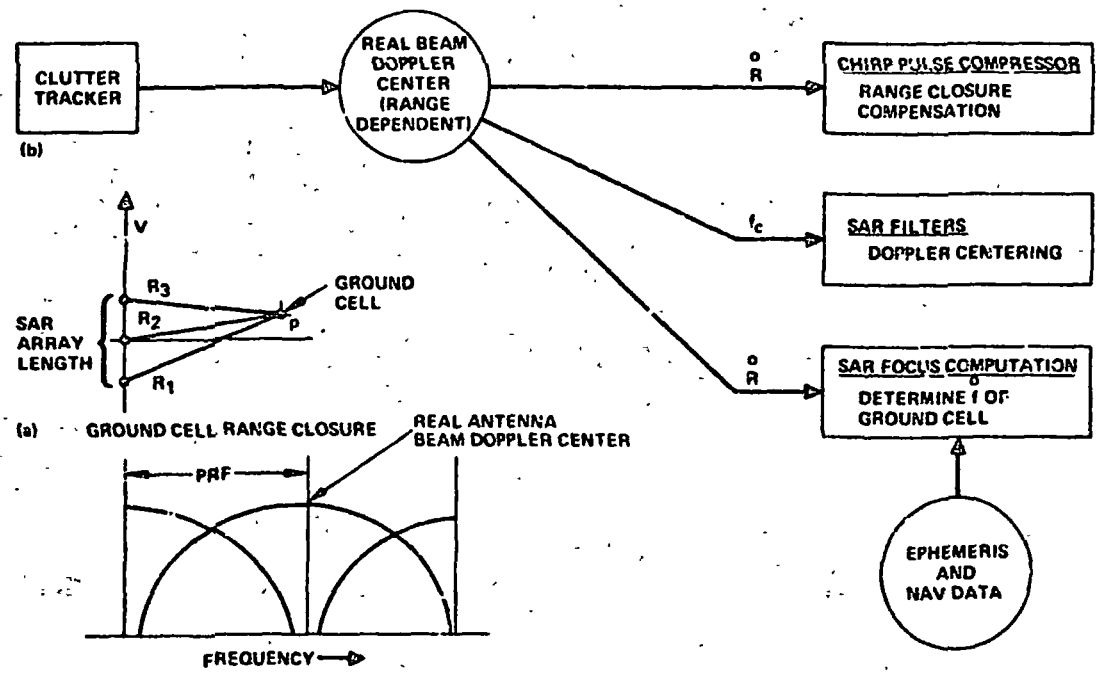

Figure 2-9. Range closure compensation, aligning SAR beams with real beam, and focusing.

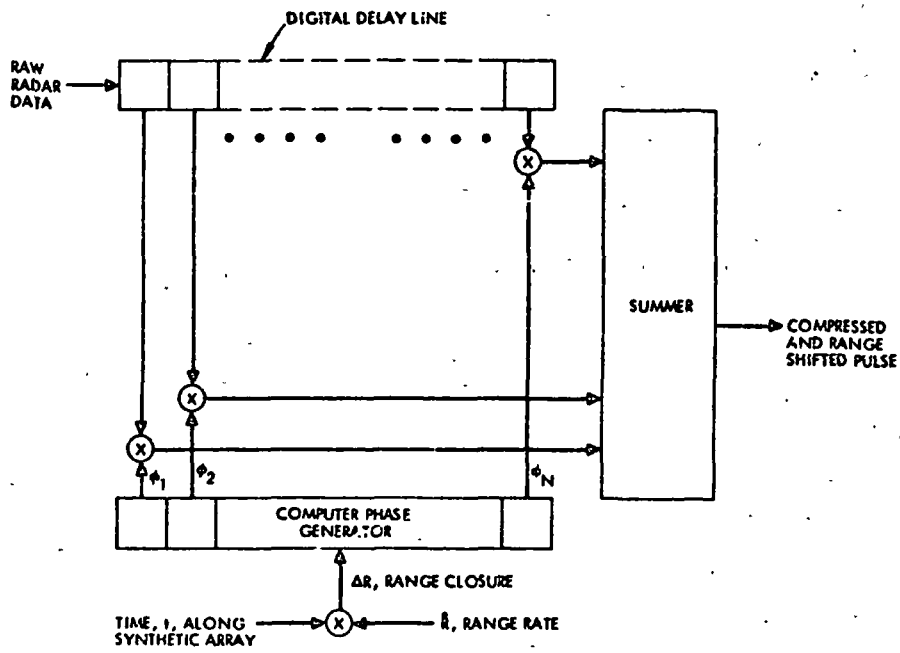

Figure 2-10. Digital delay line pulse compression and range closure compensation.

each array, the cell energy remains in the same sample position for each transmitter pulse. Range closure compensation assures that at a given range, a SAR doppler filter (after pulse compression) continues, during an array time, to receive energy from the same region of ground. If this were not so, and uncompensated range closure allowed ground cells to traverse through the range interval of the given SAR doppler filter, then it would see only part of the energy of any one ground cell. As a consequence of this range smearing of the ground cells, the spectral width of the cell would be broadened (i.e., smeared). The result is a degradation of the azimuth resolution, which becomes broader.

Applying range compensation along a SAR beam requires knowledge of the range rate. Range rate of a ground cell is a function of several factors including:

- Shuttle velocity vector
- Earth rotation rate
- Latitude of ground cell
- Direction of ground cell from shuttle

The last of these could be critical and it may be necessary to correct the payload beam pointing sensor (inertial measuring unit) with data from the clutter tracker and radar range measuring unit. In any event the data listed above are available in the computer and are used to generate the range rate. A separate range rate is generated for each SAR beam; one value is sufficiently accurate for all ranges of each beam.

The range closure compensation is applied in the processor by range shifting the radar returns in the pulse compressor as the shuttle flies down the length of the synthetic array (Figure 2-10). The amount of range shift, ΔR, is computed by multiplying the range rate by the time to the synthetic array center. The reference phase rotations, ϕ_i, which are applied to each of the radar samples along the digital delay line are selected to do both the pulse compression, and the fractional part of this required range shift. The pulse compressor range shift is specifically accomplished by translating the quadratic envelope of the phases a small amount with respect to the delay line, up to about plus-or-minue one-half a delay interval. The remaining integral parts of the range correction is done by shifting the raw data read into the compressor.

Focusing

Focusing occurs just before SAR filtering, and is the elimination of the quadratic phase variation in the radar return to which the SAR filter is tuned. If this were not done the spectral width of return from the individual resolution cells would exceed the width of the SAR filter. By focusing, the spectral width of the ground return is reduced to considerably less than that of the SAR filter by multiplying the data sequence into the filter by a unit signal vector having a progressive quadratic phase variation; this essentially linearizes the phase variation of the ground return.

SAR Filtering

The SAR filter is spectrally centered with respect to the center of the antenna main beam doppler. This is done by either translating the data before filtering when a Fast Fourier Transform is used for SAR filter formation, or in shifting the frequency of the filter reference phaser when a feed forward, line-by-line SAR filter is used.

The uncalibrated single-look image consists of a collection of SAR filter outputs, one for each range resolution interval along a single SAR beam, and a replication of these as the SAR beam sweeps along with the Shuttle. The amplitude of each cell is the square of the filter output amplitude, and is proportional to a variable quantity times the radar cross section of the cell.

Calibration of the Single Look Images

In the calibrator the amplitudes of the individual cells are adjusted to equal the product of a common known constant and the radar cross section of the cell. In order to make this adjustment several preliminary measurements must be made (Figure 2-8 and 2-11). The more important of these are:

- Antenna gain relative to the ground cell
- Transmitter output power and receiver gain
- Radar range of the cells

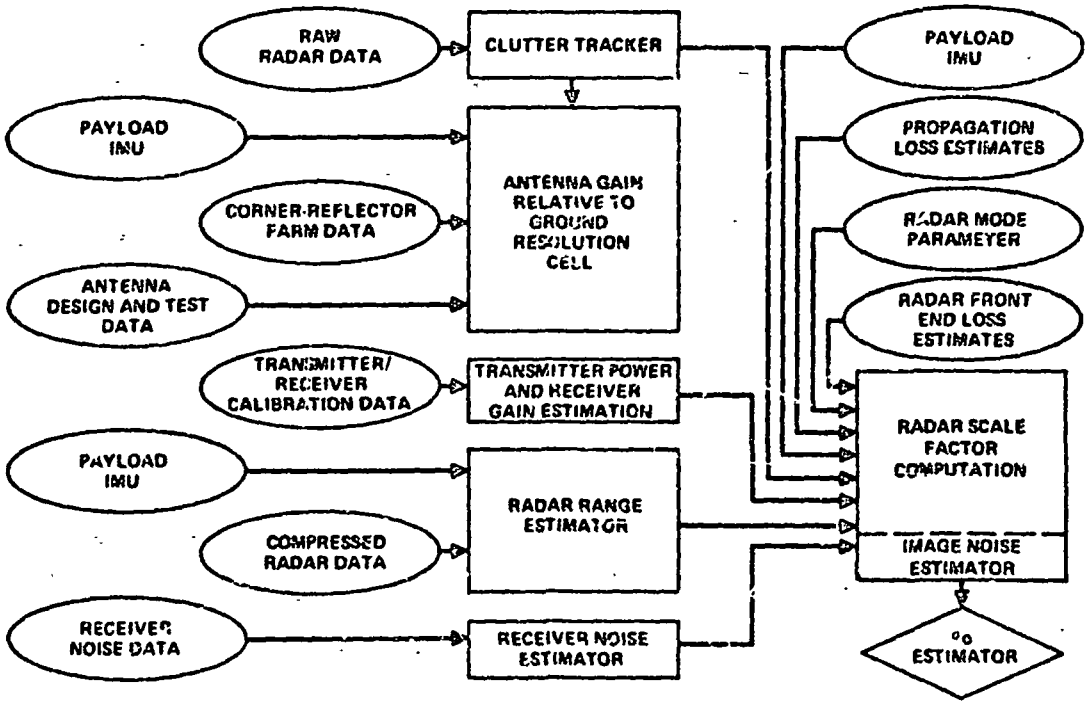

Figure 2-11. Ground processor, calibration operation.

- System loss
- Propagation loss

Data for most of these are contained on the tape with the raw radar data, but some, such as propagation loss require externally provided data.

Antenna Gain Relative to Ground Cell

Antenna gain corresponding to the ground cell of interest is mainly a function of two factors:

- Ground cell position in the real antenna beam
- Antenna gain pattern

In azimuth the position of the antenna gain pattern relative to the ground cell is determined by means of a clutter tracker which is accurate to about 5 percent of the real antenna beam. The payload inertial measuring will not be of sufficient accuracy since the X-band antenna beamwidth is only 0.15 degrees.

In elevation the position of the antenna beam relative to the ground cell will be determined by attitude data from the payload inertial measuring unit supplemented by an elevation clutter tracker.

The antenna pattern itself will be stored in memory at the ground system site. This pattern data will be derived from a series of measurements made during flights over one or more of the existing corner-reflector farms, and from pattern estimates made prior to installing the antenna in the Space Lab.

Transmitter Power and Receiver Gain

Transmitter output power will be sampled periodically during radar operation and will be recorded as ancillary data.

Data necessary for estimating receiver gain by the ground processor is recorded on the data tape during radar operation. It consists of a sequence of pilot signals of varying amplitude injected into the microwave plumbing.

Radar Range of Ground Cells

Calibration of the ground cells must include an adjustment for the effect of range on received signal power. Range from the shuttle to the ground cell cannot be determined by simply measuring the radar signal delay; the unambiguous radar range interval is only about 10 KM, while range to the target is greater than 200 KM. Because the altitude of the shuttle is known through emphemeris data and shuttle navigation data, and because the angle between the antenna beam axis and the vertical is known from the payload inertial measuring unit, the range to the ground cell can be determined. This range estimate can be improved by using the position of the ground cell in the unambiguous range interval.

System Losses

System losses are determined by periodic system measurement.

Propagation Losses

Propagation loss estimates can be made from standard atmosphere tables, and/or from meterological measurements.

3. DESCRIPTION OF ERSIR DESIGN

3.1 BASELINE DESIGN

The baseline design provides for a practical sensor that will produce high resolution imagery and require a nominal amount of power, 3.5 KW. It will be a dual frequency, dual polarization radar. It's 3 x 10.7 meter antenna is a multi-beam dual fold array, that is stored on a single pallet prior to deployment. The SAR resolution is 25 meters primarily, with a multilook resolution capability of 12 1/2 meters. Table 3-1 gives the relationship between look angle from nadir and swath width for both 25 M and 12.5 M resolutions, also for altitudes of 200 and 300 KM.

The cross-polarized imagery, in conjunction with the dual frequency feature, is essential for distinguishing pertinent characteristics of clutter signals. Three vertical beamwidths of 18.9°, 9.45°, and 6.3° are available and may be selected as required for various look angles from the nadir.

The baseline design and its significant functions are illustrated in block diagram (Figure 3-1). An unusual and significant feature is the contoured AGC, which provides for high quality imagery with a dynamic range of 50 dB.

TABLE 3-1. LOOK ANGLE-SWATH WIDTH RELATIONS

Resolution and Altitude	Look Angle	Swath Width
25 m, 200 KM	10°-61°	60-80 KM
25 m, 300 KM	10°-53°	50-85 KM
12.5 m, 200 KM	24°-56°	40-45 KM
12.5 m, 300 KM	25°-48°	40-45 KM

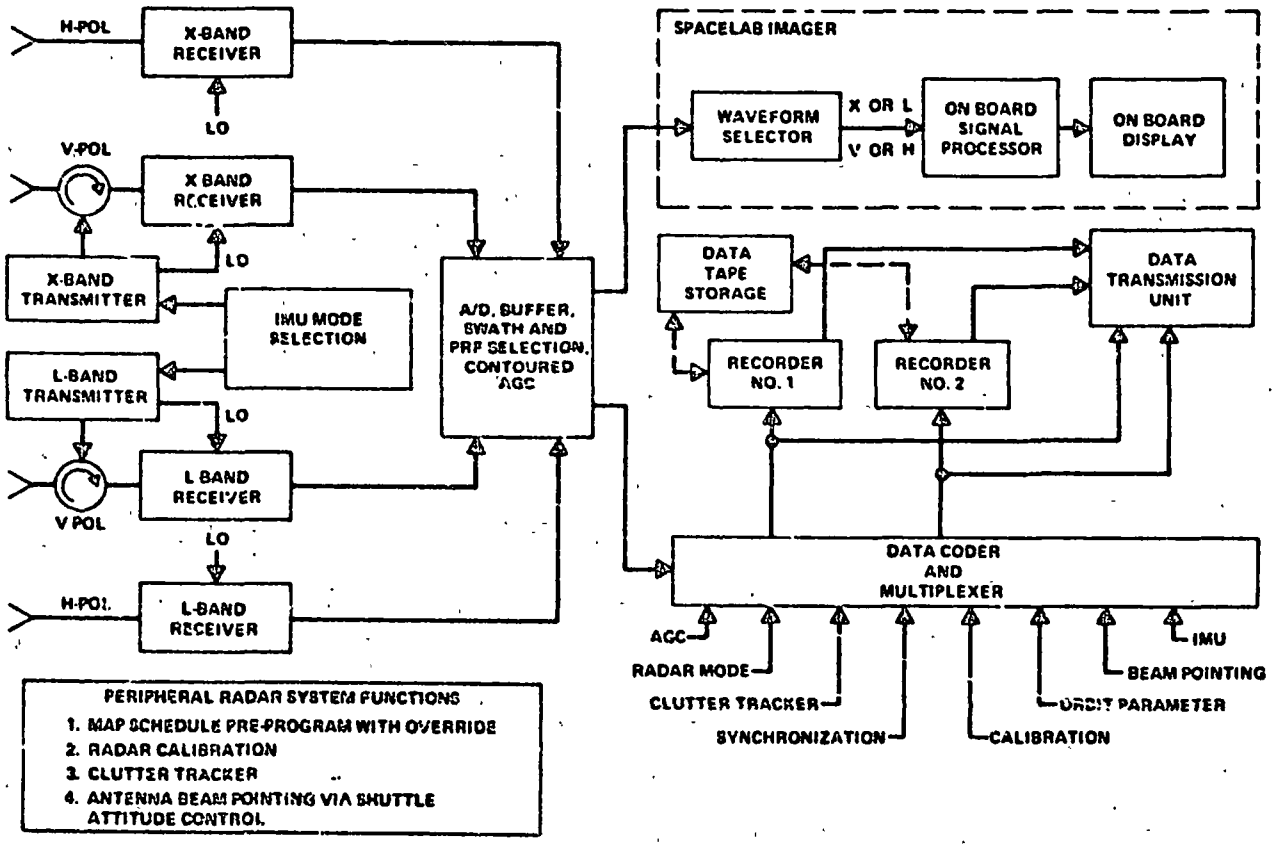

Figure 3-1. SAR space functions.

The major elements of the space sensor, shown in Figure 3-2 are the antenna, two transmitters, four receivers, two exciters, two calibrators, and related electronics. These form a group located in the space lab's pallet bay. A cold plate attached to the back of the antenna array serves as the mounting for the remaining elements in this group (Figure 3-3). The weight of the antenna and other elements in the group is 840 Kg.

A second group in the pressurized module comprises the control module, signal conditioner, buffer formatter, recorders, space processor and finally the display monitor and control console. These are shown in Figure 3-4.

The baseline parameters are summarized in three tables that follow: Table 3-2, system parameters; Table 3-3, Transmitter waveforms, and Table 3-4 Preprocessor Parameters. They are discussed further with the descriptions of the major system elements that follow in the remainder of this section.

3.1.1 Antennas

The planar array, when deployed, is 3 meters wide and 10.7 meters long. The array is shown in Figure 3-5, where it is shown deployed and folded for storage on a single pallet. Two apertures are provided for each band, a narrow one for the 18.9° beam and a wider one for the 9.45° beam. The two apertures are added to give one 6.3° beam. At X band separate apertures are paired for dual polarization with 40 dB decoupling. At L band shared apertures with crossed dipoles for dual polarization give adequate isolation, at least 30 dB. The weighting function is uniform for all apertures. The overall antenna is discussed in Section 3.3

3.1.2 Transmitters

The ERSIR will have 2 transmitters, one with a 500 Watt X band Klystron, the other with a 200 Watt L band TWT. The electrical characteristics are given in Table 3-5.

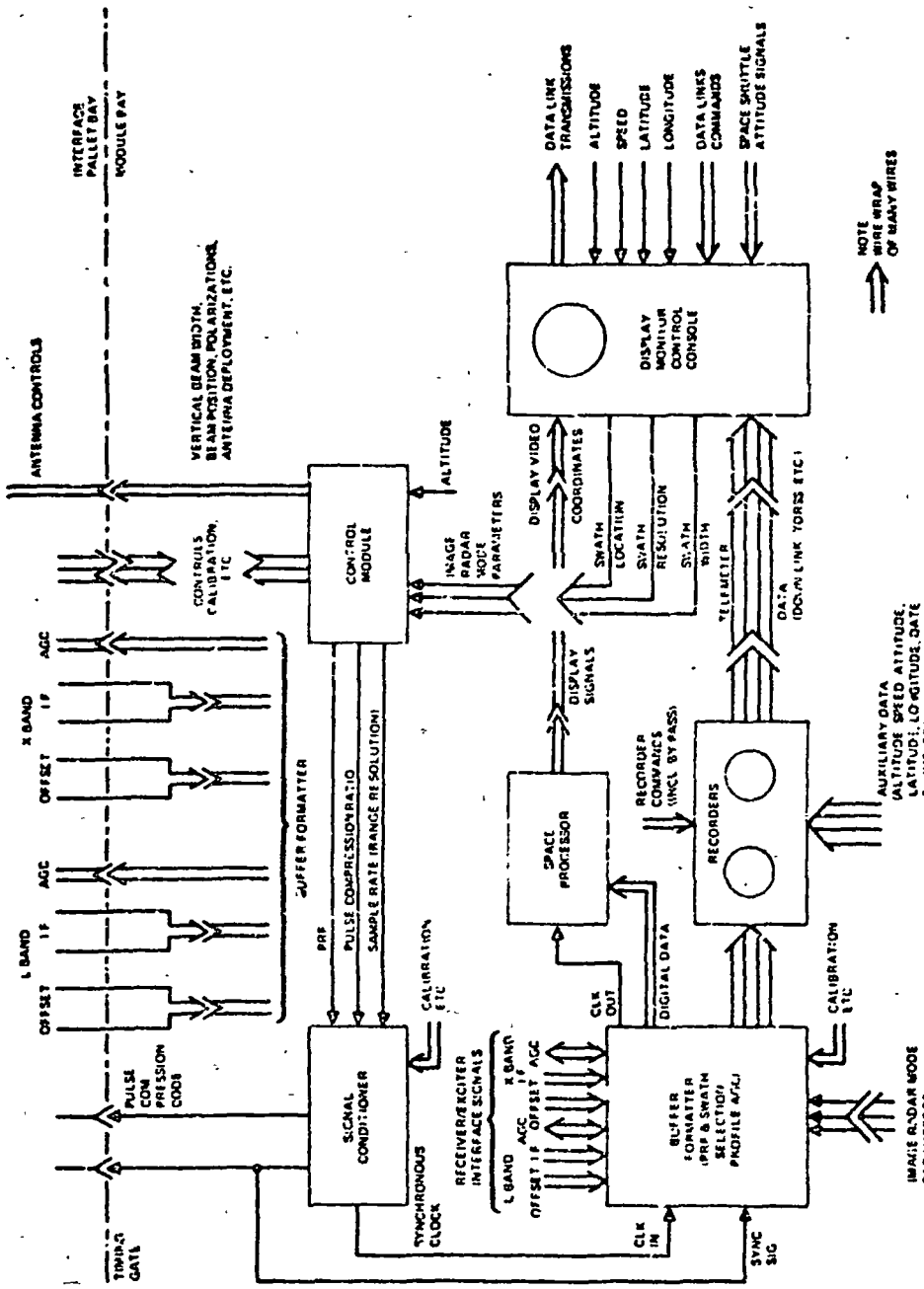

a. Module bay portion

Figure 3-2. Functional block diagram.

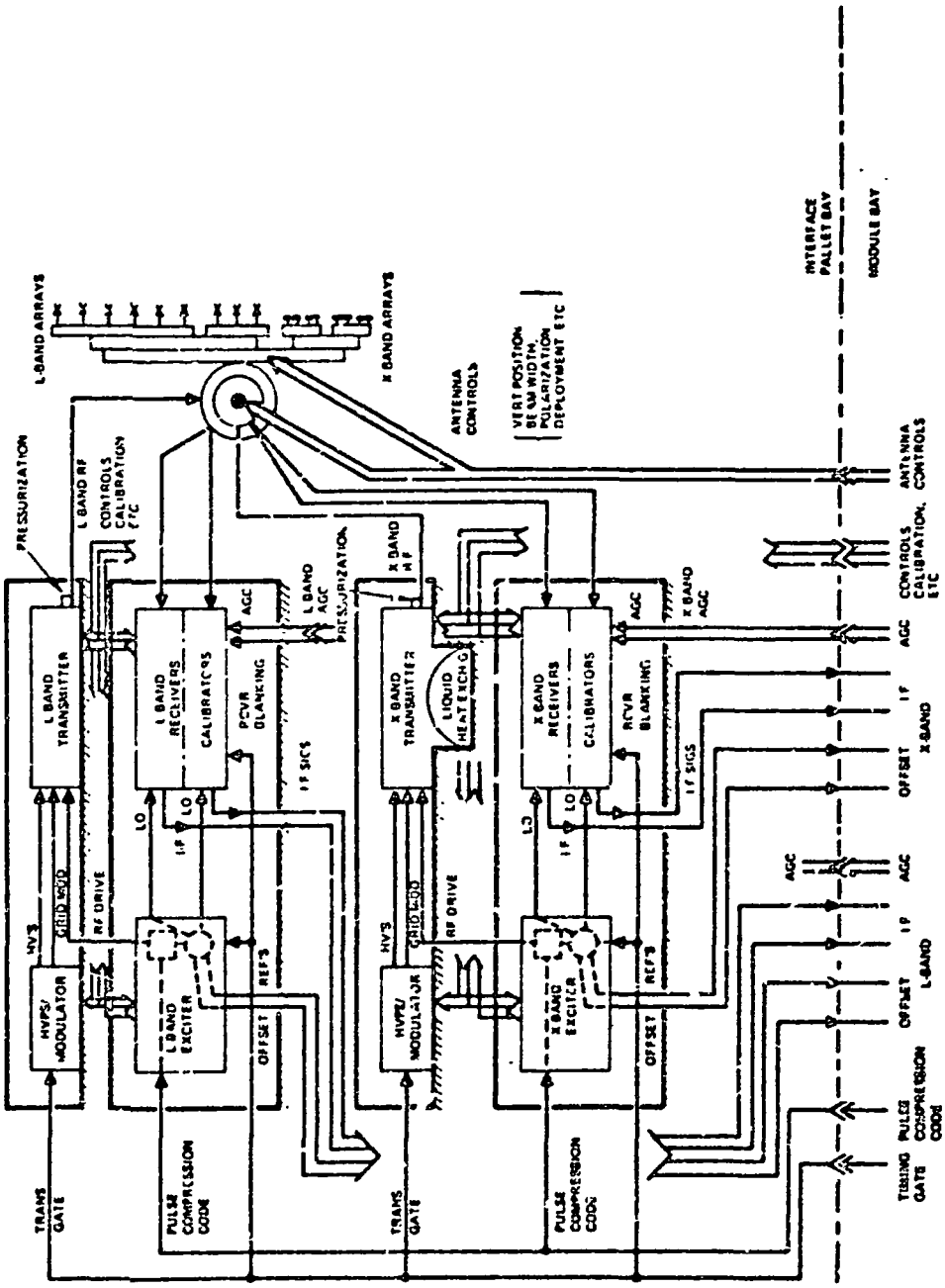

b. Pallet bay portion

Figure 3-2. Functional block diagram.

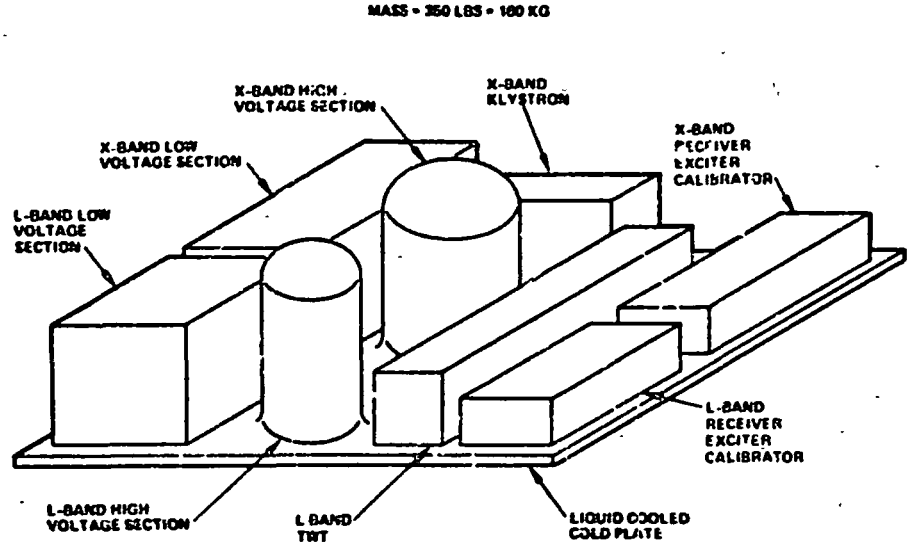

Figure 3-3. Pallet bay electronics layout.

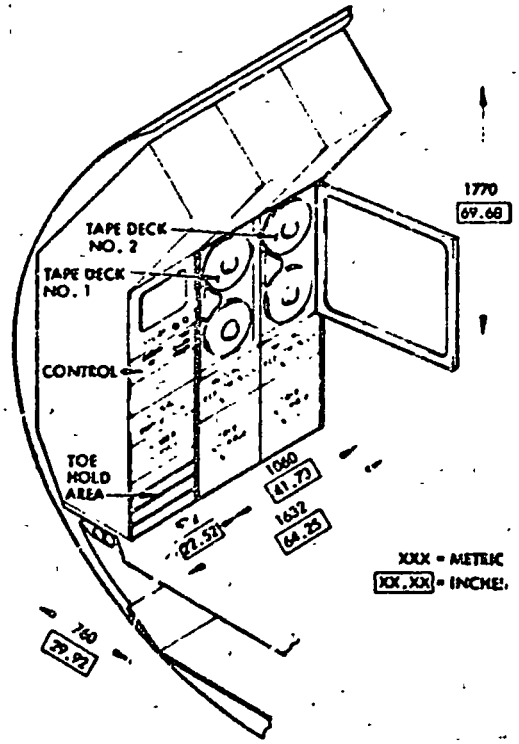

Figure 3-4. Radar equipment in module.

TABLE 3-2. BASELINE DESIGN PARAMETER SUMMARY

Parameter	L-Band	X-Band
Frequency	1.045 GHz	9.0 GHz
Polarizations (Linear)		
Transmit:	V or H	V or H
Receive:	Direct and Cross	(VV or HH) (VH or HV)
Array: Length	10.7 M	10.7 M
Height (3M)	243 CM	57 CM
Aperture Efficiency	57.5 Percent	57.5 Percent
Beamwidths (3)	6.3°, 9.45°, 18.9°	6.3°, 9.45°, 18.9°
Gains, dB	33.6, 31.8, 28.8	42.9, 41.2, 38.2

TABLE 3-3. BASELINE DESIGN PARAMETER SUMMARY

Parameter	L-Band	X-Band
Transmitter		
Peak Power:	6.8 KW	17 KW
Duty, Nominal:	2.9%	2.9%
Average Power:	200 W	500 W
PRF's, Hz:	1200 - 1800	1200 - 1800
Bandwidth, min:	75 MHz	75 MHz
Receiver		
Noise Figure, min:	2.5 dB	4.0 dB
Bandwidth, min:	35 MHz	35 MHz
System Power Demand		
L and X Bands, max:	3.5 KW Average	

TABLE 3-4. BASELINE DESIGN TRANSMITTER WAVEFORMS

Simultaneous L- and X-Band	
Selectable PRF's	F_r = 1200 - 1800 Hz
Pulse Durations	T = 15 - 25 μS
Nominal Duty	D = 2.9 Percent
Modulation; Pulsed with Linear FM Chirp (Digital Approximation)	
Selectable Bandwidths	B = 7 - 27 MHz
Selectable Pulse Compression Ratios	BT = 64, 81, 100, . . . , 324

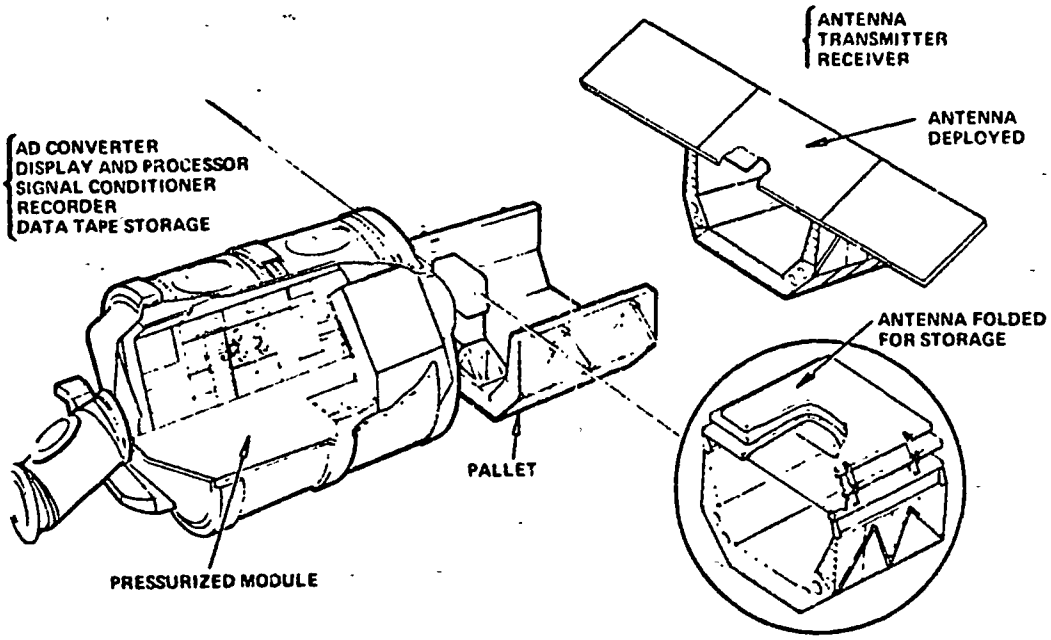

Figure 3-5. ERSIR baseline equipment locations.

TABLE 3-5. TRANSMITTER ELECTRICAL CHARACTERISTICS

	L-Band (1.04 GHz)	X-Band (9.0 GHz)
Peak Power Ratings	6.8 KW	17 KW
Average Power, Nominal Maximum	200 watts	500 watts
Power Amplifiers	Gridded TWT	Gridded Klystron
Beam Voltage	9.5 KV	17.8 KV
Bandwidths	75 MHz, min	75 MHz, min
Gain	30 dB, min	50 dB, min

High voltage components are mounted in a liquid (mineral oil) dielectric medium and the high power r-f output circuits are pressurized to prevent ionization and multipacting. High voltage power supplies and power amplifiers are mounted on a cold plate fixed to the back of the antenna. Heat from the cold plate is transferred to the space shuttle at approximately 7200 BTU per hour.

The prime power interface is at the d-c service bus. High efficiency d-c to d-c converters are employed for generating basic power forms. At nominal transmitter maximum power ratings of 700 watts (200 watts at L and 500 watts at X-band), the space shuttle prime power service will be required to supply a maximum of about 95 amperes at 26 volts or 2450 watts. Details of the transmitter design are presented in Section 3.4.

3.1.3 Receiver, Exciters, Calibrators

The remaining equipment in the pallet bay consists of the L-band and X-band receiver, exciters, and calibrators which are grouped together in an L-band and an X-band module (Figure 3-3). Electrical characteristics are summarized in Table 3-6 and requirements are discussed in Section 6.5.

The L-band receivers employ microwave bi-polar transistor amplifiers to obtain effectively low noise figures, with a 2.5 dB maximum. Low noise FET or parametric rf amplifiers are used in the X-band receivers to obtain noise figures of 4 dB maximum.

TABLE 3-6. RECEIVER/EXCITER/CALIBRATOR CHARACTERISTICS

	L-Band	X-Band
Exciter		
• RF Drive, Frequencies	1.04 GHz	9.0 GHz
Levels	7 watts	0.3 watts
Digital Phase Modulation for Pulse Compression	4 bits (0, 22 1/2°, ..., 337 1/2°)	4 bits (0, 22 1/2°, ..., 337 1/2°)
• Receiver L.O., Frequencies	1.11, 1.115* GHz	9.06, 9.065* GHz
• IF Reference Signals, Frequencies	70, 75* MHz	60, 65* MHz
Receivers		
• Noise Figures	2.5 dB max	4.0 dB max
• Gains	60 dB, min	60 dB, min
• Bandwidths	35 MHz, min	35 MHz, min
• Cross-talk	-40 dB, max	-40 dB, max
• AGC range	30 dB, min	30 dB, min
Calibrators		
• Bandwidths	35 MHz, min	35 MHz, min
• Time Delay	25 μs, nominal	25 μs, nominal
• RF Gains	0 dB, max	0 dB, max
• Output Amplitude Adjustment	8 steps at 6 dB, nominal	8 steps at 6 dB, nominal
• Transmitter Power Measurement	0.3 to 10 MW, avg	0.3 to 10 MW, avg

*Staggered IF's facilitate isolation.

Staggered intermediate frequencies help meet the specification requirement for a -40 dB maximum cross talk level. The exciters contain the stable r-f sources for the X and L band transmitter-receiver. One pair, coded for pulse compression, consists of the sources which function as the rf driver for the X and L band transmitters respectively. The other r-f sources provide local oscillator signals whose frequencies differ from the former by precisely the intermediate frequencies. These IF offset signals establish the interfaces between the exciters and the buffer-formatter in the pressurized module. The buffer-formatter uses them for down converting the respective L and X band receiver signals to quadrature phase video. These I/Q video signals are then converted to digital format and recorded or transmitted by data link for ground processing.

The calibrators are used for on board sensor calibration of data. They supply time-delayed replicas of the transmitted waveforms at precise amplitudes (adjusted in programmed steps), for calibrating receiver gain. The L- and X-band calibrators include a device for making precision power measurements. This device supplies the transmitter power data needed for the on-board calibration of sensors.

3.1.4 Buffer-Formatter

Sensor data are buffered and formatted for recording and/or telemetering. First, the input signals are filtered to approximate the signal bandwidths corresponding to the resolution at the selected swath. They are then transformed to digital form by the A/D converter. The formatter transfers digital data for a selected time interval into shift registers and then outputs them in a uniform distribution over the full interpulse interval, T = 1/PRF. The time interval selected is a fraction k of the interpulse interval T and corresponds to the slant range interval of the selected swath. The result is a time stretch of 1/k and a consequent conservation of data rate.* Pre-sum for data rate conservation is impractical because of prf

*For example, consider an image swath of 85 KM with a 25 meters resolution and an offset range of 56 to 141 KM (11° to 25° look angle at 300 KM altitude) with a PRF of 1564 Hz. The slant range interval is 27.4 KM, k = 0.286 and the time stretch factor is 3.5. Data rate is 219 MB/s for the four channels.

constraints to near the minimum values for 4 looks at 25 or 12.5 meters resolution.

The buffer formatter also develops contour AGC to establish mean levels suitable for low signal distortion in the 5-bit digital video outputs. The AGC contours are adjusted at discrete intervals of range and are controlled independently in each of the four channels (L-band with two polarizations and X-band with 2 polarizations). For this purpose, the interpulse interval corresponding to the selected image swath is divided into at least 8 time segments and AGC is applied to each segment independently. The AGC contours are up-dated at discrete time intervals that correspond to suitable distances along the AGC contour; data are supplied with the signal data as needed for calibration and data reduction. The contoured AGC approach is discussed further in Section 4.2.

Buffer-Formatter characteristics are tabulated in Table 3-7.

3.1.5 Signal Conditioner/Control Module

The signal conditioner and control module form an essential link in the production of raw data for imagery. The Signal Conditioner develops the

TABLE 3-7. BUFFER-FORMATTER CHARACTERISTICS

Input Video Filter Bandwidths	7: 3.5, 4.5, 5.5, 7, 9, 11, 17.5 MHz per receiver
A/D Converter, Bits	5I and 5Q per receiver
Max A/D Sample Rate	27 MHz
Buffer Swath Interval	85 KM, 3584 cells at 25 M Resolution
	45 KM, 3584 cells at 12.5 M Resolution
PRF Range	1200-1800 Hz
AGC Control Outputs	8 range segments; 45 dB in 3 dB steps for each receiver

sensor parameters, including prf's, pulsewidths, pulse compression codes, antenna aperture selections and pointing angle, transmitter-enable/receiver-disable gates and A/D converter clocks. It does so in response to signals from the control module. These signals are routed to the control module via the control console. Mode commands, which include calibration routines, are entered into the control console by the operator or the data link.

Pertinent characteristics of the Signal Conditioner/Control Module are listed in Table 3-8.

3.1.6 Space Processor

The Space Processor forms imagery form the raw data obtained by the sensor, utilizing one of the various possible configurations (L or X band, V or H polarization); this imagery makes it possible providing means for a to evaluate and monitor sensor performance, including image quality in real time. Range resolution is 150 meters and at X-band the unfocused strip imagery resolution is 150 meters cross-track (azimuthal, or time dimension). At L-band the cross track resolution is 150 to 200 meters depending upon

TABLE 3-8. SIGNAL CONDITIONER/CONTROL MODULE CHARACTERISTICS

• PRF's	Adjustable 1200-1800 Hz
• Pulse Compression:	Digital Approximation to linear FM
Time bandwidth product (PCR):	n^2 = 64 to 324; n = 8, 9, ... 1
Sample Rate:	f_s = 80 MHz ($1/f_s$ = 12.5 ns) resolution
Transmitter gate widths	T: 12.5 to 25 μs with 12.5 ns steps
Pulse widths (τ = 1/ft):	37.5 to 175 ns in 12.5 ns
Bandwidths (B = ft):	7 to 26.7 MHz
• A/D Converter clocks:	7 to 40 MHz

range.* A monitor viewing screen interfaces with the processor, displaying the moving scene evaluation and action.

Pertinent characteristics of the Space Processor are tabulated in Table 3-9.

3.1.7 Monitor Control Console

The Monitor Control Console is used for sensor control and for monitoring the Space Processor imagery. Visually the console is controlled by an operator and by data link communications; from the ground. Command calibration routines as well as continuous monitor calibration cycles are included in the sensor command functions. Also, the console is the interface for auxiliary sensor signals; e.g., space shuttle altitude, speed, altitude sensor inputs, latitude, longitude, etc.

The visual monitor displays a passing scene that is approximately 90 KM by 90 KM. At 150 KM resolution, the resulting display has approximately 600 x 600 elements. At an orbital speed of 7.78 KM/sec, about 11.5 seconds of passing scene will be updated continuously.

TABLE 3-9. SPACE PROCESSOR CHARACTERISTICS

Input:	L or X-band, V or H polarization 25 or 12.5 ground range resolution
Output Imagery:	Resolution 150 x (150 to 200) meters of L-Band
Swath Width:	90 KM
Display Video:	50 dB dynamic range logarithmically compressed to 6 scales of grey

*The limiting resolution of an unfocused SAR is given by the relation $d_u = 1/2\sqrt{\lambda R_s}$. For $d_u = 150$ m, λ, $R_s \leq 313.5$ KM at $\lambda = 28.7$ cms (1.045 GHz), corresponding to a look angle $\beta \leq 49.3^\circ$ at 200 KM altitude; $d_u = 200$ m, $Rs \leq 557.3$ KM ($\beta \leq 55.4^\circ$ at 300 KM altitude).

Recorders

Two high density, high data rate digital magnetic tape recorders provide storage for basic sensor data. The recorder reels are approximately 35 cm in diameter and accept tape 5 cm wide; up to 160 deparate channels of binary coded data are stored across the tape. At the maximum tape deck speed 300 cms/sec, each reel can record continuously for 12 minutes at a maximum data rate of 240 Megabits/sec. The two recorders together can record raw data continuously at maximum data rates of 350 Megabits/sec for 16 minutes.

RCA is currently developing space qualified recorders capable of recording at space shuttle sensor data rates. RCA has already developed Model HDMR-240G recorders for recording in conventional applications at maximum data rates of 240 Megabits/sec per recorder. Thus, it appears that the required high density, high data rate operational capabilities have already been demonstrated. Therefore the development of the space qualified recorder should be completed well in advance of the time needed to meet delivery schedules for the Space Shuttle.

3.2 ALTERNATE DESIGNS

Several alternate designs were examined. One variation was in the frequency pairs selected. These were (1) L and X band, (2) UHF and X band, (3) S and X band, and (4) L and K_u band. Three different L and X band systems were examined, the principal variation being in array length; those studied were 12, 8, and 16 meters. Shaped vertical beam (2 beam) arrays and simpler three beam arrays employing uniform vertical illumination patterns were also investigated. The arrays are designed for dual polarization. Vertical or horizontal polarization may be selected for transmitting; both polarizations are used in receiving and the illumination patterns are uniform in the horizontal dimension. Even though the interest was not great, a design utilizing UHF and X-bands and a design utilizing S and X-bands were considered for completeness.

Principal features of the baseline and alternate designs are listed in Table 3-10. Since the only system elements that vary for the alternate designs are the antennas and transmitters, these are described below. The

TABLE 3-10. BASELINE AND ALTERNATE SPACE SENSOR DESIGNS

Length L, M	Height W, M	Array Vertical Weighting	Estimated Weight, KG	Band	F GHz	Transmitters		System Power Demand, KW
						Average Power Watts	Estimated Weight, KG	
12*	3.0	Uniform	680	L, X	1.04, 9.0	20_,500	159	3.5
12**	3.0	Uniform	680	L, X	1.22, 11.0	200,500	159	3.5
12	3.3	Mod Taylor	750	L, X	1.22, 9.0	200,500	159	3.5
8	3.3	Mod Taylor	515	L, X	1.22, 9.0	382,764	205	4.9
8	5.0	Sin k'x/k'x	680	L, X	1.53, 10.0	200,500	136	3.5
16	3.0	Uniform	910	L, X	1.04, 9.0	120,360	136	2.8
12	3.0	Uniform	680	UHF, X	0.45, 9.0	100,500	150	3.1
12	1.6	Uniform	364	S, X	2.45, 9.0	250,500	164	3.6

*Selected design
**3 beam, shorter wavelength alternate to selected design

receiver exciter/calibration modules, signal conditioner, space processor, buffer formatter, and on-board monitor display, which were discussed in the preceding section on baseline design, are the same in the alternate designs.

3.2.1 L and X Band Dual Polarization Design

The L and X band design with dual polarization may utilize any one of three array lengths, namely: 12 meters, 8 meters and 16 meters. Each of these is described below.

3.2.2.1 L and X-Band Dual Polarization

Physical Features. The array length recommended for this design is 10.7 meters. This length contributes desirable features to swath coverage, image quality, and prf selection while the power requirement is a moderate 3.5 KW. The array is folded twice in its lengthwise dimension for stowage upon a single 3 x 4 meter pallet. No folds are required in the vertical dimension which is 3.3 meters, maximum. In service, the array is unfolded

at right angles to the space shuttle longitudinal axis and tilted for vertical positioning about a hinged edge. Figure 3-5 illustrates the deployed array in service. The space shuttle is oriented for earth observations (the space lab local vertical is earth directed) with the orbit plane normal to the space shuttle longitudinal axis (sidewise orbital motion). The image sensor functions are subsequently carried out in a stable geometrical configuration: the space shuttle attitude and control system (ACS) stabilizes the array configuration in the horizontal plane and the antenna gimbal drive maintains the vertical orientation of the array.

The single degree of freedom in the array pointing system is considered satisfactory. At additional cost, complexity and some reduction in reliability, two or even three degrees of freedom could be provided. However, motion of the relatively massive array might influence the ACS adversely. Therefore it seems reasonable to rely upon the space shuttle ACS for stabilizing the array in azimuth.

Illumination Considerations (Horizontal). Antenna length and illumination characteristics in the horizontal plane determine the lower limit for PRF selection (PRF min). Azimuth ambiguities decrease as PRF values increase, while range ambiguity increases. Included in the factors that determine the minimum acceptable prf's for image sensor applications are the following:

- V/ℓ; v ≡ orbiter speed (7780 m/s), ℓ array length (12 meters)
- d_a; swath resolution (12.5 and 25 meters)
- number of looks (4) and fractional overlap (0.45 at d_a = 25 m, 0.65 at d_a = 12.5)
- azimuth ambiguity suppression requirements (20 dB min) antenna illumination function in the horizontal plane.

Figure 3-6 illustrates the effective azimuthal suppression ratios as functions of the prf selection for 4 looks with 45 percent overlap of the doppler histories at a resolution of 25 meters and an overlap of 65 percent at 12.5 meters resolution. The figure provides a basis for comparing the effects of antenna weighting; at 25 meters resolution (4 looks, 45 percent overlap) the minimum prf is about 10 percent lower than that for corresponding suppression with a modified Taylor weighting function (-18 dB first sidelobes),

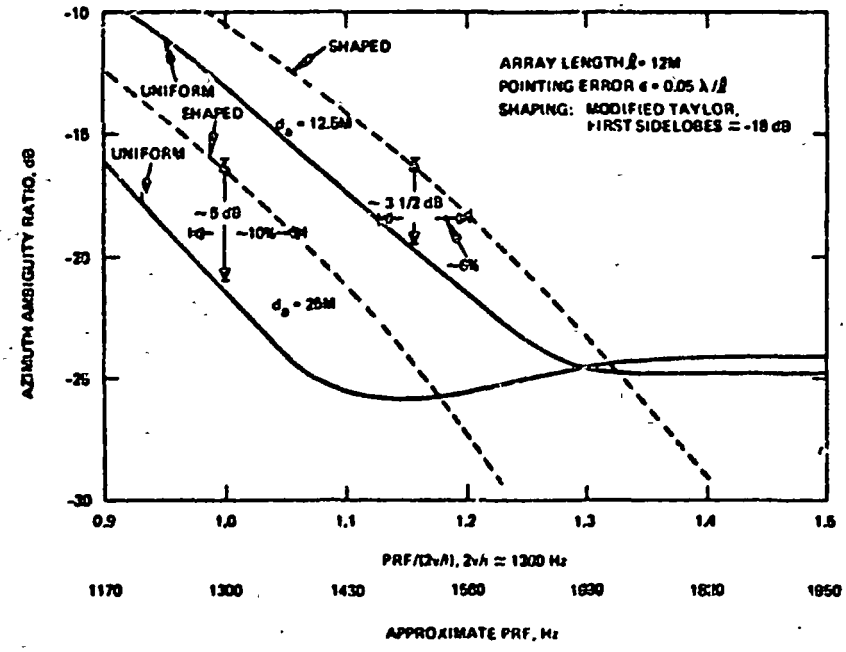

Figure 3-6. Horizontal shaping/azimuth ambiguity.

or, at a fixed near 1300 Hz, the suppression is about 5 dB more effective with uniform weighting than with the modified Taylor function. At 12.5 meters resolution, the minimum prf is about 8 percent lower (the suppression is about 4 dB better at fixed prf) for uniform weighting compared to the shaped pattern case; the advantage diminishing at larger prf's.

The simpler uniform illumination function is selected for the horizontal plane because it favors lower operational prf's in comparison to practical non-uniform weighting functions, thus facilitating large swath coverage.

The 12* meter length array with a uniform illumination function establishes the following minimum prf's upon minimum azimuth ambiguity suppression ratio requirement at 20 dB:

- 1270 Hz or PRF to 2 v/ℓ ratio = 0.98 at 25 meters resolution (4 looks, 45 percent overlap)

*Trade off comparisons are based on a 12 meter array in contrast to the recommended 10.7 meter array. The conversion is easily made by applying a correction of 11 percent.

- 1500 Hz or PRF to 2 v/ℓ = 1.16 at 12.5 meters resolution (4 looks, 65 percent overlap)

These lower limits of operational parameters used for prf selection include an allowance for pointing error of 0.05 λ/ℓ; i.e., the clutter spectrum centroid may be mis-positioned by 5 percent of its band width relative to the clutter doppler corresponding to the azimuthal boresight axis. Larger pointing errors degrade azimuth suppression ratio reducing it to less than the acceptable value, which is 20 dB for minimum prf's. The practical consequence is the requirement for a relatively high order of clutter spectrum sensing and correction (clutter tracking) for the imaging radar sensor; this clutter spectrum compensation is a part of the ground processor.

Illumination Considerations (Vertical). Vertical aperture shaping functions applied to the antenna suppress range ambiguous returns at the prf's selected on the basis of resolution, number of looks and transmitter eclipsing relative to swath location and altitude. A modified Taylor weighting function for first sidelobes of -16 dB (one-way) is applied for range ambiguity suppression in the case of 12 meter length arrays; this function has the desirable feature of reducing near vertical sidelobes by about 10 dB (two-way) relative to a uniformly illuminated array. A truncated sin kx/kx illumination function may be applied to approximate an almost ideal beam shape, with the radiant energy essentially confined to the desired swath width; however, for a dual-beamwidth system, this function requires a much larger vertical height than is practical at the 12 meter length. An application with the more nearly ideal weighting function is considered below in terms of an 8-meter array and single beamwidth 12 meter array. The modified Taylor weighting function is representative of simple vertical beam-shaping techniques and serves as a basis for selection of shaped or uniformly illuminated vertical beams for the imaging radar sensor.

Figure 3-7 illustrates the range selectivity advantage of the modified Taylor weighting function as compared to the uniformly illuminated array of comparable beamwidth. The shaped array height is 3.3 meters and the L-band frequency is 1.22 GHz, as compared to 1.04 GHz for the uniform

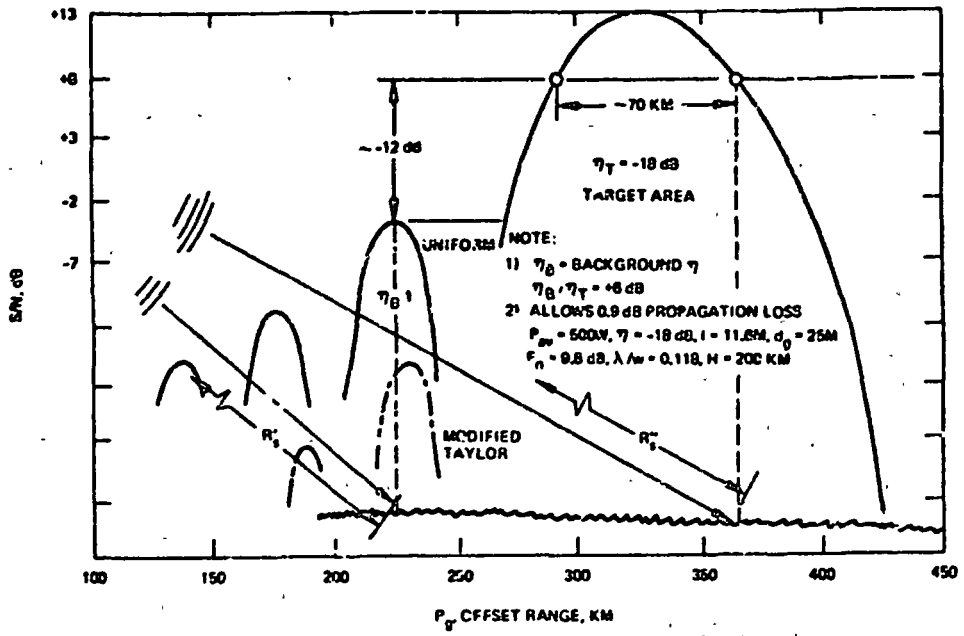

Figure 3-7.

array at 3 meters height; the X-band apertures are sized for 9.0 GHz. The shaped vertical aperture heights (and L-band frequency) are scaled to provide main lobe nulls coincident with those of equivalent uniform illumination apertures; in this instance the scaling ratio is 1.2. The main lobe shapes differ only slightly and are nearly indistinguishable in the sketch; the effective feature of the shaped array is that first sidelobe levels are down 11 dB relative to the uniform case.

The characteristics shown in Table 3-11 apply to the situation illustrated in Figure 3-7.

TABLE 3-11.

	Uniform Aperture	Shaped Aperture
Beamwidths (3 dB one-way)	~6.3°	~6°
Sidelobe levels (one-way)	~13.3 dB	~18.8 dB
Equivalent heights (wavelengths)	~8.5	~10.2
Swath center, offset rg	325 KM	325 KM
Look angle β	57.3°	57.3°
Incidence angle ϕ	60.3°	60.3°
Backscatter coefficients		
Target area, η_T	-18 dB	-18 dB
σ_{oT}	~ -21 dB	~ -21 dB
Background area$_D$ η_B	-12 dB	-12 dB
(η_B/η_T)	+6 dB	+6 dB
Signal-to-noise ratios		
Swath center	~13 dB	>13 dB
Swath edges	≥8 dB	≥8 dB
Swath widths	>60 KM	>70 KM
Transmitter power; average, X-band	500 W	500 W
L-band	200 W	200 W
System	3.5 KW	3.5 KW
Antenna array length	12 M	12 M
Resolution	~25 x 25 m	
Signal-to-ambiguity ratio	≥13 dB	
Slant range difference $R'_s - R'_s = \Delta R_s$	121 KM	
PRF f_r	1270	$1270 < f_r < 1360$
Resolution	~25 x 28 m	~25 x 25 m
Signal-to-ambiguity ratio	≥13 dB	≥13 dB
Slant range difference $R''_s - R'_s = \Delta R_s$	121 KM	121 KM

The near range first sidelobe of the uniformly illuminated array produces unacceptable range ambiguities near the far edge of the illuminated swath for prf's greater than 1240 Hz, corresponding to the slant range difference of about 121 KM. Since a minimum prf constraint of 1270 Hz is imposed by azimuth prf ambiguity considerations, the effective swath width reduces to less than 65 KM for the uniform illumination case from the greater than 70 KM width permitted by signal-to-noise ratio considerations alone and achieved with the modified Taylor illumination function. With the shaped aperture, maximum prf constraints are imposed by main lobe illumination considerations; range ambiguity constraints arise for prf's greater than 1360 Hz corresponding to the near range edge of the swath and the -27 dB relative response point at the far edge of the main lobe illumination. *

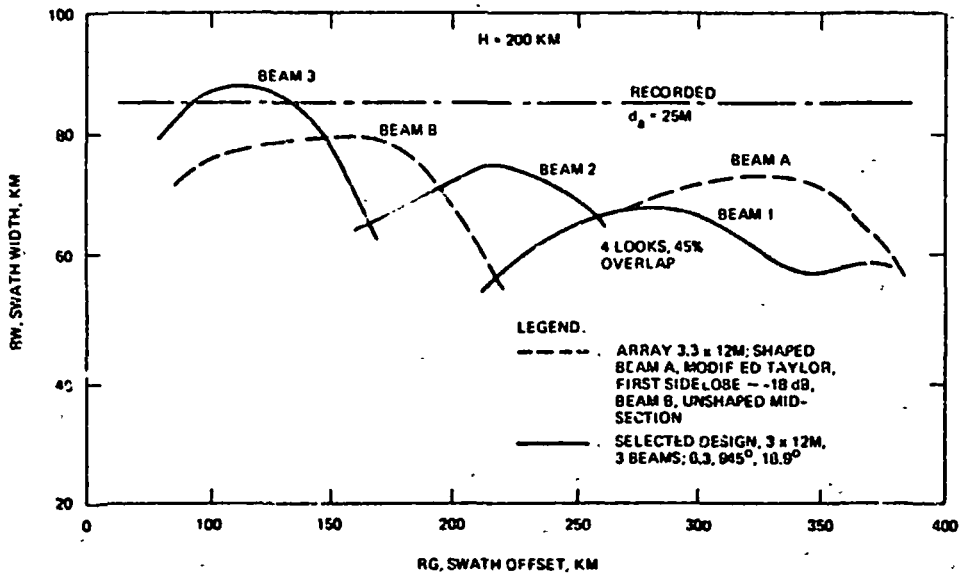

Figure 3-8. Baseline design versus shaping.

*5 dB for shading at the swath near range edge; 6 dB for the ratio of background η_B to target η_T; and 16 dB for the range prf ambiguity component.

Figure 3-8 illustrates the advantage for swath coverage at large look angles of the shaped array as compared to the uniform illuminated antenna. The minimum prf is 0.98 2v/ℓ, about 1270 Hz (ℓ = 12 m), for a ground resolution of 25 meters at swath center and 4 looks at 45 percent overlap with a minimum azimuth ambiguity suppression of 20 dB. The swath widths satisfy the following image quality requirements:

- the single look signal-to-noise ratio is at least 8 dB; the signal-to prf ambiguity energy ratio is at least 14.6 dB.*

The coverage profiles thus provide imagery with signal-to-ambiguous energy ratios of at least 13 dB. The advantage of vertical aperture shaping is evident at offset ranges of 300 KM and greater; the advantage amounts to about 15 percent at 200 KM altitude.

The shaped aperture case is a two beamwidth array of 3.3 meters height compared to a three beamwidth uniformly illuminated array of 3 meters overall height. In the modified Taylor case, the L-band frequency is 1.22 GHz as compared to 1.04 GHz for the uniform case; at 9.0 GHz for X-band, the L/X-band wavelength ratios are respectively 7.35 and 8.65. The height and frequency factors are significant in establishing comparable beamwidths for effective coverage at large look angles. The subtle factor of small changes (e.g. about 15 percent) in L/X-band wavelength ratio has a bearing upon signature distinctions in the image data (clutter synthesis) and is difficult to assess, at least at this time. Nevertheless, the wavelength ratios contemplated for the L and X-band systems discussed are consistent with expected requirements in this regard.

The shaped dual beam array is heavier and more complex than the three beam uniformly illuminated array. The three vertical beams of the dual frequency, dual polarized unshaped array are obtained with four pairs of corporate feeds, each located along the back of the structure; one pair for each polarization and one pair for each frequency. In this case, a broad

---

*See Section 4.1 for a detailed discussion of image quality, including considerations of the clutter model, scintillation smoothing with multi-looks, etc. The signal-to-total ambiguous energy ratio is 13 dB or greater with an allowance of -22 dB each for integrated azimuth and range side lobes due to the synthetic array pattern and pulse compression, respectively.

beamwidth or an intermediate beamwidth may be selected from each of two vertical apertures for which the height ratios are 1:2; a narrow beamwidth is obtained as the sum pattern of the two apertures. On the other hand, a second beamwidth from a common aperture with a non-uniform distribution function may require four sets of corporate feeds (three to a set). The broader beamwidth is selected as a mid-section of each full aperture and the narrow beamwidth is formed as the sum pattern of the mid-section connected to upper and lower portions of the aperture with separate matched corporate feeds*. The uniform illuminated array is selected for the imaging radar sensor because of its simplicity and lighter weight.

This selection of uniform aperture illumination is based in large measure upon assignment of essentially uniform weight to look angle or offset range as a sensor parameter. Thus, the broad and intermediate beamwidths readily available with the flexibility of the uniform array aperture provide near nadir and intermediate offset range coverage features which largely offset the far offset range (large look angle) advantage of the shaped array.

---

*Two alternatives are:

1. A separate array for the wide beam, requiring additional vertical aperture for an overall antenna height of at least 4 meters;
2. Sum the upper and lower portions of the array at the module level and thus combine the apertures with two corporate feeds; this solution requires more interconnection waveguide, greater weight and feed losses than the three corporate feed solution.

Power Requirements and Power Management with 12 Meter Arrays. The power requirement of the 12 meter length array radar imaging sensor is nominally 1.5 kw. The transmitters operate at about 500 watts at X-band and 200 watts maximum for L-band. At these nominal power levels, the demands upon space shuttle power are moderate and the reliability of the transmitters, high voltage supplies and modulators is good.

A higher power (5kw power demand) option is feasible. It is practicable to design the power sensitive components to operate satisfactorily at higher power levels for at least brief periods of time. Thus, it is anticipated that transmitters with an 800 watt capability could be built, but with a penalty. The weight penalty for this option is estimated to be about 40 kg for the sensor.

System power demands range from 2.6 KW to 3.5 KW for nominal operations that involve resolutions of 12.5 meters and 25 meters. The variation in system power demand is determined by a power management scheme relying primarily on pulse compression ratio PCR, according to the relations:

$$P_{sys} = \frac{\bar{P}_L}{0.28} + \frac{\bar{P}_X}{0.36} + 1.4, \text{ KW}$$

and

$$\bar{P}_L, \ \bar{P}_X = P_{L,X} * PCR * PRF * T_r, \text{ KW};$$

where

$P_{L, X} \equiv$ peak transmitter power (KW)
PCR $\equiv$ pulse compression ratio (64-324)
PRF $\equiv$ pulse repetition frequency (Hz)
$T_r \equiv$ pulse resolution time (sec)

Power P_L and P_X are fixed while pulse duration T_r is established by resolution requirements. The pulse repetition frequency PRF is selected by a method which places the transmitter eclipsing outside the illuminated swath and is thus primarily a function of offset range for a given altitude; this selection method satisfies the minimum prf requirements for multi-looks at the designated resolution. By varying the pulse compression ratios, system power is controlled to produce the best image quality possible for the maximum power constraints and resolution requirements.

Performance. The baseline design performance features are illustrated in Figure 3-9.

By narrowing the beamwidth of the baseline design to less than 6.3 degrees, the swath coverage can be improved both in width and quality for look angles greater than 50 degrees (see Figure 3-10). This alternate design is for a 3 beam system with aperture ratios of 3:2:1, the same as the baseline design, except for the beamwidths, which are 5.2, 7.75 and 15.5 degrees, respectively. The wavelengths are 24.6 cms (1.22 GHz) in L-band and 2.7 cms (11.0 GHz) in X.

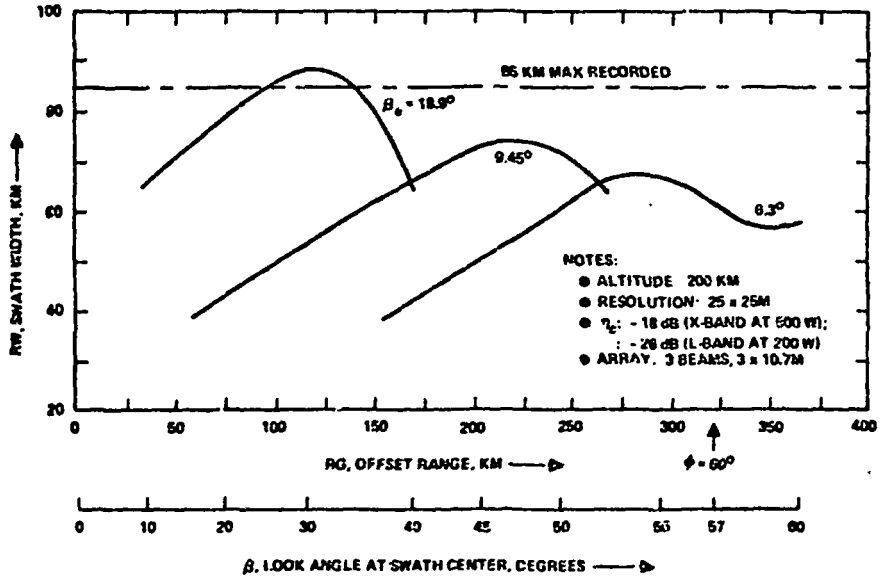

Figure 3-9. Baseline design swath width versus look angle.

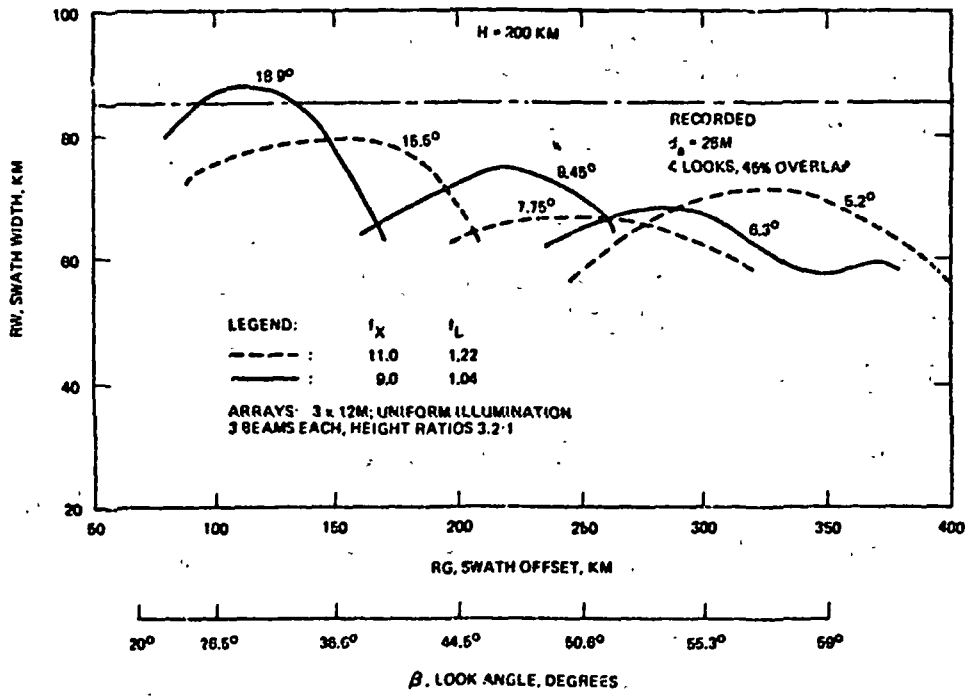

Figure 3-10. Baseline design vs frequency.

3.2.2.2. Eight Meter Length Shaped Arrays

Two 8 meter antenna length designs are discussed below. In each the narrow vertical beamwidth is shaped. Azimuth ambiguity suppression requirements for the 8 meter length necessitated an increase in minimum prf relative to that of the 12 meter antenna of nearly 50 percent. *Accordingly, range ambiguity suppression, particularly at larger look angles, favors shaping of vertical beams.

Two shaped array cases are considered, one involving a 3.3 by 8 meter array, the second a 5 by 8 meter array; the first uses Modified Taylor weighting (-18 dB for first sidelobes) and the second uses a truncated sin k'x/k'x

*PRF = kv/ℓ

v: orbital speed (≈ 7785 m/s)

ℓ: array length

k: a numerical factor increasing with ℓ for given parameters of resolution and effective number of looks; k ≈ 1.9 at ℓ = 8m, 25 meters resolution at 4 looks with 45 percent overlap.

weighting function to approximate a rectangular vertical beam. System power for the former is 4.9 KM. The five foot vertical antenna will require one vertical fold as well as a horizontal fold for stowage on a single 3 x 4 meter pallet.

3.3 x 8 Meter Arrays. Figure 3-11 compares the coverage of the baseline design with that of a two beam 3.3 x 8 meter alternate design in which the narrow vertical beam is shaped. The broader beam B (beamwidth = 15 degrees) of the alternate design is formed from a mid-section of the shaped beam and is essentially uniformily illuminated. The broader beamwidth results in a swath width of about 70 KM (η = -18 dB, S/N at swath center = 14 dB) at a look angle of 30 degrees (offset ground range of 110 KM). The narrow beam (beamwidth = 5.5 degrees) is shaped with a Modified Taylor weighting function selected

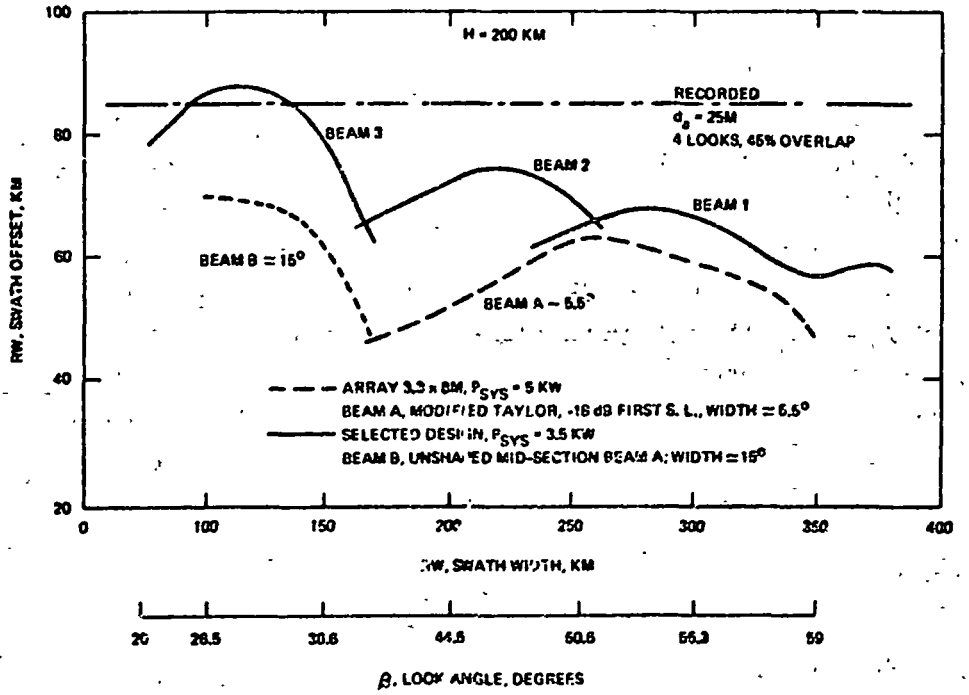

Figure 3-11. Baseline design vs. 3.3 x 8 m.

for first sidelobes of about - 18 dB. The shaped beams provide effective swath coverage from about 45 degrees look angle to nearly 60 degrees (>50 KM swath width on - 22 dB). The range selectivity characteristics of this shaped beam compared to the uniform illumination case is illustrated in Figure 3-12.

The advantages of a multi-beam antenna design are evident in the relatively effective coverage which the baseline design provides in the mid-look angle region as compared to that provided by the 2-beam shaped option. An antenna with uniform weighting that is 8 meters long, with three beams of 5, 7.5 degrees, and 15 degrees beamwidths (aperture ratios of 3:2:1, as for the selected design) in an array of 3 meters height (at an L-band wavelength of 21.5 cms) would afford effective performance and coverage. Moreover it would have the added advantage of simplicity in the corporate feed structure of the antenna, as discussed above. This uniform antenna could be effectively employed at a system power level of about 3.9 KW (600 watts at 9 GHz in X-band and 240 watts at 1.4 GHz in L-band).

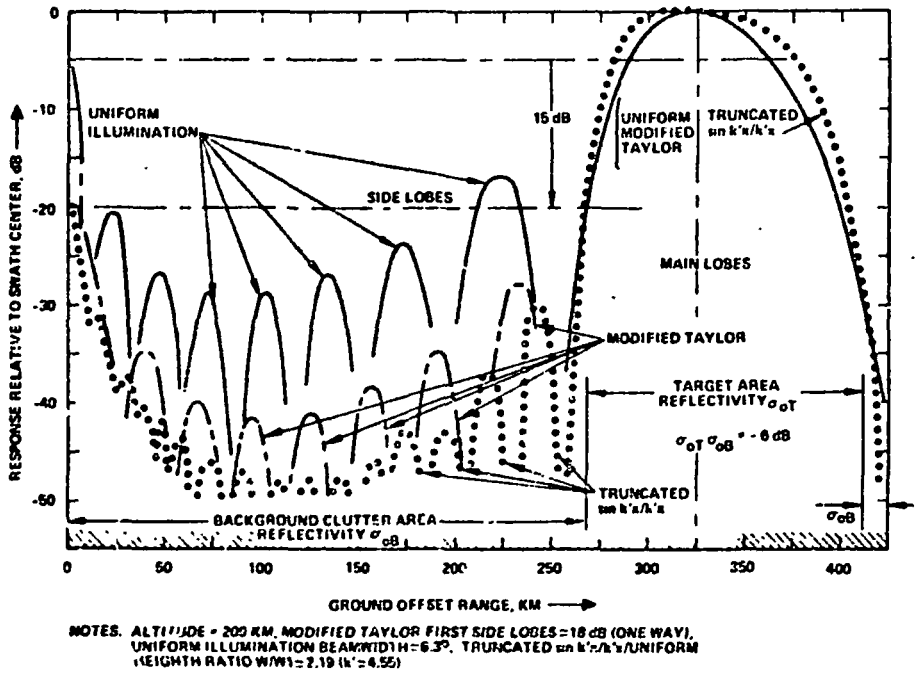

NOTES. ALTITUDE = 200 KM, MODIFIED TAYLOR FIRST SIDE LOBES = 18 dB (ONE WAY), UNIFORM ILLUMINATION BEAMWIDTH = 6.3°, TRUNCATED sin k'x/k'x/UNIFORM HEIGHT RATIO W/W1 = 2.19 (k' = 4.55)

Figure 3-12. Shaped beams/range ambiguity suppression.

5 by 8 Meter Arrays. The truncated sin k'x/k'x weighting functions of the 5 by 8 meter array provide nearly rectangular vertical illumination beams. The range selectivity advantages for the space shuttle of this nearly ideal antenna have already been discussed (see Figure 3-12) in conjunction with discussion of vertical shaping for the longer 12 meter antenna of the baseline design.

The shaped 5 x 8 meter antenna considered is a two beamwidth alternative to multi-beam antennas with beamwidths nearly matched for variable look angles over the range 20-60 degrees contemplated for the Space Shuttle. The 8 meter length is almost the minimum practical because of prf constraints for azimuth ambiguity suppression. A combination of shortened wavelength and increased antenna height relative to the selected design provides the space for shaped beams at both L-band (1.53 GHz) and X-band (10 GHz). The shaping function is applied to separate X-band arrays for vertical and horizontal polarizations and to a single L-band array with crossed dipoles for dual polarization on receive. The large antenna required for the truncated sin k'x/k'x weighting function requires a fold in the vertical plane as well as in the horizontal plane for stowage to a single 3 x 4 meter pallet. The duplicate patterns for the two wavelengths and polarizations are necessary to facilitate comparison of the space sensor data by overlay.

The aperture weighting functions for dual beamwidth vertical beams are shown in Figure 3-13; the broader beam is formed from a switched mid-section of the respective arrays. The approximately rectangular pattern of the narrow beam ($k' \simeq 1.528\pi$) has beamwidths of about 6 degrees at - 1 dB and 10 degrees at -18 dB. This improves the shading of diffuse terrain signals which results from the weighting to about 4 dB as compared to 6 dB shading for comparable swath coverage with a uniformily illuminated array. The comparable range discrimination (or, equivalently, the maximum prf constraint) is improved about 20 percent (0.6 to 1 as compared to 0.5 to 1) for the rectangular beam array approximation. Average power requirements are 200 watts in L-band (1.53 GHz) and 500 watts in X-band (10.0 GHz), with a practical aperture efficiency of 35 percent.

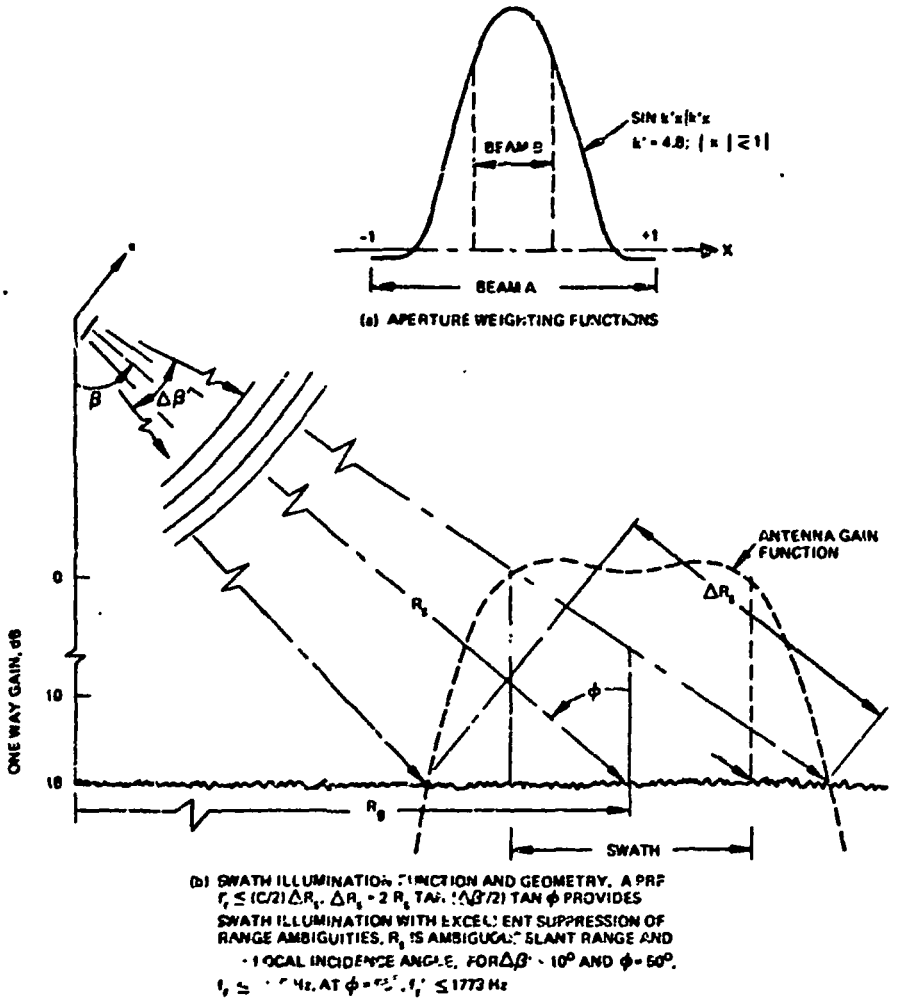

Figure 3-13. Aperture weighting functions.

Swath coverages of the dual shaped beam alternate design and the baseline design are displayed in Figure 3-14. The figure shows effective coverage for diffuse terrain, such as vegetation. This coverage is obtained for incidence angles of 25 degrees (S/N = 13.7 dB for η -18 dB) with beam B, the broader of the two beams. With the narrower beam the coverage extends to 60 degrees (S/N = 10 dB). Beyond 55 degrees (look angle about 53 degrees), the coverage decreases because of range ambiguities resulting from the minimum prf constraint (about 1900 Hz), which in turn is caused by the finite antenna length of 8 meters. With this design there is no coverage beyond 61 degrees because of prf constraints imposed by range and azimuth ambiguity suppression requirements.

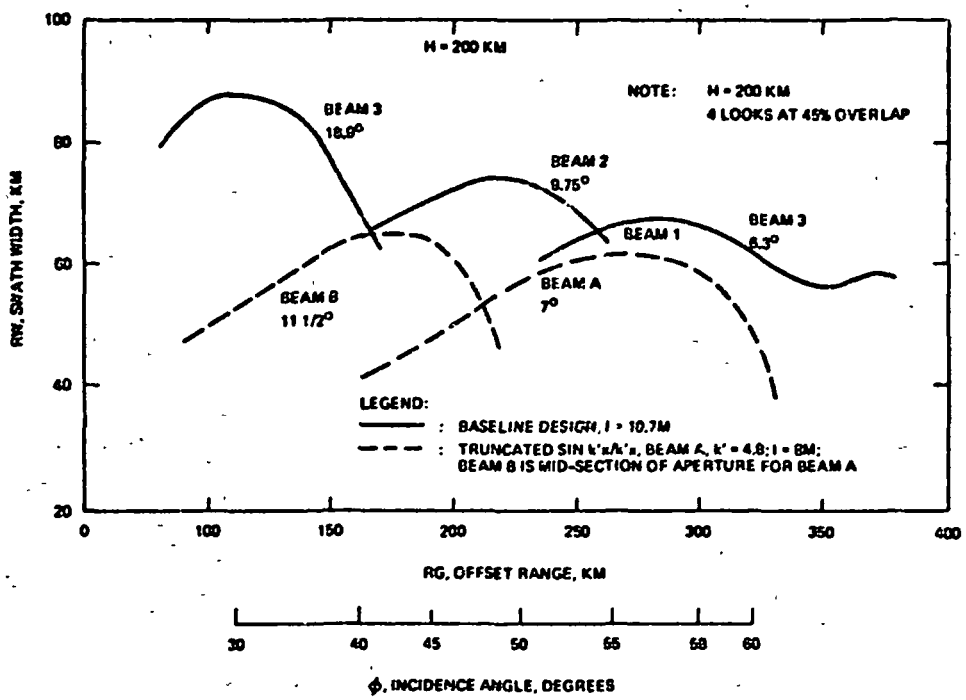

Figure 3-14. Baseline design vs. 5 x 8 m array.

The selection of multi-beam uniformily illuminated arrays is favored because they fold in a single-dimension for single pallet stowage. Similarly the simplicity of the corporate fold structure favors its selection. While shaped vertical arrays offer advantages in range ambiguity suppression, the selection of longer arrays and lower operating prf's and the choice of beam-widths more nearly matched to the various look angles compensates for this loss.

3.2.2.3 16 Meter Length Arrays

The advantages of longer arrays are primarily in the reduced transmitter power and improved swath coverage. A practical upper limit to array length for multi-look (4 looks) synthetic array radar applications is approximately the resolution (about twice the single-look resolution). Thus, for a resolution of 12.5 meters at four looks, a length of 12 meters is practical; also for a single look, 6.25 meters is practical. However, for a resolution of

25 meters, an antenna of 16 meters offers substantial reductions in the power required as well as improvements in swath coverage, particulary at look angles beyond 50 degrees.

The pros and cons of greater antenna length were investigated in a study of 15 to 16 meter planar arrays, which are essentially three-fold versions of the dual-fold deployable physical arrays of the baseline design. The height of the antenna studies is 3 meters; by selecting apertures, 3 different beams are formed – 6.3 degrees, 9.75 degrees, and 18.9 degrees in width – just as in the 11-12 meter baseline version. The increase in antenna weight for this design increase is about 1/3 (680 dg to 910 kg, approximately). It is estimated that at X-band corporate feed losses will increase by about 0.4 dB the change is anticipated; feed loss at L-band, with low loss waveguide, will be negligible. Power allocations are accordingly 360 watts at X-band and 120 watts at L-band, slightly greater than that obtained through direct scaling (338 W at X and 112 W at L-band); system power demand is 2.8 KW, a decrease of 25 percent compared to the 3.5 KW demand for the selected design.

The swath coverage of the longer antenna version is compared with that of the baseline design in Figure 3-15. Swath widths differ insignificantly at the shorter offset ranges for which the swath is determined solely by the illumination pattern of the vertical beams; however, the data rate is lower and the range ambiguity is less at the lower prf's of the long antenna design. At larger offsets, a swath width advantage is evident for the longer antenna because of improved range ambiguity suppression at the lower prf's of the alternate design. Both designs provide a swath center S/N > 14 dB for η = -18 dB and for an incidence angle of 64 degrees (look angle = 60.6 degrees). At 25 meters resolution, the minimum prf constraint (4 looks at 45 degrees overlap) to meet azimuth ambiguity suppression requirements is about 1100 Hz for the alternate and about 1300 Hz for the baseline design.

The conventional applications of synthetic aperture techniques require uniform arrays about twice the single look resolution length or less. Thus, the 15-16 meter uniform arrays of the alternate design are satisfactory for a resolution of 8 meters at a single look. However, for diffuse targets scintillation smoothing with multi-looks in time (azimuth) is desirable. Four looks at a 25m resolution, d, and 45 percent overlap is equivalent to a single

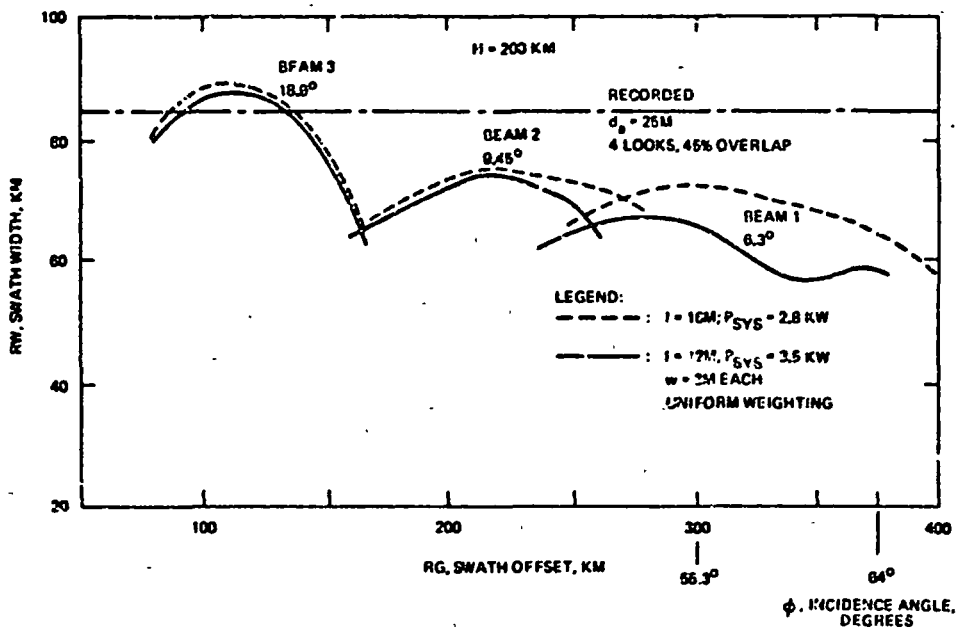

Figure 3-15. Selected design vs. 3 x 16m.

look resolution of 25/2.65 = 9.4m*, d; this provides scintillation smoothing equivalent to about 3.5 independent looks. Thus, the longer array alternate and the selected designs are satisfactory for multi-look SAR applications at 25 m resolution. However, four looks for a d of 12.5 m and 65 percent overlap are equivalent to a single resolution (d') of 12.5/2.05 = 6.1m. Thus the alternate design with an antenna length (ℓ) of 15 m is restricted to multi-look SAR applications for which resolution is equal to or more than 15-16 m and single look where the resolution d is $\ell/2$ = 7.5 m. A major factor in the choice of 11-12 m for the antenna length is its compatibility with Space Sensor SAR capabilities of 12.5 m resolutions at 4 looks (with 65 percent overlap).

The baseline design folds to stow on a single 3 x 4 m pallet, allowing room for other Space Shuttle experiments. The need to make three-folds in

*$L' = \lambda R/2d'$, $L' = L(n-(n-1)k)$; n is the number of looks and k the fractional overlap; $L = \lambda R/2d'$ is the orbit path distance vT_a (effective length of the synthetic aperture).

the horizontal plane of the 15-16 m of the alternate design to provide this room is a major factor in rejecting it in favor of the 11-12 meter length antennas.

3.2.3 UHF and X-Band Design

A UHF/X-band design is practicable. UHF is 450 MHz, the X-band frequency is 9.0 GHz. The array dimensions are 3 meters by 10.7 meters; it is stowed upon and deployed from a single pallet, as is the baseline array. The UHF aperture is dual polarized with crossed-dipoles, like the baseline's L-band array. One of three beams may be selected using vertical switching as in the baseline array. Broad beams of 24 degrees and 37 degrees are suitable for near nadir illumination (e.g. 6 degrees to 30 degrees). A 14.6 degrees narrow beam, at a look angle of 39 degrees for ground reflectivity (σ_o) of -27 dB (receiver noise figure = 2.5 dB), with 100 watts average transmitter power gives a swath center S/N of more than 14 dB. The UHF of 450 MHz was selected for two reasons. First it is below the television band (470 to 890 MHz). Secondly it is approximately an octave below the L-band (1045 MHz) frequency of the baseline design, which may be desirable for some earth resource sensor applications, such as forestry.

Parameters of the UHF/X-band alternate design are listed in Table 3-12.

TABLE 3-12. UHF/X-BAND ALTERNATE DESIGN PARAMETERS

	UHF	X-Band
Carrier Frequencies	450 MHz	9.0 GHz
Transmitter Power, Avg	100 watts	500 watts
Resolution	25 x 25 M	25 x 25 M
Vertical Beams	3:14.6, 24.0, 37.3	3:6.3, 9.45, 18.9
Array Dimensions	2.43 x 10.7 M	0.57 x 10.7 M
Swath Widths	50-85 KM	50-85 KM
Terrain Reflectivity	$\sigma_o \geq$ -27 dB	$\sigma_o \geq$ -18 dB
Received Noise Figure	2.5 dB	4.0 dB
Signal-to-Noise Ratio	≥8 dB	≥8 dB
Aperture Efficiency	57.5 percent	57.5 percent
Losses	4.2 dB	6.1 dB
Look Angles (200 KM altitude)	6 to 45 degrees	10 to 60 degrees

3.2.4 S- and X-Band Designs

An S-/X-band design at 2.45 and 9.0 GHz, respectively, was also considered. The S-band array height is 1.04 meters compared to 2.43 meters for the L-band array height. The S-band aperture uses crossed dipoles for the dual polarization feature, as does its L-band counterpart. The weight of this array, which is 1.6 meters high, is estimated to be about half that of the baseline array, while the increase in transmitter power is only 50 watts. S-band at 250 watts average power provides performance roughly equivalent to L-band, with an increase in σ_o's of 2.7 dB; losses and noise figure are approximately the same.

The S/X-band design provides coverage equivalent to the L/X-band baseline design using three switched beams of 6.3, 9.45, 18.9 degrees with uniform illumination. Remote sensor performance is also equivalent, except for any subtle difference in sensor characteristics because of the approximately one octave increase in frequency from L-band to S-band.

The S-band transmitter may be implemented with TWT's or klystrons. S-band klystrons provide a convenient means of obtaining transmitter efficiencies of 30 to 40 percent, with adequate bandwidth (at least 50 MHz), as in the X-band transmitter. TWT and Klystron tube designs suitable for the application, with perhaps some parameters scaling, are available.

TABLE 3-13. S-/X-BAND ALTERNATE DESIGN PARAMETERS

	S-Band	X-Band
Carrier Frequencies	2.45 GHz	9.0 GHz
Transmitter Power, Avg	250 watts	500 watts
Vertical Beams	3:6.3, 9.45, 18.9°	3:6.3, 9.45, 18.9°
Array Dimensions	1.04 x 10.7 M	0.57 x 10.7 M
Swath Widths	50-85 KM	50-85 KM
Terrain Reflectivity	$\sigma_o \geq$ -25 dB	$\sigma_o \geq$ 20 dB
Receiver Noise Figure	2.5 dB	4.0 dB
Signal-to-Noise Ratio	≥8 dB	≥8 dB
Aperture Efficiency	57.5%	57.5%
Losses	4.5 dB	6.1 dB
Look Angles	10 to 60°	10 to 60°

3.2.5 Dual K_u -Band and L-Band Designs

Two approaches for K_u -band alternate designs at 13.3 and 16.0 GHz were considered. The first approach uses three beams; performance is essentially equivalent to that of the X-band baseline design; the second employs a single shaped beam and provides effective coverage to a look angle of at least 40 degrees and requires less prime power than the multi-beam approach. The second K_u -band design provides a minimum swath width of 40 KM for look angles of 20 degrees to 40 degrees and a beam limited swath width of 35 KM with coverage to 10 degrees look angle. The multi-beam options provide swath widths of 60-80 KM and coverage from 10 degrees to 60 degrees look angle.

Considerations of agricultural applications motivate shorter wavelength sensor designs. In particular, X-band is not as sensitive as K_u band to differences in plant morphology and biomass. An increase in sensitivity with carrier frequency has been reported for vital crops, including corn*.

K_u -band designs have several relative disadvantages. They require more transmitter power than X-band equivalents, are more susceptible to the adverse effects of moist clouds, fog, and rain. K_u -band impose more stringent requirements on mechanical tolerances for antennas than does X-band designs. These disadvantages are significant for choice of antenna and transmitter designs, but do not preclude the use of K-band, at least for wavelengths greater than 1.8 cms. Available data for vegetation, discussed later, indicate that backscatter coefficients for a K_u -band and X-band are equivalent.

---

*1) Ulaby, F.T., T.F. Bush, P.O. Batlivala, J. Cihlar, "The Effects of of Soil Moisture and Plant Morphology on the Radar Backscatter for Vegetation". Remote Sensing Laboratory, The University of Kansas Space Technology Center, R.S.L. Technical Report 177-51, July 1974.

Experimental data for corn, milo, soybeans, and alfalfa at 9.0, 13.0, and 16.0 GHz for incidence angles of 0 degrees (vertical) to 70 degrees are reported. The effects of heavy rain on backscatter from fields of maturing corn (July 16 to August 8, 1973) are especially convincing with respect to K_u-band sensitivity to plant morphology and/or biomass.

K_u -band designs having performance equivalent to the X-band baseline design at 500 watts average transmitter power (array ≈10.7 meters long) require transmitters with average powers of 1300 to 1700 watts at 13.3 GHz and 1900 to 3000 watts at 16.0 GHz, depending upon atmospheric conditions. Table 3-14 summarizes the critical loss factors for these baseline equivalent designs. The sensitivities to propagation losses and the effects of rain are discussed below. Figure 3-16 shows the frequency dependence of transmitter power requirements and system power demand for the moderately severe propagation loss case of moist low stratus clouds without precipitation for which X-band loss at an incidence angle of 60 degrees is about 1.4 dB (Figure 3-17).

Antenna aperture weight savings of 40 to 60 kg for the shorter wavelength versions of the multi-beam baseline antenna do not compensate for the weight increases resulting from transmitter weight and power requirements. The L- and K_u -band antenna aperture area is decreased, by approximately 2.0 to 2.7 square meters (6.1 to 8.3 percent). This decrease in area results in a weight saving of up to 60 kg (aperture weight about 22 kg per M^2), which

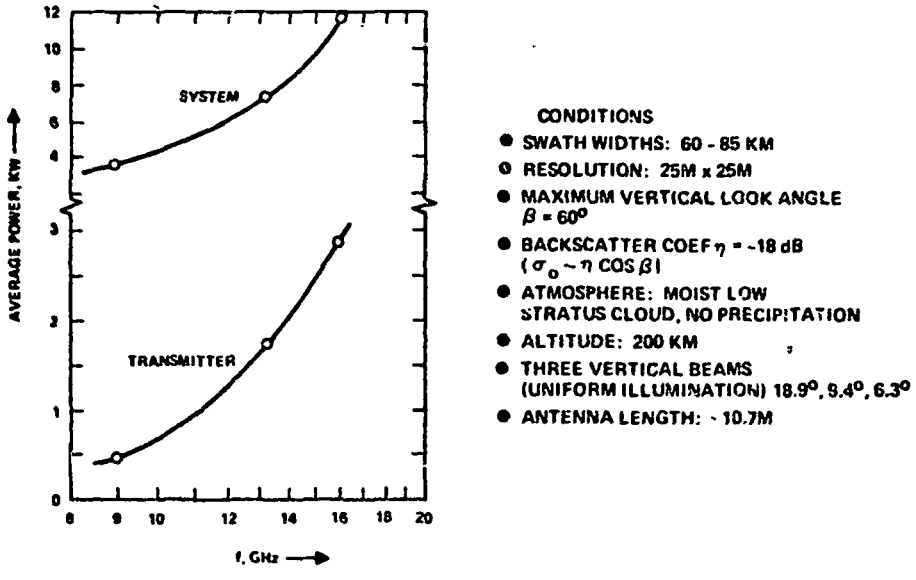

Figure 3-16. Multi-beam system frequency comparison (9.0, 13.3, 16.0 GHz).

TABLE 3-14. K_u-BAND AND X-BAND BASELINE DESIGN COMPARISONS FOR EQUIVALENT PERFORMANCE

	K_u-Band			
◦ K_u Losses relative to X-Band (9.0 GHz):	13.3 GHz		16.0 GHz	
Antenna (two-way)	+0.8 dB		+0.8 dB	
RF Coupling	+1.2		+1.2	
Receiver Noise Figure	+0.2		+0.5	
Wavelength Scaling[1]	+1.7		+2.5	
Subtotals	+3.9 dB		+5.0 dB	
◦ K_u-Transmitter Power Equivalent to 500 watts at X-Band:				
Propagation Loss Models	I[2]	II[3]	I[2]	II[3]
Propagation Losses, dB	+0.4	+1.4	+0.9	+2.6
Net Losses, dB	+4.3	+5.3	+5.9	+7.6
P_t, K_u-Band Transmitter Equivalent, watts	1346	1694	1945	2877

(1) Required transmitter power scales directly with λ for fixed clutter reflectivity (η = -18 dB), other factors being equal.

(2) Clear, warm, humid atmosphere, Model SEA 8 in Figure 3-17.

(3) Moist, low stratus clouds, Model SEA 7 in Figure 3-17.

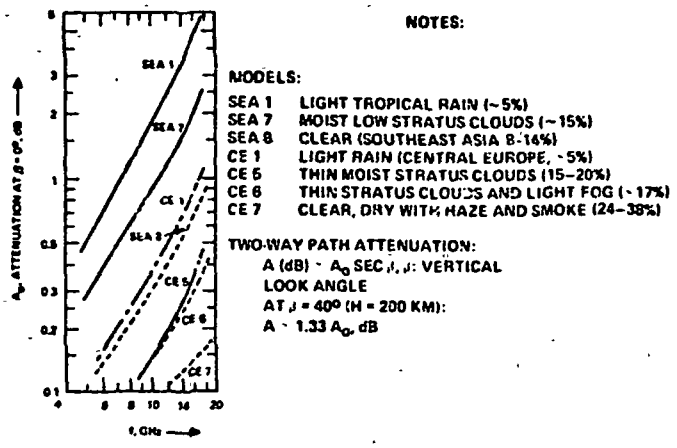

Figure 3-17. Atmospheric attenuation models.

is offset by an increase of the same magnitude in the weight of the K_u-band transmitter, necessitated by the need for more power (>1 KW*).

3.2.5.2 Single Beam Antenna Alternates to X-Band Baseline Design

The single beam alternate, with a shaped vertical beamwidth of about 12.5 degrees, provides effective coverage of 40 KM swath width for look angles of 40 degrees (200 KM altitude) with 400 to 600 watts K_u-band transmitter power. Table 3-15 summarizes the power requirements for 13.3 and 16.0 HGz K_u-band frequencies and the moderately severe propagation loss case (moist low stratus clouds, model SEA 7 in Table 3-16 and Figure 3-8). Figure 3-18 illustrates the frequency – power relationship for this design. For an equivalent single beam X-band system the average transmitter power is 130 watts.

Figure 3-19 shows the performance of the single beam design for the case of moist low stratus clouds (Model SEA 7 in Figure 3-17). The horizontal bars on the curve indicate the limits of coverage for each swath position, for example a swath width of 35 KM is obtained with the antenna at a 15 degrees look angle and covers the area between look angles of 10 degrees and 20 degrees for an altitude of 200 KM. The dashed line extension for larger look angles represents performance improvement as transmitter

*Transmitter weight is approximately proportional to the square root of power.

TABLE 3-15. SINGLE BEAM TRANSMITTER POWER REQUIREMENTS

- Shaped vertical beam (truncated SIN X/X; ~12.5°)
- K_u-Band Transmitter Power Requirements Relative to X-Band (9.0 GHz)

	K_u-Band at 13.3 GHz			K_u-Band at 16.0 GHz		
due to λ[1.]:	+1.7 dB			+2.5 dB		
due to Sensor RF Losses, dB:	+2.2			+2.5		
Sub-Total	+3.9 dB			+5.0 dB		
due to Adverse Weather[2.] {to β[3.] =	40°	45°	50°	40°	45°	50°
dB:	+1.0	+1.1	+1.3	+1.8	+2.0	+2.3
Totals, dB:	+4.9	+5.0	+5.2	+6.8	+7.0	+7.3
• Average Power: P_{AV}, Watts:	360	510	820	540	800	1300
System, Kw:	3.0	3.5	4.4	3.5	4.3	7.1

Notes:
1. Required P_{AV} α'/λ at fixed η (-18 dB) and beamwidth (~12-1/2°), other factors being equal; $\sigma_o \sim \eta \cos \beta$.
2. Propagation losses in moist low stratus cloud cover, no precipitation (Figure 3-17).
3. Look Angle β at altitude H = 200 Km.

TABLE 3-16. SELECTED WEATHER MODELS

Model	Description	Temp °C	Water Vapor g/m^3	Moisture g/m^3	Percent Annual Occurrence	
					Day	Night
SEA 1	Light Monsoon Rain, 1 to 2.5 mm/hr.	26	17	1-1.5	2.8	5.5
SEA 7	Low-Stratus Clouds Warm, Moist	26	12.7	0.5-1	12	17
SEA 8	Clear, Warm, Humid	26	14.1	—	14	8
CE 1	Light Rain 0.6 to 1.2 mm/hr.	9	6.3	0.1-0.3	5	5
CE5	Low-Stratus Clouds Cool, Broken	9	6.3	0.1-0.3	19	15
CE6	Fog and Low Stratus Clouds	9	6.8	0.1-0.3	17	18
CE7	Clear with Haze and Smoke, Dry	9	4.1	—	24	38

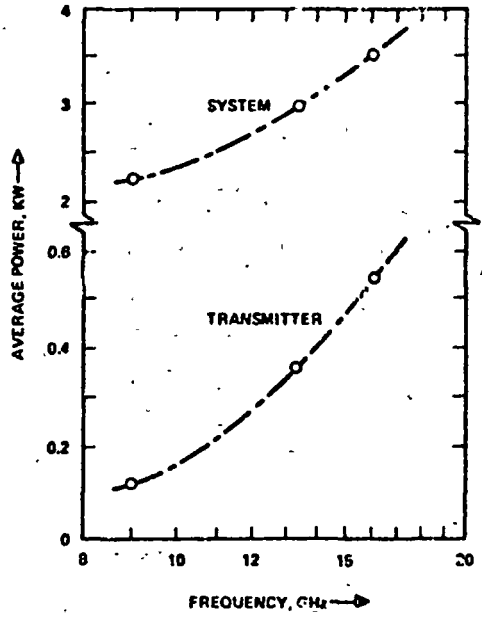

CONDITIONS

1. SWATH WIDTH: 40-50 KM
2. RESOLUTION: 25M x 25M
3. MAXIMUM VERTICAL LOOK ANGLE $\beta = 40^{o}$
4. BACKSCATTER COEF $\eta = -18$ dB ($\sigma_0 \sim \eta \cos \beta$)
5. MINIMUM S/N = 8 dB
6. ATMOSPHERE: MOIST LOW STRATUS CLOUD, NO PRECIPITATION
7. ALTITUDE: 200 KM
8. VERTICAL BEAMWIDTH $\simeq 12.5^{o}$, SHAPED: TRUNCATED SIN X/X
9. ANTENNA LENGTH: 10.7M

Figure 3-18. Single antenna beam system, frequency comparison (9.0, 13.3, 16.0 GHz)

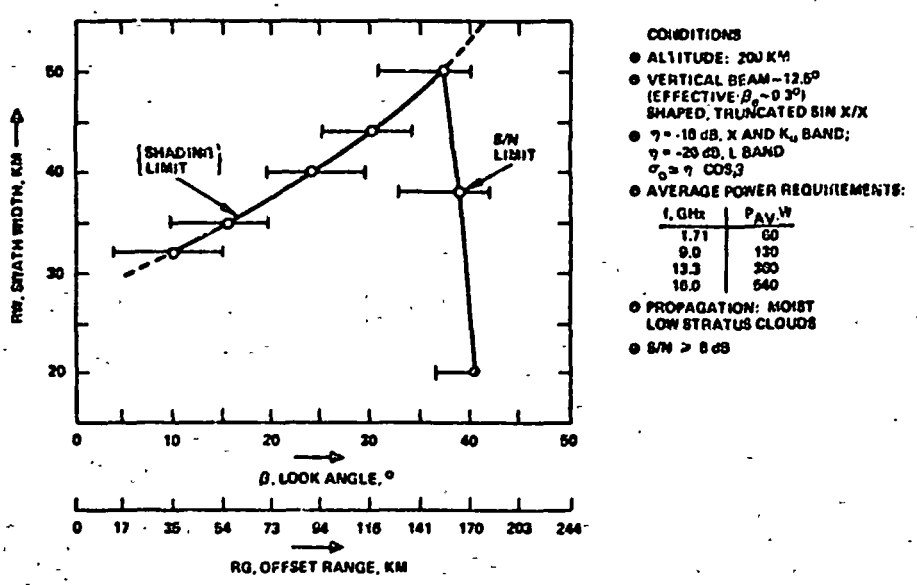

Figure 3-19. Single beam options swath coverage.

power or clutter reflectivity increase or as propagation loss decreases. Range ambiguity considerations restrict coverage to look angles that are less than 55 degrees.

The aperture dimensions and gains for the single beam designs are summarized in Table 3-17. The L-band frequency is 1.71 GHz, an increase of about 70 percent from the baseline design (1.045 GHz). The combination L-band and K_u-band single beamwidth alternate designs have apertures of 3.3 meters x 10.7 meters, consistent with deployment and single pallet stowage as with the baseline design.

3.2.5.3 Relationship of K_u-Band Planar Array and X-Band Planar Array Costs of the ERSIR

Costs of the design analysis, fabrication, and test for a K_u-band antenna at 13.3 GHz are expected to be about 25 percent more than for the equivalent X-band design at 9.0 GHz. This increase in cost with carrier frequency reflects the anticipated increase in effort needed to maintain required tolerances, which becomes greater as the antenna length increases from about 300λ at 9 GHz to 475λ at 13.3 GHz, for a 10.7 meter array.

TABLE 3-17. DUAL BAND SINGLE BEAM ALTERNATE DESIGNS
Shaped Vertical Beams
Weighting Function: Sin $k\pi x/k\pi x$
Dimensions, Aperture Efficiencies, Gains (Length = 10.7 m.):

X or K_u Band GH_z	k	Height W_L, Cms L-Band (1.71 GHz)	Height W_X, Cms X- or K_u-Band	Theoretical Efficiency %	Gain, dB L-Band (1.71 GHz)		Gain, dB X- or K_u-Band	
					Area	Effective	Area	Effective
9.0	1.646	239.1	90.9	30.1	40.2	32.6	47.4	39.8
13.3	1.698	262.5	67.5	28.1	40.6	33.0	49.5	41.2
16.0	1.717	271.9	58.1	27.4	40.7	33.1	50.5	42.1

*W_L is height of dual polarized L-band aperture (1.7 GHz), W_X is the height of two X- or K_u-band apertures; one for vertical and the other for horizontal polarization; total height is 3.3 meters, length is 10.7 meters.

The pattern requirements are tied to the SAR performance criteria and are the same for K_u-band as for X-band. The approximate relationship between cost and frequency is given by the curve shown in Figure 3-20.

The costs for the baseline equivalent K_u-band transmitters will be relatively high because of the design, development, and relevant testing costs associated with the high voltages and powers for this application. The K_u-band transmitter can be readily developed by scaling an existing K_u-band gridded Klystron design (Varian Associates), which has design center values of 14 GHz and 1000 watts to 13-16 GHz and 500 to 1500 watts. This new K_u-band transmitter will require a more powerful grid modulator than the contemplated X-band design, because of a relatively lower mu grid in the K_u-band tube.

However, the K_u-band single beam options at 360 watts (13.3 GHz) to 540 watts (16 GHz) are comparable to the baseline X-band transmitter in power and cost. The cost frequency relationship is expected to approximate that shown in the curves of Figure 3-21.

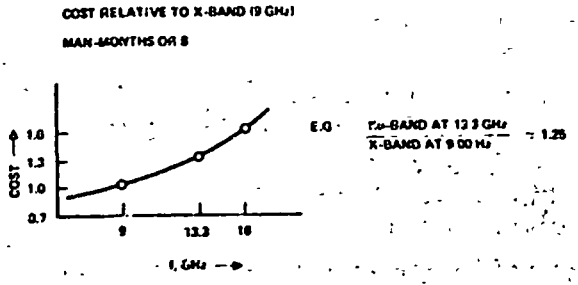

Figure 3-20. K_u-band planar arrays.

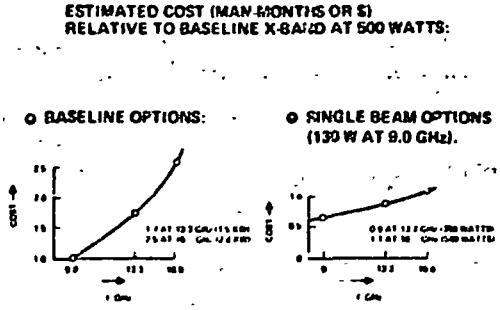

Figure 3-21. K_u - band single beam options, transmitter cost relative to baseline

Preliminary characteristics of the K_u-band transmitter at 13.3 GHz are summarized in Table 3-18.

3.2.5.4 Operating Conditions that Effect Design

Vegetation Backscatter Coefficient. Extensive experimental data on backscatter coefficients for vegetation are summarized in the literature*. The wavelength dependence for mature and maturing crops appears to be more a function of crop condition than of crop type. Condition refers to moisture content, morphology, biomass, and disease**. In general, for frequencies from 9.0 to 16.0 GHz, and for either HH or VV direct polarization, the backscatter coefficient variation because of crop type is 4 to 5 dB (incidence angles ϕ = 20 to 60 degrees); the cross-polarization backscatter coefficient is generally smaller than the coefficient for direct polarization by 5 to 15 dB, and typically is 8 to 12 dB. Following Nathanson (1969), and in general agreement with Moore (1970) an η value of -18 dB ($\sigma_o = \eta \cos \phi$) was adopted for X- and K_u-bands (to 16 GHz), HH and VV polarization, where

---

*2) Moore, R.K., "Ground Echo", chapter 25 in Radar Handbook, M.I. Skolnik, editor, McGraw-Hill Book Co., 1970; esp. pp 18-35, 42-47

3) Nathanson, F.E., "Radar Design Principles, Signal Processing and the Environment", McGraw-Hill Book Co., 1969, pp 262-273

4) Cosgriff, R.L., W.H. Peake, R.C. Taylor, "Terrain Scattering Properties for Sensor System Design", Terrain Handbook II, The Engineering Experiment Station, University of Ohio, May 1960

5) Bond, R.H., "A Summary of Measurements and Theories of Radar Ground Return", Technical Memorandum 656, Hughes Aircraft Co., September 1960

6) Ulaby, F.T., "Radar Response to Vegetation", IEEE Transactions on Antennas and Propagation, vol. AP-23 January 1975, pp 36-45

7) King, C., "Agricultural Terrain Scatterometer Observations with Emphasis on Soil Moisture Variations", Remote Sensing Laboratory, The University of Kansas Center for Research, Inc., CRES Technical Report 177-44, August 1973

**Ulaby, et al (1974), op. cit., pp 11-14

TABLE 3-18. K_u-BAND TRANSMITTER.

Based on Current State-of-the-Tube Art:

	K_u-Band
Center Frequency	13.3 GHz
Tube Type	Klystron with PM Focus
Tube Development	Scaling Existing Design
Peak Power	25 - 30 KW
Average Power	250 - 1000 W
Bandwidth	75 MHz
Duty	3 Percent
RF Drive	1 W Maximum
Modulation	Low Mu Grid (3 - 5 KV Pulse)
Pulsewidth	15 - 25 μs
PRF	1200 - 1800 Hz
Transmitter Frequency	25 - 30 percent

ϕ is from 10 degrees to 70 degrees. At L-band for which an η value of -26 dB was rather arbitrarily chosen, a tendency for smaller backscatter coefficients is noted for wavelengths larger than about 10 cms.†

Propagation Losses

The microwave sensor is valuable for its ability to penetrate cloud cover, ground fog and rain; supplementing optical wavelength sensors which are ineffective under these conditions. However, it is necessary in K_u-band to allow for increased propagation losses as compared to X-band. For this purpose, adverse weather models are used to estimate atmospheric effects.#**

---

*Nathanson (1969) op. cit., p. 273; Moore (1970) op. cit., pp. 26, 29

†Nathanson (1969), pp. 262-265

#Beam, B.R., E.J. Dutton, B.D. Warner, "Weather Effects on Radar", Chapter 24 in Radar Handbook, M.I. Skolnik editor, McGraw-Hill Book Co., 1970, pp. 16-23

**O'Reilly, Captain Patrick J., "Adverse Weather Models", USAF Environmental Technical Application Center, ETAC Report 6467, October 1970

From O'Reilly's work, the following relatively frequent low stratus cloud models have been chosen:

1. SEA 7, a model of warm (26°C), moist (~0.3 g/m^3), low stratus clouds occurring 17-22 percent of the time, September to April in Southeast Asia;
2. CE5, a cool (9°C), moist (~0.3 g/m^3) broken low stratus cloud model occurring 15-19 percent of the time in Central Europe (predominantly October – March).

Also extracted for relevance are models for light rain:

3. SEA 1, a warm (26°C), light tropical rain of 2-2.5 mm/hr typical of many regions and occurring about 5-10 percent of the time from May to September.
4. CE1 a cool (9°C), very light but extensive rain of 0.9 to 1.2 mm/hr occurring about 5 percent of the time and for all seasons in Central Europe.

These models extend to an altitude of 30 KM; the path length for the orbiting shuttle (neglecting refraction effects) is accordingly

$$\ell_p = 30 \sec \phi, \text{ KM} \qquad (1)$$

where ϕ is the angle of incidence at the ground. Thus propagation loss is simply the two-way propagation loss A_o at vertical incidence multipled by sec ϕ:

$$\ell_p = A_o \sec \phi = A_o \sec (\beta + R_g/R_e). \qquad (2)$$

The two-way vertical incidence propagation losses as functions of frequency (X- and K_u-bands) are shown in Figure 3-17. The losses for rain are those caused by absorption and scattering; the effects of rain backscatter are considered below.

The referenced models are briefly described in Table 3-16 together with estimates of their annual frequency of occurrence in Southeast Asia or Middle Europe. The models are, of course, typical of similar atmospheric phenomena in other regions, hence provide a general indication of weather effects as well as being specific for significant portions of the earth's surfaces. A cool, dry air model (CE7, 4.1 g/m^3 water vapor) exhibits low loss (0.15 dB at 16.0 GHz, equivalent to 0.3 dB at 60° incidence angle).

The Effects of Rain

Rainfall effects for the synthetic array radar are complex; turbulence, wind shear and the distribution of precipitation centers in the cloud formations are difficult to account for except in the most general cases. It will be assumed in the analysis which follows, that practical results can be obtained with a very simple precipitation model. Wind effects will be ignored. It will be assumed that the rainfall will be assumed light and extensive in area, and that it will change gradually with height above the earth. Figure 3-22 is a sketch of this simplified model for rain backscatter calculations. The propagation losses due to scattering and absorption appropriate to terrain backscatter have been accounted for in Figure 3-8 for specific light rain situations.

The simplified model for rain backscatter calculations is based on a uniform strata of precipitation parallel to the earth's surface; for simplicity, refraction effects are neglected. It is assumed that the incident rays from the illuminating sensor have fixed angles of incidence ϕ at each layer of precipitation, that each layer i is 1 KM thick with a uniform precipitation rate r_i mm/hr and that i is an index running from 1 at the top of the rainfall model to n at the earth's surface, with the precipitation exterding to a height of n KM.

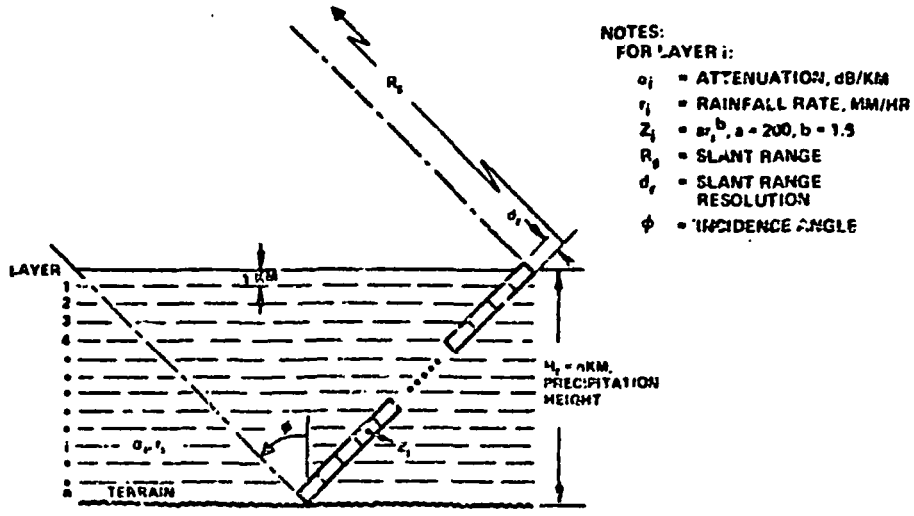

Figure 3-22. Model for rain backscatter.

The volume element for backscatter calculations consists of a slab d_r meters thick at a slant range R_s tilted at an angle ϕ from the vertical and extending distances that are large compared to SAR resolution d_a. The precipitation echoes are assumed to be random in phase relative to terrain reflections and so constitute additive white noise; further, the vertical velocity component is assumed to be sufficiently small that the apparent doppler displacement of the rain clutter spectrum is not a significant factor*. The reflections from the i^{th} layer volume element are subject to two-way path attenuation from the layers above it; for simplificy it will be assumed that the attenuation within the reflecting layer is negligible. Vertical extent is assumed small compared to the vertical illumination pattern of the sensor beam; thus terrain and rain backscatter are assumed to be illuminated at the same relative gain.

The rain reflectivity σ_r (units of square meters per m^2) is calculated for the volume element in the i^{th} layer from the following relations:**

$$\sigma_{r_i} = \frac{h_i \pi^5 |K|^2}{\lambda^4} z_i \qquad (2)$$

$$\text{with } z_i = \left(\sum_j D_j^6\right)_i = a r_i^b; \qquad (2a)$$

D_j is the diameter of the rain droplets (mm) in the j^{th} volume element of 1 m^3, r_i is rainfall rate in mm/hr, a and b are empirical constants, K is a factor related to the complex dielectric constant of the droplets and h_i is the effective distance (height) of the rain cell in the i^{th} layer ($h_i = \csc\phi_i$, KM).

---

*The rain clutter signals appear shifted in angle (azimuth) relative to the stationary ground due to the spectrum displacement of the falling rain. For gently falling rain (for example. velocities less than 5 m/s), this shift will be minor; for heavy or wind driven rain, the shift will be a significant fraction of the real array azimuthal beamwidth.

**1) Kerr, D.E. editor, "Propagation of Short Radio Waves", vol. 13 Radiation Laboratory Series McGraw-Hill Book Co., 1951, Chapter 7

2) Skolnik, M.I., Editor, "Radar Handbook, McGraw-Hill Book Co., 1970 Chapter 24, especially pp. 21-22, 28-29.

The Rayleigh scattering model is applied to the X- and K_u-band cases considered here.

Typically

$$z_i = 200\, r_i^{1.6}$$

$$|K|^2 = 0.92 \qquad (2b)$$

for rain droplets in X and K_u-bands and near a temperature of 8°C; z has the units $(mm)^6/m^3$.

The rain backscatter in the i^{th} layer is attenuated by a factor A_{i-1} due to the path in the i-1 layers above the rain cell. The terrain return signal is attenuated by a factor A_n due to propagation in n precipitation layers. Thus the terrain backscatter signal P_s and rain clutter power p_r (signal-to-noise) ratio is expressed as follows:

$$\frac{p_s}{p_r} = \frac{d_g d_a A_n \sigma_o}{d_r d_a \sum_{i=1}^{n} A_{i-1}\sigma_i} \qquad (3)$$

where d_g, d_a are SAR resolutions, σ_o is terrain reflectivity and $d_r = d_h \sin\phi$. Substituting relations (2) above with $h_i d_r = d_g \cdot 10^3 m^2$ yields:

$$\frac{p_s}{p_r} = \frac{\lambda^4 A_n \sigma_o}{2 \cdot \pi^5 |K|^2 \cdot 10^{-5} \sum_{i=1}^{n} A_{i-1} r_i^{1.6}} = \left(\frac{\sigma_o}{\sigma_r}\right) \qquad (4)$$

where λ is in cms, r_i is mm/hr and σ_r is an equivalent rain backscatter coefficient:

$$\sigma_r = \frac{5.63 \cdot 10^{-3} \sum_{i=1}^{n} A_{i-1} r_i^{1.6}}{\lambda^4 A_n} \qquad (5)$$

with $|K|^2 = 0.92$ in (2).

The equivalent backscatter coefficient σ_r as a function of frequency in X- and K_u-bands is shown in Figure 3-23 for the light rain model, SEA 1 cited above for propagation losses. The effective cross-section is observed to increase as f^p, $p > 4$ due to the frequency dependence of the attenuation factors A_{i-1} and A_n.

The signal-to-rain clutter ratio for the baseline design (η = -18 dB, σ_o = -19.2 dB at $\beta = 40^o$) is near unity at 16 GHz but still appreciable (about 12 dB) at 9 GHz. Further, the path attenuation for $\beta = 40^o$ is only 2 dB in X-band (9 GHz) but 6.3 dB at the upper end of K_u-band (16 GHz).

Moderate to heavy rains will, of course, seriously degrade X-band performance as well as inhibit K_u-band. However, severe storms are usually infrequent and restricted to relatively small areas. The light rain can be extensive in area and long in duration. Clearly, adverse weather favors longer wavelengths in the range 9 to 13.3 GHz.

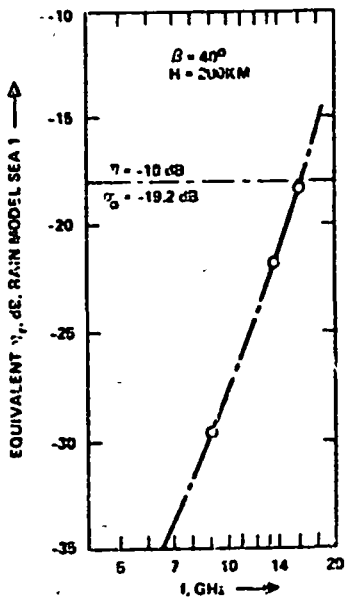

NOTES:
LIGHT RAIN MODEL, SEA 1:
PRECIPITATION HEIGHT: 6 KM
RATE: 1 - 2.5 mm/hr
SURFACE: TEMP = 26°C
WATER VAPOR 17 g/m^3
CLOUD COVER: LOW STRATUS
H_2O: 1 - 1.5 g/m^3
INCIDENCE ANGLE $\phi = 41.5^o$
ATTENUATIONS (TWO-WAY):
2 dB AT 9.0 GHz
4.3 AT 13.3
6.3 AT 16.0

Figure 3-23. Light rain backscatter versus frequency.

3.3 ANTENNA DESIGN

A preliminary antenna design has been carried out subject to the trade-offs and results of system studies. Several iterations of the conceptual design have led to the result described in the following paragraphs. Where it is considered significant, the rational for particular design choices is indicated. The dimensions of the antenna aperture are determined by a complex of system considerations and tradeoffs including resolution, swath width, gain and transmitter power, frequency, image quality, mechanical constraints, and relative economy and complexity of implementation. Based on the system performance and tradeoff studies described elsewhere (Section 3.2), and a consideration of the mechanical constraints associated with installation and deployment, a nominal aperture of 12 meters by 3 meters is recommended.

The radiating portion of the antenna consists of planar arrays at X- and L-band. The arrays are divided longitudinally into 12 sections or modules, as illustrated in Figure 3-24. The sections of the radiating structure are attached to a thermally isolated support structure by means of flexural supports. The support structure provides the mechanical strength required during boost, launch, and landing and to provide a flat stable surface that will not distort unduly with the varying thermal loads encountered in orbit. The back-up structure will also serve as a thermal shield at the back of the radiating part of the antenna to avoid the effects of a non-uniform, varying, and as yet undetermined thermal environment, encountered during exposure to portions of the Shuttle to the payload, and to space. The flexural supports serve as thermal isolators between the radiating panels and the back-up structure. They also make it possible for the radiating part of the antenna to expand or contract uniformly with temperature relative to the thermally stable back-up structure without inducing bending.

The choice of a planar radiating configuration as opposed to another configuration, such as a curved reflector with line source feeds is predicated in part on the fact that the radiating surface is exposed to space or solar radiation at varying angles, and the use of a planar surface avoids shadowing. Uneven heating or cooling and associated thermal distortions are avoided.

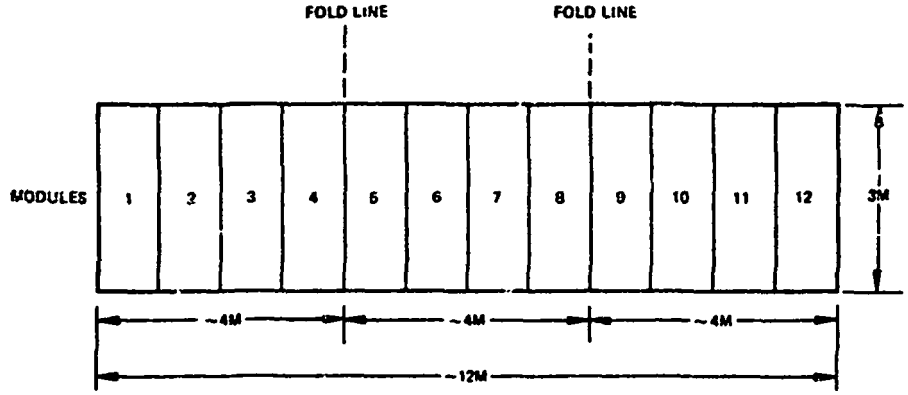

Figure 3-24. Antenna dimensions and locations of fold lines.

Induced distortions are more significant with reflector antennas, since a given displacement from the desired surface changes the distance traveled by a wave from the aperture to the reflector surface and from the surface to the feed, essentially doubling the effect. For the same reason tolerances on reflector surfaces are tighter than those on the flatness of planar arrays.

In the vertical direction the larger portion of the aperture is used for the L-band array, while the lesser portion is used for X-band. In order to provide imagery of the same areas at X-band and L-band the same beamwidths are needed in the vertical plane at both frequencies and for both horizontal and vertical polarizations. The vertical aperture height required for a given beamwidth is proportional to the wavelength or inversely proportional to frequency. For nominal frequencies of 1 and 9 GHz the aperture height for L-band is 9 times that for X-band. Since the X-band aperture is relatively narrow, it is possible to utilize separate apertures for vertical and horizontal polarization. This separation assures good isolation of the polarized beam and avoids losses and complexity without sacrificing much L-band aperture. The resulting division of the aperture is illustrated in Figure 3-25.

The antenna is divided into longitudinal sections or modules, each supported by flextures from the support structures. The division is both mechanical and electrical. Corporate feeds provide bandwidth and each longitudinal section of the antenna has separate feed inputs from a corporate feed for each polarization at each frequency. In addition to the longitudinal division, the L-band and the two X-band apertures are each divided vertically into two sections of unequal height, which provides for the generation of three different beamwidths for each type of polarization. Feeding the narrow section of each aperture produces the widest beam; feeding the wide section produces a beam of intermediate width; and feeding both sections at once provides the narrowest beam.

The calculated 3 dB beamwidths in elevation and in azimuth are given in Table 3-19. The switching that effects the changes in beamwidth is performed at the inputs to the corporate feeds. The two fold antenna has six corporate feed systems, which are illustrated in Figure 3-26. A layout of the feed for the X-band portion of the antenna for horizontal polarization is shown in Figure 3-27. For convenience, the width of the feed waveguide as shown in the figure is not drawn to scale.

The illumination of the antenna is uniform in both the azimuth and elevation directions. The uniformity in the elevation direction makes it possible to change the beamwidth with relatively uncomplicated switching located at the antenna terminals. A detailed examination of system performance shows shaping of the pattern in the elevation direction has little advantage, while it results in a considerable increase in aperture height. It also involves extreme complexity in changing beamwidth. Tapering in the azimuth direction to reduce sidelobes can be done to a good approximation with simple changes in the power distribution of the corporate feed, but this does not appear warranted since some on-axis gain would be sacrificed.

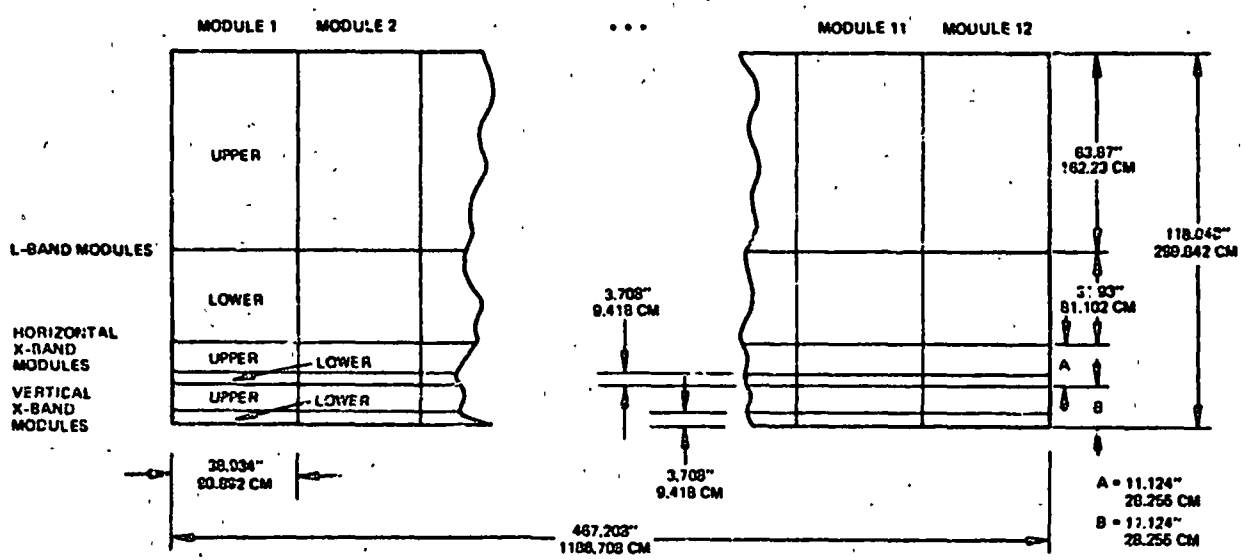

Figure 3-25. Array face – module layout.

TABLE 3-19. CALCULATED 3 DB BEAMWIDTHS – 12 M ANTENNA

Elevation Plane:		
X-Band	Both Arrays	6.29 degrees
and	Upper Array	9.44 degrees
L-Band	Lower Array	8.87 degrees
Azimuth Plane:		
X-Band	0.153 degree	
L-Band	1.287 degrees	

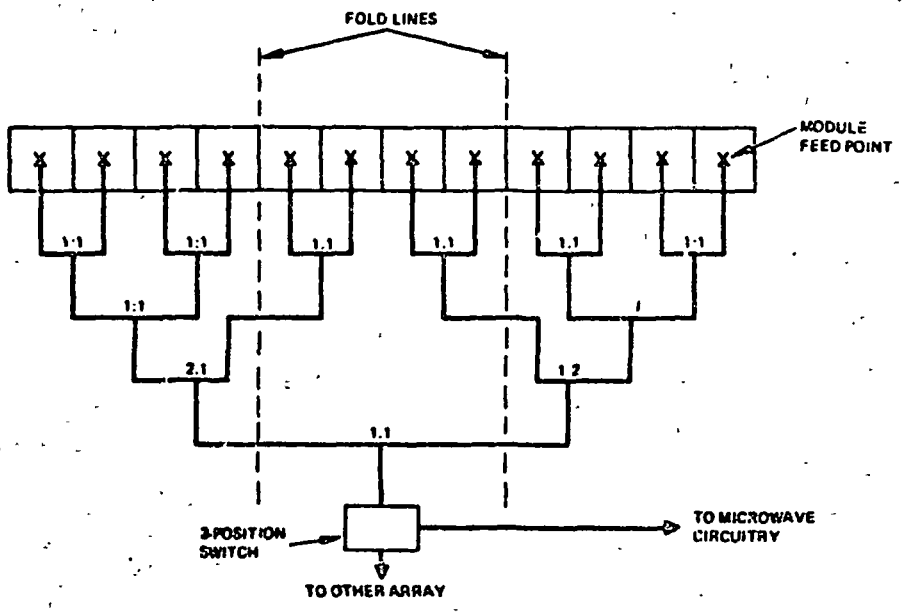

Figure 3-26. Feed schematic.

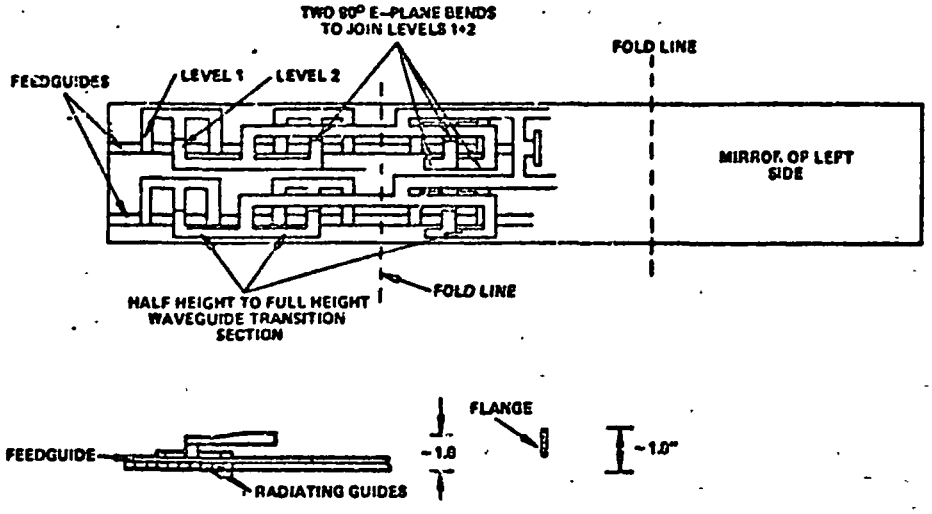

Figure 3-27. X-band feed system horizontal polarization.

Antenna gain figures for the various beamwidth frequencies and polarizations are given in Table 3-20. The table gives the area gain. From this the tabulated total losses are deducted to give the gain values as they would be measured at the antenna output to the receiver or antenna input from the transmitter. The losses include losses attributable to aperture efficiency, feed losses and effects of VSWR. Microwave devices are necessarily inserted between the transmitter and receiver terminals to provide

TABLE 3-20. ANTENNA GAIN – 12 M ANTENNA

		Area Gain dB	Losses dB	Gain dB
X-Band (9 gHz)	Both Arrays	45.79	2.4	43.39
	Upper Array	44.03	2.4	41.63
	Lower Array	41.26	2.4	38.86
L-Band (1.045 gHz)	Both Arrays	36.44	2.4	34.04
	Upper Array	34.68	2.4	32.28
	Lower Array	31.66	2.4	29.26

duplexing between transmitter and receiver, receiver protection, monitoring of the transmitter power, monitoring the power reflected from the antenna terminals, in addition to switching the beamwidth and polarization. Losses for such devices at L-band and X-band are given in Table 3-21 for the representative circuit configurations shown in Figures 3-28 and 3-29. The table includes loss values that would be specified for the procurement of the devices listed and values that could be expected to be obtained typically when so specified. The waveguide losses under item 5 of the table are for sufficient length to run all the way to the antenna from the pallet should that be necessary.

The two senses of polarization at L-band are provided by crossed dipole stripline radiators. Such a radiating element with nearly an octave bandwidth and greater than 30 dB of isolation of polarization is illustrated in the photograph of Figure 3-30. The arrangement of the elements in the L-band aperture is shown in Figure 3-31. The dipoles can be fabricated reproducibly and economically by photographing and etching from metalized board. They can then be sheared from the sheet rapidly and simply. An array of dipoles of one polarization for space application, where the dipoles were fabricated in this way, is shown in Figure 3-32 in a test configuration.

At X-band the RF power requirements are higher than at L-band and RF losses in radiating circuitry and in the long feed lines are generally higher. Losses become more significant and to minimize them a waveguide feed with slot radiators is to be recommended, and stripline and radiating and feed elements such as used at L-band are to be avoided. Both senses of polarization can be provided with broadwall, shunt, slot radiators.

The antenna installation is influenced by several factors. As installed within the shuttle it must withstand the structural loads imposed at launch and boost. It is important that it be accommodated on a single pallet. In orbit the antenna must be deployed and properly oriented. For return to earth it must be replaced within the shuttle, and safely withstand the stresses of landing. In an emergency it should be possible to jettison the deployed antenna.

TABLE 3-21. INSERTION LOSS SUMMARY (DB)

Item	L-Band					X-Band				
	Transmit		Receive			Transmit		Receive		
	Spec	Typ	Spec	One	Two	Spec	Typ	Spec	One	Two
1. Circulator, Ferrite	0.2	0.15	0.2	0.15	–	0.4	0.25	0.4	0.25	–
2. Power Monitor Couplers 2 ea	0.1	0.05	0.1	0.05	–	0.1	0.1	0.1	0.1	–
3. Waveguide Switch, Three Position	0.15	0.1	0.15	0.1	–	0.2	0.15	0.2	0.15	–
4. Receiver, Protector	–	–	0.6	0.5	0.5	–	–	1.2	1.0	1.0
5. Waveguide, Interconnecting	0.15	0.1	0.15	0.1	0.1	0.5	0.5	0.5	0.5	0.5
TOTAL	0.6	0.4	1.2	0.9	0.6	1.2	1.0	2.4	2.0	1.5

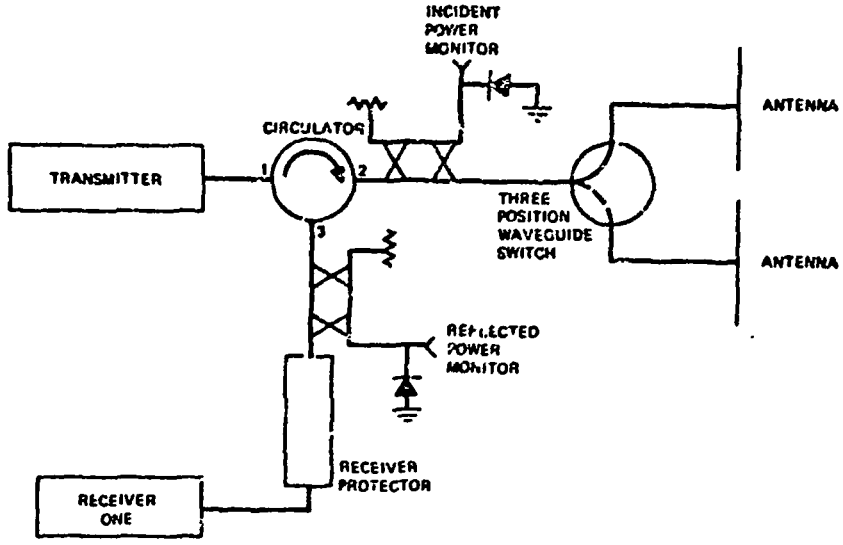

Figure 3-28. Microwave block diagram.

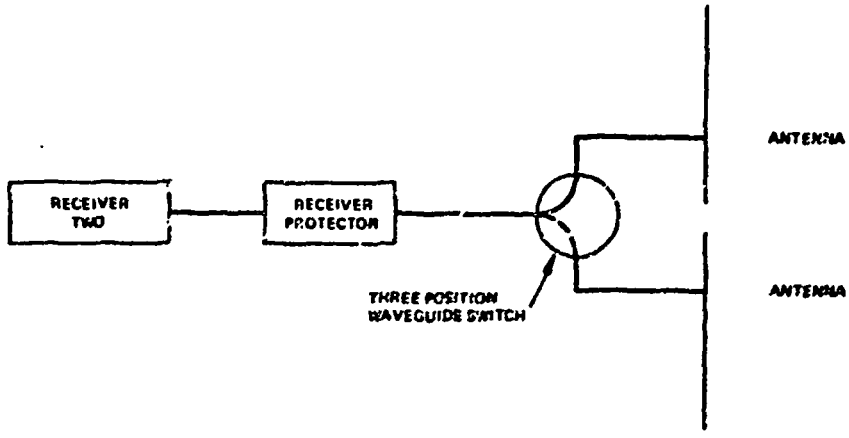

Figure 3-29. Receiving only.

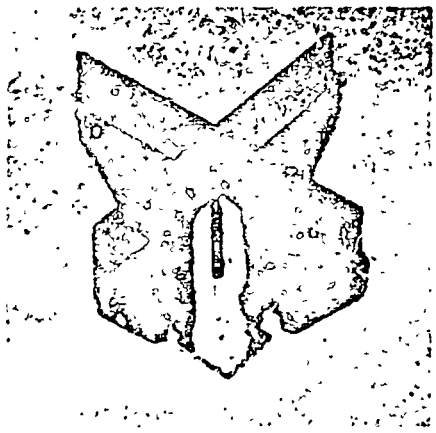

Figure 3-30. Crossed dipole.

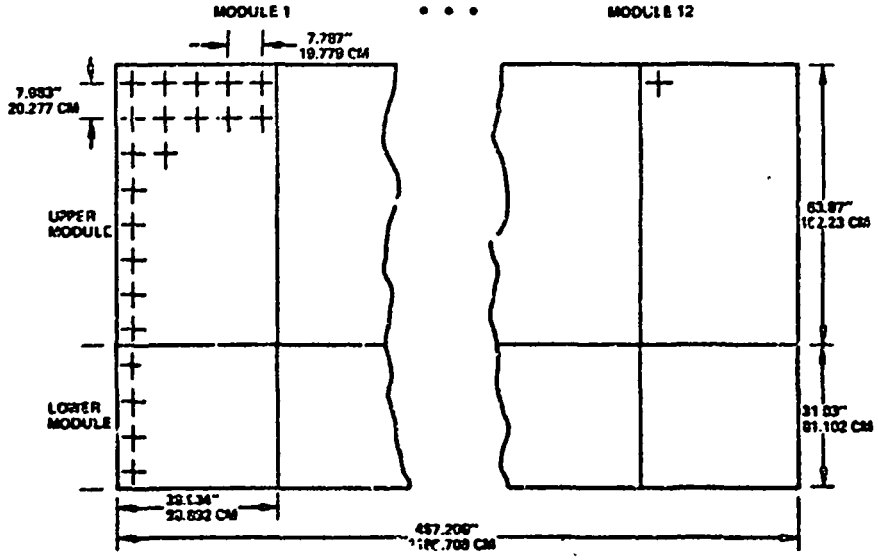

Figure 3-31. L-band element arrangement.

Figure 3-32. Dipole array.

For a nominal antenna size of 3m x 12m, it is necessary to fold the antenna about an axis that is perpendicular to the long dimension. One fold at the mid point could result in a package of about 6 meters by 3 meters and two folds would give a stowed configuration approximately 3 meters by 4 meters, which could fit on a single pallet.

Several ways of mounting and deploying the antenna have been considered. A configuration with a single fold that would require two pallets for storage is illustrated in Figures 3-33 and 3-34. As shown in the figure for deployment, the antenna would be rotated about an axis parallel to one edge and parallel to the longitudinal axis of the shuttle. It would then be unfolded about a hinge line perpendicular to the long dimension.

A second arrangement deployed from a single pallet is illustrated in Figure 3-35. For storing an antenna with a long dimension of nominally

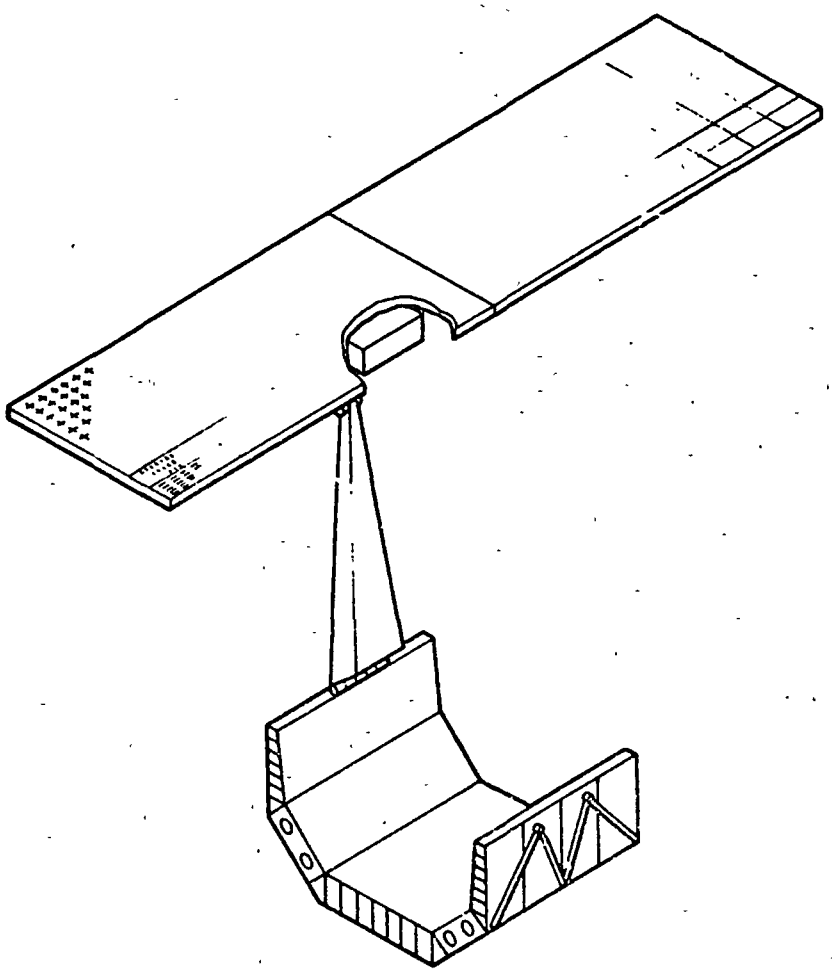

Figure 3-33. Single-fold fully deployed antenna.

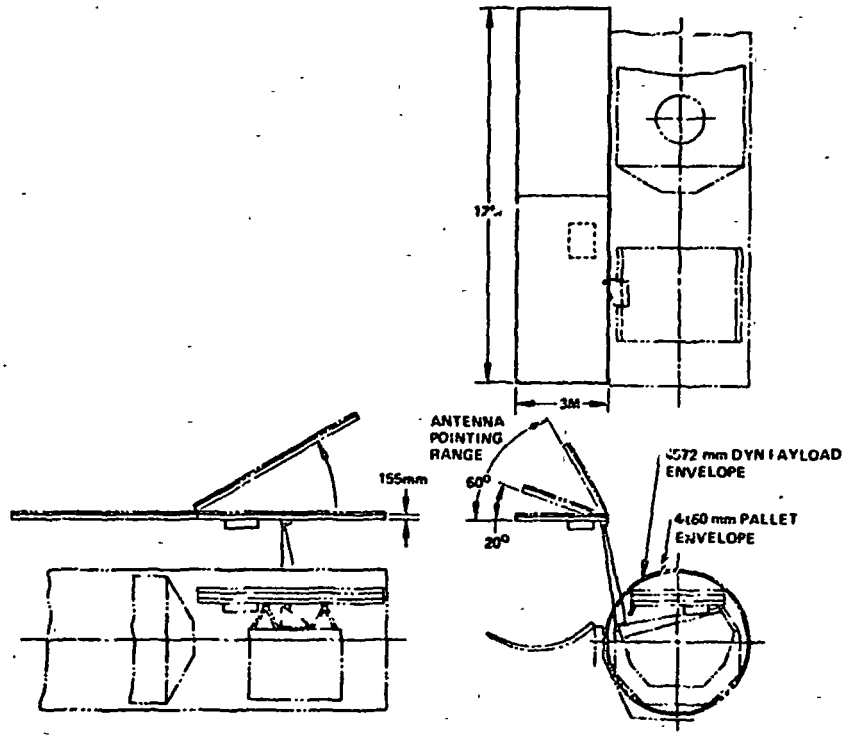

Figure 3-34. Fully deployed antenna single fold.

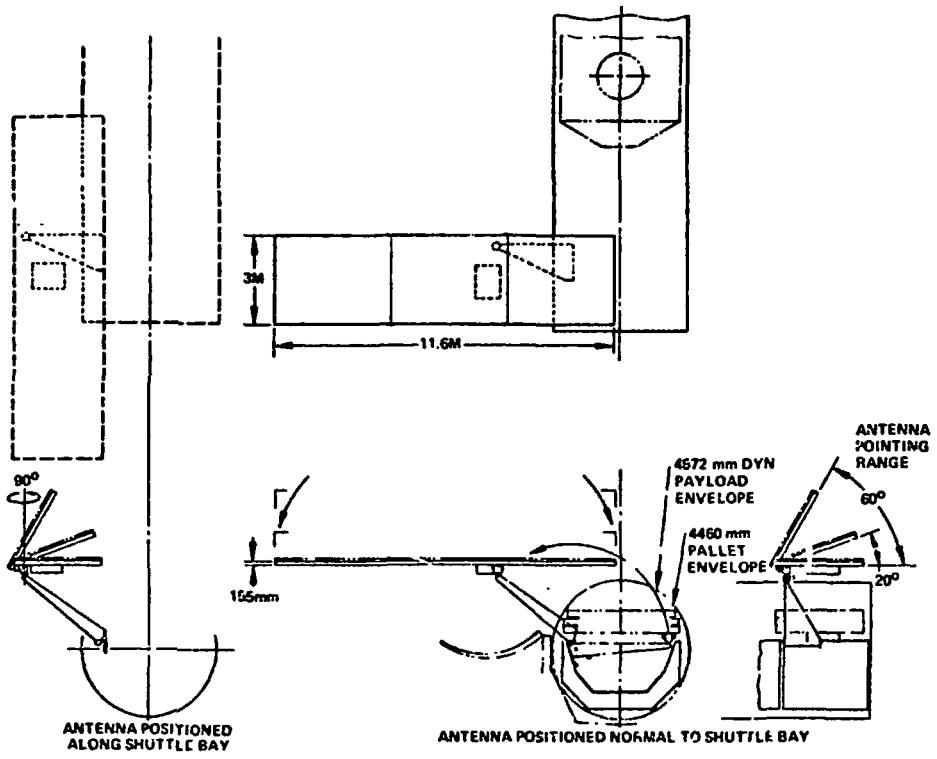

Figure 3-35. Fully deployed antenna dual fold.

4 meters on a single pallet two folds are necessary. The antenna and its support structure would be rotated out of the payload bay on a deployment arm and then unfolded. Following unfolding the antenna would be situated with the long axis transverse to the shuttle's longitudinal axis. Use in this position requires that the shuttle fly sidewise. At the cost of additional mechanism the antenna can be rotated through 90^{o} so that the long axis is parallel to the longitudinal axis of the shuttle as also shown in the figure.

A third configuration is shown in Figures 3-36 and 3-37. This arrangement is simplest in that following unfolding the antenna is simply rotated about the leading edge to give the desired elevation angles. The configuration is restricted to use with sidewise shuttle flight. As can be seen from the figure the aperture is unobstructed at an angle of 60 degrees off the nadir if one pallet length intervenes between that on which the antenna

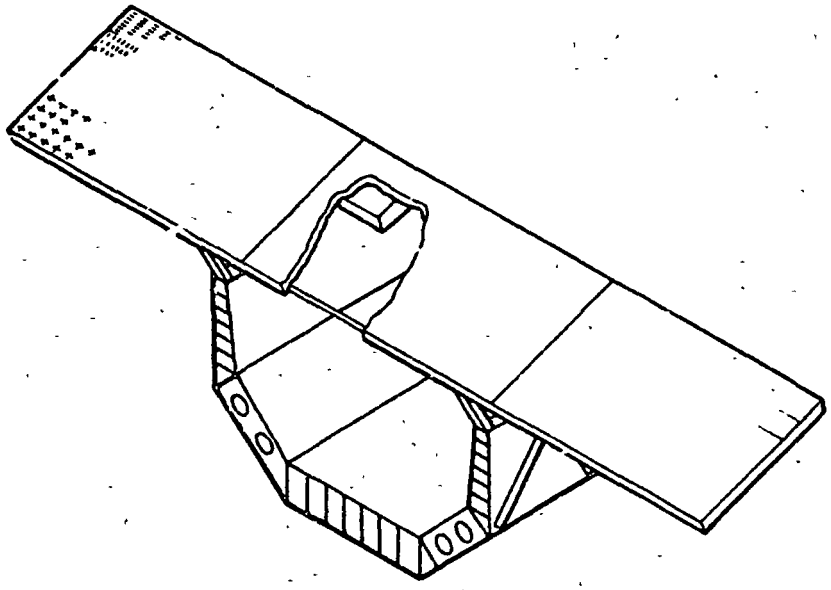

Figure 3-36. Deployed dual-fold antenna.

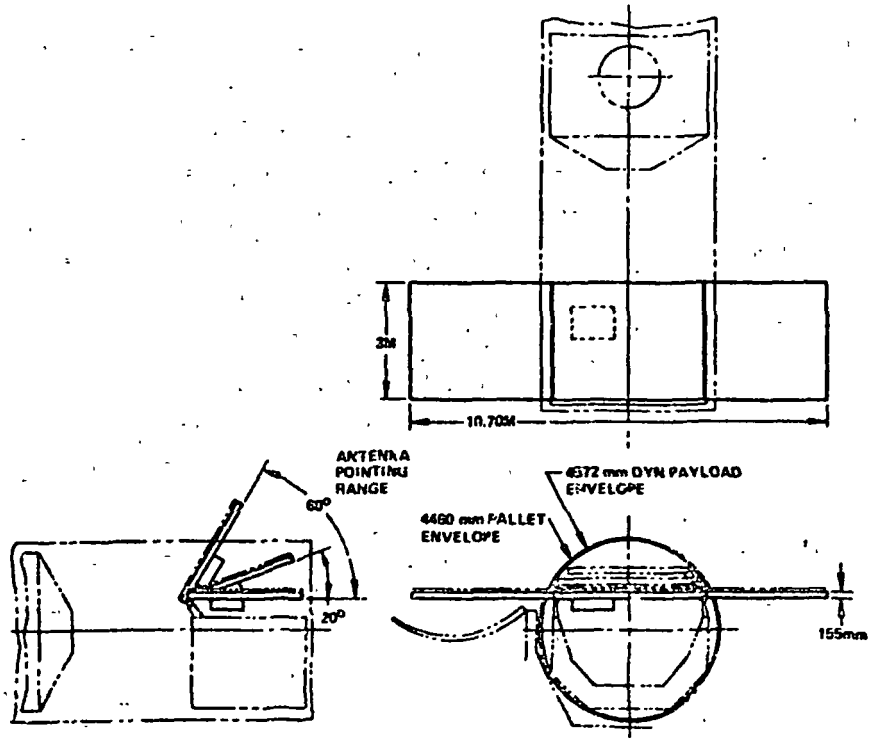

Figure 3-37. Partially deployed antenna dual-fold.

is mounted and the after end of the space laboratory and if nothing on the intervening pallet projects in front of the antenna.

In the configurations as illustrated by the figures, the receiver and the transmitter, high voltage power supply and associated low voltage circuitry are shown as mounted on the back of the antenna on a cold plate. The objective of so mounting this equipment is to eliminate the losses of rf transmission from the pallet to the antenna and the losses and complexity of rotary joints. Power, control signals, receiver outputs, and coolant would be carried in lines within or along the deployment arm. Service loops are contemplated to avoid slip rings or rotary joints.

An accurate weight for the antenna cannot be obtained until a substantial portion of the detailed structural design is completed. The weight has been estimated, however, by comparison with a previously constructed large X-Band antenna, approximately 8 meters long. The weight per unit aperture area of this device was 20.3 kg/m^2. A major portion of that weight was in the structure used to support the antenna, which was cantilevered from one end when folded once. Using 20.3 kg/m^2 value gives a weight of 731 kg for a 3m x 12m antenna, without allowing for weight of the deployment mechanism. The addition of 158 kg (350 lbs) as an estimate for the transmitter and receiver package would give an on-pallet weight of 889 kg. Considerable reduction below this figure should be practicable, but it is not entirely clear without more detailed structural and balance considerations with more firm inputs relative to dynamics and allowable loads on the shuttle whether in fact mounting the transmitter and receiver package on the back of the antenna gives the optimum configuration.

Several aspects of the design have not yet been assessed in the detail necessary for final design. This assessment is dependent on parameter data not yet available, including the following: The effects of the exhaust plumes from the reaction control system, the dynamic effects of the RCS which need to be accounted for in the structural design, the thermal environment, the possible effect of the antenna on the shuttle heat rejection system, and of course the structural detail depending upon the dynamic inputs at the pallet.

3.4 TRANSMITTER DESIGN

3.4.1 Introduction and Problem Statement

The Spacelab radar requires X and L band transmitters of relatively high peak and average power. These power levels would present little risk in terrestrial equipment, but the Spacelab application requires the solution of several problems unique to a space environment. Among these are high power microwave breakdown in antenna, feed, and other microwave components; breakdown in high voltage portions of the power conditioner; and cooling of high voltage components in the absence of convection.

Although equipment operating at these power levels has not to our knowledge been successfully flown in space, several design studies have examined the problems of high power transmitters in long-term orbital missions. Many of the findings are applicable to the Spacelab mission, although the short-term nature of the Spacelab mission requires some modification of the solutions to the design problem.

This section deals with transmitter design and the attendant design problems. The requirements of the Spacelab transmitters are summarized. A baseline design that meets these requirements is then described. It is a design that represents a good compromise among solutions that must satisfy competing criteria. Finally, alternate design approaches that utilize other compromises in meeting these functional requirements are discussed. In addition, the impact of meeting different requirements (e.g., different power levels) is also discussed.

3.4.1.1 Transmitter Functional Requirements

Electrical Requirements. The transmitter electrical requirements are summarized in Table 3-22.

Environmental Requirements. Environmental requirements are summarized in Table 3-23.

Reliability. While not specified, reliability is assumed to be 98 percent probability of success for 30 day mission after 100 hours of ground

TABLE 3-22. TRANSMITTER ELECTRICAL REQUIREMENTS

	L-Band	X-Band
Peak power (kW)	6.8	17
Center frequency (GHz)	1.04	9.0
Bandwidth (MHz)	75	75
RF drive (max) (W)	6.8	0.2
Pulse width (μs)	15-25	15-25
PRF (Hz)	1200-1800	1200-1800
Duty factor (max)	2.9%	2.9%
Average power at max duty (W)	200	500
Prime power voltage vdc	30 ±2.5	30 ±2.5
Prime power consumption (max) (kW)	4 kW total	4 kW total

TABLE 3-23. TRANSMITTER ENVIRONMENTAL REQUIREMENTS

Pressure: On-Orbit	1.4×10^{-5} to 1×10^{-10} Torr
Launch	Sea level to 8×10^{-6} Torr
Vibration, Shock, Humidity, Salt Spray, Radiation	Per JSC 07700 V. XIV Rev. C and Spacelab Payload Accommodation Handbook
Cooling Provisions:	
Cold Plate Temperature	24-40°C
Maximum Heat Load	2.5 kW*

*Up to 4.85 kW is available for all Pallet Experiments. 2.5 kW is preliminary allocation to transmitter.

testing operation. The duty cycle in orbit is assumed to be ten percent (100 on-off-cycles).

3.4.1.2 Interface With Spacelab

The Spacelab transmitter uses a significant percentage of the available Spacelab prime power and thermal dissipation capabilities. Therefore the interface between the transmitter and Spacelab must be carefully considered in the transmitter design process. The interface design is based on information obtained from References 1 and 2. Some of the more important characteristics of the interface are discussed in the paragraphs below.

Electrical Interface. All prime power utilized by the Spacelab is supplied by a dedicated fuel cell with a capacity of 7 kW of average power or 12 kW of peak power at 26-32 volts DC. Peak power is available at a duty cycle of 15 minutes three times a day. With the Spacelab in the pallet/module configuration, the power available for all Spacelab experiments, after allowances are made for Spacelab subsystem consumption, is 4 kW average and 9 kW peak. The information on the portion allocated to the radar experiment is not now available. However it is assumed that 5 kW is available to the radar and 4 kW to the transmitter. This is a conservative estimate considering the low duty cycle of radar operation. As will be shown subsequently the transmitter will use considerably less and still meet its operating requirements.

This power is available at either 26-32 volts DC or at 115 volts—400 cycle regulated three phase AC. The total power available on the AC bus appears to be insufficient for transmitter use, and there is no particular advantage in using it from a total power consumption standpoint.

The characteristics of the prime power supply, such as impedance, ripple and allowable current waveform have not been specified in detail but must be considered in completing the detailed design. In particular, the load current waveform is important in this application because the radar transmitter is inherently a pulsed load. The prime power bus current drawn by the transmitter can be expected to have strong AC components at the system PRF.

Thermal Interface. The only cooling provision available to the transmitter is the pallet cold plates. As pointed out below, it would be desirable to have a supply of liquid coolant available for the transmitter, for two reasons. First, this would allow mounting the transmitter on the back of the antenna which is desirable because it minimizes RF losses, helps counterbalance the antenna during deployment, and removes the requirement for a high power RF rotary joint. In addition, the transmitter tubes utilize liquid cooling. Thus, it would be desirable if liquid coolant were available from the Spacelab thermal control system. However, such availability is not assumed and the design is based on providing a liquid cooling loop to transfer heat from the transmitter to the pallet cold plate. With the Spacelab in the pallet/module configuration the thermal control system can accommodate a sustained heat load of 4.85 kW from the pallet experiments. To provide for a condition in which the combined heat load of all the pallet experiments exceeds 4.85 kW, heat capacitors are provided to store excess waste heat for subsequent rejection to the orbiter ATCS.

Alternate Interface if Igloo is Used. The preceeding discussion of the thermal interface assumed that the transmitter modules were mounted either on a cold plate attached to the antenna or on the pallet cold plate. One possible alternate configuration is to package the transmitter in the igloo provided by Spacelab. In this case, 1.5 kW of heat rejection is provided by an integral dry nitrogen cooling loop. A liquid cooling loop, however, would still be required by the transmitter power tubes. The dry nitrogen at one atmosphere of pressure would also serve as the high voltage insulation medium for the transmitter.

3.4.1.3 Key Design Issues

Radar transmitters at high peak and average power levels that are intended for terrestrial operation present few design problems compared to spaceborne transmitter. The technical problems encountered in designing a spaceborne transmitter are compounded by the lack of convective heat transfer in the gravity free space environment and by the problem of electrical breakdown at reduced pressure levels. These problems are discussed in the following paragraphs.

High Power Microwaves in Space. At the power levels utilized for microwave operations in space, breakdown can be expected in microwave transmission lines and components unless special precautions are taken. Two breakdown phenomenon are of interest, namely: ionization breakdown and multipacting. The power level at which ionization breakdown occurs is pressure dependent and is at a minimum in the pressure range of 1-10 torr for air. The breakdown power in this range is very low, on the order of 3 kW for WR-90 waveguide. The breakdown threshold rises for higher pressure or better vacuum. For pressures less than the maximum of 1.4×10^{-5} torr specified in orbit, the ionization breakdown threshold is theoretically adequate for these power levels. It is very difficult however, to guarantee sufficiently low pressure levels because of outgassing in confined spaces. One possible method of avoiding critical pressures is to vent waveguide and microwave components so that the pressure could be low enough to avoid ionization breakdown. This pressure would be on the order of 10^{-3} torr. If this approach were taken, the possibility of multipacting discharge would have to be considered.

An alternative approach is to pressurize the microwave circuitry. In a long-term space mission, this presents a considerable problem because of the difficulty in keeping leak rates very low. In this application, however, the mission time is short, which makes pressurization practical and straightforward. In addition, it solves the major drawback of vented vacuum systems; the possibility of local pressure buildup due to outgassing.

High Voltage in Space. The transmitter power supplies produce voltages up to 18 KV. The power supplies must be packaged in a way that prevents ionization breakdown. This can be accomplished either by thoroughly venting the equipment ("vacuum dielectrics") or by introducing a suitable dielectric medium. Each of these approaches has its advantages and disadvantages; these are summarized in a subsequent section.

The production of significant average power at high voltage imposes additional problems. The major heat removal mechanism of fluid dielectrics-convection-is absent in a gravity-free environment. Therefore either artifical convection must be provided by circulating a fluid, or else conduction must be used as the primary heat transfer mechanism.

Design Premises. Design of high power, high voltage equipment for space applications involves tradeoffs among several competing technologies. Resolution of these tradeoffs requires judgments concerning the relative emphasis to be given different aspects of transmitter performance, and this in turn is influenced by objectives. The major objective for this effort has been a simple, reliable design that involves minimum development risk. The design employs a liquid dielectric for the high voltage circuitry. While gas or solid/vacuum systems might offer some advantage in terms of weight, the technology of the oil dielectric system is much more mature and entails significantly less risk.

The baseline design approach utilizes pressurized transmission lines between the transmitter and antenna manifold. It is not expected that pressurization will be required in the antenna since the power levels are reduced to safe levels after power division in the RF manifold. The primary transmission line must handle full transmitter power and should be pressurized to eliminate any possibility of ionization breakdown. Critical components susceptible to breakdown are the duplexer devices which contain ferrite material. In the absence of pressurization it is very likely that this material will outgass sufficiently to initiate ionization breakdown at the peak power levels involved.

In a long-term space mission, pressurization would require the solution of difficult problems in sealing the microwave assembly, but these problems are not significant for the Spacelab mission. The alternative approach of venting the microwave assembly carries the risk of breakdown caused by outgassing (particularly serious in a short mission) and would require considerable component development and evaluation.

With the required RF power levels and the prime power believed available, efficiency, while an important transmitter parameter, is not a crucial one. Accordingly, we have designed for high efficiency, but not at the expense of reliability. This is reflected in the relative simplicity of the power conditioner circuitry.

It was decided to make the L-band and X-band transmitters as independent as possible. The power conditioners of the two transmitters offer

relatively little opportunity for commonality, and separating the two transmitters provides significant advantages for ground checkout and trouble-shooting. It also isolates the effects of failure modes, making it possible for operation to continue with one transmitter in the event the other fails.

3.4.2 Baseline Transmitter Designs

L-band and X-band transmitters have been configured to satisfy the functional requirements. Their major features are summarized below:

- Grid-Modulated Klystron Power Amplifier at X-Band
- TWT Power Amplifier at L-Band
- Oil-Dielectric High Voltage Circuitry
- Pressurized Waveguide and Microwave Circuitry
- Transmitter Mounting on the Rear of the Antenna

The details of the designs are discussed below.

3.4.2.1 L-band Transmitter

The major parameters of the L-band transmitter are summarized in Table 3-24. Its block diagram is shown in Figure 3-38. It uses a periodic permanent magnet focussed TWT power amplifier, whose major parameters are summarized in Table 3-25. This tube was selected because:

- It provides good efficiency (30 percent undepressed, or 35 to 40 percent with single collector depression)
- Its grid modulation capability is compatible with the PRF and pulse width flexibility required for this application.
- It is lighter and has a more favorable form factor than comparable L-band klystrons and cavity amplifiers.
- Its high gain eliminates the need for any other tube in the transmitter; it can be driven by a solid state amplifier.
- Involves only modest scaling of a production TWT (L-5476)

The tube output is protected against poor output VSWR by a three-port coaxial circulator. A second circulator followed by a diode switch-limiter receiver protector, performs the duplexing function. Incident and reverse power monitoring couplers are provided for protection and monitoring

TABLE 3-24. L-BAND TRANSMITTER PARAMETERS (TWT)

RF center frequency	1040 MHz
RF bandwidth	>75 MHz
Peak RF power	6.8 kW
Max duty	2.9 %
Max average power	200 watts
Pulse width	15-25 μs
PRF	1200-1800 Hz
Transmitter efficiency	28 %
Max prime power consumption	714 watts
Waste heat	514 watts
Transmitter weight	52 KG

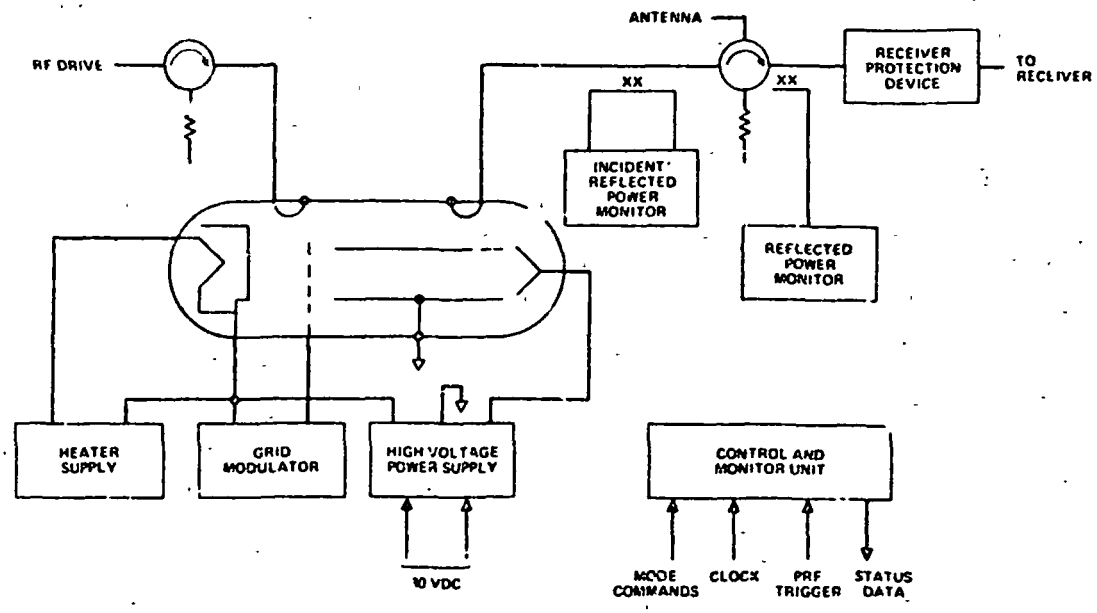

Figure 3-38. Transmitter block diagram.

TABLE 3-25. L-BAND HIGH VOLTAGE POWER SUPPLY PARAMETERS

Cathode voltage	9.5 kW
Peak cathode current	2.05 A
Average power output	570 W
Efficiency	80%
Prime power consumption	712 W
Waste heat generated	142 W
Weight	20 kg
V_K regulation	±0.5%
V_K droop	0.5%
Switching frequency	5 kHz

purposes. All these microwave devices are well within the state of the art and would require relatively little development for this application.

High Voltage Supply. The high voltage power supply block diagram is shown in Figure 3-39. Its major parameters are summarized in Table 3-26. Unregulated DC from the space shuttle is converted to an intermediate bus voltage of 150 VDC by a pulse-width modulated converter. This voltage is then used to drive a DC-DC converter which generates the cathode and collector voltages. Use of a straight (non-PWM) converter for this function avoids the need for LC-filtering of the high voltage rectifier outputs. The converter transformer drives a voltage doubler and a full wave rectifier whose outputs are placed in series to produce the 9.5 KV cathode voltage. This configuration provides good regulation while maintaining an acceptably low primary: secondary turns ratio.

The collector operates at about 35 percent depression. It is decoupled from the cathode reservoir capacitor, C_B, by diode D. C_B need only supply the TWT body current, and thus very low droop can be achieved with a reasonable size capacitor. The collector current is furnished by the voltage doubler output capacitors. Since collector voltage is much less critical,

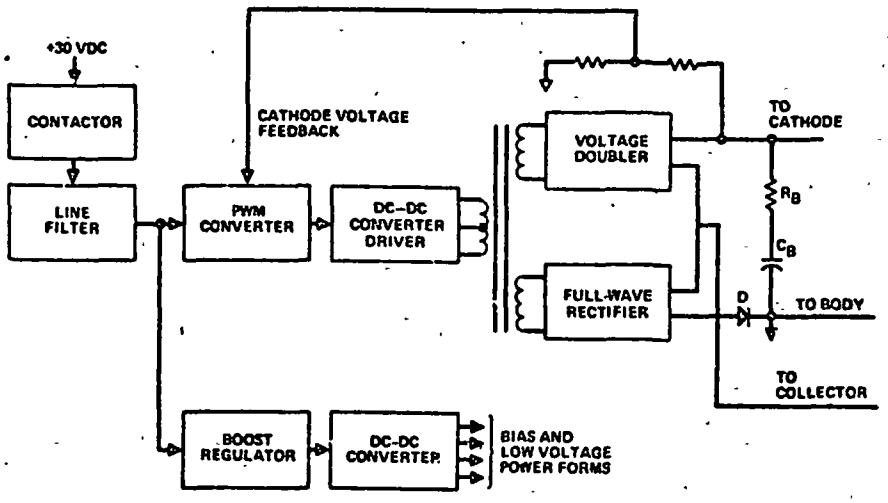

Figure 3-39. L-band TWT high voltage power supply block diagram.

TABLE 3-26. X-BAND TRANSMITTER PARAMETERS

RF center frequency	9 GHz
RF bandwidth	75 MHz
Peak power	17 kW
Max duty	2.9%
Max average power	500 watts
Pulse width	15-25 μs
PRF	1200-1800 Hz
Total efficiency	36%
Prime power consumption	1390 watts
Waste heat	890 watts
Total weight	91 KG

the collector voltage can be allowed to droop much more than the cathode voltage, and thus the capacitance needed to supply collector current in this configuration is much less than would be needed if collector and cathode were supplied from a common reservoir and the collector droop were determined by cathode droop limitations.

The cathode voltage is regulated by feeding back a sample of the cathode voltage to the PWM converter. This converter also incorporates a feedback current limiter to minimize prime power bus current transients.

A separate regulator and converter supplies low voltage power forms to the transmitter power conditioning circuitry. One of these is 150 volts regulated for the grid modulator and heater supplies.

Heater Supply. The heater supply is shown in Figure 3-40. The heater voltage is supplied by a DC-DC converter, whose output floats at cathode potential. The output voltage from the converter is sensed by a feedback winding on the converter transformer and used to control the converter input voltage. This configuration provides regulation on the order of 2 percent without direct sensing of the heater voltage, thus eliminating the need for sense circuits floating at high voltage.

The heater supply output voltage can be adjusted by changing the reference voltage for the feedback loop. Tube-to-tube variation in heater voltage requirements can thus be satisfied without adjusting any components in the high voltage portion of the supply.

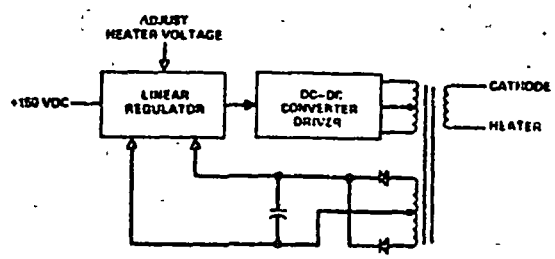

Figure 3-40. Heater supply block diagram.

Grid Modulator. A block diagram of the grid modulator is shown in Figure 3-41. Its outstanding feature is the absence of any active devices floating at high voltage. A DC-DC converter incorporating the transformer T1 establishes a B+ voltage equal to the desired grid "on" voltage with respect to cathode. It also establishes a voltage that is about 150 V negative with respect to cathode (the grid bias voltage).

In the interpulse period, the secondary voltage of transformer T2 is zero, diode D does not conduct, and the grid is held at the bias voltage. When the TWT is pulsed on, a pulse applied to T2 swings the grid positive until D conducts. The grid is then clamped to the B+ voltage for the duration of the pulse, removing the effects of ringing, overshoot, and droop attributable to T1. At the end of the pulse, the voltage across the secondary decays and reverses, D stops conducting, and the grid voltage returns to the bias level (it overshoots the bias level slightly until the core of T2 resets). The clipping action results in a very clean grid pulse.

The grid pulse voltage must be controlled to close tolerances. It is determined by the B+ voltage generated by the DC-DC converter. This voltage is regulated in a manner similar to that in the heater supply, in which the voltage from a feedback winding on the converter transformer is used to adjust the converter input voltage. Adjustment of the reference for this feedback loop allows the grid voltage to be adjusted for tube-to-tube variations.

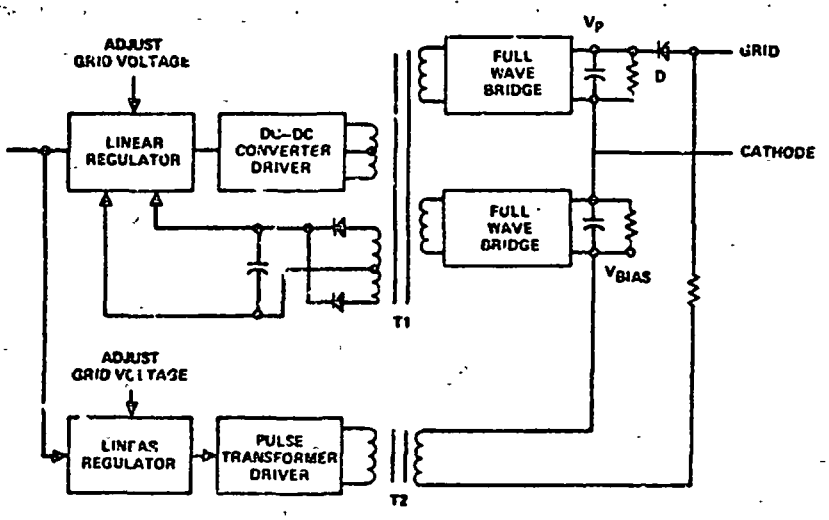

Figure 3-41. Grid modulator block diagram.

Because the output of this converter is at a higher voltage than that of the heater supply, (resulting in a turns ratio nearer unity and smaller diode drop effects) the voltage accuracy of this converter is better than that used in the heater supply; typically it is one percent.

The pulse transformer is driven by a saturated transistor switch. The pulse voltage is adjusted by varying the driver supply voltage. While not strictly necessary, allowing adjustment of the PT voltage reduces the range of load currents which must be accommodated by the converter and thus reduces power dissipation in its bleeder resistor, R_B. Since this component floats at high voltage, minimization of its dissipation is desirable.

The PT driver is driven by a pulse generated by the synchronizer portion of the transmitter's control and monitor circuitry. A duty cycle limiter is incorporated in the low-level portion of the modulator to protect the tube from anomalous operating conditions.

Control and Monitor. The block diagram of the control and monitoring unit is shown in Figure 3-42. It performs the following functions:

1. Mode Sequencing: Orderly application and removal of TWT voltage forms with appropriate delays, either in response to

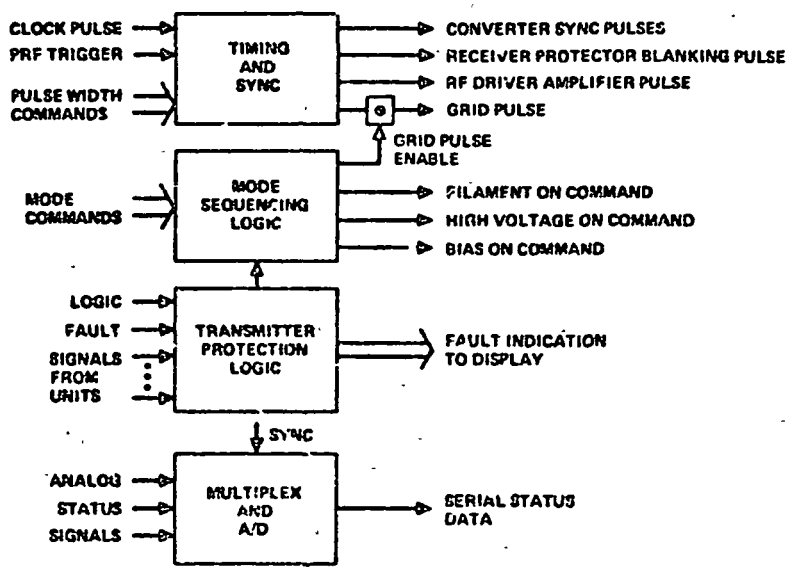

Figure 3-42. Control and monitor unit.

system turnon/turnoff commands or in response to fault conditions.

2. Fault sensing: Sensing of conditions which could damage the TWT or power supplies; also generation of appropriate mode change commands in response to the fault signals.
3. Status monitoring: Monitoring of transmitter parameters for purposes of fault isolation, checkout, and to gather long-term trend data.
4. Synchronization: Generation of the transmitter gate pulse, receiver protection device blanking pulse, and converter sync pulses, given a clock and PRF trigger generated by the radar processor.

Mode sequencing involves the modes defined below:

Dormant (D)	—	Transmitter completely off
Standby (S)	—	Heater and bias supplies energized
Ready (R)	—	Heater, bias, and high voltage supplies energized
Transmit (T)	—	Same as ready, but with TWT pulsed at the system PRF.

In the normal, turn on sequence, the transmitter changes from one mode to the next with the following delays:

D → S:	10 sec.
S → R:	10 minutes (allows heater warmup)
R → T:	10 sec (allows stabilization of high voltages)

Sequencing in the reverse order at turnoff involves no delays.

Reaction to fault conditions involves a sequence to a lower order mode with no delay. After this sequence is performed, the transmitter "locks up" and requires a reset command to clear the fault before it can be resequenced to an operational mode.

The fault signals to be monitored must be selected with care since monitoring an excessive number of signals can reduce reliability because of failure modes in the fault circuitry. The fault signals selected for this transmitter are as follows:

Signal	Fault Condition	Action in Response to Fault
TWT body current	Overcurrent	Return to Standby
Reflected power	Overpower	Return to Ready

Signal	Fault Condition	Action in Response to Fault
Cathode voltage	Overvoltage	Return to Standby
Prime power bus current	Overcurrent	Return to Dormant

The monitoring function samples a number of analog signals, converts them to digital form, and transmits them to the module bay electronics where they are multiplexed into the radar data stream and recorded on tape. They are also available for display from the operator's console. The signals to be monitored include: RF Output Power; RF Reflected Power, Cathode Voltage; TWT body current; Prime power bus voltage and current; PWM converter output voltage; and selected temperatures.

Other signals would be added in the detail design phase of the program.

The synchronization function accepts a clock, PRF trigger, and pulsewidth command, and generates internal timing signals for other C/M functions as well as the transmitter gate pulse for the modulator and a blanking pulse for the receiver protection device, which overlaps the transmitter gate pulse.

The design of the control/monitor unit is straightforward, using TTL MSI logic. LSI may well offer significant advantage in the time period in which this transmitter is to be constructed; its use should be considered at that time.

Physical Design. The high voltage portions of the power supply, modulator, and heater supply are packaged in a sealed container filled with dielectric oil (Wemco C). A spring-loaded bellows permits thermal expansion of the oil and maintains a positive oil pressure to prevent outgassing. A typical package of this type, designed for space application, is shown in Figure 3-43.

Thermal analyses of a similar power conditioner indicate that the insulating oil provides sufficient heat conduction to maintain the component temperatures within reasonable limits, allowing the high voltage module to be cooled by conduction through its mounting surface.

The low voltage portions of the high voltage supply, heater supply, modulator, and the control/monitor are mounted in a second module, which is cooled by conduction through its mounting surface.

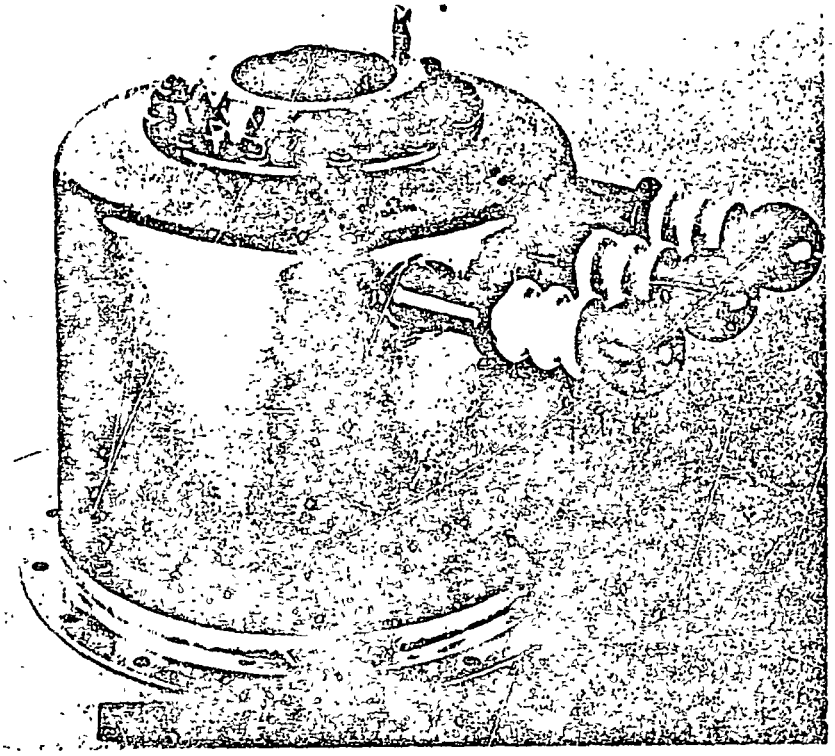

Figure 3-43. HVPS component (packaged in sealed container).

The TWT, the two power conditioner modules, and the microwave components are all mounted on a cold plate, which is in turn mounted on the back of the antenna. The cold plate temperature is controlled by a cooling loop, which circulates coolant through the transmitter cold plate, the TWT, and a heat exchanger which is cooled by the spacelab cold plate.

Mounting the transmitter on the back of the antenna reduces RF losses and avoids the need to use a rotary joint for handling the full RF power.

3.4.2.2 X-Band Transmitter

The X-band transmitter's major parameters are summarized in Table 3-27. Since its design is very similar to that of the L-band transmitter; only the differences are discussed below.

TABLE 3-27. X-BAND TRANSMITTER PARAMETER SUMMARY

Center frequency	9 GHz
Peak RF power	17 kW
Average RF power	500 W
RF bandwidth	75 MHz
RF drive (max.)	0.6 W
Pulse width	15-25 μs
PRF	1200-1800 Hz
Duty factor	2.9%
Transmitter efficiency	36%

The klystron high voltage power supply differs from the L-band unit in the absence of collector depression. The function of diode D (Figure 3-39) is the same as the L-band unit – to decouple the collector from the cathode reservoir capacitor C_b. Thus, C_b need only supply the body current and very low cathode voltage droop can be achieved with a reasonable size capacitor.

The transmitter block diagram is the same as the L-band transmitter shown in Figure 3-37. It uses a klystron as its power amplifier; its major characteristics are summarized in Table 3-28. The klystron output feeds a four-port, differential phase shift circulator which serves both to isolate the klystron and perform the duplexing function.

Several devices have been considered as receiver protection devices. A multipactor/diode limiter has been tentatively selected since it provides the best combination of power handling capacity and reliability. A ferrite/diode limiter is also attractive for the purpose. It has the advantage of not requiring auxiliary power forms, but such devices are not now capable of operation with a 500 watt average power transmitter.

The klystron operates at 17.8 kv and 500 W average power, compared to 9.5 kv and 200 W for the L-band TWT. The high voltage portion of the power conditioner will be correspondingly larger to standoff higher voltages. The high voltage power supply DC-DC converter will use three voltage doublers to obtain the higher cathode voltage. Otherwise, the basic designs of high voltage supply, heater supply, modulator and control monitor, are the same as for the L-band unit.

The X-band and L-band transmitter components are mounted on the same cold plate. The X-band klystron is cooled by liquid convection while the L-band TWT is cooled by conduction cooled. Thus, the liquid cooling loop which cools the cold plate is also routed through the klystron before returning to the heat exchanger.

3.4.3 Transmitter Tradeoffs and Alternate Designs

During the process of arriving at the baseline point design a wide range of peak and average power levels were considered. The peak power level is traded off for pulse compression ratio and average power for antenna size, image quality, etc. Rather than configure a transmitter for each point design considered, one transmitter design was configured and the major impact on transmitter design of different peak and average power levels was evaluated.

Different peak and average power levels are reflected primarily in the choice of RF amplifier and certain aspects of the physical design. Many of the circuit concepts developed for the high voltage power supply, grid modulator and control and monitor apply to all power levels considered in the tradeoff matrix. These basic concepts have evolved through years of experience in the design of high reliability high performance transmitters for a wide range of space and airborne applications. The basic tradeoffs required to arrive at these design concepts were performed in numerous design efforts of the past and were not repeated for this study.

The discussion of alternate transmitter designs will start with a discussion of some of the major breakpoints associated with different peak and average power levels.

3.4.3.1 Different RF Power Levels

The RF power levels for the baseline point design are a reasonable compromise between conflicting parameters such as antenna size, power availability, thermal dissipation capabilities, reasonable pulse compression, etc. At this time, it cannot be stated that the baseline point design is the optimum choice for the spacelab transmitter since there is some uncertainty associated with the relative importance of the various system parameters that were traded off in arriving at the point design. For example, there is some uncertainty about power availability if power must be allocated among several spacelab experiments simultaneously. The impact of different peak and average power levels on the transmitter design is discussed in the following paragraphs.

The baseline transmitter design approach is suitable, without significant modification, for a wide range of peak and average power levels. There are breakpoints however, where some modification to the baseline design occurs. These breakpoints will be identified rather than configuring transmitters for all point design considered.

In general, transmitter weight increases as the square root of the average prime power if no breakpoints are passed. If active cooling is available and no weight constraints are imposed, then the only limitation on average power is in its availability. It is desirable however, to minimize the degree to which active cooling is employed. In particular, for transmitters above a certain power level it becomes necessary to circulate the mineral oil in the high voltage containers because of the limited thermal conductivity of the mineral oil and the absence of convective heat transfer in the gravity free environment. The X-band transmitter is felt to be an upper limit for which static conduction through the oil can be used to remove waste heat from the high voltage components. Since the thermal performance may be marginal, it is felt that solid heat conduction paths (e.g., berillia standoffs) should be provided to expedite heat removal from the high voltage circuitry. For power levels much higher than this, the thermal problem becomes critical and artificial circulation of the medium may become necessary. In any event, it is felt that this would be an acceptable and

appropriate solution to the problem if higher power levels are required, in view of the short term nature of the spacelab mission.

The average power capability of transmitter tubes is essentially unlimited if solenoid focussing is acceptable. However this is considered unacceptable for the spacelab radar since the focussing electromagnets require 1-2 kW of power. Thus the average power is constrained by the inherent capabilities of PM or PPM focussed tubes. The L band klystron considered for the baseline design can be designed for average power levels up to 2 kW, and thus a comfortable margin exists. If an X-band TWT is utilized, the average power limit is about 500 watts with present state of the art. The average power limitation of the L-band TWT is 350 watts. If an L-band klystron is utilized, average power levels up to 2 kW can be accommodated with PPM focussing.

Conduction cooling of the RF transmitter tubes is desirable, however, this is not within the state of the art for 500 watts at X-band. About 100 watts of average power is a reasonable upper limit for which cooling the klystron by conduction is practical.

Since L-band waveguide is quite large, a significant saving in weight and volume can be realized through the use of coaxial transmission lines and circulators. The problem that accompanies the use of coaxial transmission lines is the removal of heat from the center conductor. This can be done by using thermally conductive dielectric material for the center conductor support structure. The breakpoint for the L-band coaxial system is provided by the coaxial circulator. Present state of the art for these devices is about 350 watts average.

Raising the transmitter peak power requires increased pressurization in the RF transmission lines to prevent ionization breakdown. There are no breakpoints within the range of peak power levels considered for the spacelab transmitter. Higher RF power levels require the application of correspondingly higher voltages to the klystrons. Again there are no clear breakpoints except that the physical design problem becomes increasingly critical as voltage levels are increased. It is expected that pressurization or solid/potted high voltage interconnections will be required in the space environment between the oil filled bellows containers and klystrons.

To simplify the physical design of the transmitter it is recommended that peak power levels be traded against increased duty factors and pulse compression ratio to the maximum extent that is consistent with the required operational characteristics.

3.4.3.2 Alternate Power Amplifier Considerations

Traveling Wave Tubes at X-Band. The Traveling Wave Tube is one of the most commonly used transmitter tubes in coherent radar systems requiring large bandwidth. Several types of TWT's can be considered. Tubes using helix-derived slow wave structures have minmum cost and very broad band widths. However, difficulties in cooling the slow wave structure limit these tubes to average powers on the order of 100 to 200 watts. Beyond this power level cavity coupled TWT's should be considered. Both PPM and solenoid focusing are used. Solenoid focusing is unattractive for this application because of the large power (1-2 kW) required for the solenoid. PPM focused coupled-cavity tubes, on the other hand, are limited to about 500 watts of power at X-band and thus a PPM focused TWT used in this application would have very little margin between the required average power and its inherent capability.

State of the art efficiency is about 30 percent for X-band TWT's. This can be increased to 35 or 40 percent by using dual depressed collectors and in at least two experimental TWT's it has been increased up to 50 percent with 10 stages of depressed collection. Since efficiency is not considered critical at 500 watts of average power, the complexity of a 10 stage depressed collector TWT/transmitter does not appear warranted for this application.

Klystrons at X-band. If bandwidth requirements do not dictate the use of a TWT, the klystron is an attractive alternative because of its inherent simplicity in design and ruggedness compared to the TWT. its gain and cathode voltage are comparable to those of the TWT and grid-control can easily be incorporated. For these reasons the klystron has been chosen for the baseline design at X band.

A point design which can be scaled within the range of peak and average power levels considered for the spacelab transmitter was offered by Varian Associates of Palo Alto, California.

The klystron is essentially an interpolation between the VKX-7765C and the V24E klystrons. The tube employs permanent magnet focussing which is not amendable to depressed collector operation. High efficiency operation is achieved through a massive permanent magnet which does not have the complexity factor associated with depressed collector design. Using samarium-cobalt magnets, an efficiency of 45 percent is obtained in a tube whose mass is 17 kg. The primary motivation for trading weight for efficiency here is to ease the thermal problems in the high voltage power supply.

The Varian klystron can be provided with average power capabilities up to 2 kW, which exceeds TWT capabilities by a factor of four. Thus a very comfortable design margin exists. Parameters for the baseline klystron are listed below in Table 3-28.

TABLE 3-28. X-BAND KLYSTRON CHARACTERISTICS

Focussing	PM
# cavities	5
Moduation	HI-MU shadow grid
RF center frequency	9 GHz
Bandwidth	75 MHz - 1 dB
Power output	17 kW
Efficiency	45% (undepressed)
Gain	50 dB
Cathode voltage	17.8 kW
Cathode current	2.13 A
Collector depr.	NA
Heater voltage	7 V
Heater current	7 A
Weight	17 kg
Dimensions	30 x 23 x 12 cm

L-Band Klystron. For the peak and average power levels given in the baseline design, the Litton TWT is the optimum choice on account of its low mass and relatively small size. If future tradeoffs lead to higher peak or average power levels, the Litton TWT becomes less appropriate because of its limited power capabilities. An L-band klystron is an attractive alternative since its bandwidth capabilities improve at higher peak power levels.

Average power levels up to 2 kW can be accommodated in the L-band klystron with PPM focussing and liquid cooling. Varian offered a point design at 12.5 kW peak output power. Parameters for this tube are listed in Table 3-29.

TABLE 3-29. L-BAND KLYSTRON CHARACTERISTICS

Focussing	PPM
# cavities	5
Modulation	HI MU shadow grid
RF center frequency	1040 MHz
Bandwidth	25 MHz
Power output	12.5 kW peak/200 W average
Efficiency	35% undepressed; 40% depressed
Gain	40 dB
Cathode voltage	13 kv
Cathode current	2.9A typical, 3.2A maximum
Collector depression	20-30%
Grid pulse voltage	+300 with respect to Cathode
Heater voltage	6.3V
Heater current	6.3A
Weight	18 kg
Dimensions	60 cm x 13 cm diameter

L-Band Cavity Amplifier:

Microwave Cavity Labs of LaGrange, Illinois offered a point design for a 3 stage cavity amplifier whose characteristics are listed in Table 3-30. The primary disadvantage for this design is the requirement for 3 separate regulated high voltage forms. Since the cavity amplifier offers no advantages over the Litton ring loop TWT in terms of efficiency, mass, volume or bandwidth, it will not be considered further for the L-band transmitter.

L-Band TWT

Two TWT's were considered for the L-band transmitter. The first is a high performance experimental TWT made by Watkins-Johnson. This tube features 50 percent efficiency with dual depressed collectors, peak power up to 31 kw and average power up to 500 watts with conduction cooling. The tube was 1.4 meters long and weighed 36 kg. Since L-band efficiency is not considered critical, the tube was rejected on the basis of excess size and mass.

TABLE 3-30. L-BAND CAVITY AMPLIFIER PARAMETERS

RF center frequency	1040 MHz
Bandwidth	50 MHz
Gain	25 dB
Efficiency	35%
Peak power	12 kW
Average power	200 W
Power forms required	
7 kv @ 6A	
5 kv @ 1A	
2 kv @ 0.25A	
# stages	3
Dimensions	46 cm x 35 cm x 20 cm
Weight	16 kg

The second TWT considered is made by Litton. It's performance characteristics are more modest compared to the WJ TWT, however, it is less than 0.5 meters long with a mass of less than 3 kg. Basic tube efficiency is 30 percent increased to 35 to 40 percent with collector depression. The transmitter specific requirements can be met with very modest scaling from off the shelf production tubes. Maximum power level for this tube is 20 kw peak and 350 w average. This tube is selected for the basline design. Parameters for the Baseline Litton TWT are summarized in Table 3-31.

TABLE 3-31. LITTON L-BAND TWT CHARACTERISTICS

Model	L-5476
Focussing	PPM
Slow wave structure	Ring loop
Modulation	High MU grid
Qualifications	MIL-E-5400
Status	Production
Frequency	L-Band
Power output	Up to 20 kW peak/350 W avg
Cooling	Conduction
Undepressed efficiency	30%
Depressed efficiency	35-40%
Depression	35%
Beam perveance	2.2×10^{-6} pervs
Cathode voltage for 6.8 kW, 35%	9.5 kv
Cathode current for 6.8 kW, 35%	2.05 A
Gain	30 dB
Length	50 cm
Mass	2.7 kg
Bandwidth	Up to 20%

There is no equivalent competition for the X-band klystron which is considered the optimum choice for all peak and average power levels considered in the tradeoff matrix.

3.4.3.3 Provision for Higher Efficiency

The transmitters were designed to have good basic efficiency, minimum complexity, maximum ruggedness and reliability, and minimum development cost. These guidelines were adopted because of the relative abundance of prime power aboard the spacelab compared to conventional satellite power sources. The transmitters do, however, consume a significant percentage of the available spacelab resources. In the event that the remaining resources are insufficient to meet the demands of other spacelab users, then an improvement in transmitter efficiency would be warranted.

The klystron power supply efficiency is very nearly optimum and little improvement is to be gained. There is some room for improving efficiency in the RF power amplifier tubes, however. It is felt that with state of the art technology, efficiency as high as 50 percent can be obtained at both X and L bands by using TWT's with multiply depressed collectors. At L-band, this has been achieved in an experimental two collector TWT operating at 30 kw peak and 500 watts average. The tube was '.4 meters long and weighed 36 kilograms. Two experimental TWT's at X-band have achieved 50 percent efficiency by using 10 stage depressed collectors. These tubes are not recommended for the spacelab transmitter except as a last resort in the event that the transmitter prime power consumption proves to be excessive.

3.4.3.4 Use of the Igloo

The Spacelab provides, as off-the-shelf equipment, a pressurized container for use in packaging components that are not being designed specifically to operate in space. The igloo includes approximately 0.7 cubic meters of volume for mounting equipment and an integral thermal control system, which circulates dry nitrogen to provide 1.5 kw of cooling capability.

The igloo may be used in any of several different ways. One is to mount all transmitter and receiver hardware inside the igloo, using one

X-band wave guide feed through and one L-band coaxial feed through. Since the tubes require liquid cooling, additional feed throughs to provide the cooling fluid would have to be installed. The dry nitrogen cooling loop would remove all transmitter waste heat not generated in the tubes. An alternate configuration would be to mount the RF tubes outside the igloo. A disadvantage is the need for high voltage interconnections in the space environment, but this approach does not require waveguide and coaxial feed throughs for the RF energy.

Use of the igloo would probably result in a minimum development cost for the transmitter. However, it is anticipated that wave guide runs and rotary joint in the transmission line between the igloo and antenna would add an additional one db loss to the system budget. It is not felt feasible to attach the igloo to the antenna.

Alternate dielectric systems have been considered for the Spacelab transmitter. These are gas, solid and vacuum. A gas system under one atmosphere of pressure was considered in the approach involving use of the igloo as a container for the high voltage power supplies. The nitrogen would be circulated to provide cooling as well as high voltage insulation. The transmitter volume could be reduced by using gases at pressures much greater than one atmosphere, but at the expense of increased weight of a stronger pressure vessel. Since thermal conductivity in gases is negligible, cooling of high voltage components would have to be cooled by conduction through solids, or else it would be necessary to circulate the high pressure gas. Such a system would provide a small weight advantage over the proposed oil system but there would be a significant increase in development cost and risk.

Solid dielectric systems have certain obvious advantages over competing systems and for this reason have been used in low voltage and low power space borne power supplies. However, the present state of the art does not allow use of solid dielectrics in high voltage high power systems because differences in thermal expansion between the encapsulated components and the insulation medium, result in voids which ultimately lead to breakdown paths caused by corona degradation.

However, the state of the art of encapsulation is advancing and techniques that overcome these problems are now being developed. Hughes has developed a proprietary process for encapsulating transformers, capacitors and circuit assemblies which is able to produce essentially corona-free encapsulation over wide temperature extremes. A reevaluation of the state of the art before completing the detailed design of the transmitter is recommended to determine the suitability of solid encapsulation techniques for this application.

Vacuum dielectric systems again have certain obvious advantages and were considered briefly for this application. Their principal advantage is the potential for large weight reductions. Their principal disadvantage is the need for an extremely hard vacuum in the vicinity of the high voltage circuitry. The presence of any outgassing products could result in breakdown and failure of the supply. The vacuum technique is particularly applicable to long term space missions where sufficient time can be allowed for outgassing to be completed. The short mission time of the space shuttle makes it unlikely that the outgassing could be completed quickly enough to satisfy space shuttle operational requirements.

Since heat can be removed only by radiation or by conduction through solids and since radiative heat transfer is not adequate, the use of vacuum dielectric would require the development of components with built-in heat removal mechanisms. At these power levels design of such components has many of the same problems that solid encapsulated components present. Therefore this approach is beyond the state of the art for these voltage and power levels at the present time. Because of this difficulty and because of the outgassing problem, this approach has been rejected.

3.5 DATA RECORDING

Maximum data rate recording requirements are 260 MB/s for the baseline design and 190 MB/s for a back-up design. Two RCA HDMR-240 tape recorders, each capable of 240 MB/s, have been chosen for the baseline design. RCA is now developing the HDMR-240 recorders, which should be available for the shuttle experiments early in 1980.

If these recorders, or their equivalents, cannot be delivered for early ERSIR experiments, the back-up design will be implemented. This will utilize two modified Ampex FR 1700 tape recorders, or equivalents, each capable of recording at 100 MB/s data rates to satisfy the data rate requirement. Characteristics of the HDMR-240 and modified Ampex FR-1700 recorders are given in Tables 3-32 and 3-33. ERSIR data recording parameters for the baseline and back-up configurations are shown in Table 3-34.

3.6 SYSTEM PHYSICAL CHARACTERISTICS

The ERSIR has been designed to interface with the space lab, which includes a pressurized module and a pallet bay. Factors that affect this

TABLE 3-32. BASELINE RECORDER

Type:	Digital
Baseline:	RCA HDMR 240
Number:	2
Bit Rate:	240 MB/S Per Recorder
Availability:	First Quarter 1979*
Power/Recorder:	200 Watts at 28 VDC Nominal*
Weight/Recorder:	90 Kg*
Reproduce Slowdown Speed:	<10:1 (E.G.: To 25 MB/S or Less
Record Time/Reel:	12 Min at 240 MB/S
Bit Error Rate:	1 in 10^6 (Max)

*Vendor Estimate (August 1975)

TABLE 3-33. RECORDER BACKUP

Type:	Digital
Backup:	AR 1700 at high density (11.8 KB/cm), 28 tracks
Number:	2
Bit Rate:	100 MB/S per recorder
Availability:	90-120 days ARO*
Power/Recorder:	~450 watts at 28 VDC nominal*
Weight/Recorder:	~40 KG*
Record Time/Reel:	15 min at 100 MB/S
Bit Error Rate:	1 in 10^5 max

*Vendor estimate (August 1975)

TABLE 3-34. ERSIR DATA RECORDING PARAMETERS

Items	Baseline	Back-up
Recorders (2 each)	HDMR-240	Modified FR 1700
Receivers (L, x-band, 2 polarizations)	4	4
Resolution	25 M	25 M
Bits per receiver	5I, 5Q	5I, 5Q
Swath widths, max	85 KM	60 KM
PRF's	1200 to 1800 Hz	1200 to 1800 Hz
Data rates	180 to 260 MB/s	130 to 190 MB/s

interface, and that in consequence must be considered in making provision for the Interface are volume, weight and power requirements. Equipment location, power sources, and signal interfaces must also be considered in designing the interface between ERSIR and the shuttle. Finally, heat transfer and discharge require attention. Design characteristics and features that deal with these considerations are described below.

VOLUME, WEIGHT AND POWER CONSIDERATIONS

Estimates for weight, volume and power are presented in Table 3-35. Values are given for each major component. These components fall into two separate groups characterized by their location, namely the group in the pallet bay and the group in the pressurized module bay. As is shown in the table, overall weight is 1271 kg, which includes the weight of 22 reels of recording tape (176 kg). Volume is 11.92 cubic meters. The power required for radar operation is 3.5 KW. The power requirement for the equipment in the pressurized module is approximately 1 KW, obtained from the dc service bus in the space laboratory. During operation provision must be made for the transfer and ultimate disposition of 11,350 BTU of heat per hour.

Equipment locations and interfaces are shown in Figure 3-44. As shown, a service loop carries power from the dc service bus to the electronics equipment in the pallet bay. During radar operations the nominal power requirement is about 2.5 KW. Maximum power requirements for the equipment in each group, pallet bay and pressurized module, are listed in Figure 3-44. Service cables which serve as interfaces between electronics equipments in the pressurized module and in the pallet bay are also illustrated. These loops, which include flexible cables, contain IF conductors, timing and control conductors, and signal conductors. The IF cables serve as a signal interface between the buffer formatter in the pressurized module and the receivers at the antenna.

The heat exchange and dissipation subsystem is made up of cold plates and flexible hoses that carry liquid coolant. While the ERSIR experiments are in progress, the nominal rate of heat exchange is 7200 BTU per hour at the pallet bay. More detailed information on thermal rates and loads

TABLE 3-35. PHYSICAL CHARACTERISTICS BASELINE DESIGN

ESTIMATED WEIGHT, POWER, VOLUMES:

	Weight(s), KG	Input Power, Watts	Volume, Cubic Meter	Location
Antenna	682		11.25	Pallet Bay
Transmitters, HVPS, Modulators, Receivers, Exciters	159	2450	0.27	Pallet Bay
Signal Conditioner, Control Module, Buffer-Formatter, Space Processor	45	250	0.025	Module Bay
Display-Control Module	27	400	0.075	Module Bay
Recorders (2)	182	400	0.1	
Sub-Total	1095 KG		11.72 M^3	
22 Reels Tape*	176		0.2	Module Bay
	1271 KG	3.5 KW	11.92 M^3	

*Storage capacity – four hours at full radar operation.

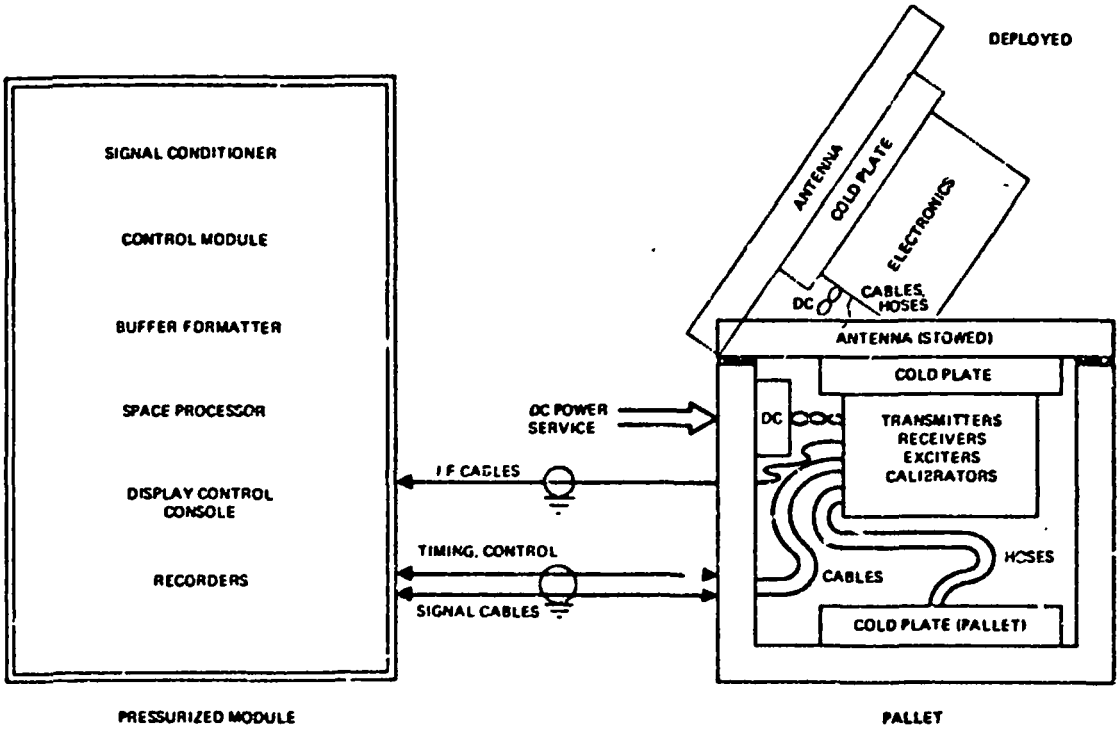

Figure 3-44. Simple schematic of ERSIR equipment interfaces.

is given in Table 3-36. A cold plate attached to the antenna support structure not only acts as a heat sink but also serves as the mount for the L and X-band transmitters, receivers, exciters, calibrators and associated electronics. An additional cold plate in the pallet takes heat from the antenna cold plate via circulating coolant in flexible hoses.

3.7 ALTERNATE DESIGN SUMMARY

The baseline design utilizes a uniformily illuminated array of 3 meters x 10.17 meters with three vertical beams. It folds twice and is stored on a single pallet. The factors listed below form the basis for establishing this design.

1. size and weight
2. transmitter power and reliability
3. simplicity of antenna feed structure

TABLE 3-36. BASELINE DESIGN POWER/ENERGY/THERMAL LOADS

	Pallet Bay	Module Bay	Total
Operating Power	2450 WDC	1050 WDC	3.5 KW DC
Current at 26 VDC:	95 A.	40 A.	135 A.
Electrical Energy, 4 Hours:	9.8 KWH	4.2 KWH	14 KWH
Thermal Rates, BTU/Hour:	7224	3584	11,348
Total Thermal Load, 4 Hours:	28,894 BTU	14,335 BTU	45,390 BTU

4. simplicity of antenna deployment mechanism
5. single pallet storage for one antenna
6. swath width and image quality

Table 3-37 is a brief summary of the baseline and alternate designs. on antenna size and weighting function. Table 3-38 is a brief summary of major design alternates and trade-off considerations.

The study of K_u-band alternate designs resulted in practical designs for 13.3 GHz with reduced swath coverage (40-50 KM) to look angles of 40°. The K_u/X-band trade-off considerations include agronomic applications in which the issue is the relative importance of sensor response to vegetation bio-mass and plant morphology. This facet of the K_u/X-band trade-off considerations has not been resolved in this preliminary design study.

TABLE 3-37. BASELINE/ALTERNATE DESIGNS COMPARISON SUMMARY

Array		Swath Widths (H = 200 KM)							
		Offsets:		100	200	300	350 KM	Estimated	
		β:		26°	45°	55°	59°		
Height X Length, M	Vertical Weighting	F_L	F_X					Weight, KG	System Power, KW
3 x 12	Baseline	1.04	9.0	85	74	66	52 KM	840	3.5
3 x 12*	Uniform	1.22	11.0	77	64	69	69	840	3.5
3.3 x 12	Modified Taylor	1.22	9.0	76	68	72	72	910	3.5
3.3 x 8	Modified Taylor	1.22	9.0	70	54	58	46	720	4.9
5 x 8	Truncated sin x/x	1.53	10.0	50	62	56	<40	910	3.5
3 x 16**	Uniform	1.04	9.0	88	74	70	66	1046	2.8
3.3 x 12	Truncated sin x/x	1.71	9.0	40	50	—	—	820	2.4

NOTES:
1. Resolution D_A = 25 M, 4 Looks, 45 Percent Overlap; except
   **4 Looks at 60 Percent Overlap for 16 MM Array
2. Uniform Illumination in Horizontal Dimension
3. * 3 Beam, Shorter Wavelength Alternate to Baseline Design

TABLE 3-38. ALTERNATE DESIGNS

Unit	Design	Remarks
Antenna	Baseline: 3M x 10.7M Uniform Illumination	Low power; large swath at 4-looks; 10-60° coverage with 3 beams
	Shaped vertical beam	3.3M height, swath coverage 10-60° with 2 beams, complicated feed
	5M x 8M, truncated sin X/X	Low power; fold in 2 dimensions for stowage
	3M x 16M, uniform illumination	Lower power, multiple folds
	3M x 12M, truncated sin X/X	Excellent image quality; low power; reduced swath
Antenna Deployment	Baseline, athwartship	Min deployment; shuttle attitude inverted, sidewise
	Extended, single pallet	Complicated mechanism; compatible with other experiments
	Extended, dual pallet	Single fold, maximum length, maximum stowage area
Recorder	Baseline: HDMR 240	240 MB/S at 200 watts each; under development
	Back Up: AR1700	100 MB/S at 450 watts each; available
Inflight Display	Baseline: Unfocused	150 M resolution 90 KM swath; 600 range cells
	Partially focused	Improved resolution (to 50 M); more storage/complication
	None	Less power; minimum monitor
Short Wavelength	Baseline: X-Band	Moderate power and sensivity to weather
	K_u-Band at 13.3 GHz	Greater power and sensivity to weather; more responsive to vegetation bio-mass

4.0 CRITICAL DESIGN FACTORS

4.1 IMAGE QUALITY

4.1.1 Introduction

The radar output is an imperfect image of the object field viewed by the radar. As examples, a point scatterer in the object field images as a diffuse principal spot surrounded by subsidiary spots; images of low reflectivity regions are contaminated by the radar's response to adjacent regions; and radar noise may obscure the images of weak scatterers.

Over the years, the radar design community has used special measures to evaluate radar image quality. Some of these measures are resolution, maximum sidelobe level, integrated sidelobe level, signal-to-noise ratio, minimum target radar cross-section, number of independent resolution cells for smoothing, small signal suppression ratio, maximum target radar cross-section, ambiguity levels and dynamic range. The need for measures of radar image quality arises for two reasons: 1) the various characteristics associated with the radar imaging process, such as non-zero resolution sidelobes and ambiguities, and 2) the finite variation in received power which can be accommodated by the radar, particularly by the radar signal processor, display and observer.

The following sections discuss the terrain (object field) to be imaged, the radar impulse response, the effects of the radar impulse response on the image, techniques for smoothing the images of diffuse terrain, A/D converter effects and an estimate of the image quality expected from the selected radar design.

4.1.2 Terrain Reflectivity

Some example terrain models are 1) diffuse terrain (many scatterers per resolution cell with no one scatterer giving a large portion of the power returned), 2) a hole (no scatterers within a resolution cell) and 3) an isotropic point scatterer. These three models are illustrated in Figure 4-1.

Diffuse terrain gives a radar return whose amplitude and phase (for each resolution cell) depend both on the within-cell positions and amplitudes of the scatterers and on the encounter geometry between the radar and the resolution cell. Thus, the image of terrain with a given average backscattering coefficient exhibits a wide variation in image power from resolution cell to resolution cell. Furthermore, the image power for any given resolution cell changes with radar frequency and encounter geometry. This characteristic variation in image power from cell to cell or with changes in encounter geometry is usually called scintillation. Holes and isotropic point scatterers do not exhibit scintillation, but any combination of two or more scatterers within a resolution cell can exhibit scintillation.

Figure 4-2a shows a radar impulse response (or imaging aperture) idealized to exclude sidelobes. Figure 4-2b shows the image of diffuse terrain, holes and an isotropic point scatterer made with such an ideal impulse

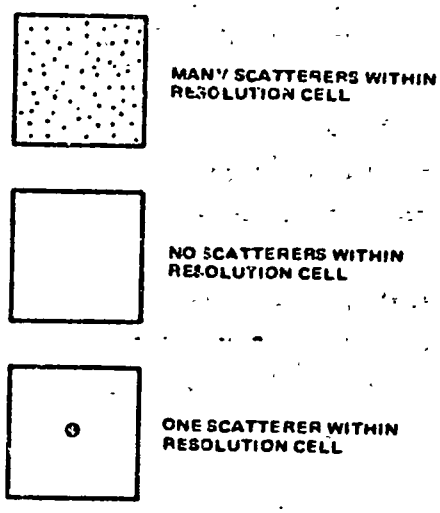

Figure 4-1. Terrain models.

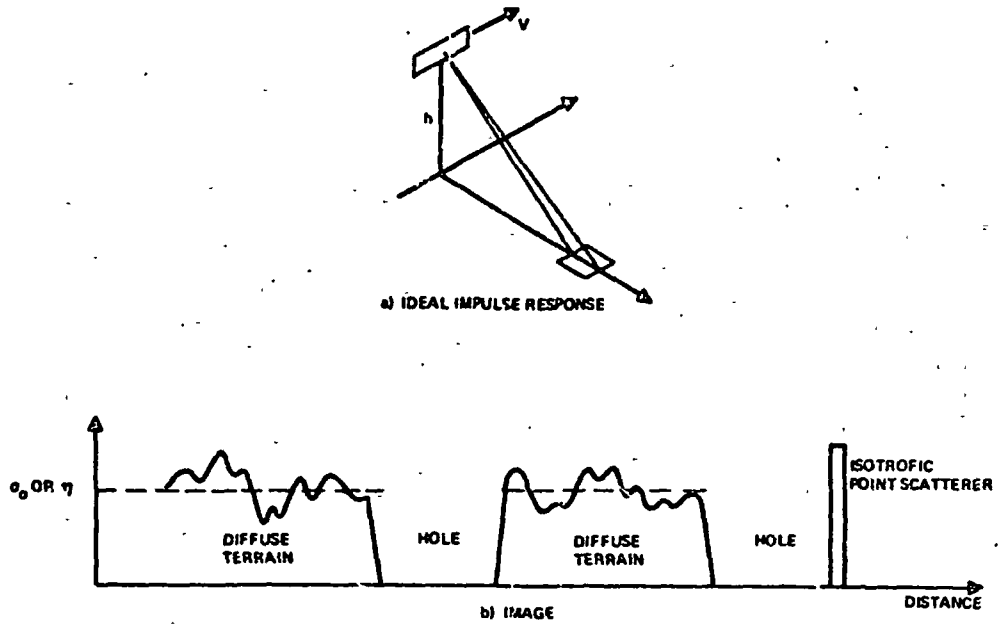

Figure 4-2. Image with ideal impulse response.

response. The diffuse terrain images vary from cell to cell about the back-scattering coefficient, which is characteristic of all resolution cells; the image of the isotropic point scatterer has non-zero width because the ideal impulse response chosen was of non-zero width.

4.1.3 Non-Ideal Radar Impulse Response

Figure 4-3 shows a synthetic array radar moving with a given velocity and illuminating an isotropic point scatterer in an otherwise zero-reflectivity background. The image of this isotropic point scatterer is the radar impulse response and is illustrated in Figure 4-4. Some features of interest are the range and azimuth sidelobes, the mainlobe, the impulse response width (or resolution), the maximum sidelobe levels in range and azimuth and the ratio of total sidelobe energy to mainlobe energy.

Figure 4-5 shows the impulse response discussed above together with range and azimuth ambiguities. (Strictly speaking, Figure 4-5 represents the complete impulse response while Figure 4-4 shows the local desired impulse response.)

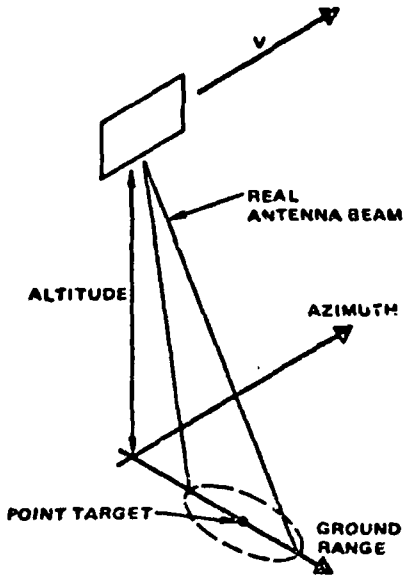

Figure 4-3. Impulse response geometry.

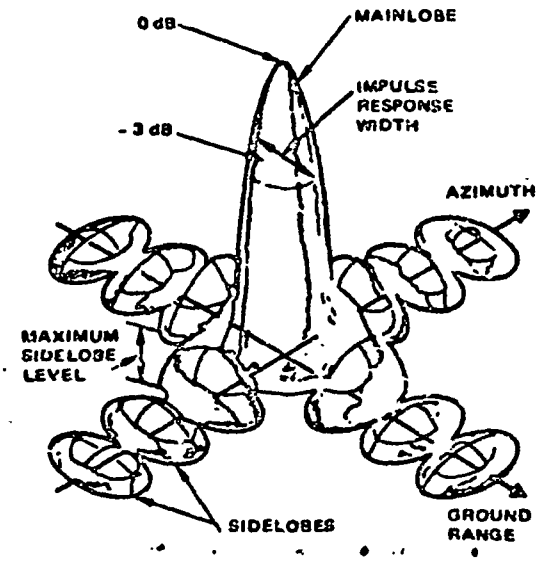

Figure 4-4. Non-ideal radar impulse response.

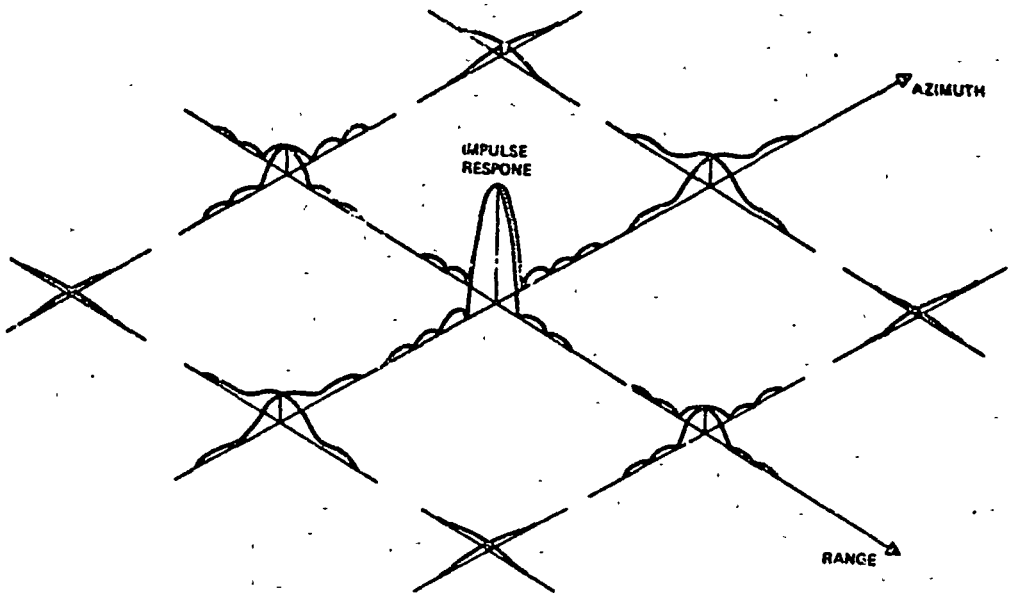

Figure 4-5. Ambiguities.

4.1.4 Effects of Non-Ideal Impulse Response on Images

Figure 4-6a shows the same terrain models used in Figure 4-2 – diffuse terrain with holes and an isotropic point scatterer. Figure 4-6b shows a possible azimuth impulse response for the synthetic array radar and Figure 4-6c shows the image brightness which results from scanning the model terrain with the impulse response. The image brightness of Figure 4-6c exhibits the following characteristics:

1. The image of the isotropic point scatterer is essentially the azimuth impulse response.
2. The images of the diffuse terrain regions have lower (spatial) frequency variations about the average value. Also, the image average value is higher than the true average value, the results of additions of receiver noise, ambiguities and sidelobe energy.
3. The image power in the holes is not zero, again due to receiver noise, ambiguities and sidelobe energy.

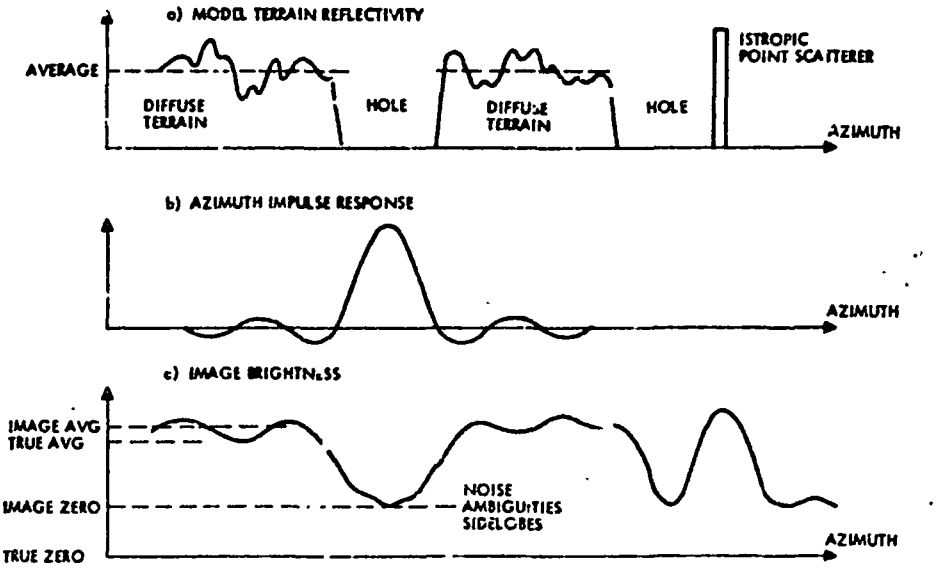

Figure 4-6. Effects of non-ideal impulse response on images.

4.1.5 Unsmoothed versus Smoothed Images

Usually smoothed images are generated in an effort to minimize the diffuse terrain image power variations about the average value. The solid and dashed curves of Figure 4-7a represent two independent images of the model terrain discussed above. These two images could have been generated, for example, by transmitting two widely separated frequency bands and processing them separately. If these two images are added, then the variations of the resultant are less extreme as illustrated in Figure 4-7b. It is to be noted that the resultant image averages and true averages are still not identical and that the images of the holes are not zero.

Smoothing techniques can be separated into two categories: a) within-cell averaging and b) area averaging.

The within cell averaging technique makes high resolution images of each cell with essentially independent portions of the pulse or Doppler spectrum. Figure 4-8a shows a pulse spectrum broken up into four sub-bands, each of which yields a pulse (range) resolution, τ. The four independent

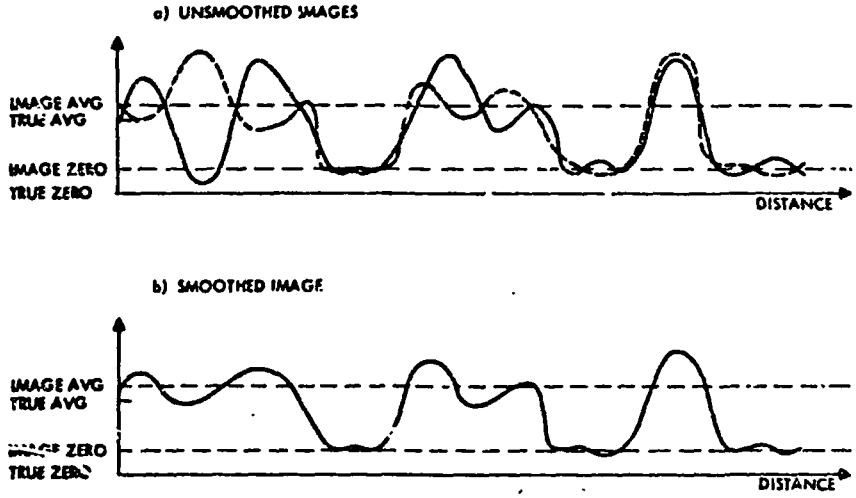

Figure 4-7. Unsmoothed and smoothed images.

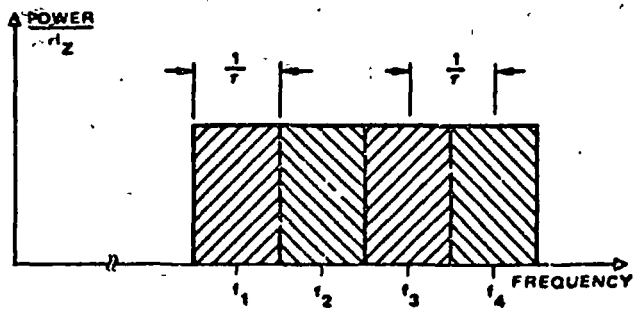

a) Pulse Spectrum Diversity (Range Diversity)

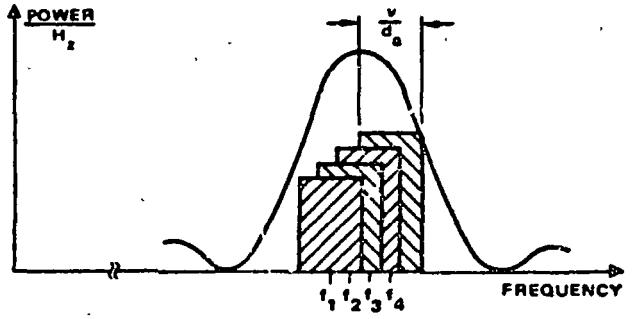

b) Doppler Spectrum Diversity (Azimuth Diversity)

Figure 4-8. Within-cell averaging.

synthetic array images made from these sub-bands are then added (non-coherently) to produce a smoothed resultant image. This technique is sometimes called range diversity. Figure 4-8b shows a doppler spectrum broken up into four (overlapping) sub-bands, each of which yields an azimuth resolution, d_a. The four almost independent synthetic array images made from these sub-bands are then added (non-coherently) to produce a smoothed resultant image. This technique is sometimes called azimuth diversity.

The area averaging technique makes one high resolution image of the large area of interest and then (non-coherently) adds the values of several adjacent cells for every cell position producing a lower resolution smoothed

resultant image. Figure 4-9 illustrates how this technique might be used to add a large number of independent cells to produce a better estimate of area backscattering coefficient. Referring to Figure 4-9, note that a particular field has been assigned the value η_3 for the backscattering coefficient. Here, the radar design parameters and the size of the field allow 28 independent resolution cells to be combined into one estimate of η_3. (It is implicit that the experimenter recognizes the boundaries of this field and only adds image powers from cells within the boundaries.)

For a fixed bandwidth (doppler, pulse or both), the trade-off can be made between resolution and image smoothing. Figure 4-10a shows measured backscattering coefficient versus true backscattering coefficient for an unsmoothed (single-look) image. Here, the image power variation from cell to cell (for the same terrain type) makes the measured value of η in each cell uncertain. The curve shown in Figure 4-10a assumes a measurement confidence interval equal to the step size shown, thus only five values of measured η are statistically significant in this example. Figure 4-10b shows measured backscattering coefficient versus true backscattering

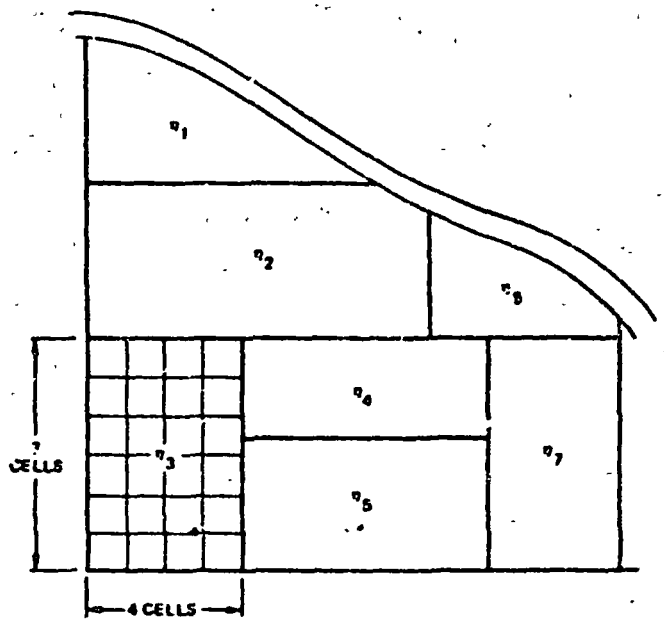

Figure 4-9. Area averaging.

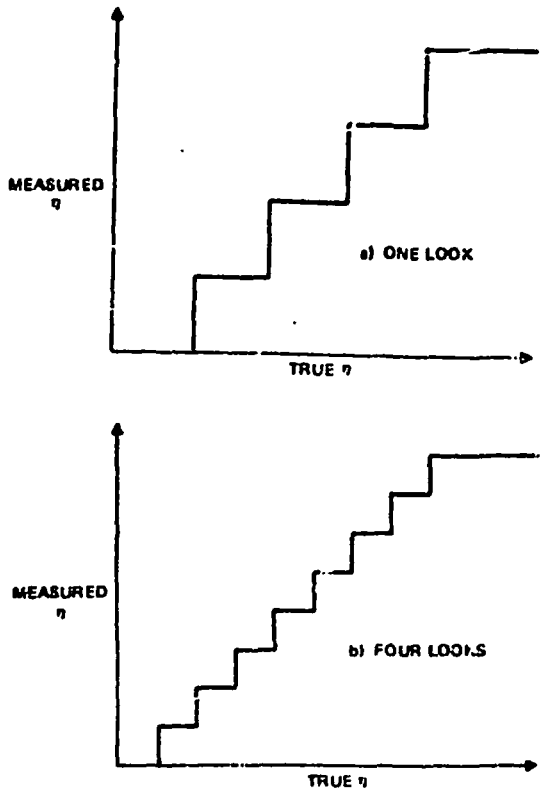

Figure 4-10. Improved measurement of η through smoothing.

coefficient for a smoothed (four-look) image. Here the confidence interval is narrower than before due to the smoothing so that more steps are shown. In this example, nine values of measured η are statistically significant after four-look smoothing. Figure 4-11 shows how the final image resolution varies with azimuth resolution for an assumed set of conditions. Here the larger number of significant measured η values of Figure 4-10b (obtained from four-look smoothing) are seen to be gotten by degrading the one-look resolution from 6.2 meters to 12.6 meters. (Overlap of the doppler bands used to get the four looks is assumed for this example.)

4.1.6 A/D Converter Effects

The basic radar block diagram is shown in Figure 4-12. Coherent radar pulses are generated in the Transmitter and Local Oscillator,

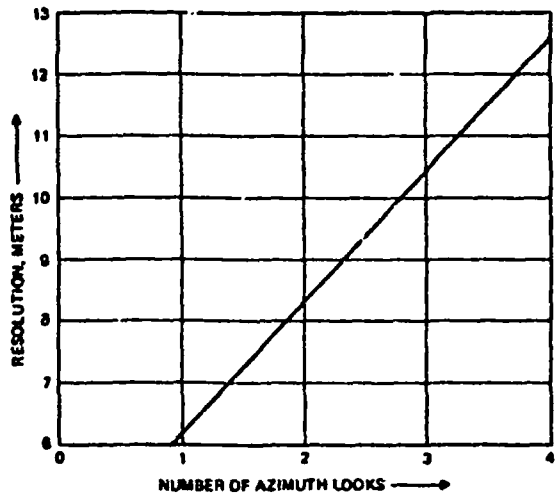

Figure 4-11. Improved azimuth resolution with less smoothing.

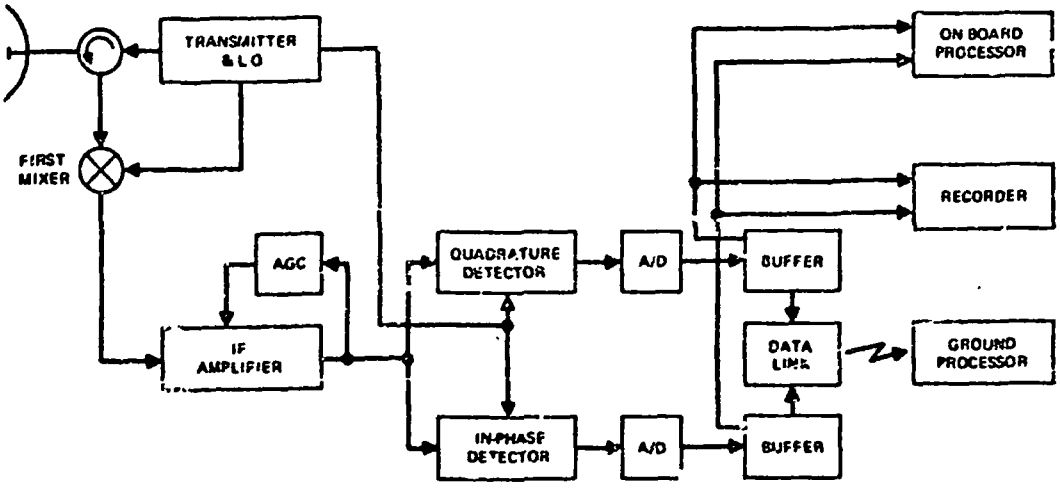

Figure 4-12. Basic radar block diagram.

radiated and received by the antenna, and converted to i.f. by the First Mixer. The output of the first mixer is supplied to In-phase and Quadrature Detectors through the I. F. amplifier (with its associated AGC). Each of the detectors drives an A/D Converter; the outputs of theA/D Converters

are supplied to an On-board Processor, a Recorder and a Buffer (which drives a Data Link for final Ground Processing). In the absence of round-off and truncation effects, in the on-board or ground processors, the A/D converters are the devices which limit the final image dynamic range. Even for cases where round-off and truncation in the processors affect the final image dynamic range, the maximum dynamic range that can be obtained is determined by the characteristics of the A/D converters and the manner in which the AGC controls the input levels of the A/D converters.

The A/D converter samples the input signal and encodes the sampled value into a digital number. As a result, sampling effects (such as aliasing), saturation effects and quantization errors are present in its output. It is customary to assume that the aliasing errors are negligible because of analog filtering before the A/D converters and, in some cases, because of oversampling. The quantization and saturation effects are illustrated in Figure 4-13 where the input-output characteristic of a 4-bit A/D converter has been modeled as a simple voltage-in/voltage-out relationship and the input signal statistics have been assumed to be gaussian. Referring to Figure 4-13a, it is seen that a continuous input voltage has been converted into a finite number of output voltage levels through the staircase-like amplitude characteristic. Note that above a certain input voltage, V_{SAT}, the output voltage is a constant, saturated value. Referring to Figure 4-13b, it is seen that if the input rms voltage is too high (e.g. k = 1.25), then a large portion of input voltage values exceed V_{SAT} and produce a large amount of saturation noise. If, on the other hand, the input rms voltage is too low (e.g. k = 5), then the majority of the input voltage values fall within only a few of the available number of output voltage values, producing a large amount of quantization noise. It turns out that there is a drive level which produces the minimum amount of total (saturation plus quantization) noise; for the 4-bit A/D converter, the optimum rms input voltage levels is 0.4 V_{SAT} (k = 2.5).

Figure 4-14 shows quantization noise, saturation noise and total noise versus k for the 4-bit A/D converter model, above.

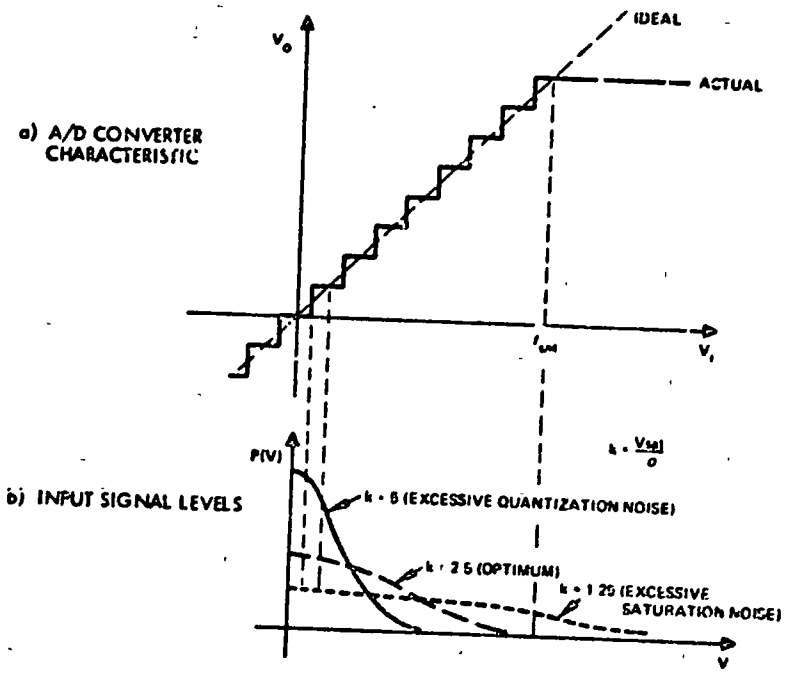

Figure 4-13. 4-bit A/D converter characteristic and input signal levels.

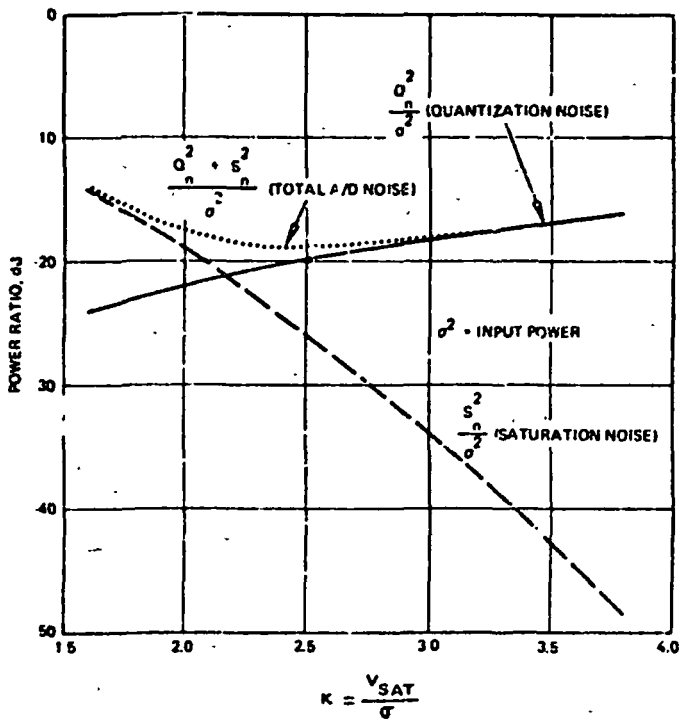

Figure 4-14. 4-bit A/D converter quantization and saturation noise.

4.1.7 Image Quality Estimates

In order to estimate the radar output image dynamic range, the evaluation terrain model of Figure 4-15 will be used. The terrain area of immediate interest has a range extent equal to the uncompressed pulse length and an azimuth extent equal to that subtended by the real antenna beamwidth. This area contains a hole, a bright scatterer and average terrain. The hole is two synthetic array resolution cells in diameter and the bright scatterer occupies one synthetic array resolution cell. All other cells contain terrain with average backscattering coefficient.

Three definitions are associated with this evaluation terrain model:

1. Minimum Cell Power. The power mapped on the radar image at the position of the hole.

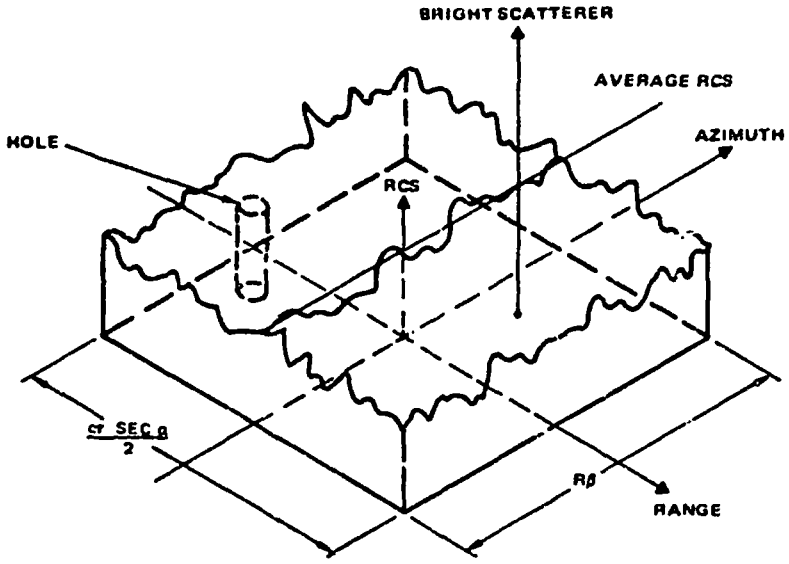

Figure 4-15. Evaluation terrain model.

2. Maximum Cell Power. The power mapped on the radar image (at the position of the bright scatterer) which produces an acceptable value of minimum cell power.

3. Dynamic Range. The ratio of maximum cell power to minimum cell power at a given gain setting.

The image dynamic range is estimated by the following procedure:

a. Specify the most minimum cell power allowable relative to average terrain.

b. Under-drive the A/D converter (large values of k) with the returns from average terrain until the allowable minimum cell power is achieved.

c. Drive the A/D converter with the evaluation terrain model, and increase the bright scatterer power until the allowable minimum cell power has been reached again. (As the bright scatterer power increases, the A/D noise will first drop as the quantization noise decreases and then increase as the saturation noise dominates.)

d. The dynamic range is then calculated with definition 3), above, including the range and azimuth compression ratios.

This procedure was used for the ERSIR selected design at mid-range, at 25 meters resolution and with a pulse compression ratio of 100. The dynamic ranges at X- and L-band for several A/D converters are given in Table 4-1, below.

As can be seen in Table 4-1, at X-band, a 4-bit A/D converter falls short of the 50 dB dynamic range originally requested. Although it could be argued that scatterers 50 dB above minimum cell power (corresponding to radar cross-sections of about 500,000 square meters) are very rare, the choice of 5-bit A/D converters (in the I and Q channels) was made on the basis that they are feasible and desirable in a radar experiment.

The image quality performance of the selected design is given in Table 4-2, below. The performance given is worst-case since the values tabulated are estimated at the swath edges.

TABLE 4-1. DYNAMIC RANGE FOR A/D CONVERTERS

No. Bits in A/D Converter	Dynamic Range, dB	
	X-Band	L-Band
4	49.6	58.9
5	57.3	66.7
6	63.8	73.2
7	70.00	79.4

TABLE 4-2. WORST-CASE IMAGE QUALITY PERFORMANCE

Parameter	Performance	
	X-Band	L-Band
Resolution	25 m	25 m
Single-look S/N, η = -18 dB	8 dB	8 dB
Number of looks	4	4
Ambiguity Ratio	-14.5 dB	-14.5 dB
Integrated Sidelobe Ratio	-16 dB	-16 dB
Dynamic Range	57.3 dB	66.7 dB

4.2 CONTOURED AGC

4.2.1 Introduction

A major consideration in ERSIR, more so than in most radar systems, is the design of the Automatic Gain Control system. AGC is required because of variations in received signal power seen by the radar sensor and because dynamic range is limited at critical points in the receiver-recording data path. A technique known as contoured AGC, in which the reciver gain is varied digitally over the sampled range swath, after A/D conversion, preserves the calibration integrity essential for accurate σ_0 estimates without sacrificing image quality.

This section begins with a discussion of the sources of received signal power variation and a discussion of the sensor dynamic range limitation. Image quality measures related to AGC are then reviewed. This review is followed by a discussion of AGC approaches, with emphasis on contoured AGC. The last discussion includes AGC inversion in the ground processor, a function necessary for producing high image quality. Performance of alternative AGC approaches is also discussed, in terms of distortion noise, a relevant measure of performance for contoured AGC.

4.2.2 Sources of Received Signal Power Variation

Received signal power varies because of the following: range variation across the swath (R^3); antenna gain variation (elevation pattern); terrain reflectivity variation (σ_0); and transmitter power and receiver gain variation. These items contribute to both short term variations (variations over the range sampling interval) and long term variations in received signal power. The first two items contribute to long term variations, the last item (transmitter power and receiver gain) contributes to short term variations, and the remaining item (terrain reflectivity) contributes to both short and long term variations. The AGC system comprises two portions, the calibrated slow AGC portion, which is utilized for the long term variations and the contoured AGC, which is utilized for the short term variations. The short term variations and contoured AGC are emphasized in this discussion.

The magnitude of the short term variations can be estimated from the contributions of the first three sources listed. The combination of the [illegible] and elevation pattern variations produces about an 8 dB variation across the swath. This variation is characterized by an approximately parabolic shape as shown in Figure 4-16. Variations in σ_0, the other contributor, can be considerable on a cell-by-cell basis, but radar reflectivity data at X-band and L-band, for various terrain types, averaged over areas comparable to a square kilometer or greater, exhibit a variation confined to about 8 dB. (Special cases, such as land-water boundaries, will, of course, exceed this range.) The two 8 dB variations sources combine to produce the simplified short term variation model of Figure 4-16. The critical characteristic of this model is that the maximum slope is about 6 dB variation in received power over an 8 Km segment of the swath.

4.2.3 Dynamic Range Limitations

The critical system elements which limit dynamic range are the digital tape recorder and data link. The limitation is caused by the fact that the rate at which data are recorded and transmitted over the data link is proportional to the number of bits per sample. This data rate is the key parameter in determining the cost and complexity of the recorder and data link. In addition, high data rates mean shorter recording times. They also mean an increase in the weight and volume of stored tape. Clearly, the minimization of data rate is an important design goal.

Other radar design parameters are of secondary importance in limiting dynamic range. The RF portion of the receiver is not a limitation. The IF portion has more than adequate dynamic range, and with slow AGC, can

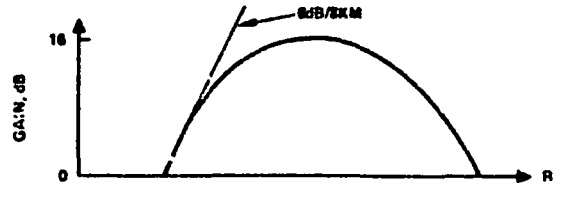

Figure 4-16. Signal power variation — range dimension.

keep the level of signal entering the A/D converters in the proper range. The state of the art permits the design of reliable 8 to 10 bit A/D converters for use at the 6 to 18 MHz sample rate required for 25 meter resolution. The number of bits per sample is reduced from the 8 to 10 bit quantity before transmission and recording by the use of contoured AGC. Before this approach is discussed, however, the effects of some AGC alternatives on image quality are examined.

4.2.4 AGC/Image Quality Interactions

AGC minimizes A/D converter distortion noise by controlling receiver system gain. However, in doing so, it introduces step changes in gain within processed data sets, with the potential of degrading resolution and integrated sidelobe ratio (ISLR). This negative effect is illustrated by Figure 4-17, which shows the affect of a 6 dB gain change in the center of a $\cos^2 x$ weighting function. The solid line shows the unperturbed compressed pulse (in either range or azimuth) while the dotted line shows the mainlobe broadening and increased sidelobe level resulting from the gain change.

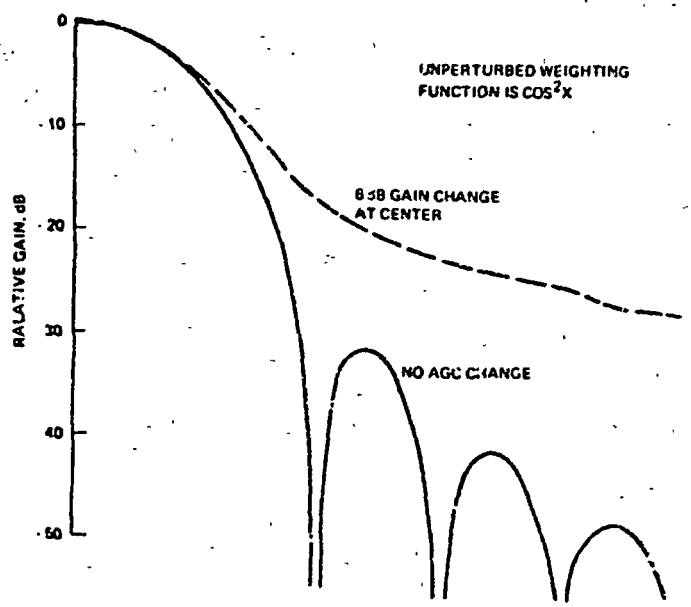

Figure 4-17. AGC'd weighting function.

The effect of distortion noise is illustrated in Figure 4-18. This figure plots the combination of saturation and distortion noise resulting from A/D conversion, for different ratios of A/D saturation voltage to RMS signal level, as discussed in Section 4.1.6. The total of quantization and saturation noise is referred to as distortion noise. The figure shows that a signal whose average power varies over an 18 dB range can result in a maximum ISLR of -27 dB, for an optimum gain setting using an 8 bit A/D converter. In contrast, a 16 dB variation of average power results in a much poorer -15 dB ISLR for a 5 bit A/D converter. Figure 4-18 is useful for determining distortion noise performance and will be referred to again in the section which follows.

4.2.3 AGC Approach

In the ERSIR AGC approach, slow AGC accommodates long term gain variations, and digital contoured AGC accommodates short term variations. Slow AGC causes neither image degradation, because of its long time constant, nor calibration inaccuracy, because calibration is accomplished once each PRI, as discussed in Section 4.4. It is the function of slow AGC to reduce the operating range required of the contoured AGC to the approximately 16 dB discussed in Section 4.2.2.

Conventional fast AGC, designed to respond to short term variations, is illustrated in Figure 4-19. Here, the range swath is divided into 8 sections, each with its own long term AGC loop. Gain is controlled by fast control of IF amplifier gain.

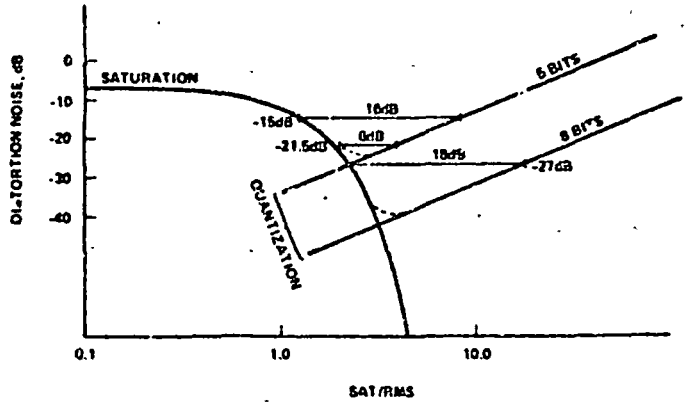

Figure 4-18. Distortion noise.

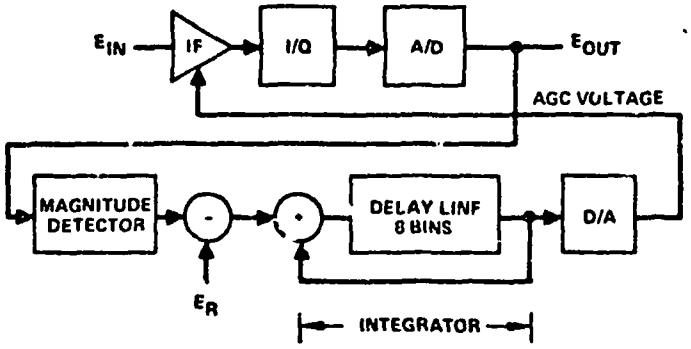

Figure 4-19. Conventional fast AGC (simplified).

This approach suffers from calibration inaccuracy as well as from the defects of image quality mentioned in Section 4.2.4. One of these defects, resolution and ISLR degradation, can be remedied by using the AGC inversion technique. This technique, illustrated in Figure 4-20, permits the gain settings for the different range segments to be recorded and transmitted along with the image data. In the ground processor, the gain variation is reversed by multiplying the received signal by a function proportional to the inverse of the IF gain. The extra bits per word which result from AGC inversion in the ground processor do not increase data rate as would have been the case

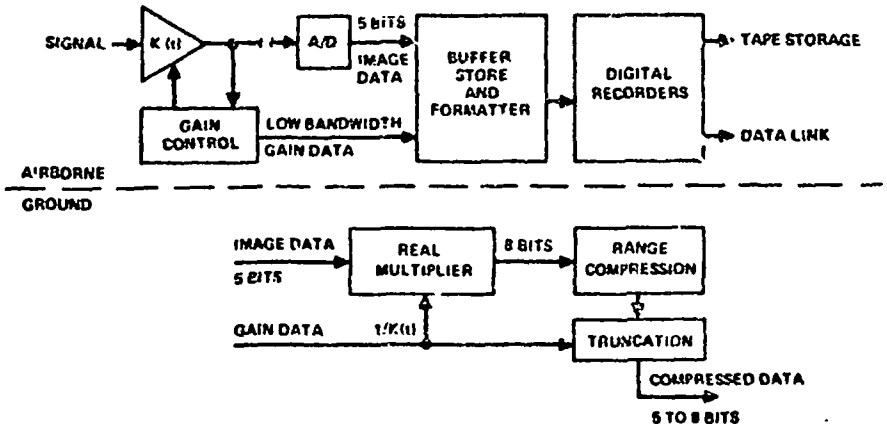

Figure 4-20. AGC inversion.

had they been recorded and transmitted. After processing, the data can then be rounded off as desired.

The increase in bandwidth needed to transmit the gain data is negligible. For example, consider the 80 Km swath divided into 20 segments, each of which has 160 range of 25 meters resolution elements. Following the arguments of Section 4.1.7 this calculation will use 5 bits per I and Q word (based on the dynamic range requirement) This will result in 1600 sample bits per range swath segment. If 6 bits are used to transmit the gain data for this segment, then the bandwidth or data rate increase is less than 1/2 percent.

Contoured AGC, which utilizes the digital inversion technique just described, eliminates the calibration inaccuracy associated with conventional fast AGC. It also eliminates resolution and ISLR degradation, while providing tight control over distortion noise. The output of an 8 bit A/D converter, as illustrated in Figure 4-21, is sent to a digital multiplier. The multiplying coefficient is determined from a range cell average, and is updated for each range swath segment. This multiplying coefficient is used for digital AGC inversion in the same way as was the gain data of Figure 4-20, which shows digital AGC inversion for conventional fast AGC. After multiplication, the data is rounded-off to 5 bits, which meets the dynamic range requirement.

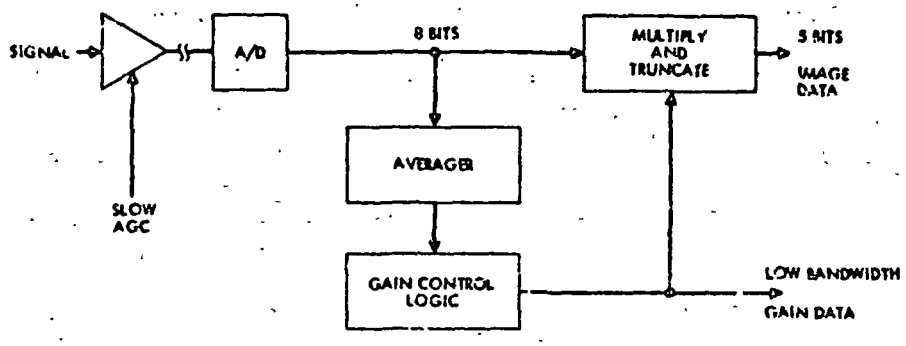

Figure 4-21. Contoured AGC.

Because the multiplication and round-off is optimum, the resulting distortion noise is the same as if a 5 bit A/D converter had been used at an optimal input gain setting, but without calibration inaccuracy. It is assumed here that the number of range swath segments is great enough to limit the systematic variation derived from the gain model of Figure 4-16 to 1 or 2 dB. Ten or twelve segments should suffice.

Two approaches to digital multiplication can be used, either simple point shift or a standard (6-bit, eg.) digital multiplication. Simple point shift involves choosing which 5 of the 8 available bits will be recorded. This choice, which requires less than 2 bits of gain data per swath segment, is equivalent to varying the voltage gain in steps of two. The resulting 6 dB variation in input signal power causes the -24 dB distortion noise achievable with an optimally controlled A/D converter to degrade to -21.5 dB, as illustrated in Figure 4-18. The use of a standard digital multiplier will result in -24 dB performance. These results are shown in Table 4-3, which

TABLE 4-3. COMPARISON OF AGC APPROACHES

Type	A/D Converter	Digital Multiplier and Round-Off	Distortion Noise	Remarks
Slow AGC	5 bits	N/A	-15 dB	Simple. Low performance.
Conventional Fast AGC	5 bits	N/A	-24 dB	Calibration difficult. Requires fast IF gain control. Resolution and ISLR degradation.
Conventional Fast AGC with Digital Inversion	5 bits	N/A	-24 dB	Calibration difficult. Requires fast IF gain control. No ISLR or resolution degradation.
Contoured AGC	8 bits	Point shift 5-bit round-off	-21.5 dB	Good calibration performance. No resolution or ISLR degradation. Simple multiplier.
Contoured AGC	8 bits	6-bit multiplier 5-bit round-off	-24 dB	Good calibration performance. No ISLR or resolution degradation.

summarizes the AGC approaches discussed herein, and tabulates their performance characteristics.

4.3 SAR ANTENNA BEAM POINTING

Antenna beam pointing, with the Spacelab inertial pointing system (IPS), is a critical factor in designing the ERSIR. With or without IPS, the antenna beam pointing direction, in the baseline design, is determined by a combination of the Spacelab attitude and the vertical tilt angle of the single axis gimbal of the antenna. The Shuttle Orbiter's reaction control system could establish the spacelab's attitude without the fine vernier control of the IPS. However, this would be at the cost of adding complexity to ground processing and at the risk of error resulting from imperfect compensation for range closure and doppler. With the IPS, increased beam position accuracy and rate control permit considerable simplification of the ground processing equipment and algorithms.

There are two basic problems associated with beam pointing. First, beam motion reduces the effective number of looks and as a result image measurement accuracy. Secondly, beam position error induces range closure and doppler compensation complexities in ground processing.

4.3.1 SAR Antenna Beam Pointing Error Rate

Antenna beam motion in the azimuth plane degrades measurement system accuracy. The SAR system depends upon smoothing with multi-look processing for measurement accuracy and the number of looks available decreases with azimuth beam slewing. The effects of azimuth slewing of the SAR Beam are illustrated in Figure 4-22. In (a), the real beam is at azimuth A and has an angular rate $\dot{A}$; the point p accordingly moves through the beam at a higher velocity than the orbital velocity v, about half the time.

Accordingly, the point p will often be imaged for a time T, which is less than the time T_n required to image the point for N looks. The percentage loss p in the number of available looks is

$$p = \frac{100\,(T_n - T)}{T_n} = \frac{100}{(V/\dot{A}R_s) + 1} \qquad (1)$$

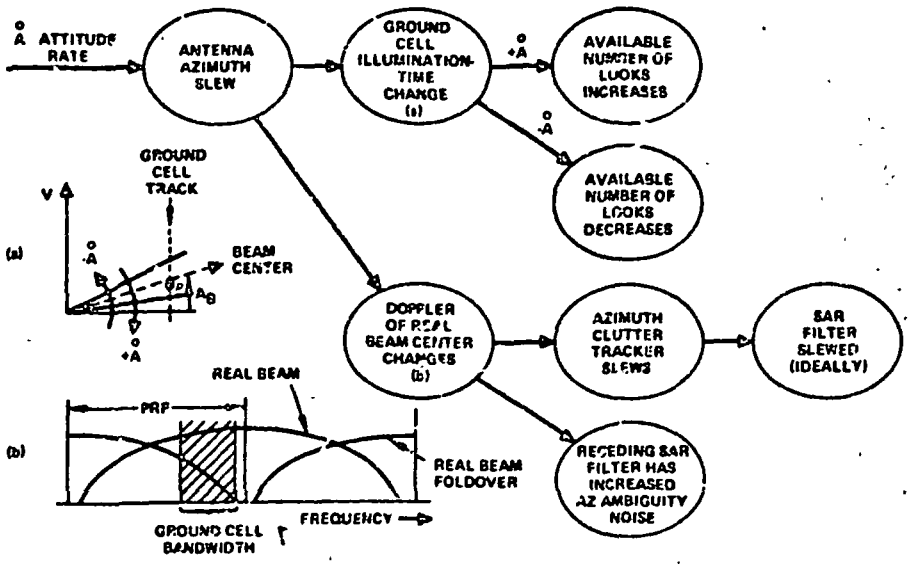

Figure 4-22. Payload pointing error rates.

where R_s is the mean slant range to the point p. For example, p = 20 percent for V = 7.8 KM/s, $\dot{A} = 0.275^{\circ}$/sec, and R_s = 420 KM, a worst case for an altitude of 200 KM (look angle $\beta = 60^{\circ}$).

Table 4-4 is a summary of the angle rate effect for this "worst case", maximum R_s at a look angle near 60° (H = 200 KM). The SAR filter must be slewed to retain its alignment with the antenna boresight axis and to prevent excessive azimuth ambiguity noise (the SAR processing filters should be distributed symmetrically about the beam center). To maintain track, the clutter tracker will slew at the rate of doppler frequency change induced by motion of the beam axis, $\dot{A}$.

4.3.2 Antenna Beam Position Error

Compensation for range closure at L-band and for doppler shift at X-band, when the data are acquired with the space sensor at non-optimum azimuth angles, complicates the ground processing.

The geometrical factors involved in range closure compensations are illustrated in Figures 4-23a and 4-24b; the point p is displaced from the

TABLE 4-4. PAYLOAD POINTING ERROR RATES

$\dot{A}$ Azimuth Attitude Rate	Worst Case**		Acceptable?	Is SAR Filter Slewing Needed
	Percent of Looks Lost	Cell Doppler Spreading ÷ SAR Filter Width / SAR Filter Slew Rate (Hz/Sec) X (Array Time)^2		
(–) 0.008°/sec	0.7	0.20	Yes	No
(–) 0.02°/sec	1.8	0.50	Yes	?
(–) 0.275°/sec*	20	6.8	Yes	Yes
(–) 1.1°/sec	50	27.0	No	NA

*Baseline system

**V = 7.78 KMs, Altitude = 200 KM, R_s = 420 KM.

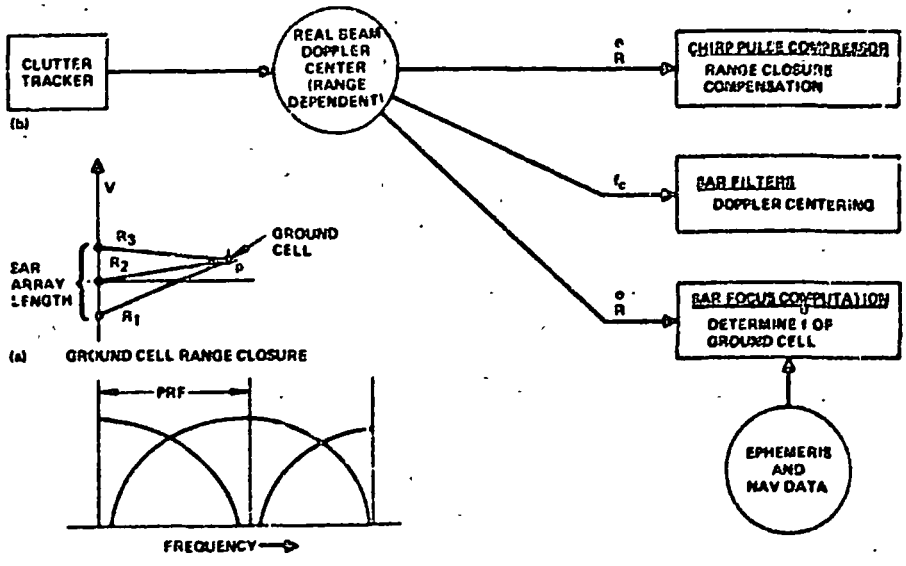

Figure 4-23. Aligning SAR beams with real beam, and focusing.

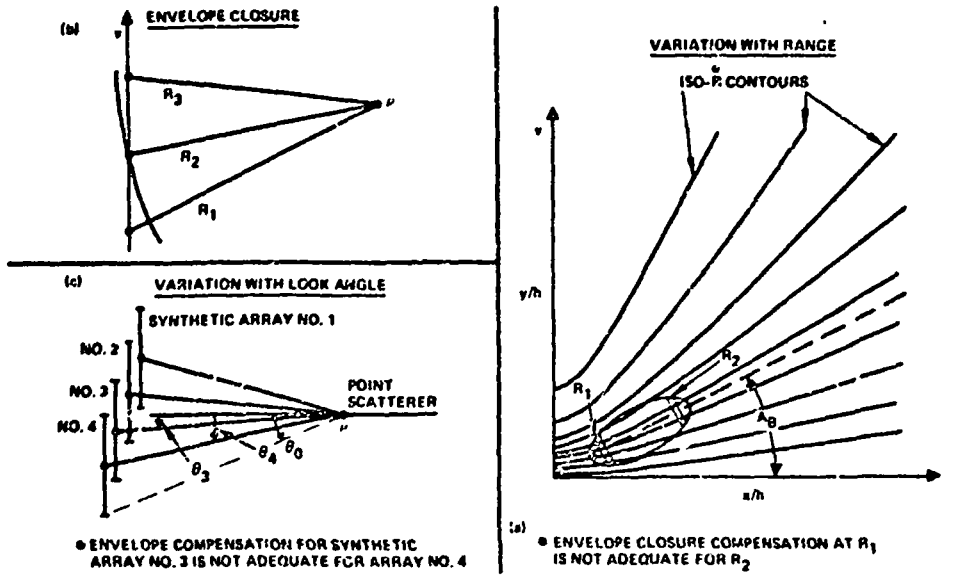

Figure 4-24. Envelope closure variations.

optimum position, broadside to the velocity vector. At the optimum pos $A_B = 0$ in Figure 4-24(a), the range closure compensation is zero, for circular orbits. The range closure compensations required at L-band a large and vary from the near range edge of the antenna footprint to the fa for near nadir look angles and non-zero A_B (Figure 4-24a). The magnit of the range closure compensations are shown in Figure 4-25 for an ante beam with look angle coverage from 10° to 30°, (offset range 35 to 116 K at H = 200 KM). The ideal squint angle is A_{so}, the azimuth angle relativ to the Orbiter's velocity vector. The angle A_{so} corresponds to the minir change in range closure across the swath, A_{so} is also the squint angle fo zero range closure compensation (single look) for circular orbits.

For elliptic orbits, the angle A_{so} corresponds to a non-zero rang closure; the effects of ellipticity rotate and displace the constant $\dot{R}$ (dopp contours to preclude a zero iso-doppler ($\dot{R}$) contour (Figure 4-26). The range closure curves are normalized by the slant range resolution d_r, wl corresponds to the transmitted waveform bandwidth. The ordinate values

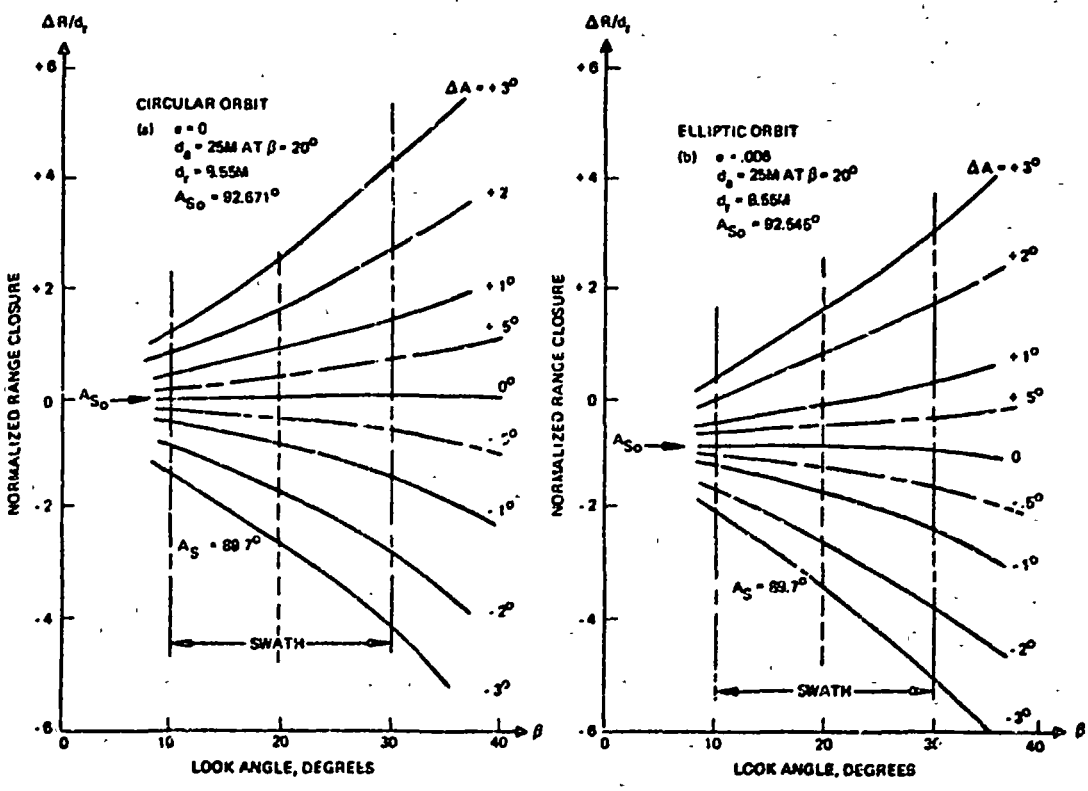

Figure 4-25. Normalized range closure ΔR vs look angle β, L-band (1.04 GHz) H = 200 km, i = 80°, ϕ = 40° N latitude.

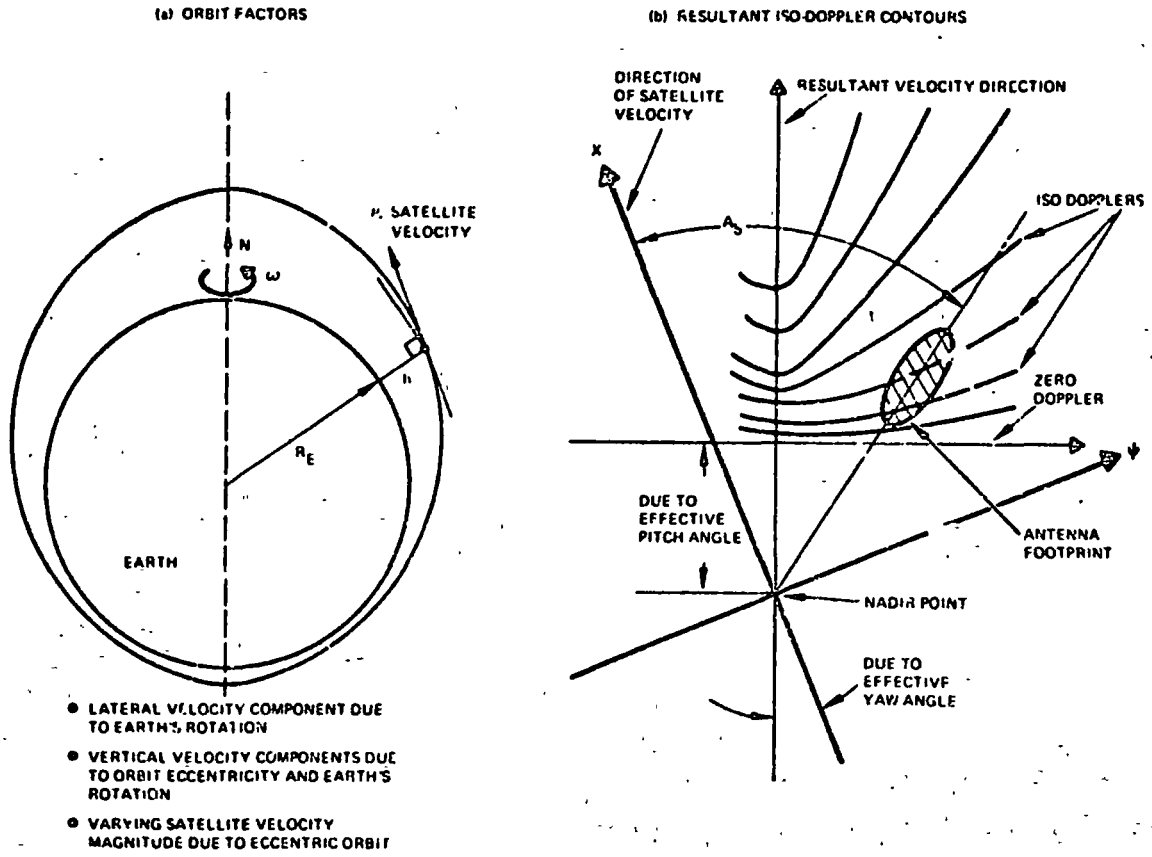

Figure 4-26. Eccentric orbit velocity effects on SAR.

$$Y = \frac{\Delta R}{d_r} = \frac{\dot{R}\, T_a}{d_a \sin \phi_o} = \frac{\lambda \dot{R} R}{2 v d_a^2 \sin \phi_o}$$

where T_a is the array time; $T_a = \lambda R/2vd_a$; d_a is ground cell resolution; ($d_r = d_a \sin \phi_o$; ϕ_o is the incidence angle ($\phi_o \sim \beta_o$, the look angle); λ is wavelength; R_s is slant range; and v is velocity.

Range closure compensations for L-band multi-look ground processor imaging may differ for individual looks. This is shown in Figure 4-24c. With the IPS available for beam positioning, it should be possible to maintain A_s within $\pm 0.3^o$ of A_{so}. At 1.04 GHz for L-band and d_a = 25 meters, the angle

θ_o is at most 0.5^o (45 percent overlap, 4 looks). The maximum position error for this fourth look is 0.8^o. For this condition, with signal range closure compensation equivalent to A_s at swath center, the uncompensated error will be about 0.6 cell resolution (at $\beta = 30^o$), which is acceptable.

The range closure compensation is proportional to wavelength and inversely proportional to ground cell resolution squared, $d_a \times d_a = d_a * d_r \csc \phi_o$. Therefore an approximate doubling of the L-band frequency from 1 to 2 GHz will reduce the expected range closure compensation error to 0.3 cell resolution at the swath edge, a clearly acceptable value. Conversely, a grosser cell resolution of about 35 meters in contrast to the 25 meters resolution of the baseline design has the same desirable effect and retains the long wavelength L-band feature (~ 28 cms).

In X-band, the compensation of doppler shifts associated with non-optimum beam position complicates ground processing. Normalized doppler shifts versus look angles are shown in Figure 4-27 for the circular and elliptic orbits with coverage from 10^o to 35^o look angle. In this figure, the doppler shift values are normalized by the factor $2v/\ell$ (= 1455 Hz) where v = 7.78 KM/s and ℓ = 10.7 meters, the SAR real array length. The optimum squint angles A_{so} correspond to the minimum change in $\dot{R}$ across the swath. For the elliptic orbit squint angle A_{so}, the doppler shift is nearly constant (~ 3 KHz) across the swath, which greatly simplifies the compensation algorithm and clutter tracking functions of the ground processor.

The critical factor of IPS beam positioning for the potential implementation of ERSIR with K_u-band should be a major consideration. Clutter doppler compensation for K_u-band (13.3 GHz) is more sensitive to beam position errors than X-band (9.0 GHz) by a factor of nearly 1.5; the variation of doppler compensation across the swath ($\beta = 10^o$ to 30^o) in Figure 4-27 will be about 2070 Hz at 13.3 GHz as compared to 1400 Hz at 9.0 GHz for $\Delta A = 0.3^o$.

Antenna squint angle positioning to A_{so} is needed to simplify that part of the ground processor design concerned with range closure compensation at L-band and doppler compensation at X-band. The 0.3^o accuracy for A_{so} previously mentioned may be obtained by using a pallet bay sensor and the inertial pointing sub-system (IPS) for spacelab attitude control. With the

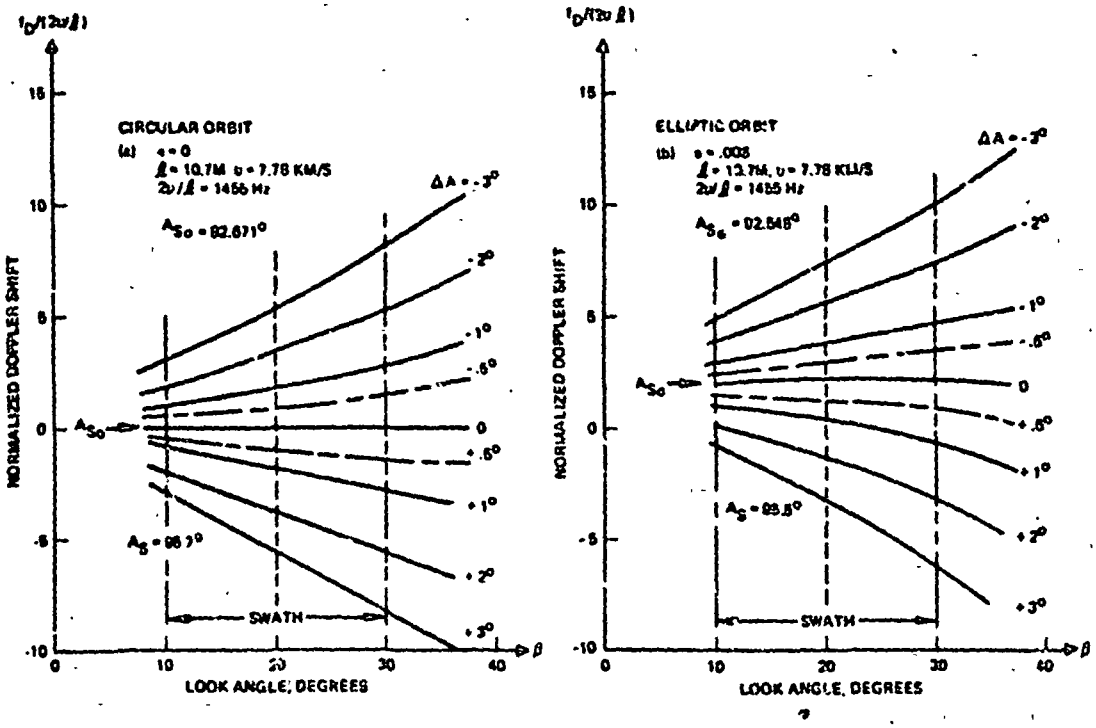

Figure 4-27. Doppler shift f_D vs look angle β, X-band (9.0 GHz), H = 200 km; i = 80°, ϕ = 40° N latitude.

orbiter reaction control system (RCS) alone; accuracies better than ±2.0° are not assured, because of the length and flexibility of the coupling between the pallet bay location and the Orbiter. Table 4-5 shows that the relevant accuracy of 0.3° may be obtained with the IPS.

TABLE 4-5. NAVIGATION ACCURACIES*

Reference Direction	STDN Accuracy (degrees)	TDRSS Accuracy (degrees)
Local Vertical	0.16.	0.16
NADIR Earth Target	0.18	0.28
30° Off Vertical	0.20	0.29

*Reference: Space lab payload accommodation handbook, April 1974, pp 27-28.

Conditions:

Payload sensor

- Alignment ±0.07°
- Drift ±0.04° per hour
- Deadband ±0.1°

185 KM orbit altitude
Payload Inertial Pointing system (IPS)

4.4 CALIBRATION

4.4.1 Model of Calibration Errors

The response S of the measurement system to the backscatter parameter σ_o characteristic of terrain is expressed by the range equation for SAR:

$$S = P_{av}\left(\frac{\lambda}{4\pi R_s}\right)^3 \frac{G_o^2 G_r d_r g(\theta,\phi)\sigma_o}{(2v/\beta_t)F_\ell F_p \sin\phi\sin\theta} \qquad (1)$$

where S has the units of P_{av};

P_{av} is the average transmitter power;

λ is the wavelength of the radiation;

R_s is the slant range;

G_o is the peak antenna gain;

G_r is the receiver/processor gain to the point of measurement S;

$g(\theta,\phi)$ is the antenna pattern function relative to the angular coordinates θ, ϕ of the resolution cell;

ϕ is the angle of incidence at the ground*;

θ is the angle of the line-of-sight relative to the velocity vector ($\theta \approx 90^o$);

v is the magnitude of the velocity;

β_t is the bandwidth of the transmitted waveform;

$d_r = c/2\beta_t$ is the slant range resolution ($c/2 \approx 150$ m/μs)#

$F_\ell > 1$ is a loss factor for sensor plumbing and all appropriate processing losses;

$F_p > 1$ is a loss factor due to the propagation medium.

---

*$\phi = \beta + R_g/R_e$ where R_g is the ground offset range to the resolution cell and R_e is the radius of the earth and β is look angle.

#Ground resolution d_g is given by $d_g = d_r/\sin\phi$

The wavelength λ, slant range R_s, bandwidth β_t, and resolution d_r are known very accurately in the proposed SAR system. The system wavelength is established by a stable fixed frequency source; the range R_s is resolved to the unambiguous interval containing the swath and corresponding to an accurately established prf. The range to an individual resolution cell is accurately metered and tagged by precision clocks and counters; the slant range resolution d_r and transmitted waveform bandwidth β_t are accurately established by the linear FM digital approximation for pulse compression. The proposed calibration approaches replicate each transmitter waveform (pulse by pulse) and facilitate precise measurement of d_r. The relevant calibration accuracy involving λ, R_s, β_t, and d_r should be better than ±0.3 dB RSS (seven percent root-sum-squared).

The angles ϕ and θ are derived from Space Shuttle inertial referenced signals and from active sensor sensing of clutter (terrain backscatter) signals. These angles must necessarily be determined with mean errors very near zero, that is to a small fraction of the respective vertical and horizontal beamwidths of the antennas. The effects of angular errors are especially severe at the near and far edges of the swath corresponding to the steep slopes of the vertical gain pattern of the antenna. For this reason, the following discussion of errors will be restricted to the middle third of the swath; i.e. the calibration error model is applied to the central third of the vertical beamwidth. Local terrain slopes average to zero over substantial distances and their effects can be partially compensated using topological survey maps with "ground truth" knowledge; the model does not treat this source of error.

For convenience, the signal response S of (1) is rewritten:

$$S = K_o \sigma_o^* = K_o \sigma_o (1 + \mu) \tag{2}$$

where K_o is the "true value" of the proportionality factor

$$K_o = P_{av} \left(\frac{\lambda}{4\pi R_s}\right)^3 \frac{\sigma_o^2 C_r g(\theta, \phi) d_r}{(2v/\beta_t) F_\ell F_p \sin\phi \sin\theta} \tag{3}$$

The signals S and σ_o^* are expressed in logarithmic units (dB's):

$$S(dB) = 10 \log S = 10 \log K_o + 10 \log \sigma_o^* \tag{4A}$$

$$\sigma_o^*(dB) = \sigma_o(dB) + 10 \log(1 + \mu) \tag{4B}$$

Thus the error μ is conveniently expressed in dB (logarithmic) form:

$$\mu(dB) = 10 \log(1 + \mu) \tag{5}$$

In the following discussion, as in the discussion in Section 1.4, the error μ will be understood as a logarithmic unit made up of the sum of similar error components μ_i (in decibel units):

$$\mu(dB) = \sum_{i=1}^{N} \mu_i \tag{6A}$$

with $\mu_1 = 10 \log (1 + \Delta P/P)$,

$\mu_2 = 20 \log (1 + \Delta G/G)$,

$\mu_3 = 10 \log (1 + \Delta G_r/G_r)$,

$\mu_4 = -10 \log (1 + \sin(\phi + \Delta\phi)/\sin(\phi))$, (6B)

$\mu_5 = -10 \log (1 + \Delta F_\ell/F_\ell)$

$\mu_6 = -10 \log (1 + \Delta F_p/F_p)$,

$\mu_7 = 10 \log (1 + \Delta g(\theta,\phi)/g(\theta,\phi))$,

Etc, etc.

In some instances, the individual μ_i are made up of a sum of diverse source errors peculiar to the generic error type; the losses in F_ℓ, for example, are due to component losses in transmitter plumbing, receiver connections, and various sources of processing losses. Figure 4-28 is a sketch of error sources.

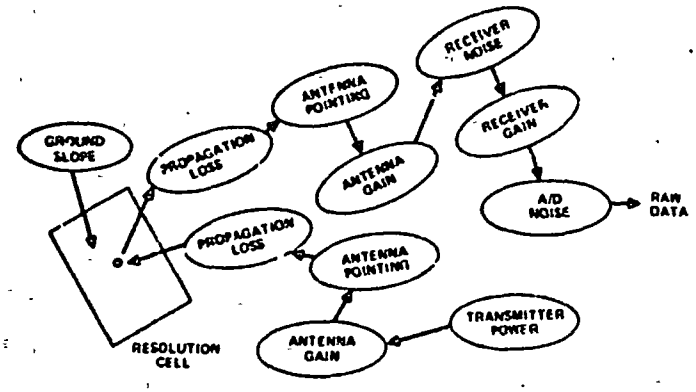

Figure 4-28. Sources of uncertainties in σ_o measurement.

The error model treats the μ_i and the component parts of μ_i as mutually independent. Thermal cycling, for example, will produce predictable effects on some critical parameters; such systematic error sources are to be compensated with the best available knowledge. The assumption of independence on the basis of compensation for known and monitored stresses (primarily thermal) is reasonable. Further, the ensemble of errors both individually (μ_i(dB)) and collectively (μ(dB)), will be treated as normally distributed with zero mean in logarithmic units (a log-normal distribution of linear errors). Thus the variance in calibration error (in dB) is the sum of variances of the individual μ_i's (in dB).

4.4.2 Spectrum of Calibration Errors

The limiting envelope of the power spectrum of calibration errors is modeled by Figure 4-29; the autocorrelation function corresponding to the spectrum is sketched in Figure 4-30. These curves reflect the following modeling:

1. Each Space Shuttle mission with ERSIR involves a steady component of calibration error; i.e. an unknown "d-c" component having zero-mean expectancy (over a large ensemble of systems) but a standard deviation presently estimated at 0.9 dB;
2. A uniform power density "low frequency" component with a cut-off frequency proportional to the orbit rate (f_{orbit} = 0.302/orbit period); this variation involves orbit-to-orbit changes, arising primarily from imperfectly compensated thermal stresses;

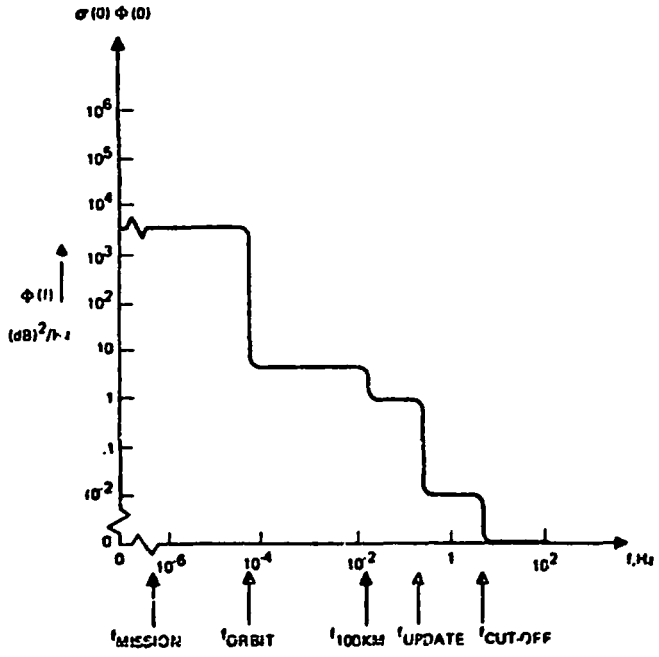

Figure 4-29. Limiting envelope density function $\Phi(f)$ of calibration error μ (in dB).

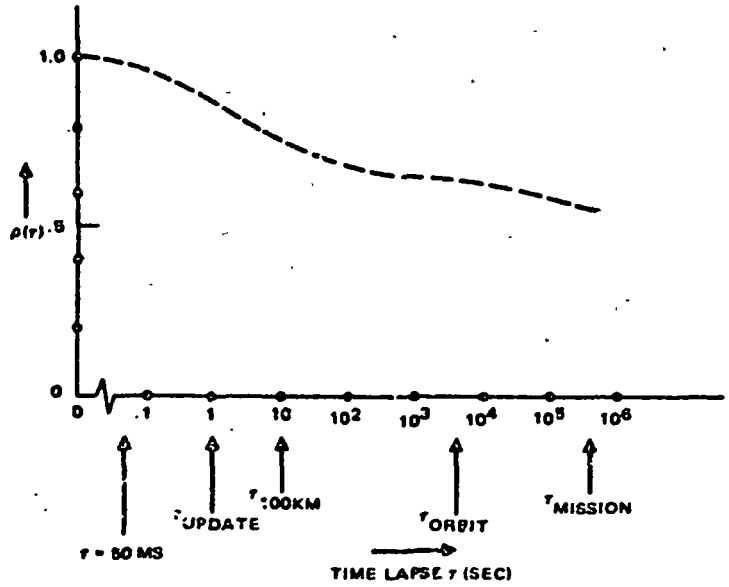

Figure 4-30. Autocorrelation function $\rho(\tau)$ (normalized autocovariance function) of calibration error μ (dB).

3. A uniform power density component, which reflects rates of change within an orbit period but of a relatively slowly fluctuating nature; cut-off for this component is proportional to the rate 100 km strips are imaged;

4. A moderate frequency component related to changes slower than the update rate (for AGC and clutter sensed corrections to angle estimates of θ and ϕ, cut-off $f_{update} = 0.302/\text{update interval } \tau_{update} = 24$ Hz);

5. A high frequency component associated with measurement changes for path lengths of a few hundred meters to the up-date interval at about 10 km; these changes result from uncompensated components of the Space Shuttle attitude and control system plus geometrical factors associated with the terrain and the local atmospheric propagation fluctuations (significant only at X-band);

6. Negligible error power density above the cut-off frequency $f_{co}=6$ Hz, corresponding to a time interval of 50 ms or a path length of about 400 meters.

4.4.3 Preliminary Estimate of Calibration Error

Table 4-6 summarizes tentative, preliminary estimates of ERSIR calibration error components. Time periods correspond to the time lapses

TABLE 4-6. PRELIMINARY ESTIMATED COMPONENT ERRORS (dB)

Error Source	μ_i	68%/95% Confidence Levels*				
		$\tau_{50\ ms}$	τ_{update}	$\tau_{100\ km}$	τ_{orbit}	$\tau_{mission}$
Trans power, P_{av}	μ_1			0.1/0.2	0.15/0.3	0.3/0.6
Antenna Gain, G_o^2	μ_2				0.4/0.8	0.7/1.4
Receiver Gain, G_r	μ_3		0.25/0.5	0.1/0.2	0.1/0.2	0.25/0.5
Sensor Loss, F_ℓ	μ_4		—	—	0.1/0.2	0.2/0.4
Vert Angle+, sin ϕ	μ_5		0.25/0.5	0.1/0.2	—	—
Pattern Gain, $g(\theta,\phi)$	μ_6	0.1/0.2	0.3/0.6	0.1/0.2	—	0.2/0.4
Prop Loss, F_p and misc.	μ_7	0.25/0.5	0.25/0.5	0.1/0.4	0.15/0.3	0.35/0.7
Clutter Sensing, Az and El	μ_8	0.1/0.2	0.4/0.8	0.3/0.6	—	—
Epoch RSS	σ_e	0.29/0.57	0.66/1.32	0.41/0.82	0.47/0.95	0.92/1.84
Net Expected	μ	1.32/2.64	1.29/2.57	1.1/2.2	1.0/2.0	0.92/1.84

Notes: *Based on normal distribution of μ_i's in dB.

+Vertical Pointing Error at $\phi = 20^o$; worst case.

#Includes net calibration error for wavelength λ, slant range R_s, transmitter bandwidth β_t and slant range resolutions d_r.

τ in Figure 4-30. The intervals range from short intervals of about 50 milliseconds through the 90 minutes of an orbital period, to the time (7 to 30 days) of an entire mission. The dc component of error (τ mission, Figure 4-29) is the expected bias error for a particular mission and ERSIR sensor. It has a standard deviation of 0.92 dB, corresponding to a confidence level of 68 percent for the lognormal distribution of errors. For twice the standard deviation (1.84 dB) the confidence level is 95 percent; 50 ms values of 1.32 dB and 2.64 dB give confidence levels of 68 percent and 95 percent, respectively, for specific measurements.

A briefer summary of the tentative ERSIR calibration error components is presented in Table 4-7. The first four intervals of Table 4-6 are grouped to show net components.

TABLE 4-7. BRIEF SUMMARY OF SENSOR CALIBRATION

Calibration Performance*		
Calibrated Parameter	Estimated Error (95% Confidence)	
	Long Term	Temporal
Transmitter power	0.6 dB	0.4 dB
Receiver Gain	0.5	0.5
Sensor RF Losses	0.4	0.2
Antenna Peak Gain (2-way)	1.4	0.8
Vertical Angle, Sin $(\Delta+\phi)/\text{Sin}\phi$:	—	0.6 ($\Delta=3^{o}$, $\phi=20^{o}$)
Gain Pattern (2-way)	0.4	0.7
Clutter Sensing (Az and El):	—	1.0
Prop Loss and Misc	0.7	0.5
Net RSS	1.84 dB	1.82 dB
	TOTAL = 2.6 dB	

Notes: *Applicable to middle third of swath;
at swath edges: +2 dB gives net RSS = 3.3dB

Detailed studies of calibration error sources and the calibration mechanisms are necessary to refine the accuracy of the tentative and preliminary estimates given here.

4.4.4 Implementation of Calibration

The ERSIR utilizes specific operations and routines to supply data used by the ground processor for calibration. The calibration routines and equipment appropriate to ERSIR are discussed below. These approaches to implementation are preliminary and tentative. The approaches will be defined more specifically in detailed design studies.

The ERSIR system will require calibration for antenna gain and pattern. Calibration routines and special tests for this purpose are not discussed. However, it is expected that existing calibration facilities will be used, these include special test ranges with standard targets such as corner reflectors. The on board calibration routines discussed apply to the measurement of antenna gain and patterns using available test ranges and facilities.

ERSIR Sensor

Calibration Operations. Shuttle ERSIR sensor calibration operations are divided into two broad categories, namely, calibrate routines and built-in-test. Calibrate routines consist of programmed operations which provide calibration data for:

- Transmitter Power
- Receiver Gain, and
- Sensor Noise.

In actual operation, transmitter power and receiver gain are measured together; the proposed implementation employs the transmitter waveform for receiver gain calibration data.

The sensor noise calibration routine provides the calibration data used for estimating ERSIR system noise, composed largely of receiver thermal noise and A/D converter noise. This noise is a component of measurement bias error for signals of finite magnitude. To provide very accurate estimates

of clutter signal reflectivities, the ERSIR measurement system requires an accurate estimate of the sensor noise component. The ground processor will use the sensor noise calibration to correct for bias error.

Built-in-test consists of two parts:

- Special routines to test various parts of the sensor and supply critical status data (voltages, etc)
- Continuous monitor routines, which provide status data during normal sensor operations

Only the continuous monitor function is directly related to calibration. This function provides "continuous" data on transmitter power, waveform, and receiver gain. During each transmission, the receiver responds to a sample of the transmitter waveform in a controlled manner; this receiver gain "monitor" provides quantitative data on (a) receiver gain and (b) transmitter waveform. Additionally, the continuous monitor function provides accurate data on the average transmitter power, duplicating the power measurement function of the calibration routines discussed below.

Transmitter/Receiver Calibration. The calibrate routine for transmitter power and receiver calibration is executed in a special purpose mode of ERSIR. In this mode the antenna may be disconnected and the transmitter power coupled into an internal dummy load, or the antenna may be directed skyward, or the antenna might be tilted to look near the horizon (large look angles); the purpose being to avoid earth reflected signals of sufficient magnitude to significantly degrade calibration accuracy.

Figure 4-31 is a functional block diagram of the implementation of the transmitter/receiver calibration routine. A sample of the L-band and X-band transmitter waveform are coupled from a port very near the respective antenna. These transmitter waveform samples are then routed to respective L- and X-band calibration transponders where they are reproduced, range delayed and measured for power. The range delayed RF reproductions of the transmitter waveforms are then coupled to the respective L-and X-band receivers. In the case of the direct polarization (V-POL in the figure), the transponder RF outputs couple to the receiver port over a path shared by

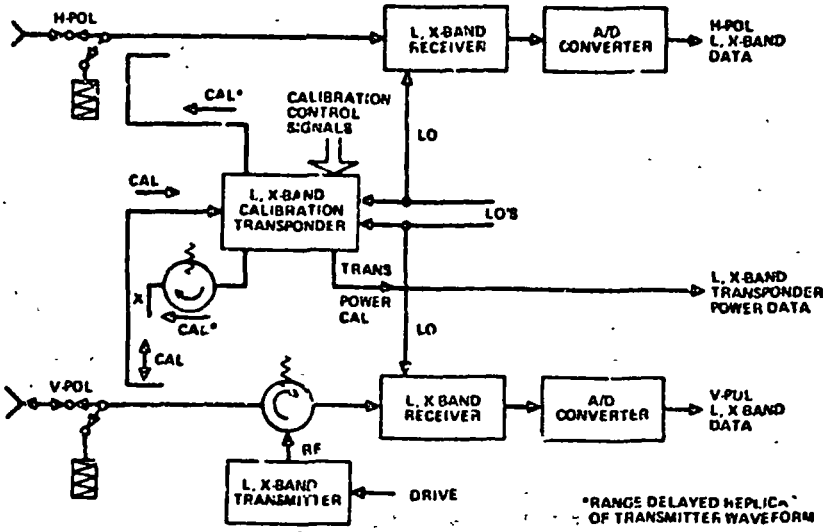

Figure 4-31. Transmitter/receiver calibration.

the transmitter waveform. The cross-polarized receiver (H-POL in Figure 4-31) is coupled to the RF calibration signal at a port very near its antenna. For both cases, much of the RF plumbing path is traversed by both calibration and actual sensor signals. In consequence a significant portion of the RF plumbing signal path is utilized for the calibration.

Signals from the Control Module control the calibration process; the transmitter waveform is reproduced at other ranges and amplitudes for completness.

The calibrator (calibration transponder) makes power measurements on the transmitter waveforms and sends the transmitter power data to the recorder. The L-band and X-band receiver calibration data are recorded in the same way as the sensor signals obtained during ERSIR experiments.

The operational parameters for calibration (transmitter waveform, bandwidths, pulse durations, prf's) are established by the normal sensor control system. The parameters may or may not be sequenced over a range of values, depending upon operator option or planning. However, it is expected that the calibration routine would be repeated for each experiment.

Sensor Noise Calibration. The sensor noise calibration routine is a special purpose mode of ERSIR. The antenna may or may not be connected. The connected antenna receives signals from external radiation sources. In appropriate cases these signals may be used to make the assessments of measurement errors attributable to these sources. The routine should include measurements with and without the antenna coupled where this is practicable.

Figure 4-32 illustrates the implementation of the sensor noise calibration routine. There are, basically, two parts:

1. A "passive" part in which the receivers have no external input; this provides the baseline measurement data
2. An "active" part in which a calibrated noise source is coupled to the receiver inputs; this provides the means of making noise figure or effective noise temperature estimates for the receivers.

The RF wideband noise sources are time gated. This feature facilitates radiometric type measurements which may be appropriate for antenna gain assessments and will, in any case, permit quantitative assessments of external radiation sources which can be of value for planning ERSIR experiments.

In all cases, the transmitter are in "standby" or "sniff" modes to prevent transmitter RF energy from interferring with the calibration.

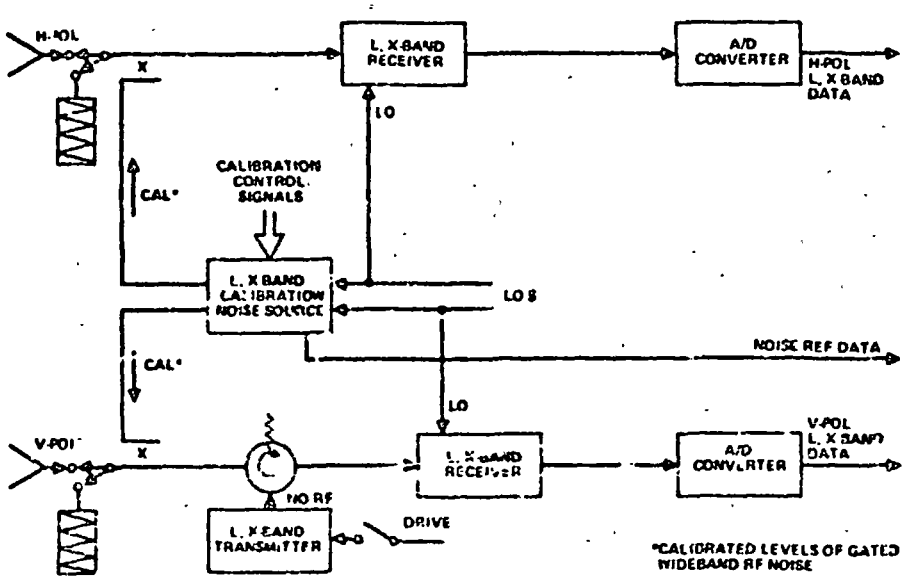

Figure 4-32. Sensor noise calibration.

Built-In-Test Continuous Monitor. Built-in test continuous monitor functions are performed during normal ERSIR sensor operations. Transmitter power, waveform and receiver gain data are the primary outputs of the continuous monitor function and they are the status data of most significance for ERSIR measurement system accuracy.

Figure 4-33 is a functional block diagram of the built-in-test continuous monitor functions of immediate interest. Samples of the L- and X-band transmitter waveforms are coupled from a port near the antenna and serve as inputs to a calibration transponder as in the transmitter/receiver case. However, in this case the RF signals are down-converted to IF, and inserted into the receiver at an intermediate stage of amplification. The IF reproductions of the transmitter waveforms, delayed very slightly because of the finite bandwidths of the calibrator (35-50 MHz), have a nearly fixed level relative to transmitter power. Consequently, they supply continuous monitor data on very significant portions of the receiver gains. Furthermore, they provide monitor data on the waveforms themselves, their bandwidth duration and phase codes for pulse compression. These receiver monitor continuous data complement the data from transmitter/receiver calibration routines, which are separated by significant intervals of time.

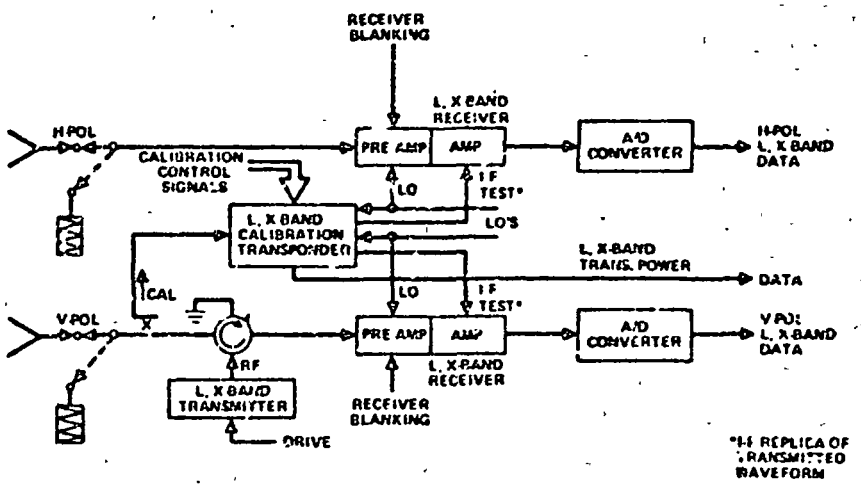

Figure 4-33. BIT continuous monitor.

The continuous monitor routine provides for L and X-band transmitter power measurements. Continuous monitor data consequently serve the dual purpose of determining transmitter power status and updating the calibration.

The continuous monitor functions illustrated in Figure 4-33 impose a design requirement on receivers. The usual receiver blanking function, which eclipses the transmitter feed-through signal, must attenuate the IF transmitter feedthrough signals to levels well below the IF test signals from the calibration transponder. The requirements for the receiver in Section 6.5 anticipate this need.

4.5 SAR IMAGE NOISE SOURCES AND MEASUREMENT QUALITY

4.5.1 Image Noise Sources

Various elements of the SAR measurement system, including the ground processor, contribute to image noise (signal to noise ratio). Sources of image noise are briefly reviewed in this section. An itemized list of distortion noise source is presented, together with a preliminary and tentative budget of their contributions to the Integrated Side Lobe Ratio (ISLR).

The sources of noise that contribute to the image signal are shown in Figure 4-34. The usual noise sources are receiver noise, range and azimuth PRF ambiguity, and A/D quantization. Additional sources are the integrated sidelobes which accompany the pulse compression waveform and

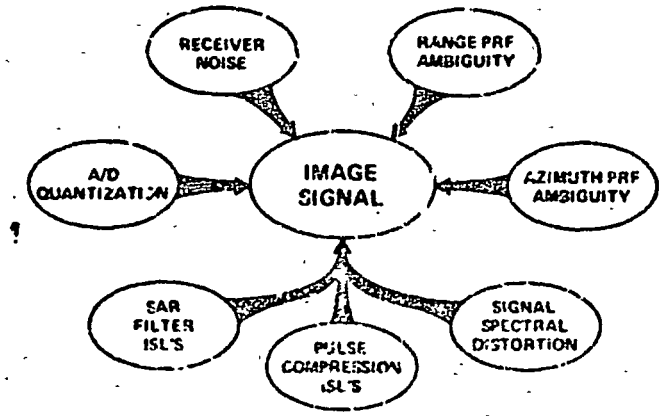

Figure 4-34. Image noise sources.

processing and the SAR filter processing. A general category, "signal spectral distortion" accounts for such sources as phase distortion in propagation and from vehicle motion (acceleration).

In estimating image and measurement quality, the contributions of receiver noise and PRF ambiguities are treated independently. The remaining items are sources of signal spectral distortion (see Figure 4-35) or sidelobe energy. They are listed in the ISLR budget, Table 4-8.

The SAR ISLR budget shown in Table 4-8 reflects a preliminary and tentative judgment of the contributions from the sources of sidelobe energy itemized. A detailed design study will be required to make the list complete. This will involve adding any significant sources not listed and possibly deleting some items, such as propagation and motion effects, that may not be significant. Error analysis of the detailed SAR sensor design as it evolves will be used to revise and up-date the ISLR budget in order to estimate performance realistically.

The major contributor to the ISLR budget, Table 4-8, is A/D converter quantization noise. The value, -22 dB, anticipates a contoured AGC which sets A/D converter signals near their optimum values (±3 dB), see Figure 4-36.

The transmitter, receiver, A/D, and pulse compression (digital linear FM approximation) are other large contributors to the ISLR budget. Time jitter is the principal cause of this contribution. The contribution is

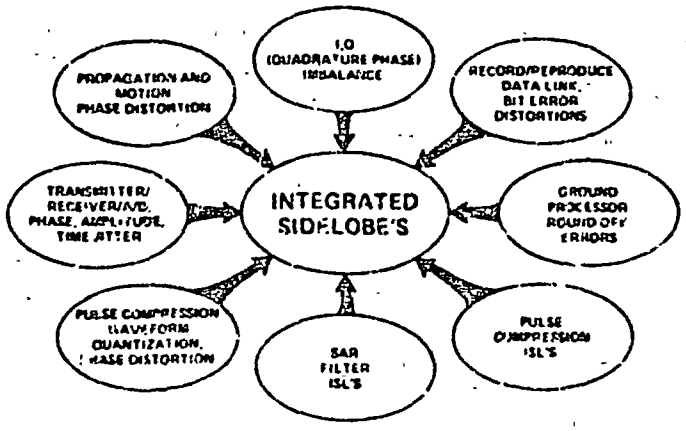

Figure 4-35. Sources of signal spectral distortion.

TABLE 4-8. SENSOR SAR ISLR BUDGET

Sidelobe Energy Source	Contribution
Propagation and Motion Effects	@ - 40 dB ea
Transmitter/Receiver/A/D	- 27
Pulse Compression Quantization	- 26
I, Q Imbalance	- 33
A/D Converter Quantization	- 22
Record/Reproduce	- 36
TDRSS Data Link	- 36
Range/Doppler Compensation	@ - 40 ea
Processor Round-off	- 33
Sub-Total	- 19 dB
SAR Processing	
Range Compression	- 22 dB
Angle Compression	- 22 dB
Total	- 16 dB

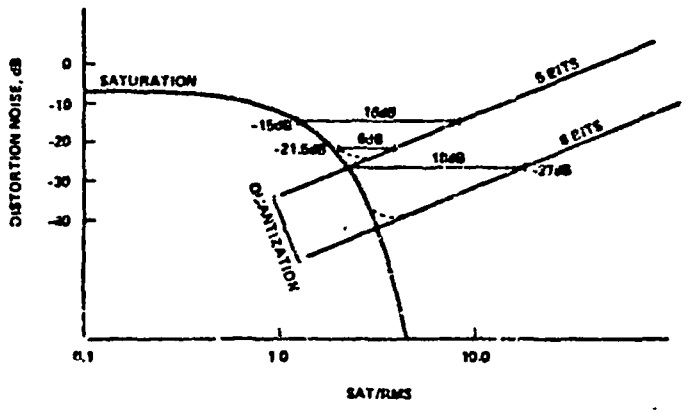

Figure 4-36. Distortion noise.

related to bandwidth, since the time jitter to be appreciable must be a significant portion (3 percent rms) of the reciprocal bandwidth of the transmitted waveform (37 ns at 27 MHz bandwith).* A substantial contribution of time jitter at look angles near nadir is anticipated; beyond look angles β of 30 degrees the time jitter contribution should rapidly diminish (as cosecant β).

The value for the pulse compression quantization effect (-26 dB) listed in the table is largely an estimate. It should be significant for the digital approximation to linear FM ISLR contribution and to correspond, approximately, to non-ideal pulse compression by any technique. The contribution is separated from the ISLR budgeted contribution (-22 dB) for range compression to signify its importance; the net contribution is -20.5 dB.

The quadrature phase channel (I, Q) imbalance contributions arise from imprecise quadrature phase relation (90 degrees ideally) and gain imbalances in the video down conversion process; for example, PM of 1.3 degrees rms or an AM index of 2.2 percent rms (0.1 dB) imply contributions of -36 dB.

The following relatively minor contributers make an aggregate contribution of -28.5 dB:

Propagation and motion effects,	-37 dB
Data storage and transmission,	-33 dB
Range/doppler compensation,	-37 dB
Processor round off,	-33 dB.

SAR processing, with suitable weighting, results in a net ISLR contribution of -19 dB for range and angle compression at -22 dB each. The net result is -16 dB for this preliminary and tentative SAR ISLR budget.

4.5.2 Measurement Quality

The implications of image quality for the ISLR budget at -16 dB are seen in Table 4-9. At the edge of the swath, the signal-to-thermal (receiver)

*This bandwidth of 27 MHz corresponds to a range resolution of 5.7 meters and a ground resolution of 25 meters at a look angle β = 13 degrees and 12.5 meters at β = 27 degrees).

TABLE 4-9. IMAGE QUALITY

Image Noise Source	Contribution		
	Swath	Edge	Center
Thermal Noise	-8 dB	-8 dB	-14 dB
SAR ISLR	-16	-16	-16
Angle PRF Amb.	-20[1]	-22	-22
Range PRF Amb.	-16[2]	-22	-22
Net	-6.6 dB	-7.1 dB	-11.1 dB

Notes: 1. $PRF = PRF_{min}$
2. $PRF = PRF_{max}$

noise ratio, S/N, is -3 dB minimum. Two cases of PRF ambiguity are treated. In the first, a worst case, the PRF is simultaneously near its minimum value for angle ambiguity and its maximum value for range ambiguities, which is characteristic of the worst case condition. The net contribution to relative noise level for this case is, therefore, -6.6 dB. In the second case (far swath edge) the improvement in angle and range ambiguities from a net relative noise level of -14.5 dB to -19 dB, results in a 0.5 dB improvement in relative noise level (from -6.6 dB to -7.1 dB). At swath center, the S/N improvement of 6 dB, with the favorable PRF ambiguity making a net contribution of -19 dB, results in a 4 dB improvement in the net image signal-to-total noise ratio, from +7.1 dB to +11.1 dB.

This image quality feature of SAR processing is responsible for textural distinctions in imagery; the contrast between sharply defined terrain surface features and a general background level of "clutter" is improved with the improvement in the image signal-to-total noise ratio.

Image quality, a figure-of-merit for imagery, is also an index of measurement quality for a large class of ERSIR measurement systems. Applications of ERSIR to agronomy, for example, include crop and soil moisture assessments in which the backscatter parameter σ_o for sizeable

areas of terrain is estimated. For homogeneous areas smaller than 100 hectares (1 square kilometer, about 250 U.S. acres), the ISLR contributions extend beyond the borders of the region for which the σ_o estimate is desired and must be included in the measurement problem as interference or noise.

The figure-of-merit measurement quality for one class of SAR measurement system applications is somewhat better than the figure-of-merit generally. This class of SAR measurement system applications is for homogenous, extensive backscattering surfaces for which σ_o estimates are required; for example, the estimation of backscatter reflectivity σ_o for wheat fields on a generally level plain. In this case, the integrated noise sidelobes of the SAR image are produced by the same reflectivity surfaces as those producing the mainlobe signal image (a hypothesis susceptible to verification at the image quality figure-of-merit); in this case, the SAR ISLR component (-16 dB) belongs to the signal. The result is an improvement of 0.5 to 1.7 dB in the net measurement signal-to-total noise ratio, from +11.1 dB to 12.8 dB at swath center (S/N = 14 dB), as shown in Table 4-10.

TABLE 4-10. MEASUREMENT QUALITY, HOMOGENEOUS TERRAIN

For homogeneous terrain include SAR integrated sidelobes in σ_o estimate:

Measurement Noise Source	Contribution		
	Swath	Edge	Center
Thermal Noise	-8 dB	-8 dB	-14 dB
Angle PRF Amb.	-20[1]	-22	-22
Range PRF Amb.	-16[2]	-22	-22
Net	-7.1 dB	-7.7 dB	-12.8 dB

Notes: 1. $PRF = PRF_{min}$
2. $PRF = PRF_{max}$

An area of roughly 200 hectares (2 square kilometers, about 500 U.S. acres) is required to make effective use of the larger of the two figures-of-merit. Homogeneous areas not so large must, of course, be estimated as the reduced measurement quality; 11.1 dB signal-to-total noise ratio at swath center (S/N -14 dB) rather than 12.8 dB. This is, of course, the general situation. It is impractical to attempt extension of the concept to PRF ambiguities, either in range (distance > 100 km) or angle (distances > 5 km at X-band, 45 km at L-band).

5.0 GROUND PROCESSING SYSTEM

5.1 DESCRIPTION OF GROUND PROCESSING SYSTEM (GPS)

The Ground Processing System (GPS) plays back the magnetic tapes which were recorded in the spacecraft, processes the reproduced raw data, and generates a film copy of the synthetic aperture image data. The system contains a tape unit, which reproduces and formats the original 5-bit I/Q digital video; a signal processor unit which compresses the digital data in range and azimuth; and a high resolution laser beam recorder, which records the image data on 5-inch film.

A basic configuration of the GPS is shown in Figure 5-1. It consists of a Programmable Signal Processor (PSP), film recorder and tape recorder. The signal processing element is the PSP, which is a special purpose, high speed computer designed to execute, under program control, signal processing algorithms. In this configuration of the GPS, the PSP would be

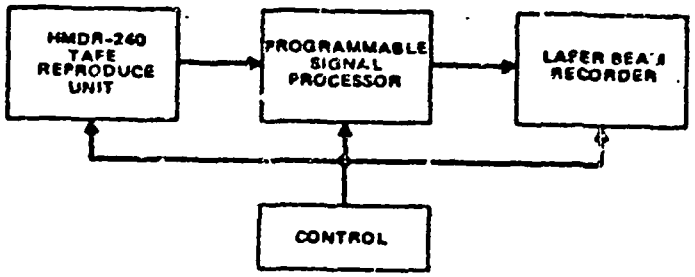

Figure 5-1. Ground processing system.

programmed to perform synthetic aperture processing of the raw data. With these components the GPS can generate high quality strip maps on photographic film.

Use of the PSP as the processing element allows the GPS to grow into a more efficient configuration. A disadvantage of the basic GPS is the need to perform data analysis on the photographic film. The film is then analyzed either visually or with an image scanning system that converts the data into a format suitable for analysis. Signal processing parameters such as azimuth and range processing algorithms, dynamic range, and image integration can be varied but require a repetition of the film recording process. With the basic system therefore, time spent on non-productive tasks such as data search, film recording, and film processing can be excessive. The efficiency of the GPS can be improved considerably by adding a second tape unit, a general purpose computer, and a means of displaying the image data.

A more optimum configuration of the GPS is shown in Figure 5-2. In this configuration, the operator can view the image in real time. Four CRT displays are used to display the image data for each transmitted frequency and polarization. An additional color display integrates the data observed on the black and white displays to a color composition. The data

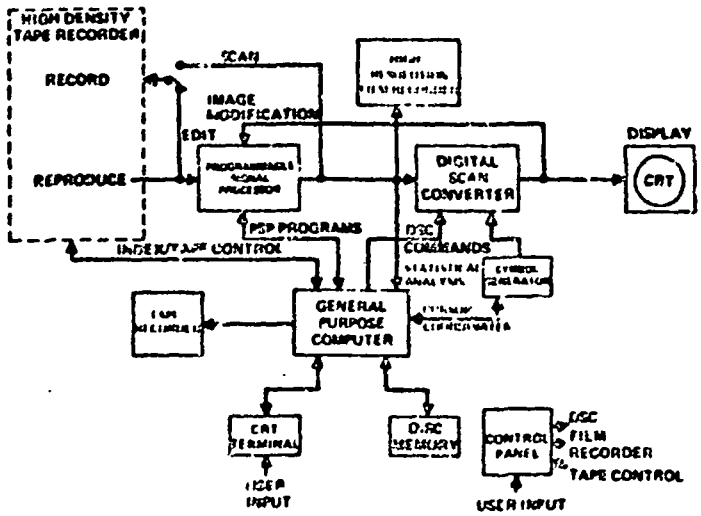

Figure 5-2. Ground processing system.

corresponding to each frequency and polarization can be encoded in color and presented on the color display. A typical composition format is shown in Figure 5-3.

The image data from the PSP is sent to the Digital Scan Converter (DSC). The DSC converts the synthetic aperture image data into a flicker-free TV raster, which is then displayed on the CRT's. The DSC contains sufficient memory to store four images at reduced resolution (1000 x 1000 elements) or a complete image at full resolution (4000 x 4000 elements). This storage capability allows the user to freeze the image on the display and perform real time analysis of the image data. The DSC in conjunction with the CRT displays provides rapid monitoring and anslysis of the data.

The DSC and the PSP in this configuration are controlled by a general purpose minicomputer. PSP programs are stored in the computer. Typical programs select dynamic range, resolution, image to be processed, and image processing functions. These programs are loaded into the PSP at the user's command. The computer also controls the DSC and tape reproduce functions. User input commands are entered via a CRT terminal. The user selects the section of the recorded tape to be processed, PSP functions, and the display format. The user also has the capability of sending the image data to the computer. He then performs statistical analysis of the data or records the data on computer compatible tape for analysis at a different

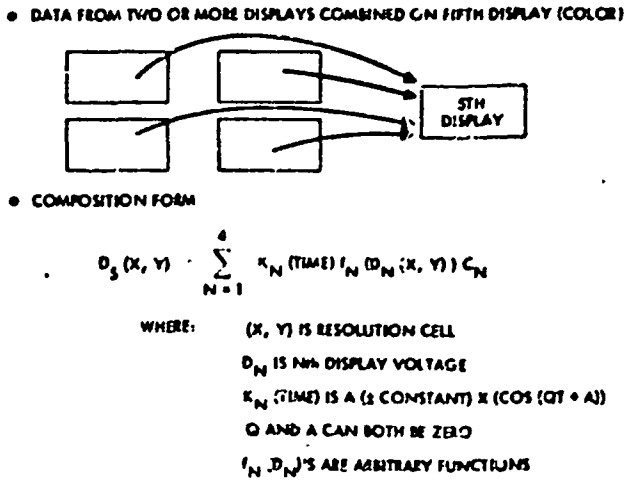

Figure 5-3. Data composition.

location. The disc memory is for storage of PSP programs. The disc storage contains a library of processing algorithms.

A tape recording function has also been added to the system. The recorder with the reproduce unit gives the GPS an editing function. This feature allows the user to selectively edit the mission tapes, thus reducing the large amount of recorded data that must be handled.

The final function in this configuration of the GPS is the symbol and cursor generator. A symbol generator provides annotations on the display. These designate the parameters recorded during the mission. The cursor generator positions a cursor on the display to allow the user to designate areas of the image for closer examination or further processing by the PSP or the computer. The computer performs a statistical analysis of the data enclosed within the cursor. A copy of image data within the cursor can also be recorded on computer compatible tape. A high resolution film copy of the image data can be made on the film recorder.

The control panels allows the user to control manually operational modes in the GPS. These functions include:

1. Freeze Mode – The image data can be stored on the display.
2. Repeat Mode – The tape playback is continuously cycled through the same data. If desired, the processing can be altered on each pass through the data.
3. Data Copy – Image data is recorded on the film recorder. Annotations generated by the symbol generator are also recorded.
4. Cursor Control – The cursor can be manually positioned on the display. The cursor coordinates are transferred to the computer and to the PSP.

5.2 PHYSICAL CHARACTERISTICS OF GPS

An artist's conception of the Space Shuttle Ground Processor is shown in Figure 5-4. The system contains two RCA high density tape recorders (HDMR-240), which reproduce the raw data and perform the editing function of the GPS. The five displays and the four Programmable Signal Processors provide real time viewing of the processed data. Four PSPs are used for real time high resolution processing of the raw data. A high resolution laser beam recorder (RCA LR71) provides a hard copy of the

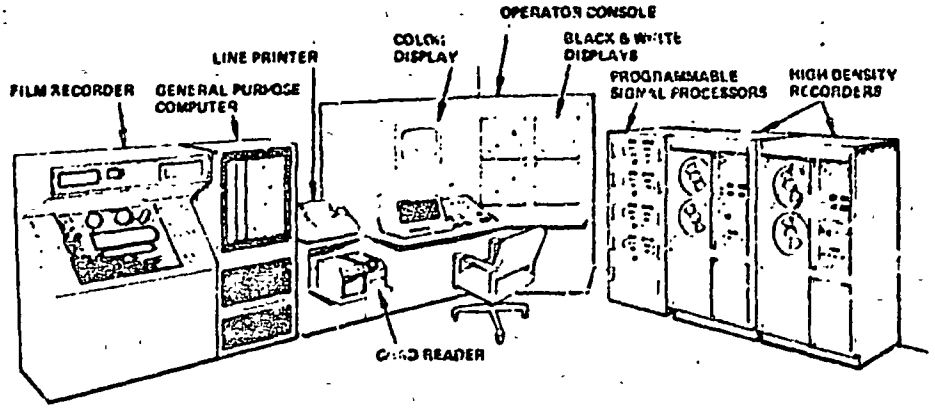

Figure 5-4. Space shuttle ground processor.

image data. This unit can record 20,000 elements per range line and has a capacity of 1500 feet of 5-inch film. The entire system is controlled by the general purpose computer. The computer with a control panel simplifies the interaction between the user and the system. The computer peripherals (disc memory, tape recorder, CRT terminal, card reader, and line printer) provide program and data storage as well as input and output of programs, data, and analytical results. All components within the system are operated from the control panel.

5.3 MODES OF OPERATION

The sequence of operations for the Ground Processing System is shown in the operation flow charts in Figures 5-5, 5-6, and 5-7. After each mission a scan tape is prepared as shown in Figure 5-5. Each of the mission tapes is played back into the PSP. The PSP is programmed by the computer to select vertically polarized X-band data and process the data in a low resolution mode (100 meters). The image data is then recorded on magnetic tape with the recorder operating at a tape speed of 8 inches/sec. This scan tape when played back into the CRT display provides the user with a quick look at the image for the complete mission. The tape can be played back in real time or at high speed (120 IPS). Also recorded on the scan tape will be a

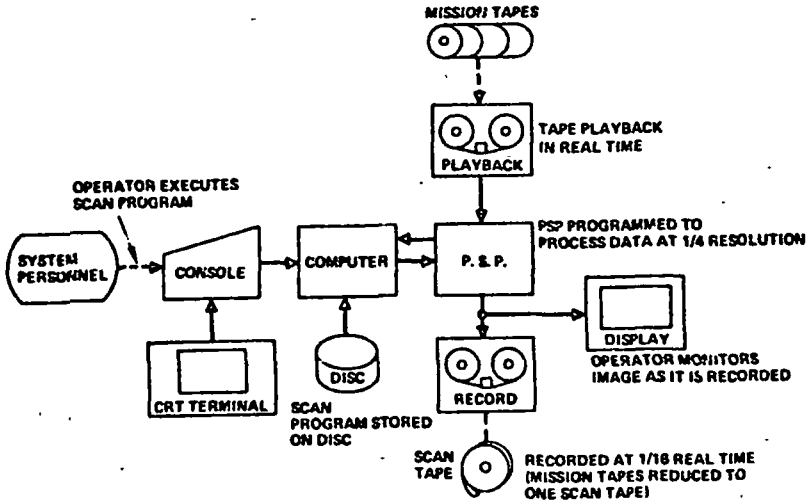

Figure 5-5. Space shuttle ground processor operational flow – scan tape generation.

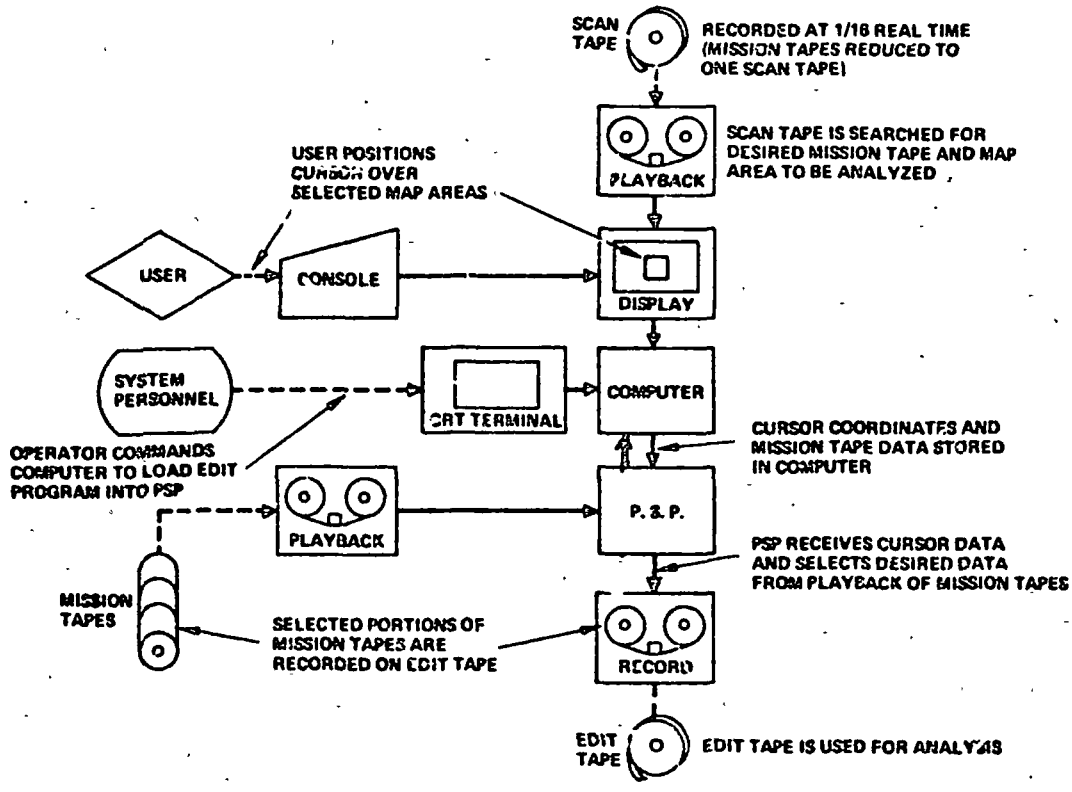

Figure 5-6. Space shuttle ground processor operational flow – edit tape generation.

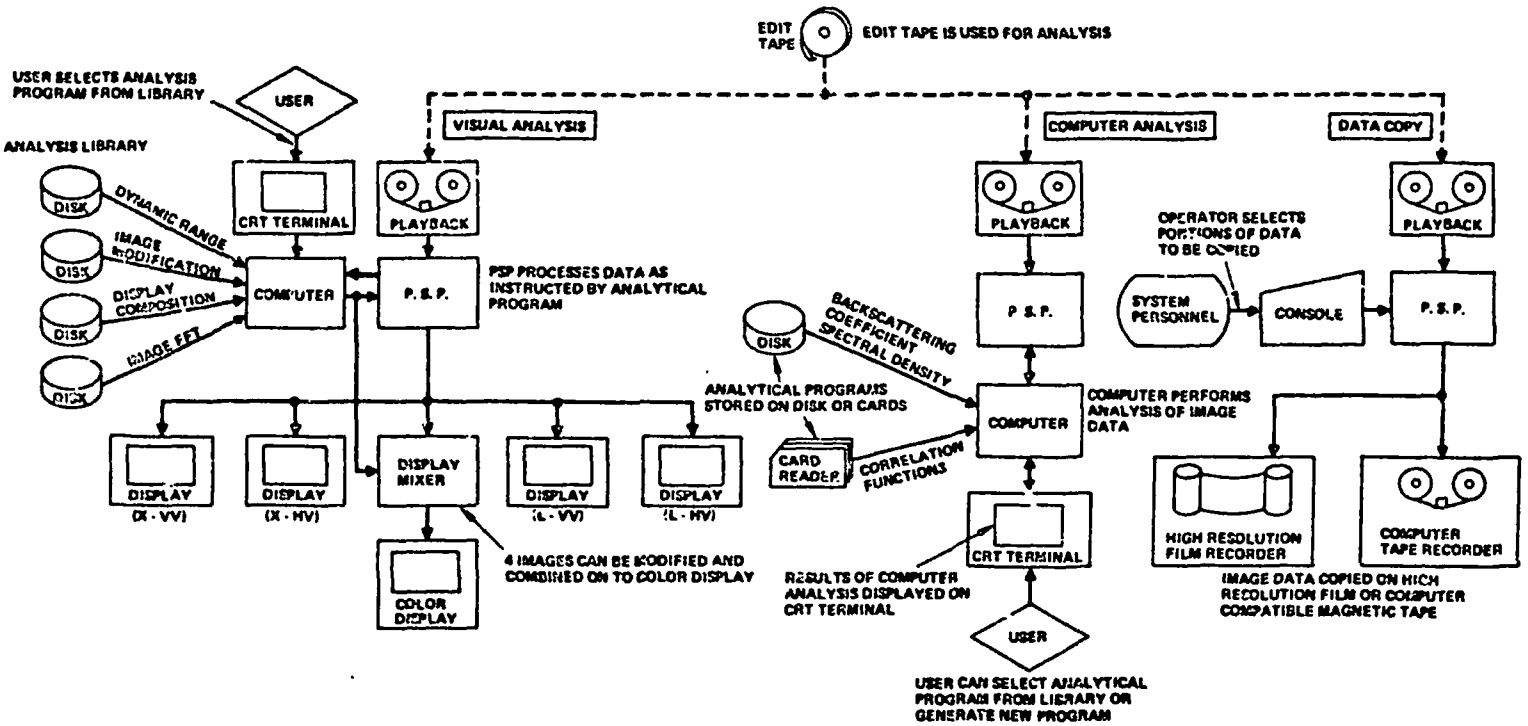

Figure 5-7. Space shuttle ground processor operational flow — analysis and copy.

location code, which will designate on the display the mission tape and the time code for the particular ground area that is being displayed.

With the scan tape, the operator can then generate an Edit tape as shown in Figure 5-6. The user plays back the scan tape and the image data is sent directly to a CRT display. A passing scene of the mapped area is presented on the display in either real time or at a 16/1 speedup. When an area of interest appears, the user freezes the display and positions a cursor over the selected area. The location code and the cursor coordinates are then sent to the computer for storage. The user continues the review until he has selected all ground areas he wishes to analyze. The system operator then prepares an Edit tape. He plays back each of the mission tapes that contain the desired data. The location code and cursor coordinates are sent to the PSP and the raw data corresponding to the location is sent to the tape recorder where the Edit tape is prepared. The Edit tape will contain the synthetic array raw data with both frequencies and polarizations of the selected areas which are to be analyzed.

The Edit tape is used for analysis and copy as shown in Figure 5-7. The data is processed by the PSP. The signal processing parameters (resolution, motion compensation, dynamic range, etc.) are controlled by the computer. A PSP program, which is stored on disc, is sent to the PSP by the computer. The PSP operates on the data and sends the process data to the displays. Each of the displays has a resolution of 1000 elements. The four black and white displays can then be used to show a complete range swath at a single frequency and polarization with maximum resolution. Alternately the displays can show each of the frequencies and polarizations at a reduced resolution. The choice is controlled by the user via inputs to the computer. If the user wishes, he can generate a composite display on the color monitor. He can assign colors according to a stored algorithm or he can control the display manually by inputs at the CRT terminal.

The computer also has a more accurate means of analyzing the image data. On command by the user, the display freezes the image and a cursor appears along with the map. The user positions the cursor over an area on the map. The data within the cursor is then sent to the computer. When the transfer is complete, the computer operates on the data. Analytical

programs such as correlation functions, scattering coefficient measurement, and spectral density functions can be called from disc memory and the computer will perform these measurements on the data. The results of this analysis will be presented to the user on the CRT terminal. At this time the user can also record on computer compatible tape a copy of the selected image data. The data can then be analyzed off-line with a large scale computer.

The data copy mode provides a high resolution film copy of the image data. The film recorder receives data and synchronizing signals from the PSP. The image data is then recorded on 5-inch film. Since the recorder has a capacity for 1500 foot reels, the image data from a mission can be recorded on two reels of film.

Analysis is the primary mode of the GPS. In this mode the user can analyze the synthetic array data on the CRTs with the computer. He can generate data copy with the computer for off-line analysis or with the film recorder for analysis at other locations. The analytical programs available to the user are stored on disc and constitute a portion of the GPS software library.

The GPS software library contains utility programs and applications programs. The utility programs are designed to minimize the data handling required by the user. They are generated and executed by the GPS personnel. Applications programs are executed by the user and define the type of processing that is to be performed on the data. The programs are described below:

Utility Programs

1. SCAN – This program is used to obtain a recorded catalog of the mission tapes. The PSP processes the mission data at 1/4 resolution and displays the X-band (VV) image data. The operator then records each of the missions on the scan tape. Auxiliary data specifying the mission, date, and time code will also be recorded.
2. EDIT SEARCH – This program searches the scan tape to locate areas that will be processed by the user. The scan tape is played back into the PSP. The PSP sends the data directly to the display. The operator designates the desired area by

positioning the cursor onto the area and transferring the cursor coordinates to the computer.

3. EDIT COPY – This program searches the mission tape, selects those areas defined during the search operation, and records the raw data onto an edited tape. The PSP is set to process the data at 1/4 resolution so that the operator can monitor the image data on the display.

Applications Programs

There will be three types of applications programs. Processing programs determine the type of synthetic array processing performed by the PSP. These programs affect the pre-detection functions. The image modification programs define the post processing functions of the PSP. These will operate on the image data. The third set of programs defines the statistical analysis that will be performed by the computer.

SAR Programs

1. Resolution – The PSP will process the data at either full or 1/4 resolution as selected by the user.
2. Select Data – The PSP will process either all of the raw data or only that data selected by the user or designated by the cursor.

Image Modification Programs

1. Linear – The PSP processes the image data linearly.
2. Log Compression – The data is log converted prior to display.
3. Dynamic Range – The user designates which bits will be displayed.
4. Display Composition – The image data to the color display will be a composite of the four images according to the equation:

$$D_5(X, Y) = \sum_{1}^{4} Kn\,(T)\ fn\left(Dn\,(X, Y)\right) Cn$$

where

Dn	is the image data to the Nth display
X, Y	are the coordinates of the resolution cell
Kn(T)	is an image fade function
fn	is an arbitrary function

5. Image Enhancement – This program will optimize the assignment of CRT gray levels to enhance the image contrast.
6. Image FFT – This program will perform a two-dimensional FFT on the image data.

Statistical Analysis

1. Histogram – An amplitude versus frequency histogram of the image data will be displayed.
2. Auto-Correlate – The computer will perform a two-dimensional auto-correlation of the image data.
3. Cross-Correlate – The four sets of image data will be correlated by a two-dimensional cross-correlation function.
4. Spectral Density – The spectral density function of the data will be calculated.
5. Scattering Coefficient – The radar scattering coefficient will be averaged across selected areas of the image.

In addition to these programs other programs can be generated by the user and added to the permanent library file. The operating system allows the user to write his programs in a high-level or problem oriented language. A compiler will be designed to translate the program to machine language required by the PSP.

5.4 GROUND SYSTEM OPTIONS

The Programmable Signal Processor offers complete flexibility in the design of the Ground Processing System. Initially, a low cost system can be developed for processing the synthetic aperture data and generating a film copy of the ground map. This basic system would contain a tape reproduce unit, the PSP, and a film recorder. Ground processing parameters could be varied by changing the PSP software. This basic system would be sufficient to verify the performance of the Radar Imaging System and also define the

ground processing parameters. As the amount of collected data increases, the GPS will become overloaded and other functions can be added to the system, which will increase the processing efficiency. The addition of a DSC and CRT will provide a quick look at the image data and thereby reduce the amount of image data that must be recorded on film. A tape record unit will provide editing capability and reduce the data handling required by the user. Finally, other PSPs and CRTs can be added which will increase the processing rate and provide the user with an efficient system for processing and analyzing radar imagery data.

6.0 PRELIMINARY SYSTEMS SPECIFICATIONS

These specifications are in the most part abstracted from the preliminary design work reported earlier in this report and from References 1 and 2. The purpose is to establish a starting point for a detailed design phase of the ERSIR Program. To some extent the requirements specified may be too rigorous in that a detailed design effort may show that the specified image quality cannot be obtained with the specified subsystem parameters. As an example, the specified transmitter power may, because of a better estimate of antenna efficiency, be insufficient to provide the required signal-to-total noise ratio specified under "Image Quality Requirements."

6.1 OPERATING MODES

Operating modes are described in terms of those parameters and functions that are to be controllable or selectable respectively (see Tables 6-1 and 6-2).

6.2 OPERATING ORBITS AND OFF-DESIGN POINT PERFORMANCE

ERSIR is required to operate in a 200 km altitude circular orbit. It is required to perform at up to 400 km and to produce useable data at this altitude, although reduced performance is acceptable. Table 6-3 shows the variation of performance with altitude.

6.3 IMAGE QUALITY REQUIREMENTS

Noise background on the output image is attributable to several sources. Among these are:

receiver front end - (thermal noise)
A/D converter step size - (quantization noise)

TABLE 6-1. CONTROLLABLE RADAR PARAMETERS.

Controllable Radar Parameter	Maximum Value	Maximum Value	Step Size
Swath Offset (km)	275 km	360 km	1 km
Swath Width Recorded	45 km	85 km	1 km
Ground Range Resolution	12.5 m	25.0 m	12.5 m

TABLE 6-2. SELECTABLE RADAR FUNCTIONS.

Selectable Radar Function	Options
Transmitter Frequencies	X and L, or X or L
Receiver Channels Recorded	All or any combination of their two frequencies with their two polarizations or none.
Data Link Transmission	From data tape, real time, or no data transmission.
Spaceboard Unfocused Display	Any 40 km swath width within selected swath parameters.
AGC Type	Gain as a function of range, local average of scatterer magnitude, or a combination of these.

TABLE 6-3. OFF DESIGN-ALTITUDE PERFORMANCE.

Performance Parameter	Required Performance		
	200 km Altitude	300 km Altitude	400 km Altitude
Maximum Available Swath Width	85	70	60
Minimum Signal-to-Total Noise Ratio	7 dB	7 dB	7 dB
Resolution (ground)	25m x 25m	25m x 25m	25m x 25m

A/D limit - (saturation noise)

pulse compression - (range integrated and peak side lobe noise)

pulse repetition frequence - (range ambiguities and azimuth ambiguities)

azimuth compression - (azimuth doppler filter integrated and peak side lobe noise)

In the specifications the signal-to-total noise ratio is determined by dividing the average signal power by the sum of the noise powers contributed by the above sources. The primary image quality specified is this signal-to-total noise ratio; however, the contributing components are also individually specified as they are not entirely equivalent. For example, azimuth ambiguities can cause ghosting whereas quantization noise will not. Also, azimuth ambiguities are more sharply focused than range ambiguities. Still, a large number of noise contributions, some of which are further effected by scintillation (such as the ambiguities and side lobe contributions), and by defocussing tend towards a randomized noise. That is, the noise tends towards less specific image dependence, and more towards dependence on average, image σ_o's.

To a first approximation, then, the image dependent noise is specified in terms of a uniform, homogenous, diffuse terrain having a constant average radar cross section per unit area (σ_0). Thus the desired resolution cell has the same σ_0 (σ_0 = -17 dB) as does the terrain contributing to the ambiguity noises, and the range and azimuth side lobe noises.

Image quality is specified further by considering a hole located in the uniform terrain model, to which is added a few large discrete backscatterers. By a hole is meant a small region of 3 or 4 resolution cells over which σ_0 is zero; an example is a small, very still pond of water. The amount of image noise from the discrete backscatters and from the other noise sources already listed is termed the "hole noise". Dynamic range is now defined as the ratio of the maximum discrete scatterer power-to-hole noise that could be available at the digital correlator (ground processor) output. Figure 6-1 shows the terrain backscattering characteristics assumed for this case.

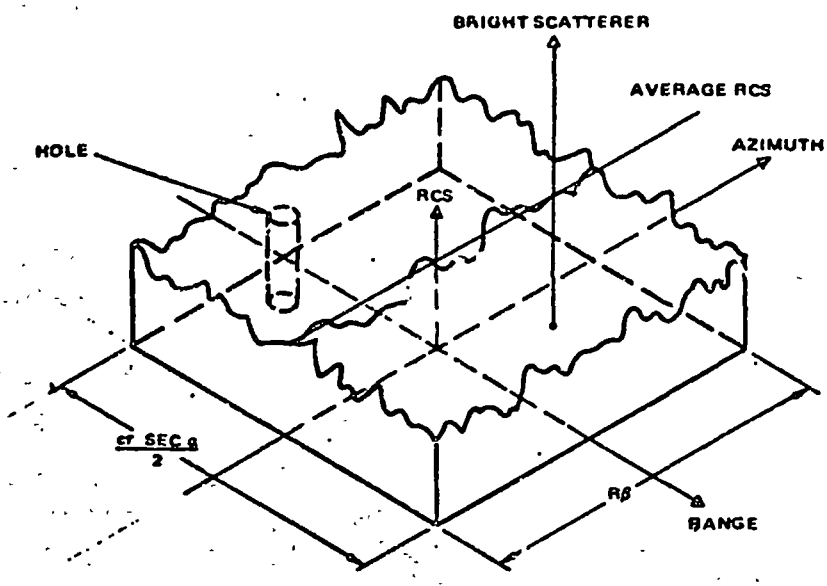

Figure 6-1. Evaluation terrain model.

6.4 SPACE SYSTEM CALIBRATION

Uncertainty in the measured image power is caused principally by uncertainties in the following parameters:

(1) antenna gain (including overall efficiency); (2) receiver gain; (3) transmitter peak power; (4) propagation path losses; (5) terrain factors (terrain slope for difuse backscatterers); in terms of these parameters, the measured power, S, for a single resolution cell is

$$S = \frac{K_M P_0 G_0^2 \sigma_0}{L_{att} \sin \phi_0} \left(1 + \frac{\xi_P}{P_{00}}\right) \left(1 + \frac{\xi_{rec}}{G_{rec}}\right) \left(1 + \frac{\xi_G}{G_0}\right)^2 \left(\frac{\sin \phi}{\sin (\phi + \xi_\phi)}\right)$$

where: (1) P_0, G_0 and G_{rec} are the measured values of transmitter power, antenna gain in direction of resolution cell, and receiver gain respectively; (2) L_{att} is the atmospheric propagation loss; (3) ϕ_0 is the wave incidence angle at the resolution cell (includes ground slope); (4) ξ_P, ξ_G and ξ_{rec}

are the errors in the transmitter power measurement, the antenna gain estimate pertaining to the resolution cell, and the receiver gain measurement respectively, (5) ξ_ϕ is the error in the incidence angle at the resolution cell; (6) σ_0 is the actual average backscattering cross section per unit area of terrain at the resolution cell; and (9) K_M is a function of the other radar parameters which do not contribute significantly to the uncertainty in the image power estimate (or the ultimate estimate of σ_0),

$$K_M = \frac{K \lambda^2 d_r d_a f_r T_A}{(4\pi)^3 R^4}$$

k	= constant	f_r	= PRF
λ	= wavelength	T_A	= synthetic array length
d_r	= slant range resolution	R	= range
d_a	= azimuth resolution length		

Here only the radar sensor uncertainties are considered; i.e., ξ_p, ξ_{rec} and ξ_G. If Equation 6-1 is normalized, an expression for the uncertainty in the σ_0 measurement contributed by the radar sensor is

$$\log \left(\frac{\sigma_0^*}{\sigma_0}\right) = \log u$$

where:

$$u = \left(1 + \frac{\xi_p}{P_0}\right) \left(1 + \frac{\xi_{rec}}{G_{rec}}\right) \left(1 + \frac{\xi_G}{G_0}\right)$$

Here the logarithm of u is assumed to be normally distributed; consequently u in dB is also normally distributed.

Two characteristics of u are considered in these specifications; its power spectral density function and its magnitude. Knowledge of its spectral density (or, equivalently autocovariance function) aids in the quantitative comparison of data collected within a given time interval, and, of course, magnitude is needed for reference to standards. Actually, the integral of the spectral density is equal to the variance of u plus its mean squared ("mean" is here the time average over a single mission; over the ensemble

of missions it is assumed to be normally distributed about zero; i.e., log u is normally distributed about zero).

The limiting envelope of the power spectral of u in dB (Figure 6-2) is defined in terms of a delta functior at zero frequency and its values at three frequencies:

$f_{mission}$ = 0 Hz
f_{orbit} = 0.302 + orbit period in secs
f_{update} = 0.302 + calibration update interval in seconds

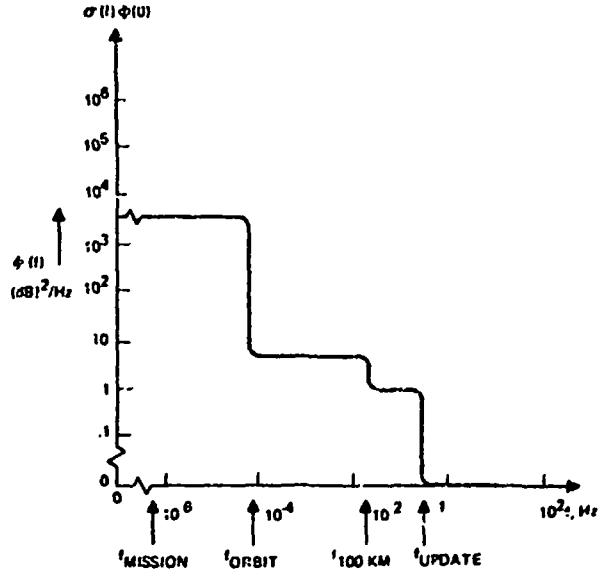

Figure 6-2. Limiting Envelope of u (in dB) Power Spectral Density

Roughly speaking during a single orbit the mean of u (in dB) is given by the integral of $\phi(f)$ to the left of f_{orbit}, and fluctuating component is the integral of $\phi(f)$ to the right. A similar remark applies to the other break points. These integrals for the limiting envelope of Figure 6-2 are listed in Table 6-4.

Allocation of the allowable contributions of antenna, transmitter, and receiver to total integral of $\Phi(f)$ are given in Table 6-5.

TABLE 6-4. CALIBRATION ERROR MODEL

f_i	"MEAN" $\mu_o = \sqrt{\int_o^{fi} \Phi(f)df}$	"FLUCTUATING" $\mu_f = \sqrt{\int_{fi}^{\infty} \Phi(f)df}$
$f_{mission}$	.92 dB	.91 dB
f_{orbit}	1.06	.73
$f_{100\ km}$	1.10	.66
f_{update}	1.22	.39
f_∞	1.28	-

TABLE 6-5. CALIBRATION ERROR CONTRIBUTIONS SOURCE

Source / f_i	Antenna*		Transmitter		Receiver	
	μ'_o	μ'_f	μ''_o	μ''_f	μ'''_o	μ'''_f
$f_{mission}$	0.7 dB	0.4 dB	0.3 dB	0.2 dB	0.25 dB	0.30 dB
f_{orbit}	0.73	0.35	0.33	0.13	0.27	0.29
$f_{100\ km}$	0.81	0.05	0.35	0.08	0.29	0.28
f_{update}	0.82	—	0.36	—	0.38	0.10
f_∞	0.82	—	0.36	—	0.40	—

Notes:

*Peak gain, two way

$$\mu'_o = \sqrt{\int_o^{1i} \Phi'(f)df} \quad ; \quad \mu'_f = \sqrt{\int_{f_i}^{\infty} \Phi'(f)df}$$

6.5 SUBSYSTEM PARAMETERS

6.5.1 Transmitter/Receiver Subsystem

Stable L- and X-band transmitter/receiver subsystems are required. The subsystems will operate at fixed frequencies determined by stable, low noise reference sources from corresponding L- and X-band exciters. The transmitter/exciter/receiver subsystems include modulators controlled by master timing waveforms from electronics in the pressurized module bay; thus waveforms that are identical with respect to pulse compression, transmitter pulsed output timing, and receiver enabling signals are supplied to the L- and X-band subsystems. A means is provided for replicating the transmitter waveform and inserting the resulting down-converted i-f test signal into the respective receiver to serve as a continuous monitor test signal. This signal is used for built-in-test and for calibration of the measurement system. Receiver AGC signals have a long time constant. Their control signals come from module bay electronics.

Major parameter requirements of the L- and X-band transmitter/receiver systems are listed in Table 6-6. Frequency requirements are largely determined by available spectrum allocations, availability of transmitter tubes, and user community preferences. The recommended system parameters with respect to frequencies (1.045 and 9.0 GHz) are guides which provide L-band near the maximum useable wavelength together with a convenient X-band frequency for a large ratio (9:1) of wavelengths. Shorter L-band wavelengths reduce antenna aperture height and processing requirements. The X-band wavelength can be shortened to about 2.6 cms with some increase in power requirements or reduction in coverage. The transmitter subsystems assume an array of 10.7 meters length similar to the recommended design. Power requirements are based upon resolutions of 25 meters with swath width coverages >60 KM for terrain backscatter coefficients of $\eta = -18$ dB in X-band (8.5 to 11.8 GHz) and $\eta = -27$ dB (1 GHz) to -24 dB (2 GHz) in I-band.

TABLE 6-6. MAJOR PARAMETER REQUIREMENTS FOR L- AND X-BAND TRANSMITTER/RECEIVER SUBSYSTEMS

Parameter	L-Band	X-Band
Wavelengths[1] λ, cms	28.7 (15-30)	3.33 (2.6-3.5)
Average Transmitter Power[2], Nominal Watts	200	500/.3λ
Receiver Noise Figure, Max, dB	2.5	4.0
Operating PRF's, Min-Max, Hz	1200-1800	1200-1800
Pulse Compression Ratios	64-324	64-324
Peak Power Ratings[2], Nominal, Kw	6.6	17/.3λ
Duty Factors, Nominal Max	3%	3%
Transmitted Waveform, Bandwidth Max	27 MHz	27 MHz
Transmitter Tube Bandwidths, Min	75 MHz	75 MHz
Receiver Bandwidth, Min[3]	35 MHz	35 MHz

Notes:

1) Baseline frequencies are 1.045 and 9.0 GHz, respectively; L- and X-band operate at fixed frequencies in the indicated ranges.

2) Power requirements are based upon an array of 10.7-12 meters length; in X-band power should be scaled linearily with frequency, 500 watts at 9.0 GHz (λ in cms).

3) Filters matched to transmitted waveform are provided with the signal processing

6.5.1.1 Transmitter Requirements

Preliminary requirements for the transmitter are given in Tables 6-6 and 6-7. The operating temperatures specified are design limits. The Spacelab thermal control system (TCS) and auxiliary payload supplied facilities are to be employed for a nominal operating temperature from

TABLE 6-7. TRANSMITTER REQUIREMENTS

Parameter	L-Band	X-Band
Operating Temperature Range, °C	-20 to +40	-20 to +40
Average Power, Minimum	200 W	500 W
Gain, Minimum	30 dB	50 dB
Drive, Maximum	7 W	0.3 W
Gain Deviation, Maximum	TBD	TBD
Gain Drift Rate, Maximum[1]	TBD	TBD
PM and AM Sidebands, Maximum[2]	-45 dB	-45 dB
RF Power Droop in 25 μs, Maximum	0.3 dB	0.3 dB

Notes:
1. In any 1 second period.
2. For any frequency >100 Hz, measured in 100 Hz bandwidth.

(TBD)°C to (TBD)°C at the pallet bay electronic cold plate, mounted on the back of the antenna in the baseline design. (References 1 and 2)

6.5.1.2 Exciter Requirements

Preliminary requirements for the exciters are given in Table 6-8. Stability requirements for the exciter apply to the local oscillator outputs as well as to the transmitter drive signals. The transmitter drive outputs are gated and the leakage levels at CW are specified for the purpose of avoiding excessive zero-doppler feed-through in the receiver channels.

The maximum deviation per state for the digital phase modulator is to be determined; maximum deviations of $\pm \pi/24$ are desired. Since ERSIR is not to be mass produced, a (TBD) screening process for (TBD) maximum phase state deviation is allowed.

TABLE 6-8. EXCITER REQUIREMENTS

Parameter	L-Band	X-Band
Operating temperature, °C	-20 to 40	-20 to 40
Carrier frequency, GHz[1.]	F_L ±100 PPM	F_X ±100 PPM
Carrier drift rate, max[2.]	$F_L \cdot 10^{-9}$ per sec	$F_X \cdot 10^{-9}$ per sec
FM, PM, and AM noise, max[3.]	-75 dB/C at F> 1000 Hz	-75 dB/C at> 1000 Hz
	-97 dB/C at F> 10 KHz	-97 dB/C at F> 10 KHz
RMS frequency deviation, max:		
In 20 Hz band centered at 100 Hz	0.8 Hz	0.8 Hz
In 1 KHz band centered at 600 Hz	2.7 Hz	2.7 Hz
Drive power output, gated, min peak	7 watts	0.6 watt
Drive power leakage, max	-100 dB/MW	-100 dB/MW
Power output stability, max dev	±0.5 dB	±0.5 dB
Power output drift rate, max[4.]	0.1 dB/minute	0.1 dB/minute
Local oscillator power, frequency	20 MW at F_L + 70 MHz	20 MW at F_X + 60 MHz
	20 MW at F_L + 75 MHz	20 MW at F_X + 65 MHz
Digital Phase Modulator		
(4 bit); phase states	16	16
Quantization size	$\pi/8$	$\pi/8$
Max deviation per state[5.]	TBD (desired $\pm \pi/24$)	TBD (desired $\pm \pi/24$)
State transition time, max	TBD	TBD
Peak amplitude modulation, max	0.2 dB	0.2 dB

Notes:

1.) For baseline: $F_L = 1.045$, $F_X = 9.0$; F_L F_X to be assigned in band 1 to 2 GHz and 8.5 to 11.5 GHz, respectively.

2.) In any 10 ms period.

3.) In 100 Hz bandwidth at frequency F; dB relative to carrier.

4.) In any 1 sec period.

5.) Phase states are: ϕ_o (quiescent) and $\phi_i = \phi_o + \frac{\pi}{8}(i \pm 1/3)$, $i = 1, 2, \ldots, 15$.

6.5.1.3 Receiver Requirements

Preliminary requirements for the receivers are given in Table 6-9.

The receivers are to be blanked by means of a receiver blanking signal synchronous with the transmitter timing gate. Allowable transmitter feed through is specified at levels consistent with the use of a continuous monitor IF test signal. This built-in test signal is applied in the receiver before AGC. Its purpose is to supply up-dated receiver gain data.

Cross-talk between any pair of receivers is specified at levels consistent with requirements for minimum mutual coupling between cross-polarized antennas; the antenna specification at L-band is -30 dB and is the limiting applicable specification. Staggered IF's are specified to facilitate mutual channel isolation.

6.5.2 Antenna Subsystem

Preliminary antenna subsystem requirements are summarized in Table 6-10. These requirements reflect the baseline choice of a planar array with dual polarized L-band antennas in a common aperture and separate apertures for horizontally and vertically polarized X-band antennas.

The antenna subsystem provides three vertical beams to effectively illuminate terrain at vertical pointing angles of 20° to 57° and thus provide for terrain imaging at 10° to 60° look angle. Three beamwidth choices in the range 5.7° to 20.8° are a satisfactory compromise with the ideal of continuous adjustment to match desired swath width coverage versus look angle. A broad beamwidth vertical antenna pattern (15.4° to 20.8°) is formed with a narrow section of the vertical dimension of the L- and X-band apertures; an intermediate beamwidth pattern (8° to 10°) is obtained from a broader section of about twice the narrow section height. The two sections are combined with suitable switching of corporate feeds to form a narrow vertical beamwidth (5.7° to 6.3°) antenna pattern.

A relatively long array of 10.7 meters minimum is specified for two reasons:

1. A long array permits sensor operations at the low prf's needed for swath illumination at large offsets and look angles with acceptable range ambiguity suppression;

TABLE 6-9. RECEIVER REQUIREMENTS

Parameter/Function	Requirement	
	L-Band	X-Band
Operating temp, °C	-20 to +40	-20 to +40
Noise figure, max	2.5 dB	4.0 dB
Image rejection, min	20 dB	20 dB
AGC range, min	30 dB	30 dB
Gain, min*	60 dB	60 dB
Gain deviation, max**	±0.7 dB	±0.7 dB
Gain drift rate, max***	0.1 dB/min	0.1 dB/min
Transmitter feed through, peak[1]	-85 dB/mw	-85 dB/mw
Cross talk, max[2]	-40 dB	-40 dB
Output saturation level, min[3]	+16 dB/mw	+16 dB/mw
Input saturation level, min[3]	-35 dB/mw	-35 dB/mw
Bandwidth, min	35 MHz	35 MHz

Notes:

*RF input to i-f output at quiescent (0) AGC level

**At any fixed AGC level

***In any 10 sec period at fixed AGC level

1. At the input of AGC'd i-f circuits with application of suitable blanking signal
2. Between any pair of receivers
3. At 1 dB small signal suppression

TABLE 6-10. ANTENNA REQUIREMENTS

Parameter	Requirement
Carrier wavelengths, cms[1.]	L-band: 28.7 (15-30) X-band: 3.33 (2.6-3.5)
Bandwidth, min	75 MHz, L- and X-band
Length, min	10.7 m
Height, max	3.3 m
Weight, max	TBD
Stowage:	Dual fold to single pallet, 3.3 x 4 m max horizontal area
Deployment:	Unfolded, tilted from hinged edge athwartship orientation
Jettisonable:	Yes, by mechanical means
Type:	Planar array
Polarization:	L- and X-band, linear vertical and horizontal, selectable on transmit, each on receive
Mutual coupling, max:	-10 dB between polarizations, each band
Multiple vertical beams:	3 co-planar, each polarization, each band
Beam axis misalignment, max: (any pair of beams)	±3 mr vertical; ±1 mr horizontal
Narrow vertical beamwidth:	6 ±0.3°
Vertical beamwidth ratios:	1, 1.5 ±0.1, 3 ±0.3
Vertical plane tilt	10° to 60° from horizontal
Peak sidelobes, max deviation relative to uniform illumination pattern:	±1.0 dB
Gain measurement	Yes, on suitable antenna range
Accuracy estimate, 2σ[2.]	±0.7 dB, each beam
Main lobe pattern measurement	Yes, on suitable antenna range
Accuracy estimate, 2σ[3.]	±0.5 dB, each beam

1. Baseline frequencies: 1.045 GHz (L) and 7.0 GHz (X); design center frequencies to be selected from indicated range.
2. Gain measurement to include corporate feed losses and effect of VSWR; thermal stress effects to be evaluated.
3. Measurement relative to principal axis in principal plane to -12 dB points (one-way). Thermal stress effects to be evaluated.

2. It favors economic Shuttle energy resources management and expeditious development of transmitter hardware because of the decrease in RF power requirements with antenna length.

Maximum length of the antenna is restricted to about 12 meters by the need for single pallet stowage with at most two folds and Illumination requirements for multiple-look imaging at 25 meters resolution, at least 4 looks with an overlap between successive looks of about 50 percent.

The minimum antenna length (about 10.7 meters) is determined by dynamic payload envelope constraints and the baseline choice of simple deployment and antenna pointing mechanisms, as discussed in Section 3.3 and illustrated by Figure 3-37. A detailed antenna design study should consider the possibility of practical implementations of the simple deployment and antenna pointing concepts which permit extension of the antenna length to 11 meters or more.

A vertical height of 3.3 meters maximum is adequate for a minimum beamwidth of 5.7° at L- and X-band wavelengths of 28.7 and 3.33 cms, respectively, and is consistent with a requirement for single pallet stowage. Final detailed design choices of carrier frequencies and beamwidths should result in a total antenna height of 3 meters or less.

Thermal considerations require thermal isolation of the antenna's radiating surface and the thermal mass of the payload supporting structure and electronics. As a practical consequence, operating temperature specifications for the antenna subsystem in the conventional sense are largely irrelevant. In the baseline design the pallet bay electronics are mounted on a cold plate fixed to the back of the antenna, and provision is made for heat exchange with payload thermal resources. The antenna radiating surface is thermally isolated. Specification of operating temperature conditions for the pallet bay electronics and the cold plate is properly part of the transmitter/receiver subsystem.

Ideally, each pair of antenna beams are coaxial. The specification of 3 milliradians maximum relative vertical beam axis misalignment is about 3 percent of the narrowest beamwidth (5.7° minimum) and consistent with practical overlay registration considerations for dual frequency or dual polarization imagery. The relative horizontal beam axis misalignment of

1 milliradian is approximately one-third the X-band beamwidth and is a practical compromise between the achievable and the impractical ideal, micro-registration of dual polarization X-band imagery. It will be necessary to compensate for the incremental doppler because of X-band horizontal axis misalignment in ground processing. The horizontal axis misalignment specification is equivalent to 4 to 5 percent of the L-band beamwidths. Resolution element spacings of 25 meters correspond to about 100 microradians (e.g., 25m at 250 km range). Along track registration of dual polarization or dual frequency imagery to a resolution cell width is a function for ground processing.

Mutual coupling of dual polarization apertures is specified at -30 dB, a practical and attainable value for the common aperture L-band case and a value readily exceeded by the separate aperture X-band approach. The isolation of 30 dB provides a cross polarized to direct signal interference ratio of at least 15 dB for practical applications, for which direct to cross polarization ratios are typically less than 12 dB. Cross talk in the receiver channels is specified at -40 dB maximum to assure a satisfactory margin at the mutual coupling specification for the antenna.

Gain and pattern measurements of the antennas must be made prior to their use in Shuttle experiments. However, the length of the antennas and the relatively large vertical beamwidths impose stringent requirements on an antenna range; and facilities must be adequate for measurement accuracy. The objectives of such measurements are to provide calibration data for gains, beamwidths and patterns for use in earth resources measurements with ERSIR sensor. The requirement for making gain and pattern measurements prior to Shuttle installation should be waived if suitable facilities cannot be provided at reasonable cost. In either case, specially designed Shuttle experiments for the purpose of gain and pattern measurements are recommended.

Evaluation of thermal stress effects on antenna gain and pattern on the basis of analysis and appropriate test data are planned. Resulting antenna test data will be used to correct nominal antenna gain and pattern calibration data for various incident solar radiation angles during Shuttle experiments.

6.5.3 Space System Preprocessor Requirements

The preprocessor generates timing and control signals and preprocesses receiver IF signals for data storage on magnetic tape. Data are recorded in a digital format. Preliminary requirements for the ERSIR space system preprocessor are given in Tables 6-11 and 6-12.

Signal conditioning requirements include the generation of analog AGC signals independently for each of the four receivers. The AGC levels are smoothed with a time constant of (TBD) seconds. AGC signals are recorded for subsequent use in data reduction.

Contoured AGC is adjusted to accommodate varying signal levels in a number of range segments that will be determined in subsequent detailed design studies. Ultimately the number of range segments should be at least 8 (about 10 km intervals) and possibly as many as 80 (about 1 km intervals). The contoured AGC levels are adjusted independently for each of the four receivers and the range segment AGC signals are recorded for subsequent use in data reduction. The contoured AGC levels are updated at intervals that correspond to the equivalent range segments. The two dimensional AGC segments are to be approximately square; e.g.: 4 x 4 km.

Video signals are processed in matched quadrature phase filters before A/D conversion. Specifications on quadrature channel phase and gain balances include the contributions of the filters. One of the seven selectable bandwidths will approximate the signal bandwidth for 25 meter ground range resolution, for look angles of 15° to 60°.

Buffer output data rates for the baseline design are 260 mB/s maximum. The data storage requirements are satisfied by two high density, multi-track tape recorders. If such recorders are not available, two 90 to 100 mB/s recorders are acceptable as an alternate solution, which will be implemented in the back-up design.

6.6 BUILT-IN-TEST

The space radar subsystem incorporates built-in test (BIT) circuitry for checking operating status of the equipment. It provides for checking performance of the major subassemblies and for the continuous monitoring of critical parameters. The continuous monitor performs calibration functions

TABLE 6-11. SPACE SYSTEM PREPROCESSOR REQUIREMENTS

1. Signal Conditioning:

Function/Parameter	Requirement
Operating temp, °C	-20 to +40
PRF timing gates:[1]	
Rates f_r, Hz	1200 to 1800
Duration T, μs	15 to 25
Accuracy in f_r, T	±0.01%
Time jitter, $\Delta\sigma$, ns[2]	1
Video Signal Conditioning[3]	
I-F input saturation level, min[4]	+10 dBM
Selectable video bandwidths, MHz	7; 1.5, 4.5, 5.5, 7, 9, 11, 17.5
Quadrature channel balance:	
Phase deviation, Δφ	±4°
Gain deviation, Δg	±0.2 dB
A/D Converter[5]	
Precision, bits	8I, 8Q
Oversampling, min	5%
Speed, MHz	7 to 10
AGC'd output to buffer, bits	5I, 5Q
Pulse Compression[2]	
Type	Digital approximation to linear FM (4 bits phase quantization)
Clock rate f_c, MHz	80 MHz ±50 PPM
Bandwidths B, MHz	6 to 27
Accuracy in B	±0.01%
TB products, PCR	64 to 124
Time jitter, max, ns[6]	0.5
Receiver AGC[7]	
Type	Fixed, analog
Update interval, min	TBD
AGC range, min	10 dB
Processor AGC[7]	
Type	Digital, contoured to range profile
Range segments	8 to 32 segments/swath
AGC range	Point shift, 8 bits (in) to 5 bits (out)

Notes:

1) Simultaneous L- and X-band channels

2) Pulse position errors at PRF intervals

3) Independently, each of 4 receivers

4) At 1 dB small signal suppression

5) Simultaneous L- and X-band channels

6) Pulse position errors at PRF intervals

7) Independently, each of 4 receivers.

TABLE 6-12. SPACE SYSTEM PREPROCESSOR REQUIREMENTS

2. Space Preprocessor:	
Function/Parameter	Requirement
PRF-buffer	
Storage capacity, max	87.5×10^3 bits/channel; 350×10^3 bits
PRF-buffer	
Output rate, max	65×10^6 bits/sec/channel; 260×10^6 bits/sec
Monitor display	Unfocused strip map, any of four channels, 150 m x 150 m resolution (6:1 range collapsing)
Processor	
Scan converter capacity	3.6×10^5 elements; 3 bits/element
Display	600 x 600 elements, to 90 km swath coverage at 150 m resolution
Dynamic range, min	6 grey scales, logarithmically compressed video
Recorder requirements	
Rate requirements, max	65×10^6 bits/sec/channel; 260×10^6 bits/sec
Bit error rate, max	1 part/in 10^5 (random)
Number, max	2 at 240 MB/s each
Record time per reel	16 min at 240 MB/s
Reel size, max	Diameter = 35 cm., width = 5 cm
Reel weight, max	8.5 kg

that are described in Section 4.4. In addition to calibration, it provides for continuous monitoring of such critical parameters as voltages, currents, pressure, coolant flow and temperature. The remaining BIT will isolate failure to the pallet bay or pressurized module subassemblies.

6.7 ENVIRONMENT

The EPSIR design will include provisions for performance in the anticipated space environment. Since it is intended for the space shuttle, the environments encountered will differ in some respects from those

experienced by equipment designed for other satellite operations. Details will be worked out in the final design. The ERSIR will be required to meet environmental requirements of the applicable NASA documents and some consideration has been given to these requirements in this study. Environmental factors that will influence the antenna design are listed in section 3.3. Those that influence design of the pallet bay electronics (transmitter/receiver subsystems) are covered in section 3.4. The remaining equipment is located in the pressurized module and for this reason should present no unusual problems.

REFERENCES

1. Spacelab Payload Accommodation Handbook, Intermediate Issue (Revision A), April 1974, European Consortium, ERNO VFW-FOKKER

2. Space Shuttle System Payload Accommodations, Level II Program Definition and Requirements, Vol. XIV, Revision C, July 3, 1974, JSC, Houston, Texas.